

ICCE

2008
Hamburg

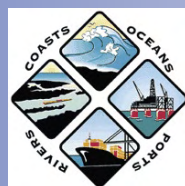
31st

International Conference on Coastal Engineering

«meeting coastal challenges»

31 August to 5 September 2008
Hamburg | Germany

**Morphodynamic Processes
and Modeling**



Short Course

Morphodynamic Processes and Modeling

Short Course held at ICCE2008 Hamburg, 31 August 2008

Rainer Lehfeldt (editor)

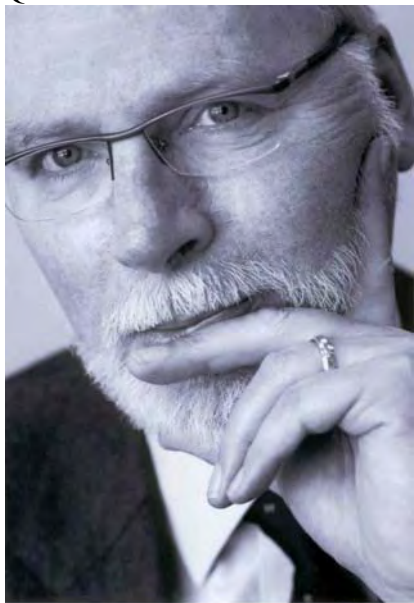
Marcel J.F. Stive: Sea Level Rise and Coastal Erosion	1-20
Hanz D. Niemeyer: Field Measurements and Morphodynamical Modeling of Tidal Inlets and Basins	21-48
Ida Brøker: Effects of coastal structures	49-81
Tim J. Chesher: Siltation Studies	82-94
Dano Roelvink: Modelling of geological processes	95-107
Jørgen Fredsøe: Small Scale Morphodynamics	108-125
Andreas Malcherek: The Morphodynamics of Estuaries	126-143
Chris Sherwood: Introduction to the Community Sediment- Transport Modeling System	144-173
Peter Mewis: Tidally Induced Morphodynamics	174-179



Short Course on Morphodynamics

- Marcel J.F. Stive

August 31 – September 05

NAME - DATE OF BIRTH - NATIONALITY:	Marcel J.F. Stive - February 25, 1951 - Dutch
EDUCATION:	PhD Civil Engineering, Delft University of Technology MSc Civil Engineering, Delft University of Technology
PRESENT POSITION	Professor of Coastal Engineering, Delft University of Technology, Faculty of Civil Engineering and Geosciences, Section of Hydraulic Engineering Scientific Director Water Research Centre Delft Course Director Erasmus Mundus Master Program Coastal and Marine Engineering and Management
<p>KEY QUALIFICATIONS:</p> 	<p>Marcel Stive received an MSc degree in Civil Engineering in 1977 and a PhD degree in Civil Engineering in 1988, both at Delft University of Technology. He has plus 30 years experience in research and projects in the fields of hydraulic engineering, coastal morphodynamics, coastal biogeomorphology and coastal and estuarine management, as team member, as team leader and as advisor. His record involves coasts, estuaries, harbours and offshore projects in Europe, Asia, Africa and the Americas, using fieldwork and experimental physical and mathematical physical models. He spent two years as visiting professor on the Universitat Polytechnica de Catalunya, and was part-time professor Coastal Morphodynamics at Delft University of Technology from 1994 to 2000. In 2001 he accepted the fulltime chair of Coastal Engineering at the Faculty of Civil Engineering and Geosciences of Delft University of Technology. Since 2003 he is scientific Director of the Water Research Centre of Delft University of Technology, and since 2006 is course director of the EU Erasmus Mundus MSc course on Coastal and marine Engineering and Management. He is a member of the Coastal Engineering Research Council of the American Society of Engineers. He has written many publications on a variety of topics, ranging from geology to hydraulic engineering and coastal zone management. His current Hirsch-factor is 14.</p>
PUBLICATIONS	<p>Selection of recent journal publications</p> <p>2008 Van Koningsveld, M.; Mulder, J.P.M.; Stive, M.J.F.; Vander Valk, L., And Vander Weck, A.W., 2008. Living with sea-level rise and climate change: a case study of the Netherlands. <i>Journal of Coastal Research</i>, 24(2), 367–379. West Palm Beach (Florida), ISSN 0749-0208.</p> <p>2005 Jonkman, S.N., Stive, M.J.F. and Vrijling, J.K., 2005. New Orleans is a lesson to the Dutch, <i>Journal of Coastal Research</i>, 21 (6), XI-XII</p> <p>2005 Elias, E.P.L., Stive, M.J.F. and Roelvink, J.A., 2005. Impact of back-barrier changes on ebb-tidal delta evolution, <i>Journal of Coastal Research</i>, SI, 42, 460-476</p> <p>2004 Stive, M.J.F., 2004. How important is global warming for coastal erosion? <i>Climatic Change</i> 64 (1-2): 27-39</p> <p>2004 Kragtwijk, N.G., Zitman, T.J., Stive, M.J.F. and Wang, Z.B., 2004. Morphological response of tidal basins to human interventions, <i>Coastal Engineering</i> 51: 207 - 221</p> <p>2003 Cowell PJ, Stive MJF, Niedoroda AW, de Vriend HJ, Swift DJP, Kaminsky GM, Capobianco M, 2003. The coastal-tract (part 1): A conceptual approach to aggregated morphodynamics of low-order coastal change, <i>Journal of Coastal Research</i> 19 (4): 812-827</p> <p>2003 Cowell PJ, Stive MJF, Niedoroda AW, Swift DJP, de Vriend HJ, Buijsman MC, Nicholls RJ, Roy PS, Kaminsky GM, Cleveringa J, Reed CW, de Boer PL, 2003. The coastal-tract (part 2): Applications of aggregated morphodynamics of lower-order coastal change, <i>Journal of Coastal Research</i> 19 (4): 828-848</p> <p>2003 Van Goor, M.A., Zitman, T.J., Wang, Z.B. and Stive, M.J.F., 2003. Impact of sea-level rise on the morphological equilibrium state of tidal inlets. <i>Marine Geology</i> 202 (3-4): 211-227</p> <p>2003 Hibma, A., de Vriend, H.J., and Stive MJF. 2003. Numerical modelling of shoal pattern formation in well-mixed elongated estuaries, <i>Estuarine Coastal and Shelf Science</i>, 57 (5-6): 981-991</p> <p>2003 M.J.F. Stive and A.J.H.M. Reniers, 2003. Sandbars in motion, <i>Science</i>, 299, 1855 – 1856</p>

SEA LEVEL RISE AND COASTAL EROSION

Marcel J.F. Stive^a, Roshanka Ranasinghe^{b,c} and Peter J. Cowell^b

^a *Department of Hydraulic Engineering, Delft University of Technology
P.O. Box 2600 GA, Delft, Netherlands, E-mail: m.j.f.stive@tudelft.nl*

^b *School of Geosciences, University of Sydney, NSW 2006, Australia*

^c *Department of Environment and Climate Change, Sydney, NSW 2001, Australia*

IPCC projections indicate that the rate of sea level rise (SLR) during the 21st century may be about an order of magnitude greater than the 20th century rate of 1-2mm/yr. This accelerated sea level rise will in turn result in much faster coastline retreat with particularly severe impacts on low-lying areas. The socio-economic impact of such accelerated coastline retreat could be massive due to the rapid growth of coastal communities and infrastructure over the last five or six decades. The method most commonly used to estimate coastline retreat due to SLR is the simple two-dimensional mass conservation principle known as the Bruun Rule. However, in view of the high level of predictive accuracy that is clearly needed to facilitate informed planning decisions for the future, can we continue to depend on the Bruun Rule? This chapter discusses the evidence for and against the Bruun Rule and suggests alternative methods that may be more suitable for the 21st century.

1. Introduction

The IPCC¹ projections for 21st century sea level rise (SLR) range from 0.18m to 0.79m by 2090-2099 relative to 1980-1999, including an allowance of 0.2m for uncertainty associated with ice sheet flow. Very recent research also suggests that the measured SLR over the last decade is under predicted by the IPCC models (Rahmstorf et al.²), and that a maximum SLR of 1.4m by 2100 (relative to 1990 levels) is not unlikely (Rahmstorf³). Compared to the 1-2mm/yr rate of SLR that was experienced in the last century, these 21st century projections constitute an order of magnitude increase in the rate of SLR.

It has been long known that, in the absence of other compensatory mechanisms, any rise in the mean sea level will generally result in the retreat of unprotected coastlines (Bruun⁴). Fortunately, the still-stand (slow) conditions of sea level rise (SLR) during the last century has resulted in slow and mostly manageable coastline retreat (recession). However, the potential order-of-magnitude increase in the rate of SLR in the 21st century is likely to result in much faster coastline recession. The socio-economic impact of such accelerated coastal recession could be massive due to the unprecedented growth of coastal communities over the last 50 years or so which has led to \$ billions worth of developments and infrastructure within the coastal zone. To ensure the safety of growing coastal communities and to avoid massive economic losses in the future, it is now imperative that any predictions of coastal recession due to SLR be highly accurate.

The IPCC has successfully raised awareness on political and societal levels, which in many nations has resulted in including SLR scenarios in new designs of shore protection works, both hard (structures) and soft (nourishment) or combinations thereof (Hamm et al.⁵). In this context, it is crucial that the impact of SLR in low-lying coastal areas be quantified accurately. The inundation of such low-lying areas will result in significant coastline retreat, the magnitude of which is governed by the local coastal slope. As coastal slopes in such areas may be as mild as 1 in 1000, the resulting coastline retreat could be three orders of magnitude greater than the rate of SLR.

Quantifying the impact of SLR on dune and barrier coasts is less straightforward. This is because the response of dune and barrier coasts to SLR is a complex morphodynamic issue. The most commonly used method to quantify the recession due to SLR at such coastal locations is the simple two dimensional mass conservation principle known as the Bruun Rule, which predicts a landward and upward displacement of the cross-shore profile in response to a rise in the mean sea level. For many of the world's coastlines, where the nearshore beach slope is about 0.01 to 0.02, the Bruun Rule predicts a coastline retreat between 50xSLR and 100xSLR, which are proportionalities that are commonly used as a '*rule-of-thumb*'.

Although, coastal scientists and engineers have been routinely using the Bruun Rule for almost 5 decades, mainly due its simplicity and the lack of any other easy-to-use alternative methods, it has been receiving some heavy criticism in the recent past (Pilkey and Cooper⁶; Cooper and Pilkey⁷). While the many attempts to verify the Bruun Rule against field and laboratory data over the last 4 decades (e.g. Rosen⁸, Hands⁹, Everts¹⁰, Pilkey and Davis¹¹, Dean¹²) have qualitatively confirmed the basic concept of the Bruun Rule, not many have

resulted in convincing quantitative comparisons between measurements and Bruun Rule predictions (SCOR¹³). Zhang et al.¹⁴, who undertook a large-scale study of a 220km stretch of the US East coast is the only study which resulted in reasonably good comparisons between measured shoreline recession and Bruun Rule predictions.

However, does even a good comparison between measured and predicted values under present still stand SLR conditions (1-2mm/yr SLR) mean that the Bruun Rule is conclusively validated? Based on observations made in the USA, the Netherlands, the Mediterranean and Australia, Stive¹⁵ showed that the net natural shoreline change due to cross shore processes is $\sim 1\text{m/yr}$, while the net natural shoreline change due to longshore processes is $\sim 0.1\text{-}1\text{m/yr}$. However, the Bruun Rule predicts a recession rate between 0.1 to 0.2m/yr for the current long term SLR rate of about 2mm/yr (using the *rule-of-thumb* approach). Thus, the Bruun effect (i.e. the coastal recession due to eustatic SLR alone) is, at best, an order of magnitude less than observed net natural shoreline changes. This means that the Bruun effect is likely to be overridden by other coastal processes under present still stand SLR conditions. Therefore, any good comparisons between shoreline recessions measured in the last century and corresponding Bruun Rule predictions is likely to be fortuitous and cannot be considered as conclusive verification of the Bruun Rule. However, it should be noted that the quantitative accuracy of the Bruun Rule has been validated for contemporary systems that have undergone a strong relative sea level rise due to subsidence (Mimura and Nobuoka¹⁶). Holocene coastal evolution modeling using the Bruun concept under considerable rates of sea level rise and fall also lends convincing support to the concept (Cowell et al.¹⁷, Storms¹⁸). It is also noteworthy that large- and small-scale laboratory tests of dune erosion under high storm surge levels (e.g. Steetzel¹⁹, Van Gent et al.²⁰) suggest a Bruun-type response at the much shorter time-scales of storm duration (hours-day).

Although, available evidence suggests that the Bruun Rule is most likely conceptually correct, arguably, it addresses only one potentially important effect of a range of effects. If no other sediment sources or sinks are present or if no other sediment transport gradients in cross-shore and longshore directions prevail, the Bruun effect is the only operational effect. However, this idealized situation is the exception rather than the rule, and there are other effects of SLR on the coastal sediment budget, which are generally much larger, or at least of the same order of magnitude as the Bruun effect. In the following section we present the available evidence pointing to the presence of mechanisms other than the Bruun effect, which may play an equal or more crucial role in governing coastline retreat/advance.

2. What is the Evidence?

A general point-of-view, triggered by Bird²¹, is that since 70% of the world's sandy beaches are in a state of erosion, global sea-level rise has to be the most probable cause (c.f. Leatherman et al.²²). However, there are numerous coastal systems that have been accretive in the Holocene, even though sea level was rising. A few examples are the Australian coast (Short²³), deltaic coasts (Mississippi, Ebro, Po, Yangtze, and many other deltas at earlier stages of the Holocene) and composite coasts such as the US Northwest Washington coast and the Dutch coast (Cowell et al.¹⁷). This implies that there must be a number of other processes that can override the Bruun effect, which is generally erosive, to such an extent that the resultant response is coastline advance. In contrast, many other coasts experience larger erosion than is explained by the Bruun effect. This implies that there must be coastal processes other than the Bruun effect that contribute to coastline retreat/advance. The important question then is, what are these other processes and are they likely to be affected by the accelerated sea-level rise that is likely to occur in the 21st century?

The other processes that may govern coastline retreat/advance may be collectively referred to as “sediment availability”, which is implicitly included in earlier first approximation kinematic models of long-term (millennia) coastal change (Curry²⁴). Swift²⁵ extended Curry's ideas into a general framework for long-term coastal change entailing *transgression* (landward retreat) and *regression* (seaward advance) of the shoreline due to sea-level rise and fall respectively, with corresponding tendencies toward *retrogradation* and *progradation* due to net sediment losses or gains from alongshore gradients in sediment transport.

Cowell et al.²⁶ show how Swift's concepts can be quantified and related back to the Bruun Rule, when upper shoreface sediment balance is considered. Cowell et al. assume that, to a first approximation, the upper shoreface is form invariant relative to mean sea level over time periods for which profile closure occurs ($\gg 1$ year) (Nicholls et al.²⁷). The upper shoreface is represented by an arbitrary, but usually concave-up, profile $h(x)$ to a depth h_* (a morphologically active depth) and a length L_* , in which x is the distance from the shore (Dean²⁸). Assuming that the cross-shore profile shape remains constant over time, sediment-volume conservation for profile kinematics requires (for a Cartesian coordinate system with seaward and upward directions positive) that

$$\frac{\partial h}{\partial t} + c_p \frac{\partial h}{\partial x} = 0 \quad (1)$$

where c_p is the horizontal profile displacement,

or via $h = MSL - z_b$, where MSL is Mean Sea Level and z_b is the bottom level:

$$\frac{\partial z_b}{\partial t} + c_p \frac{\partial z_b}{\partial x} = \frac{\partial MSL}{\partial t} \quad (2)$$

where c_p is the horizontal translation rate of the shoreline position. The sediment-transport balance equation for a fixed spatial control volume is

$$\frac{\partial z_b}{\partial t} + \frac{\partial q_x}{\partial x} + \frac{\partial q_y}{\partial y} + s = 0 \quad (3)$$

where $q_{x,y}$ are the cross-shore and alongshore sediment transports, and s is a local source or sink. These equations may be combined to yield

$$c_p = -\frac{\partial MSL}{\partial t} \left(\frac{\partial h}{\partial x} \right)^{-1} - \frac{\partial q_x}{\partial h} - \frac{\partial q_y}{\partial y} \left(\frac{\partial h}{\partial x} \right)^{-1} - s \left(\frac{\partial h}{\partial x} \right)^{-1} \quad (4)$$

or, after cross-shore integration over L_* ,

$$c_p H = -\frac{\partial MSL}{\partial t} L - (q_{x,sea} - q_{x,dune}) - \frac{\partial Q_y}{\partial y} - s \quad (5)$$

in which Q_y is the alongshore transport integrated over L_* .

In the absence of littoral transport gradients and other sources or sinks (including sand exchanges with the lower shoreface and backbarrier) the above reduces to the standard Bruun Rule^{4,13}:

$$c_p = -\frac{\partial MSL}{\partial t} \left(\frac{L}{H} \right) \quad (6)$$

Equation 5 is similar to the Dean and Maurmeyer's²⁹ generalized version of the Bruun Rule, an analytical precursor of the coastal-tract concept (see below).

The source and sink terms in equation 5 allow the qualitative Curray-Swift model of coastal evolution to be quantified as a time trajectory in sediment source/sink phase space: e.g., evolution of the well-documented central Netherlands coast between Hoek of Holland and Den Helder in Figure 1. The trajectory is derived by applying equation 5 and based on a) estimates derived from radiometric data by Beets et al.³⁰, for the period 5000 - 0 years BP; and b) the results of reconstruction simulations for 7200 - 5000 BP. The line separating advance and retreat of the coast is fitted for the trajectory in the top-right quadrant, with its mirror image assumed for the bottom-left quadrant in the absence of other data. The trajectory bifurcates after 2000 BP because differences

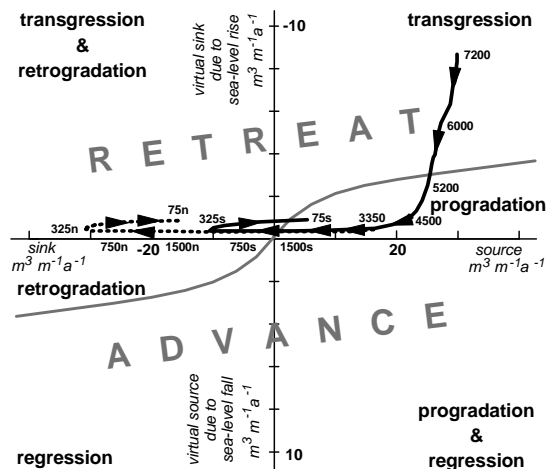


Fig. 1. Evolution of the central Netherlands coast (Hoek of Holland to Den Helder) as a time trajectory in sediment-supply/accommodation phase space (abscissa and ordinate respectively, scaled in cubic meters per year per meter of shoreline). Numbers along the trajectory indicate time (years BP); suffixes n and s denote north and south of Haarlem respectively (after Cowell et al.²⁶).

develop in rates of shoreline change averaged alongshore north and south of Haarlem. The shape of the advance/retreat-threshold curve demonstrates that coastal evolution is governed mainly by a) sediment supply (+/-) under near-still stand sea-level conditions (such as those predominating in the late Holocene), and b) change in accommodation space when sea-level changes rapidly (such as during global *glaciation* and *deglaciation*).

What do we learn from this evidence? In periods of near still stand sea-level conditions the Bruun effect is operational, but is commonly overridden by the sediment availability terms in equation 5. Therefore, an understanding of the relative magnitudes of these sediment availability mechanisms and the Bruun effect appears to be crucial in attempting to predict future coastline retreat/advance accurately. Sediment availability mainly consists of three potential contributions: a) cross-shore contributions, b) alongshore contributions, and c) other sources/sinks such as inlets and deltas. General quantifications of these three contributions are presented in the following three sections (section 3-5).

3. Cross-shore Processes

A general estimate of the contribution of cross-shore processes to coastline retreat/advance can be obtained by considering geological reconstructions and associated sediment balances.

Geological reconstructions of the Australian (Short²³) and the Dutch coast (Cowell et al.²⁶) have strengthened the hypothesis (Cowell et al.³¹) that middle shoreface wave-induced sediment transport is generally onshore on concave shaped shorefaces. This is associated with wave asymmetry and wave boundary layer induced net flow (Bowen³²). While this is a contribution that results in shoreline advance, there are also two contributions that result in shoreline retreat, which should be generally considered. One contribution is due to aeolian loss, i.e. wind-driven onshore transport of sediment that is lost from the active upper-shoreface profile and. The other is a virtual loss due to the Bruun effect. The Bruun Rule can quantify this virtual loss, theoretically. This latter loss due to the Bruun effect amounts to 500 to a 1000 times the SLR rate (in $\text{m}^3/\text{m}/\text{unit time}$), assuming an active depth of 10 m. Under recent near still stand SLR conditions of typically 20 cm/century (2mm/yr), the Bruun effect leads to a shoreline retreat of 0.1 to 0.2m/year, and an associated virtual loss of 1 to $2\text{m}^3/\text{m}/\text{year}$ (assuming an active profile slope h^*/L^* of 1/50-1/100 and an active profile height of 10m) The loss due to aeolian transport is often an order-of-magnitude larger (Cowell et al.²⁶). Therefore, on average, long-term cumulative losses due to sea-level rise and aeolian loss in cross-shore direction are 5 to $10\text{m}^3/\text{m}/\text{year}$. However, Australian and Dutch observations indicate net cross-shore gains of the order of 0.1 to $10\text{m}^3/\text{m}/\text{year}$ leading to coastline advance. Hence, onshore asymmetry- and boundary layer induced onshore transport on the middle shoreface should amount to 5 to $20\text{m}^3/\text{m}/\text{year}$.

In the absence of longshore sediment transport gradients one might therefore observe net chronic (i.e. long term) and extreme event driven ephemeral shoreline changes as indicated in Table 1. Chronic changes are due to long term processes such as the Bruun effect and Aeolian losses, while ephemeral changes are those that are associated with extreme storm events, which cause dune erosion. The ephemeral changes will be restored in the long term, if no upper shoreface losses due to alongshore transport gradients occur (List and Farris³³). The values given in table 1 are validated for the Dutch and Australian coasts, and are expected to be generally applicable for moderate (lower bound values) to high (higher bound values) energy coasts.

What can we conclude from these cross-shore process quantifications? Under present sea level rise conditions the Bruun effect is at least an order of magnitude

smaller than contributions from other processes and is therefore negligible. Obviously, if the rate of SLR increases 5 or 10 fold, then the losses due to the Bruun effect will be of the same order-of-magnitude as the gains due to chronic accretionary processes (e.g. wave asymmetry, boundary layer flow), which may even reverse the net shoreline change from advance to retreat.

Table 1. Typical cross-shore losses (-ve) and gains(+ve) and associated shoreline changes (-ve=retreat) ¹⁵	
Ephemeral processes ^A	O(-10 ²) m ³ /m/year or /extreme event
Chronic processes	O(+10 ¹) m ³ /m/year
Effective profile height	10 m
Rate of shoreline change due to chronic processes	O(+1) m/year
Rate of shoreline change due to ephemeral processes (extreme events or adverse years) ^A	O(-10) m/year or /extreme event
Rate of shoreline change due to Bruun effect only	O(-0.1) m/yr
^A the net ephemeral loss will be zero, as these losses will be recovered in time	

4. Longshore Processes

In this section we consider shoreline changes due to gradients in longshore sediment transport. Here, we distinguish low- and high-energy coasts in terms of wave energy, and assume wave-induced surf zone longshore flow to be the driving agent. This is a reasonable assumption along coasts that are not influenced or interrupted by coastal inlets and associated tidal basins or major engineering structures.

Tables 2 (low energy coasts) and 3 (high energy coasts) summarise typical longshore sediment transport rates (integrated cross-shore over the surf zone) associated with chronic (ambient transport gradients) and ephemeral (storms) processes, natural and human-induced length scale variations and associated longshore transport gradients, and resultant (net) shoreline changes. The length scale of natural variations, such as coastline curvature, is usually an order-of-magnitude larger than human-induced length scale variations (eg. harbor moles and shore protection structures).

Table 2, 3 and 4 indicate that cross-shore effects dominate coastline change along low-energy coasts, while along high-energy coasts cross-shore and longshore effects are comparable and are of equal importance where coastline change is concerned. In the case of human-induced changes, the effects of cross-shore and longshore processes are comparable on low-energy coasts, while on

high-energy coasts longshore effects are dominant. This may explain why cross-shore impacting structures, such as offshore breakwaters and perched beaches, perform better on low-energy coasts than on high-energy coasts. It is also clear that both on low- and high-energy coasts the Bruun effect is of similar or lower magnitude when compared to other effects. However, if the rate of SLR increased by 5 or 10 fold, increased erosion or decreased advance due to an enhanced Bruun effect will be noticeable.

Table 2. Typical longshore sediment transport rates (integrated across the surf zone) along low-energy coasts (e.g. the Mediterranean coast) and associated shoreline changes (-ve = retreat)¹⁵

Ephemeral processes	$O(10^5)$ m ³ /year or /extreme event
Chronic processes	$O(10^4)$ m ³ /year
Length scale of natural variations	10 km (long term scale)
Length scale of human-induced variations	1 - 10 km (medium-term scale)
Transport gradients due to natural variations	1 m ³ /m/year
Transport gradients due to human-induced variations	1 - 10 m ³ /m/year
Effective profile height	10 m
Rate of shoreline change due to natural processes	$O(+ \text{ or } - 0.1)$ m/year
Rate of shoreline change due to human-induced processes	$O(+ \text{ or } - 0.1 - 1)$ m/year
Rate of shoreline change due to Bruun effect only	$O(-0.1)$ m/yr

Table 3. Typical longshore sediment transport rates (integrated across the surf zone) along high-energy coasts (e.g. Holland coast, Eastern US coast) and associated shoreline changes (-ve = retreat)¹⁵

Ephemeral processes	$O(10^6)$ m ³ /year or /extreme event
Chronic processes	$O(10^5)$ m ³ /year
Length scale of natural variations	10 - 100 km (long term scale)
Length scale of human-induced variations	1 - 10 km (medium-term scale)
Transport gradients due to natural variations	1 - 10 m ³ /m/year
Transport gradients due to human-induced variations	10 - 100 m ³ /m/year
Effective profile height	10 m
Rate of shoreline change due to natural processes	$O(+ \text{ or } - 0.1 - 1)$ m/year
Rate of shoreline change due to human-induced processes	$O(+ \text{ or } - 1 - 10)$ m/year
Rate of shoreline change due to Bruun effect only	$O(-0.1)$ m/yr

5. Backbarrier Sources and Sinks

The effect of backbarrier sources and sinks are represented by the last term on the RHS in Equation 5. This term could play a significant role when the backbarrier consists of a river, estuary or tidal lagoon. In case of a river or an estuary there may be a natural supply of sediment to the coastal system that can compensate for all cross-shore and longshore losses mentioned above in sections 3 and 4. In this case, a delta will form and evolve with time. The delta evolutionary characteristics will depend on the relative role of waves, tides and river flow. In the Holocene, many deltas have been outbuilding as a result of abundant sediment supply due to erosion of the catchment basin. Over the last 5 decades many deltas have started to disintegrate due to human intervention in the form of dam regulated river discharge, which decimates downstream sediment supply.

In case of a tidal lagoon or an estuary with low fresh water inputs, the backbarrier tidal basin area may act as a source or a sink for the coastal sediment budget. Classic examples of sink behavior are the Frisian Wadden basins along the Dutch and West German North Sea coast. Dronkers³⁴ analyzed the net sediment transport behavior of these basins and showed that these basins are generally flood dominant, i.e. there is a tendency to accumulate sediment within the basin as sea level rises, restoring dynamic equilibrium geometry. Stive and Wang³⁵ further analyzed this response and showed that, in this case, the Bruun Rule can be extended as follows to express the impact of sea-level rise on inlet-influenced coasts:

$$c_p = \frac{\partial MSL}{\partial t} \frac{L_*}{h_*} + \frac{\partial MSL}{\partial t} \frac{A_b}{h_* L_{ac}} \quad (7)$$

where A_b is the tidal basin area and L_{ac} is the length of the adjacent coast impacted.

In the above equation the first term on the right-hand side expresses the Bruun effect and the second term expresses the basin accommodation effect. The Bruun effect is exceeded by the basin effect when:

$$A_b > L_* L_{ac} \quad (8)$$

Typical orders of magnitude for L_* and L_{ac} are 1 km and 10 km respectively, meaning that the direct impact of basin areas larger than $O(10 \text{ km}^2)$ on coastline retreat overrides the Bruun effect.

Friedrichs and Aubrey³⁶ presented a similar analysis for a large number of schematized tidal basins in eastern USA. They showed that depending on basin hypsometry, tidal basins could be either flood- or ebb-dominant. This implies that sea-level rise may lead to both importing and exporting basins. Figure 3 of Zhang et al.¹⁴ indicates that long stretches of coastline, which they denote as

inlet-influenced, experience stronger recession rates than the non inlet-influenced stretches of coastline where the Bruun Rule was used. This gives rise to the hypothesis that backbarrier basins along that coastline are flood-dominant. However, when the basins are ebb-dominant, sea-level rise may cause an export of sediment. This will decrease or even compensate for the Bruun effect to such an extent that shoreline advance may occur.

If sea-level rise forces positive accommodation in flood-dominant basins, surf zone generated sediment transport will be diverted into the tidal basin by flood-currents. These sediments will be trapped in the flood delta. Typical barrier length scales are $O(10\text{km})$. Therefore, typical values for shoreline changes in the vicinity of backbarrier sinks can be estimated as shown in Table 4.

Ephemeral processes	$O(10^6)$ m ³ /year or /extreme event
Chronic processes	$O(0.5*10^6)$ m ³ /year
Length scale of natural variations	10 km (long term scale)
Length scale of human-induced variations	1 - 10 km (medium-term scale)
Transport gradients due to natural variations	50 m ³ /m/year
Transport gradients due to human-induced variations	50 - 500 m ³ /m/year
Effective profile height	10 m
Rate of shoreline change due to natural processes	$O(-5)$ m/year
Rate of shoreline change due to human-induced processes	$O(-5 - 50)$ m/year
Rate of shoreline change due to Bruun effect only	$O(-0.1)$ m/yr

Table 4 indicates that along inlet interrupted coastlines the tidal basins linked to the inlets have a considerable influence on coastline change. Interestingly, the magnitude of tidal basin influenced coastline change (as indicated above) is significantly larger than the coastline changes estimated by Zhang et al.¹⁴ along their non inlet-influenced coastline (cf. Figure 3 of Zhang et al.¹⁴).

In essence, therefore, while the underlying concepts of the Bruun Rule have been verified, its quantitative accuracy remains unverified; largely due to the presence of other coastal processes that easily override the Bruun effect under present still stand SLR conditions. Furthermore, the numerous restrictive assumptions associated with the Bruun Rule preclude its application in most natural environments, and especially in the vicinity of inlets linked to tidal basins larger than 10km^2 . However, what is needed now, in view of the massive socio-

economic impacts along the world's highly developed coastal margins that are likely to result from accelerated SLR, is a robust and widely applicable method that can be confidently applied to obtain accurate predictions of coastline retreat due to SLR. From the above discussion, it is apparent that the Bruun Rule is of limited use in this context. Therefore, alternative methods to address this critical issue must now be considered. In this regard, a promising alternative philosophy is the "Coastal Tract" concept presented by Cowell et al.^{26, 37}.

6. An Innovative Approach: the Coastal Tract

The Coastal tract approach introduces the concept of a meta-morphology, defined as the morphological composite comprising the lower shoreface, upper shoreface and backbarrier (where present). It is the first order-system within a cascade hierarchy that provides a framework for aggregation of processes in modeling the evolution of coastal morphology over decades to millennia (low-order coastal change). This type of coastal change involves parts of the coast normally ignored in predictions required for management of coastal morphology: i.e., shoreline evolution linked to behavior of the continental shelf and coastal plain. The Coastal tract approach adopts a temporally and spatially cascading framework, where appropriate boundary conditions and internal dynamics are defined to separate low-order from higher-order coastal behavior for site-specific applications. This procedure involves preparation of a data-model by templating site data into a structure that complies with scale-specific properties of any given predictive models.

Each level of the *coastal-tract cascade* is a self-contained system that shares sediments with other levels. This sediment sharing constrains morphological responses of the system on given temporal and spatial scales. The internal dynamics of these responses involve morphological coupling of the upper shoreface to the backbarrier and to the lower shoreface. The coupling mechanisms govern systematic lateral displacements of the shoreface, and therefore determine trends in shoreline advance and retreat. These changes manifest as the most fundamental modes of coastal evolution upon which higher-order (shorter-term, i.e. sub decadal scale) changes are superimposed.

Prediction of shoreline change adopts different approaches, depending on the space and time scale over which predictions are required. For short-term (sub-decadal) coastal change (event and synoptic-scale changes occurring over hours through seasons to years), the focus is generally on the local sediment dynamics. These affect the shoreline plan form and the cross-shore profile (e.g., shoreline and profile models) in response to fluctuations in environmental conditions (i.e.,

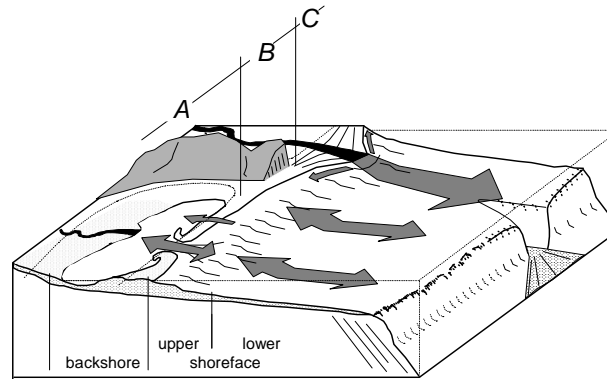


Fig. 2. Physical morphology encompassed by the coastal tract (after Cowell et al.³⁷; see text for explanation).

the wave climate, littoral sediment budgets, sea level and the effects of anthropogenic activities). Theoretical and empirical approaches to these sub-decadal time scales generally focus on changes to the upper shoreface (defined loosely as the *active zone*; cf. Stive and De Vriend³⁸), which correlate with shoreline movements. These changes are moderated by littoral sediment budgets and by sediment ‘production’ via shoreline erosion cutting into onshore sand reserves (e.g. eroding dunes or cliffs), or through artificial nourishment of beaches.

The practical imperative for long-term prediction (decades or longer) requires an expanded scope as included in the coastal tract concept that includes the lower shoreface and the interaction between the shoreface and backshore environments (Fig. 2). The upper shoreface has cross-shore length scales that are typically two to three orders of magnitude less than for the lower shoreface (depicted in Fig. 2). This scale difference means that changes on the lower shoreface are associated with disproportionately larger changes on the upper shoreface, due to mass continuity for sediment exchanges between the two zones (Roy et al.³⁹; Cowell et al.⁴⁰). The upper shoreface is subject to a similar interaction with the backshore, which comprises a morphologically active zone located between the upper shoreface (ocean beach) and the mainland. This zone may variously include dunes, wash over surfaces, flood-tide deltas, lagoon basins, tidal flats (Fig. 2A), mainland beaches (Fig. 2B) and fluvial deltas (Fig. 2C). Each of these may be present or absent, depending on local conditions, especially the regional substrate slope (Cowell et al.¹⁷).

The sediment exchanges depicted by the arrows in Figure 2 occur in principle during any average year and on all longer time scales. These exchanges are

summarised schematically in Figure 3, which differentiates sediment fluxes into sand and mud fractions. For coastal change on any scale, antecedent morphology, sea-level change, fluvial discharges and littoral sediment budgets can be regarded as boundary conditions for the coastal area of interest.

For sub-decadal prediction of horizontal movements in the upper shoreface, sand exchanges with the lower shoreface (Fig. 3B) are usually ignored because these fluxes are so small that resulting morphological change is negligible: i.e. the annual closure-depth concept (Hallermeier⁴¹; Nicholls et al.²⁷). The fluxes of fine sediments (Fig. 3, C and D) are not directly relevant to the upper-shoreface sediment budget because mud deposition there is negligible. For long-term predictions, like on the scale of climate change, however, none of the internal sediment exchanges depicted in Figure 3 can be ignored. This is because systematic residual fluxes, that are small on the sub-decadal time scale, eventually cumulate through time enough to produce non-negligible (i.e., measurable) morphological changes. Moreover, the changes in morphology of the backbarrier, lower shoreface and upper shoreface cause these three zones to interact dynamically: i.e., the sediment exchanges themselves become influenced by the morphological changes.

7. Conclusions

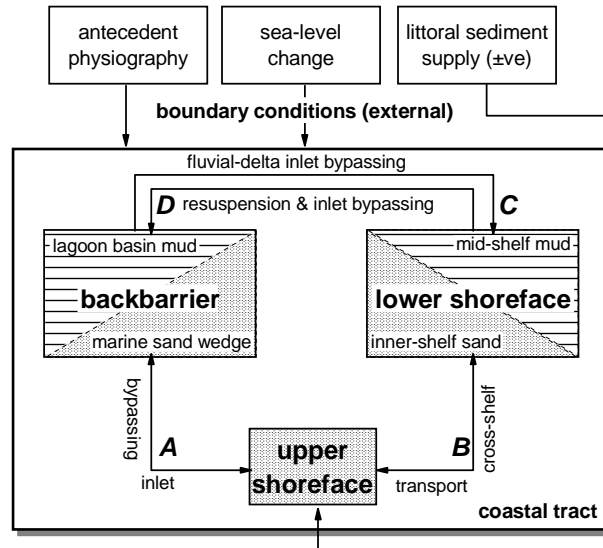


Fig. 3. Schematic representation of mechanisms steering the location of the upper shoreface (after Cowell et al.³⁷).

The characteristics of coastline response to SLR suggested by the Bruun Rule seem conceptually correct. However, under present near still-stand sea level rise conditions, the Bruun effect can easily be sub-ordinate to a host of other processes. Therefore, any good comparisons between shoreline recessions measured in the last century under near still stand SLR and corresponding Bruun Rule predictions is likely to be fortuitous and cannot be considered as conclusive verification of the Bruun Rule. Furthermore, due to the many restrictive assumptions associated with the Bruun Rule, it is not applicable in most natural environments, as exemplified by Zhang et al.¹⁴'s exclusion of almost 70% of the study area from their analysis. The applicability of the Bruun Rule is particularly compromised in the vicinity of tidal basins associated with inlets as the Bruun effect can be overridden by the response of the tidal basin when the basin area is larger than 10 km² (Stive¹⁵).

Clearly the Bruun Rule is not suitable to obtain exact and site-specific predictions of coastal recession due to SLR, particularly in view of the accelerated SLR projected for the 21st century. At best, any predictions obtained via the Bruun Rule should be considered only as broadly indicative, order-of-magnitude estimates that are not suitable for direct use in making planning decisions. The only robust solution to the problem lies in comprehensive bottom-up (small-scale, process-based) and top-down (large-scale, behavior-based)

numerical modeling that adopts the coastal tract philosophy as a conceptual template. Once comprehensively validated by field data, such numerical models can be strategically applied to determine quantitative forcing-response relationships of complex, non-linear coastal processes. These relationships can then be aggregated and/or parameterized and embedded into a robust and easy-to-use numerical model, which accounts for at least the primary physical processes governing coastline response to SLR. Such a process-based approach would constitute a significant step forward from the Bruun Rule and is likely to provide more scientifically robust and reliable predictions of coastline retreat due to future sea level rise.

In closure we note that here we have only discussed the impact of a change of the rate of SLR on coastline evolution and not the impacts associated with other climate change driven impacts such changes in regional hurricane or typhoon climates, changes in dominant wave direction, storm frequency and intensity (Ranasinghe et al.⁴²), and ENSO, NAO and SOI oscillations (cf. the Chapter by Komar et al., Ranasinghe et al.⁴³), which may have local and/or regional impacts as important as or even exceeding the impact due to SLR alone.

Acknowledgments

MJFS was supported by the project ‘Sustainable development of North sea and Coast’ (DC-05.20) of the Delft Cluster research project dealing with sustainable use and development of low-lying deltaic areas in general and the translation of specialist knowledge to end users in particular.

References

1. IPCC, Contribution of Working Group I to the Fourth Assessment Report of the Intergovernmental Panel on Climate Change. Summary for Policymakers. 18 pp (2007)
2. S. Rahmstorf, A. Cazanave, J. Church, J. Hansen, R. Keeling, D. Parker, R. Somerville, *Science*, 316, 709 (2007).
3. S. Rahmstorf, *Science*, 315, 368 (2007)
4. P. Bruun,. Sea-level rise as a cause of shore erosion. *Journal of Waterways Harbors Division*, American Society of Civil Engineers, 88, 117-130 (1962)
5. L. Hamm, M. Capobianco, H.H. Dette, A. Lechuga, R. Spanhoff, and M.J.F. Stive. Soft engineering intervention: A view on shore nourishment. *Coastal Engineering* (2002)
6. O.H. Pilkey, and J.A.G. Cooper, Society and sea level rise. *Science*, 303, 1781-1782 (2004)
7. J.A.G. Cooper and O.H. Pilkey, Sea level rise and shoreline retreat: time to abandon the Bruun Rule. *Global and Planetary Change*, 43, 157-171 (2004)
8. P.A. Rosen, A Regional Test of the Bruun Rule on Shoreline Erosion. *Marine Geology*, 26, M7-M16 (1978)

9. E.B. Hands, The Great Lakes as a Test Model for Profile Responses to Sea Level Changes. In: Komar, P.D., (ed.) *Handbook of Coastal Processes and Erosion Boca Raton*. CRC Press, 176-189 (1983)
10. C.H. Everts, Sea Level Rise Effects on shoreline position. *Journal of Waterway, Port, Coastal and Ocean Engineering*, 111(6), 985-999 (1985)
11. O.H. Pilkey. and T.W. Davis, An analysis of coastal recession models: North Carolina coast. In: Nummedal, D., Pilkey, O.H., Howard, J.D., (eds), Sea-level Fluctuation and Coastal Evolution: SEPM (Society for Sedimentary Geology) Special Publication No. 41, Tulsa, Oklahoma, p. 59-68 (1987)
12. R.G. Dean, Beach Response to Sea Level Change. In Vol. 9 of *The Sea*. Wiley, 869-887 (1990)
13. SCOR Working Group 89, *J. Coastal Research*, 7(3), 895 (1991).
14. K. Zhang, B. C. Douglas, S. P. Leatherman, *Climatic Change*, 64, 41 (2004).
15. M. J. F. Stive, *Climatic Change, Editorial Comment*, 64, 27 (2004).
16. N. Mimura and H. Nobuoka, Verification of Bruun Rule for the estimate of shoreline retreat caused by sea-level rise. In Dally, W.R. and Zeidler, R.B. (eds.), *Coastal Dynamics 95*. American Society of Civil Engineers, New York, 607 – 616 (1995).
17. P.J. Cowell, P.S. Roy and R.A. Jones, Simulation of LSCB using a Morphological Behaviour Model. *Marine Geology*, 126, 45-61 (1995).
18. J.E.A. Storms, Event-based stratigraphic simulation of wave-dominated shallow-marine environments. *Marine geology*, 199(3-4), 83-100 (2003).
19. H.J. Steetzel, Cross-shore transport during storm surges, *PhD thesis* Delft University of Technology (1993).
20. M.R.A. van Gent, E.M. Coeveld, D.J. Walstra, J. van de Graaff, H.J. Steetzel, M. Boers. Dune erosion tests to study the influence of wave periods on dune erosion, *Proceedings International Conference on Coastal Engineering*, ASCE, San Diego (2006).
21. E.C.F. Bird, *Coastline Changes*. Wiley & Sons, New York, p.219 (1985).
22. S.P. Leatherman, K. Zhang and B.C. Douglas, Sea level rise shown to drive coastal erosion, *EOS Transactions*, 81 (6), 55-57 (2000).
23. A.W. Short, A survey of Australian beaches. Keynote Lecture, *Coastal Sediments 2003*, Clearwater, Florida (2003).
24. J.R. Curray. Transgressions and regressions. In: Miller, R.C. (ed.), *Papers in Marine Geology*, New York: McMillan, 175-203(1964).
25. D.J.P. Swift,. Continental shelf sedimentation. In: Stanley, D.J. and Swift, D.J.P., (eds.) *Marine Sediment Transport and Environmental Management*, New York: Wiley, 311-350 (1976).
26. P.J. Cowell, M.J.F. Stive, A.W. Niedoroda, D.J.P. Swift, H.J. de Vriend, M.C. Buijsman, R.J. Nicholls, P.S. Roy, G.M. Kaminsky, J. Cleveringa, C.W. Reed, and P.L. De Boer. The Coastal-Tract (Part 2): Applications of aggregated modelling to lower-order coastal change. *Journal of Coastal Research*, 19 (4), 828-848 (2003).
27. R.J. Nicholls, W.A. Birkemeier, and G-H. LEE.. Evaluation of depth of closure using data from Duck, NC, USA. *Marine Geology*, 148, 179-201 (1998).
28. R.G. Dean. Equilibrium beach profiles: characteristics and applications. *Journal of Coastal Research*, 7, 53-84 (1991).

29. R.G. Dean and E.M. Maurmeyer. Models of beach profile response. In: Komar, P. and Moore, J. (eds), *CRC Handbook of Coastal Processes and Erosion*, Boca Raton, CRC Press, 151-165 (1983).
30. D.J. Beets, L. van der Valk and M.J.F. Stive. Holocene evolution of the coast of Holland. *Marine Geology*, 103, 423-443 (1992).
31. P.J. Cowell, M.J.F. Stive, P.S. Roy, G.M. Kaminsky, M.C. Buijsman, B.G. Thom and L.D. Wright. Shoreface Sand Supply to Beaches. *Proc. 27th International Conference on Coastal Engineering*, American Society of Civil Engineers, 2495-2508 (2001).
32. A.J. Bowen. Simple models of nearshore sedimentation, beach profiles and longshore bars. In: McCann, S.B. (ed.), *The Coastline of Canada*, Geological Survey of Canada Paper, 80-10, 1-11 (1980).
33. J.H. List and A.S. Farris. Large-scale shoreline response to storms and fair weather. *Proc. Coastal Sediments '99*, ASCE, Reston, VA, pp. 1324-1338 (1999).
34. J. Dronkers. Morphodynamics of the Dutch Delta. In: J. Dronkers and M. Scheffers (eds.), *Physics of estuaries and coastal seas*, Balkema, Rotterdam, pp 297-304 (1998).
35. M.J.F. Stive and Z.B. Wang. Morphodynamic modeling of tidal basins and coastal inlets. In: *Advances in coastal modeling*, Ed: C. Lakhan, Elsevier, Chapter 13, 367-392 (2003).
36. C.T. Friedrichs and D.G. Aubrey. Non-linear tidal distortion in shallow well-mixed estuaries: a synthesis. *Estuarine, Coastal and Shelf Science*, 27, 521-545 (1988).
37. P.J. Cowell; M.J.F. Stive, A.W. Niedoroda, H.J. De Vriend, D.J.P. Swift, G.M. Kaminsky and M. Capobianco. The Coastal-Tract (Part 1): A conceptual approach to aggregated modelling of low-order coastal change. *Journal of Coastal Research*, 19 (4), 812-827 (2003).
38. M.J.F. Stive and H.J. De Vriend. Modelling shoreface profile evolution. *Marine Geology*, 126, 235-248 (1995).
39. P.S. Roy, P.J. Cowell, M.A. Ferland and B.G. Thom. Wave dominated coasts. In: Carter, R.W.G. & Woodroffe, C.D. (eds), *Coastal Evolution: Late Quaternary shoreline morphodynamics*, Cambridge Univ Press, Cambridge, 121-86 (1994).
40. P.J. Cowell, D.J. Hanslow and J.F. Meleo. The Shoreface. In: SHORT, A.D. (ed.), *Handbook of Beach and Shoreface Morphodynamics*. Chichester: Wiley, 37-71 (1999).
41. R.J. Hallermeier. A profile zonation for seasonal sand beaches from wave climate, *Coastal Engineering*, 4, pp. 253-277 (1981).
42. R. Ranasinghe, D. Lord, D. Hanslow, and K. McInnes.. Climate Change impacts on NSW coasts and estuaries. *Proceedings of Coasts and Ports '07, Melbourne, VIC, Australia. CD ROM Published by Engineers Australia* (2007).
43. R. Ranasinghe, R. McLoughlin, A. Short and G. Symonds. The Southern Oscillation Index, Wave Climate, and Beach Rotation. *Marine Geology*, Vol. 204, 273-287 (2004).



August 31 – September 05

Short Course on Morphodynamics

- **Hanz D. Niemeyer**



Current Position:

**Director of Coastal Research Station, Norderney,
Lower Saxony Water Management, Coastal Defence and Nature Conservation Agency**

Education Background:

1. Graduated at Hanover Technical University in Civil Engineering (1975)
2. Research Engineer at the Franzius Institute for Hydraulic and Coastal Engineering, Hanover University (1975)
3. Visiting researcher at the Coastal and Hydraulics Laboratory of the Corps of Engineers and at the Institute for Hydraulic Engineering of the Polish Academy of Science.

Email: hanz-dieter.niemeyer@nlwkn-ny.niedersachsen

Professional Career :

1. Group leader for Hydrodynamics at Coastal Research Station (CRS) (1976)
2. Section Head for Hydrodynamics and Coastal Engineering at CRS (1984)
3. Director of Coastal Research Station (2003)

Position in Professional Association:

1. External advisor for Rijkswaterstaat with respect to design of coastal structures with special emphasis on design waves
2. Lecturer at Kiel University for Coastal Processes and Coastal Protection in the International Master Course on Coastal Geosciences and Engineering

Publications:

1. Über den Seegang an einer inselgeschützten Wattküste. BMFT-Forschungsbericht MF 0203 (Waves at an Island-sheltered Wadden Sea Coast). (in German), 1983.
2. Jan van de Graaff, HDN & Jan van Overeem: Beach Nourishment, Philosophy and Coastal Protection Policy. *in:* J. v. d. Graaff, H. D. Niemeyer, J. v. Overeem (eds.): Special Issue Artificial Beach Nourishments. *Coast. Engg.*, Vol. 16, No. 1, 1991.
3. Long-Term Morphodynamical Development of the East Frisian Islands and Coast. *In:* B. L. Edge (ed.): Proc. 24th Int. Conf. Coast. Engg. Kobe/Japan, Am. Soc. Civ. Engs., New York, 1994.
4. Müller, J.-M., Zitman, T., Stive, M.J.F., Niemeyer, H.D.: Long-Term Morphological Evolution of the Tidal Inlet "Norderneyer Seegat". *In:* J. McKee Smith (ed.) Proc. 30th Int. Conf. Coast. Engg. San Diego, Ca./USA. World Scientific, New Jersey/London/Singapur, 2006.
5. A. Herman, R. Kaiser, H.D. Niemeyer: Medium-term Wave and Current Modelling for a Mesotidal Wadden Sea Coast. *In:* J. McKee Smith (ed.) Proc. 30th Int. Conf. Coast. Engg. San Diego, Ca./USA. World Scientific, New Jersey/London/Singapur, 2006.

Lower Saxony Water Management, Coastal Defence and Nature Conservation Agency

Field Measurements and Morphodynamical Modeling of Tidal Inlets and Basins

Hanz Dieter Niemeyer
Coastal Research Station
 Lower Saxony Water Management, Coastal Defence and Nature Conservation Agency

Coastal Research Station

Lower Saxony Water Management, Coastal Defence and Nature Conservation Agency

CONTENTS

1. Introduction
2. Morphodynamical response to accelerated sea-level rise
 - 2.1 Motivation
 - 2.2 Conceptual long-term modeling
 - 2.2.1 Database
 - 2.2.2 ASMITA-model and approach
 - 2.2.3 Results
 - 2.3 Process-based modeling
 - 2.3.1 Tool and set-up
 - 2.3.2 Boundary conditions
 - 2.3.3 Results
- 2.4 Conclusions

Coastal Research Station

Lower Saxony Water Management, Coastal Defence and Nature Conservation Agency

CONTENTS

3. Field measurements, model validation and improvements
 - 3.1 Accuracy of data
 - 3.2 Validation procedures,
 - 3.3.1 Aggregated Parametrization
 - 3.3.2 Model improvements by consideration of field measurements
 - 3.3 Conclusions
4. Final remarks

Coastal Research Station

Lower Saxony Water Management, Coastal Defence and Nature Conservation Agency

WADDEN SEA – NORDERNEY INLET AND BASIN

Coastal Research Station

Lower Saxony Water Management, Coastal Defence and Nature Conservation Agency

EFFECTS OF CLIMATE CHANGE AT A WADDEN SEA COAST

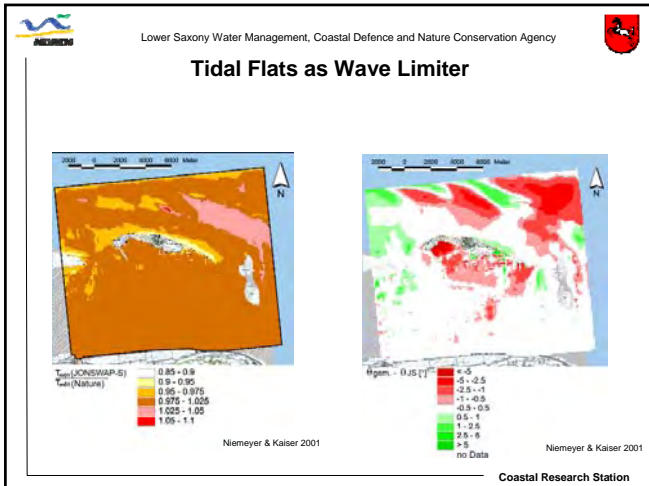
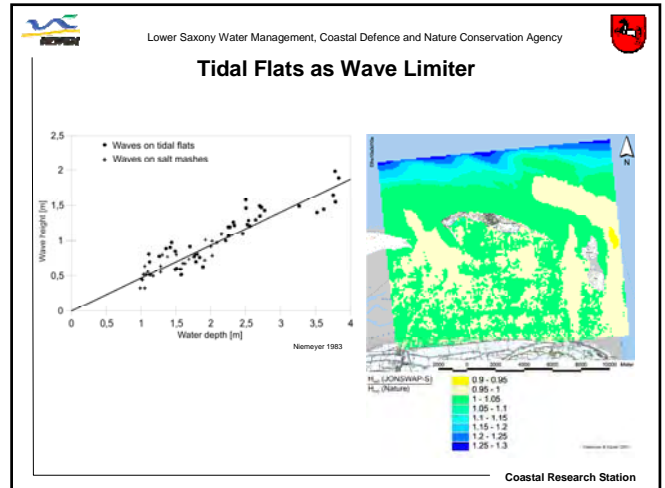
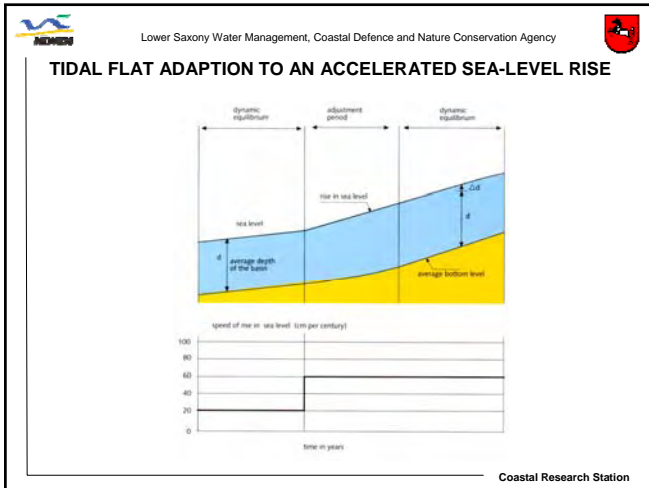
Coastal Research Station

Lower Saxony Water Management, Coastal Defence and Nature Conservation Agency

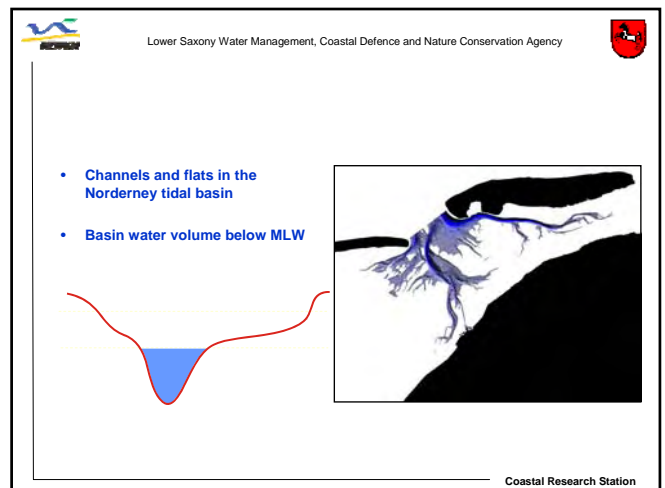
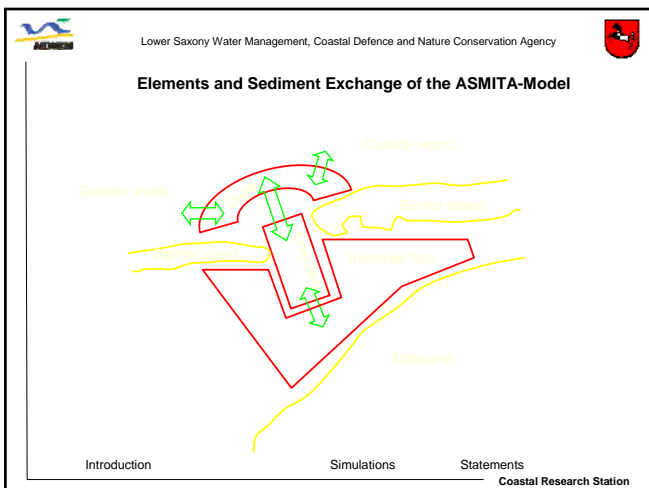
SEA-LEVEL RISE AND COASTLINE ADAPTION

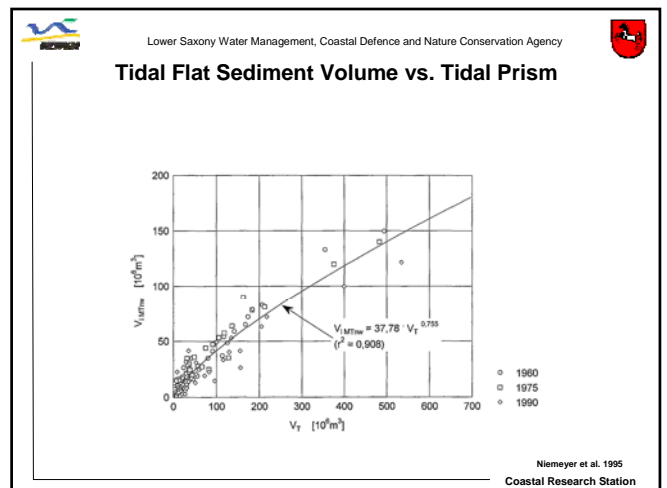
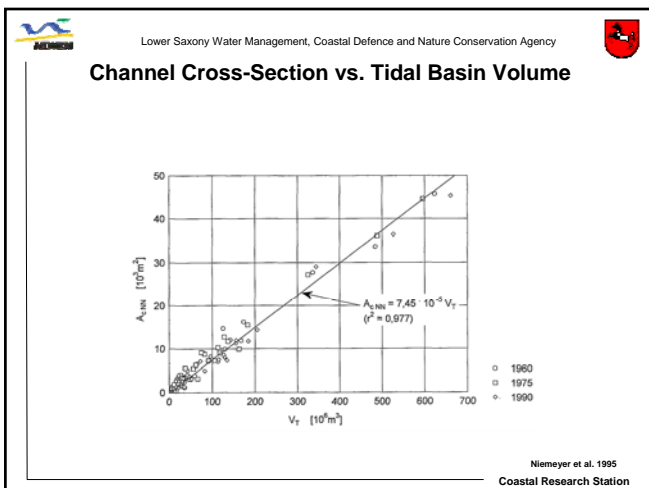
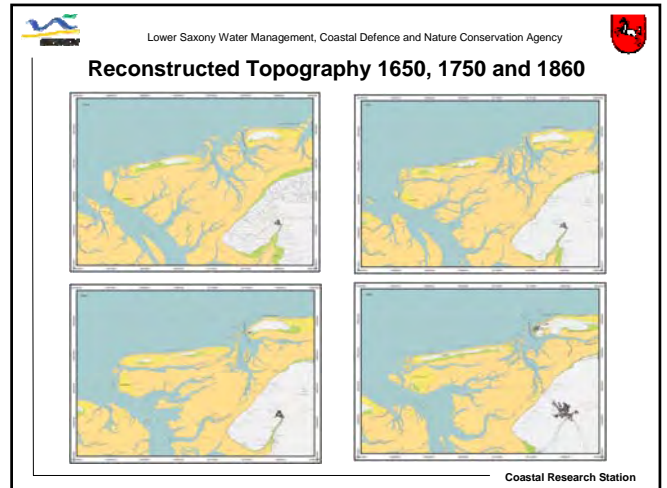
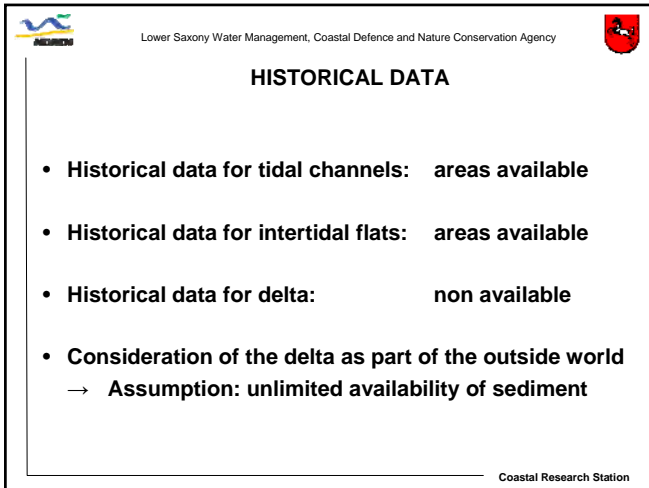
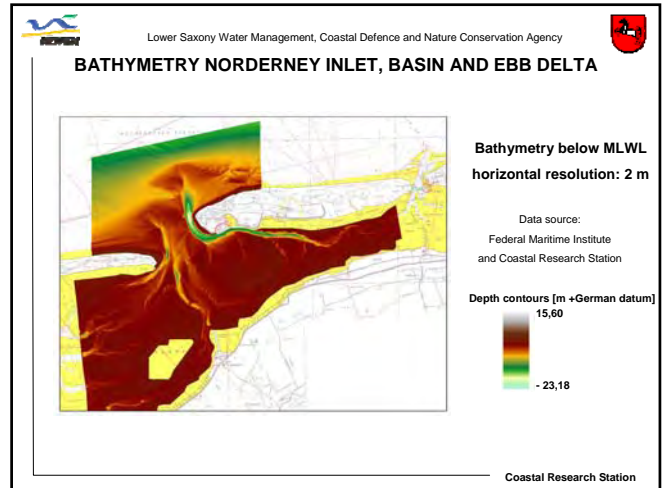
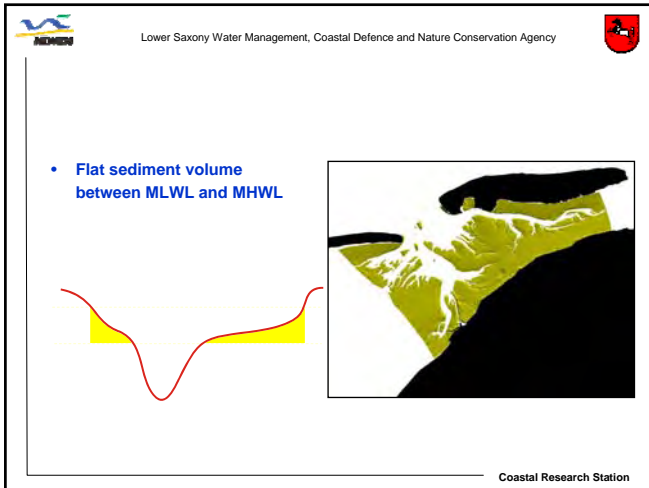
Veenstra 1973

Coastal Research Station



- Lower Saxony Water Management, Coastal Defence and Nature Conservation Agency
- ### APPROACH
- Available: data of the tidal basin + ASMITA model
 - Calibration of the ASMITA-model for detailed data sets from 1960, 1975, 1990
 - Use of these data sets for the determination of empirical relationships for incorporation of historical 2D-data sets
 - Application of ASMITA for historical situations
 - Applying ASMITA for long-term evolution of tidal channels and flats due to distinct rates of sea-level rise
- Coastal Research Station





Lower Saxony Water Management, Coastal Defence and Nature Conservation Agency

Empirical Model Parameters

- For each element a morphodynamical equilibrium exists and is defined by
→ empirical equilibrium relations
- Specific character of areas is represented by empirical parameters

Norderney inlet and basin:

- Flat sediment volume $V_S = \alpha_f \cdot A_b \cdot TR$ $\alpha_f = 2,8 \cdot 10^{-4}$
- Basin water volume $V_B = \alpha_c \cdot P^a$ $\alpha_c = 0,375$
 $a = 1,37$

Coastal Research Station

Lower Saxony Water Management, Coastal Defence and Nature Conservation Agency

TIDAL ASYMETRY

- $T_{flood} = 6:04$
- $T_{ebb} = 6:21$
- $T_{flood} < T_{ebb}$ ($\Delta = 17 \text{ min}$)

→ slightly flood dominant

Coastal Research Station

Lower Saxony Water Management, Coastal Defence and Nature Conservation Agency

AIMS

- Prediction of long-term evolution of tidal inlet and basin for distinct sea level rise scenarios
- Check on capability of the tidal system to adapt to changing boundary conditions
- Long-term evolution for distinct rates of sea-level rise
- Evaluation of a critical rate of sea-level rise for drowning of flats

Coastal Research Station

Lower Saxony Water Management, Coastal Defence and Nature Conservation Agency

MODEL VERIFICATION AND APPLICATION (Sea-level Rise 1,5 mm/year)

Coastal Research Station

Lower Saxony Water Management, Coastal Defence and Nature Conservation Agency

TIDAL CHANNEL RESPONSE ON SEA-LEVEL RISE RATES

MÜLLER et al. 2007

Coastal Research Station

Lower Saxony Water Management, Coastal Defence and Nature Conservation Agency

TIDAL FLAT RESPONSE ON SEA-LEVEL RISE RATES

MÜLLER et al. 2007

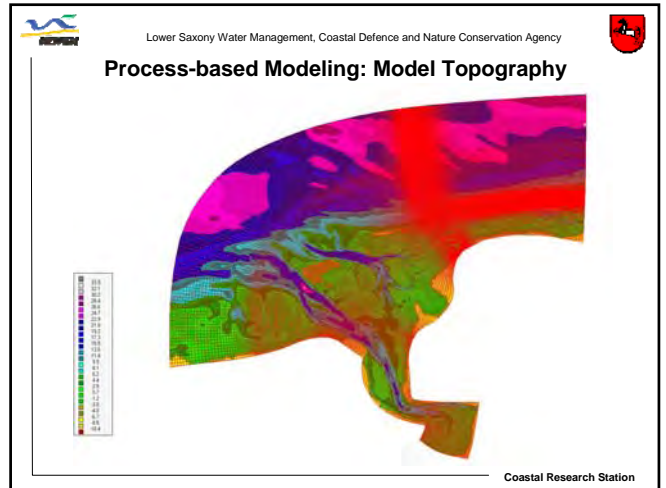
Coastal Research Station

Lower Saxony Water Management, Coastal Defence and Nature Conservation Agency

CONCLUSIONS

- Reconstruction of long-term processes of tidal channels and flats are achievable with conceptual models like ASMITA
- ASMITA delivers valuable insights into the morphodynamical response of tidal channels and flats for distinct rates of sea-level rise
- A sea-level rise of about 10 mm/year might provoke a drowning of the tidal flats in the Wadden Sea

Coastal Research Station

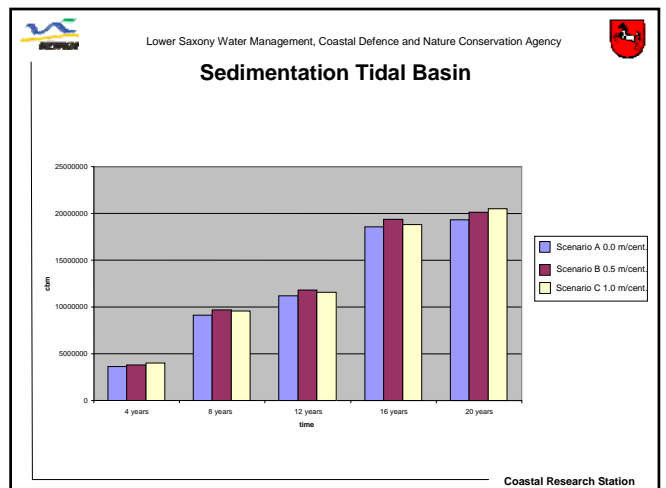
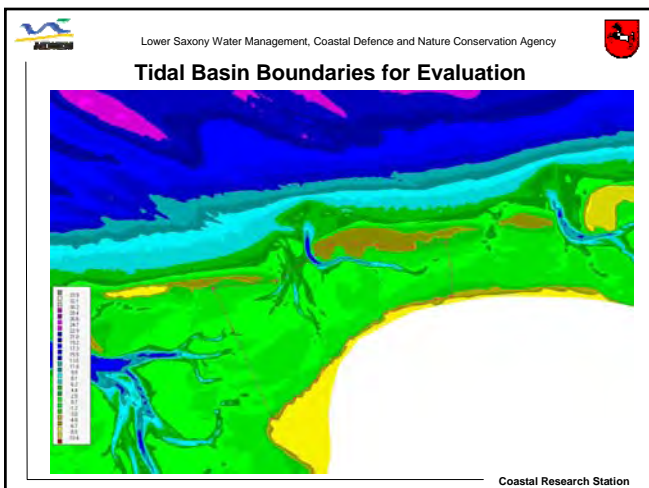
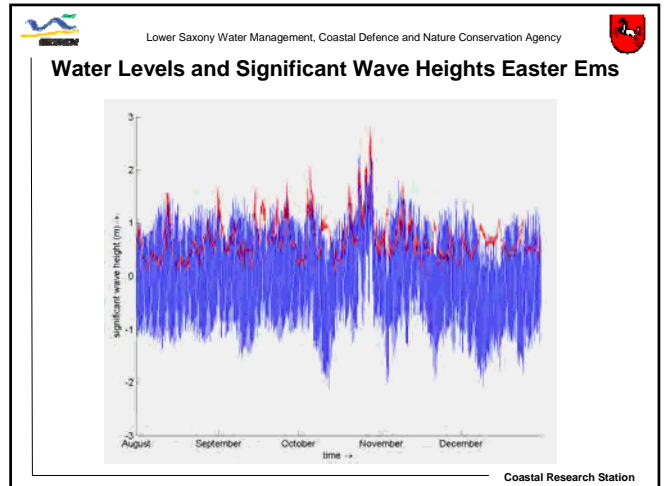


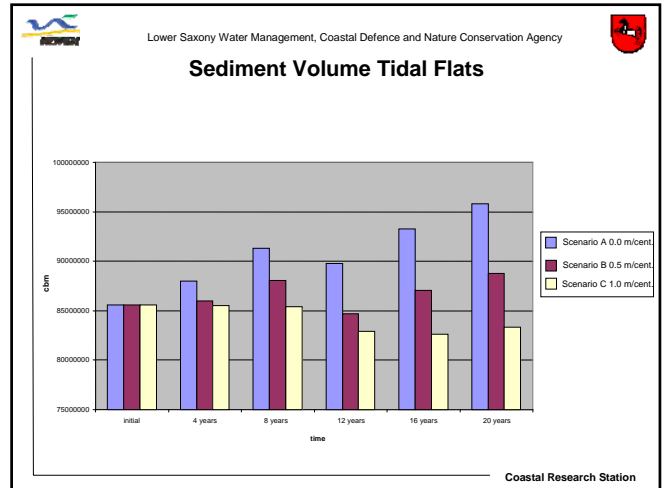
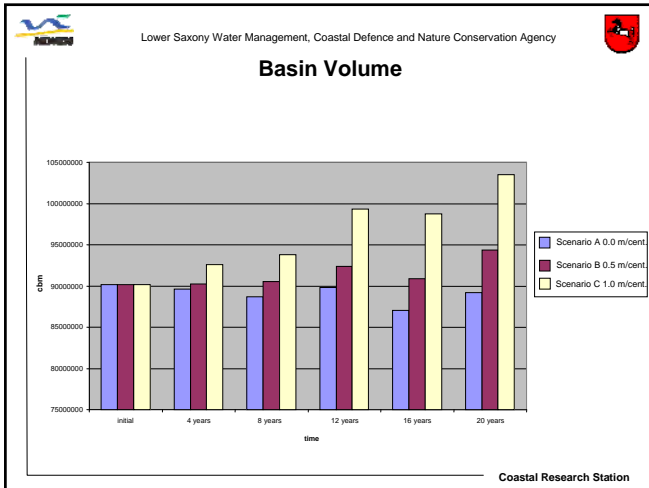
Lower Saxony Water Management, Coastal Defence and Nature Conservation Agency

Process-based Modeling: Boundary Conditions

- Water levels, currents waves for 5 months
- Morphological factor: 50 → ~ 20 years
- Constant tidal range
- Uniform sediment diameter: 0,3 mm
- Three sea-level scenarios
 - a. 0,0 m/century
 - b. 0,5 m/century → rise: ~ 12 cm
 - c. 1,0 m/century → rise: ~ 24 cm

Coastal Research Station





Lower Saxony Water Management, Coastal Defence and Nature Conservation Agency

CONCLUSIONS-1

- Simplified process-based modeling produces reliable results; trends are similar to those from long-term conceptual modeling
- A sea-level rise of about 1 m/century is critical with respect to drowning of the tidal flats in the Wadden Sea
- For deeper insights more sophisticated modeling approach is necessary → success is highly probable

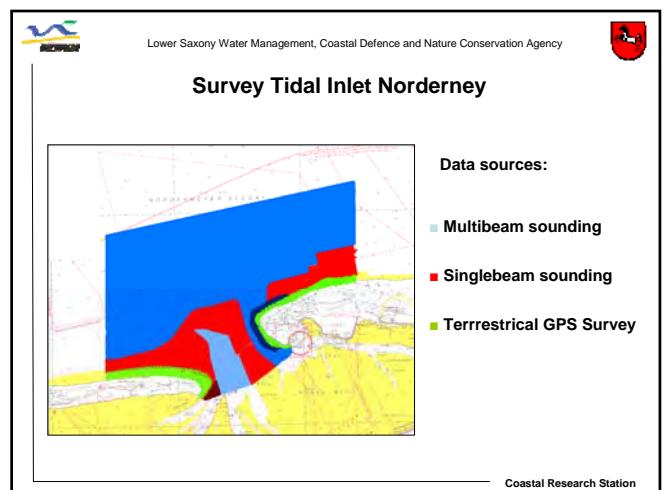
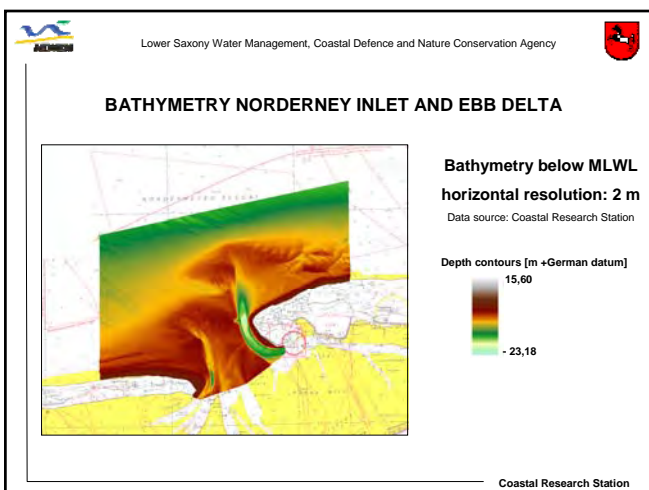
Coastal Research Station

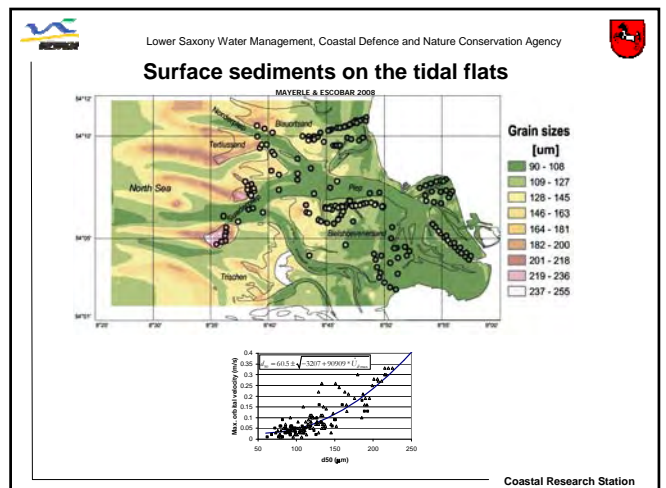
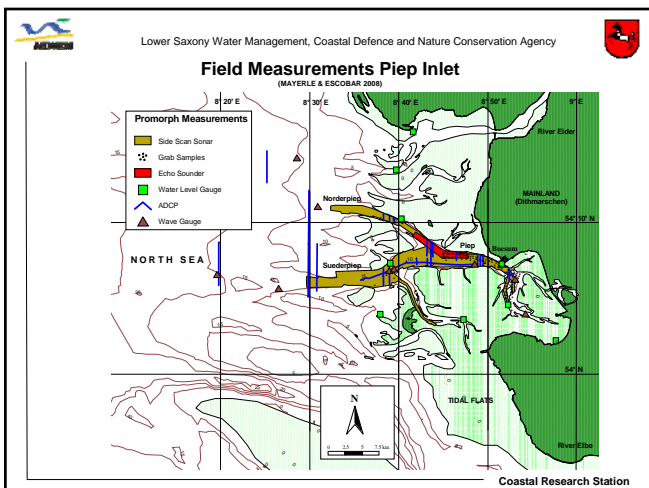
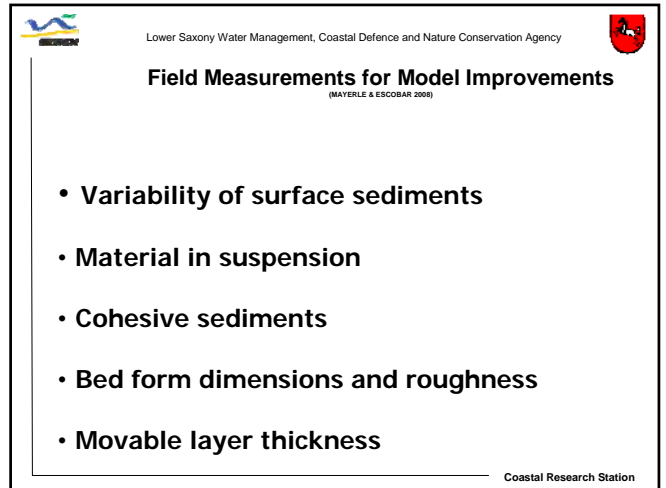
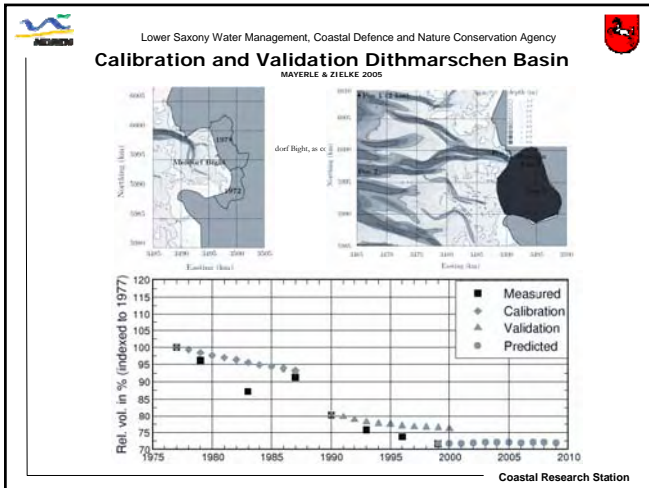
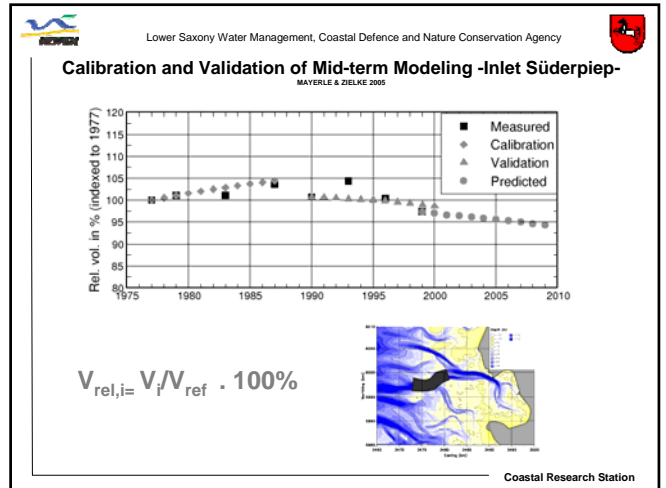
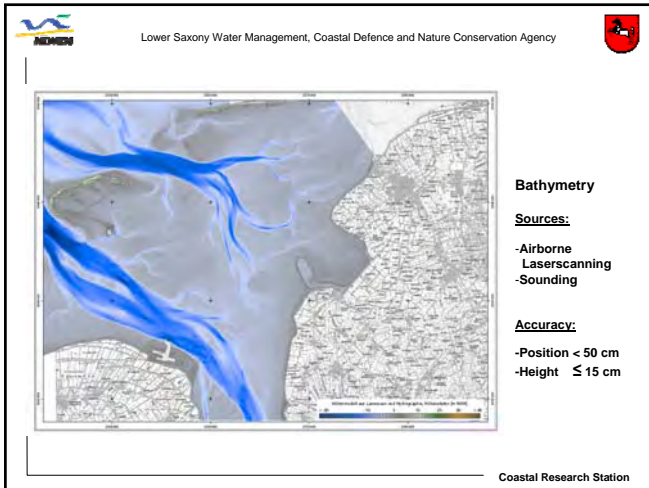
Lower Saxony Water Management, Coastal Defence and Nature Conservation Agency

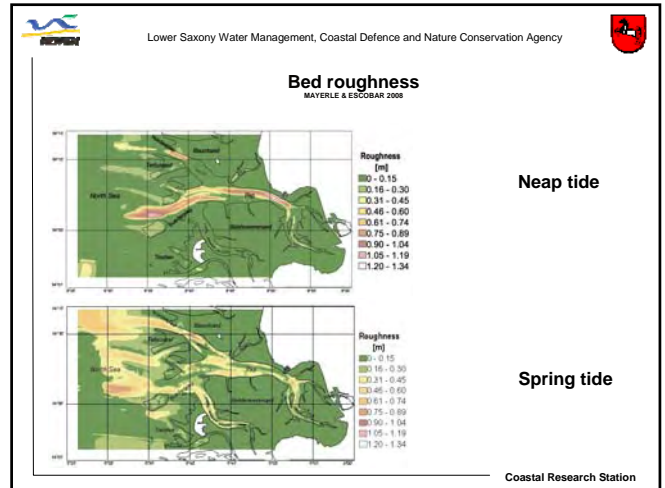
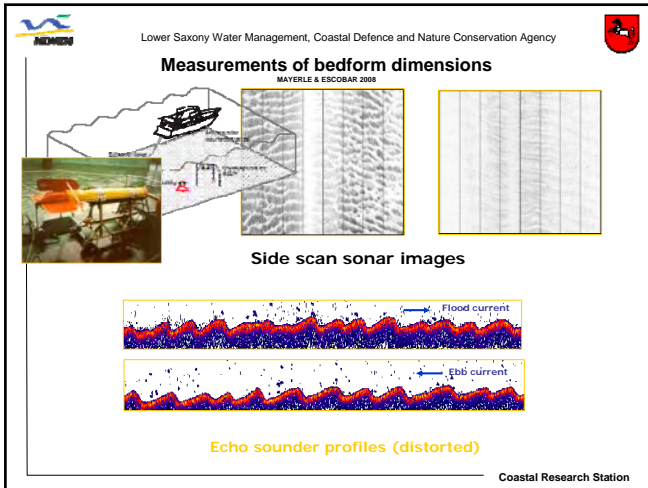
CONCLUSIONS-2

- Detailed process-based modeling for longer periods should be ensemble with sensitivity studies for distinct impacts and boundary conditions
- Combination with conceptual models is urgently recommended

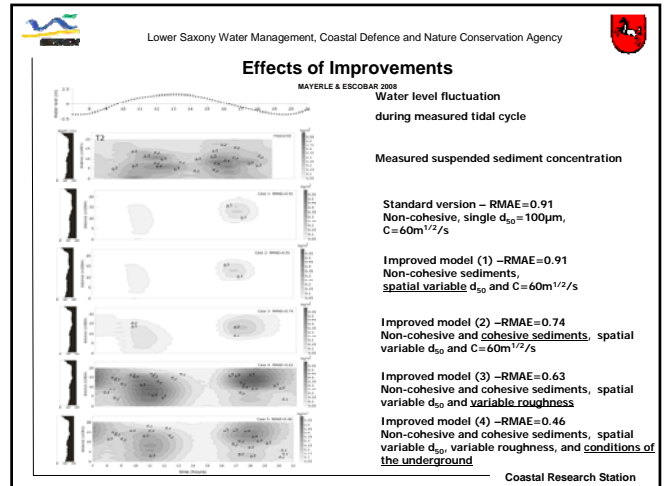
Coastal Research Station







- Lower Saxony Water Management, Coastal Defence and Nature Conservation Agency
- ### Consideration of bedform variations
- Small variation during a tidal cycle
 - Major variations of bedform dimensions due to fluctuation of tidal range
 - Dimensions of bedforms depend mainly on local maximum shear stress
 - Extension of existing relationship for bedform dimensions in dependence of local maximum shear stress
- Coastal Research Station



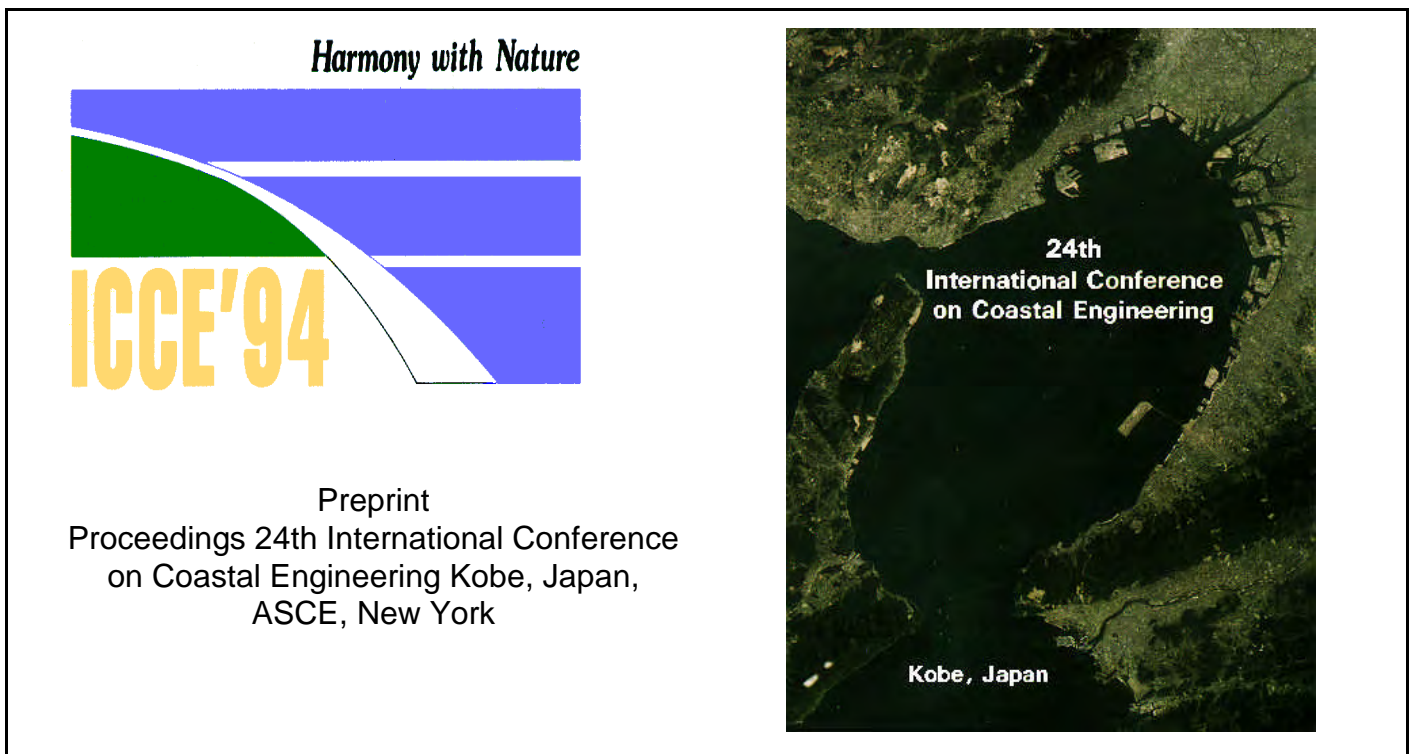
- Lower Saxony Water Management, Coastal Defence and Nature Conservation Agency
- ### Final Remarks
- Both conceptual and process-based modeling deliver valuable insights into the morphodynamical response of intertidal areas to be expected due to an accelerated sea-level rise
 - Validation of morphodynamical modeling is recommended on an aggregated scale
 - Field measurements could deliver valuable inputs for model improvements
- Coastal Research Station



Forschungsstelle Küste



Niedersächsisches Landesamt
für Ökologie



Hanz D. Niemeyer

**LONG-TERM MORPHODYNAMICAL DEVELOPMENT
OF THE EAST FRISIAN ISLANDS AND COAST**

LONG-TERM MORPHODYNAMICAL DEVELOPMENT OF THE EAST FRISIAN ISLANDS AND COAST

Hanz D. Niemeyer¹

Abstract

The morphology of the East Frisian Islands and Coast has experienced enormous changes in the course of the last centuries. The resedimentation of medieval sturm bays has played a dominant role within these morphodynamical processes which could no longer only be credited to the impacts of littoral drift. Reconstructions of former coastal morphology have been used to quantify the long-term development of significant parameters for the tidal basins of the East Frisian Wadden Sea. Additionally also the tidal volumes for situations since 1650 could be determined. On this basis the long-term stability of common empirical relationships was checked.

Introduction

The East Frisian Islands and Coast are part of the Frisian Wadden Sea which ranges from the eastern part of the Dutch across the German to the southern part of the Danish North Sea coast (fig. 1) and consist of a chain of seven barrier islands separated by tidal inlets from each other through which the tidal basins with intertidal areas and supratidal salt marshes are filled and emptied during each tidal cycle. The tidal range is about 2,5 m and the yearly mean offshore significant wave height is about 0,7 to 1,0 m. It is therefore a mixed energy tide-dominated coast according to the classification of HAYES [1975]. The littoral drift is predominantly eastward directed.

The East Frisian Islands and Coast have been performed at the end of the holocene transgression [KRÜGER 1911; LÜDERS 1951; STREIF 1990] and have experienced enormous morphological changes since then. Though no detailed information is available for that time firstly a superposition of human impacts on this natural development is expected to have been effective when the mainland coast was closed consecutively against the sea by constructing sea dykes since the beginning of this millenium [HOMEIER 1969]. Later on and particularly for the last 350 years the morphological behaviour of the East Frisian Islands and Coast is well documented by the horizontal position of the morphologically representantive markers tidal low and high water lines, dune foot and border lines of supratidal salt marshes [HOMEIER 1962]. Additionally there is even information with lesser accuracy on certain areas available concerning situations until more than 600 years ago (fig. 2). The migration of tidal inlets and barrier islands

¹Coastal Research Station of the Lower Saxonian Central State Board for Ecology
Fledderweg 25, 26506 Norddeich/East Frisia, Germany

has been superimposed interactively by further large scale human impacts interfering with the natural processes. In the course of the last centuries the two most important ones have were:

1. Artificial acceleration of resedimentation of the medieval storm surge bays at the mainland coast in respect of land reclamation and afterwards consecutively executed partial enclosures of these areas by dyking.
2. The fixation of the four migrating ones of the six tidal inlets separating the East Frisian barrier islands since the middle of the 18th century in order to protect there developing holiday and health resorts.

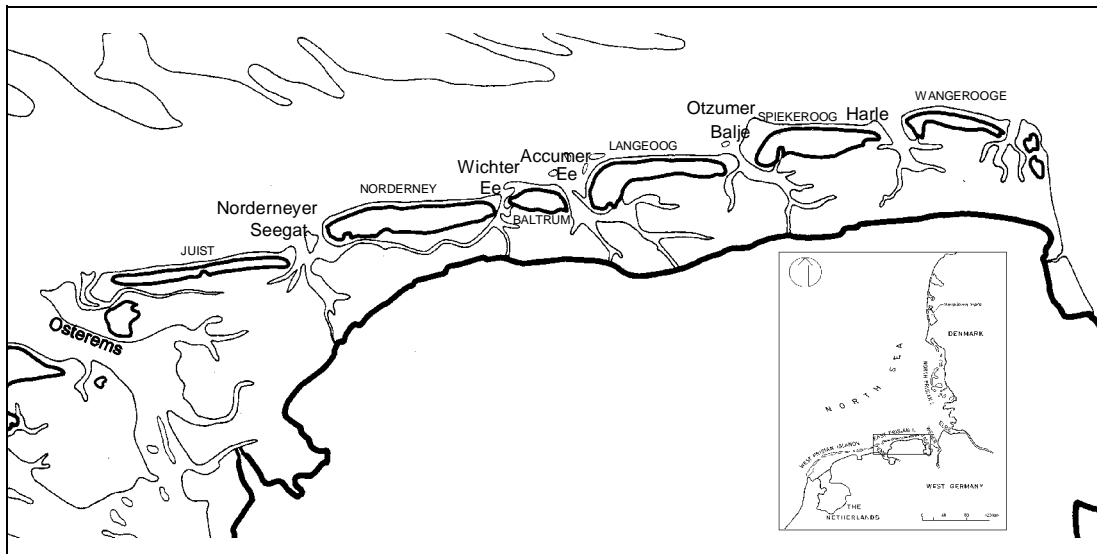


Figure 1. East Frisian Islands and Coast with inserted overview of the North Sea

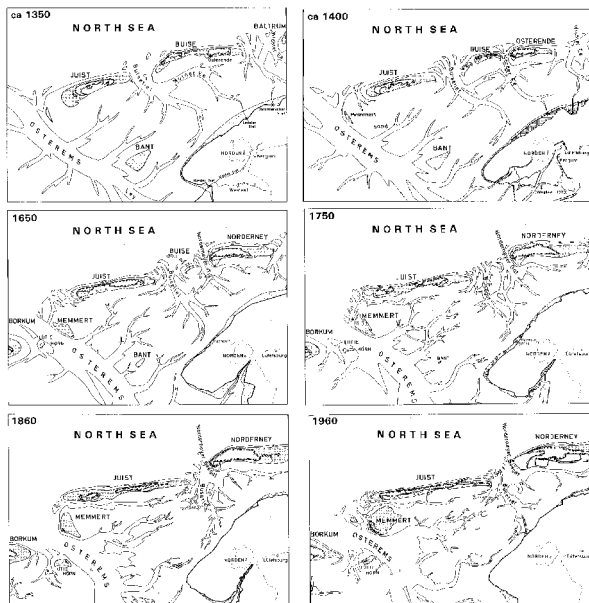


Figure 2. Reconstruction of the western East Frisian Wadden Sea since 1350 by HOMEIER [1964]

These large scale morphodynamical processes have mainly taken place in the western and eastern part of the East Frisian Wadden Sea whereas the tidal inlet Accumer Ee and its basin in the central part have remained rather stable in the course of the recent centuries. Beside geological boundary conditions it is also remarkable that in this area no large storm surge bay was ever existent. A detailed knowledge about the background of these developments is of high interest. Not only for improving backward directed process knowledge but also for the development of long-term prognostic tools like empirical morphodynamical models. In order to create a data basis for this purpose the charts containing historical reconstructions of coastal morphology elaborated by HOMEIER [1962] and hydrographic charts have been transferred into a Geographical Information System (GIS) which is used as a database for further evaluation and parametrization.

Extension and enclosure of medieval storm surge bays

Ley Bay

The Ley Bay ever got its largest extension due to the erosional effects of the catastrophic storm surges of the 14th century and especially due to those of the "First Dyonysis Surge" in 1374 [HOMEIER 1972]. The storm surges in that time were very effective in respect of eroding the flooded areas after dyke failures as their soil consisted predominantly of very erodible peat. Due to that fact the losses of land to the sea were much higher than usual, the extension of the bay did afterwards not fit with the hydrodynamical boundary conditions in order to reestablish a morphodynamical equilibrium. This imbalance caused sedimentation leading to the rise of salt marshes at the borders of the bay supported and accelerated by interfering human reclamation works. These processes changed the system again resulting in further sedimentation [NIEMEYER 1984, 1991b]. The rise of salt marshes allowed a subsequent reclamation and partial enclosures of formerly lost areas (fig. 3). In the course of the centuries the areal extensions of the enclosures decreased until the beginning of this century. But in recent years the advanced tools then available in coastal engineering made even the dyking of intertidal flats possible and not only of those areas which had already reached the stage of supratidal salt marshes. These measures interfered with hydrodynamical-morphological interactions to a much higher extent than the dyking of salt marshes.

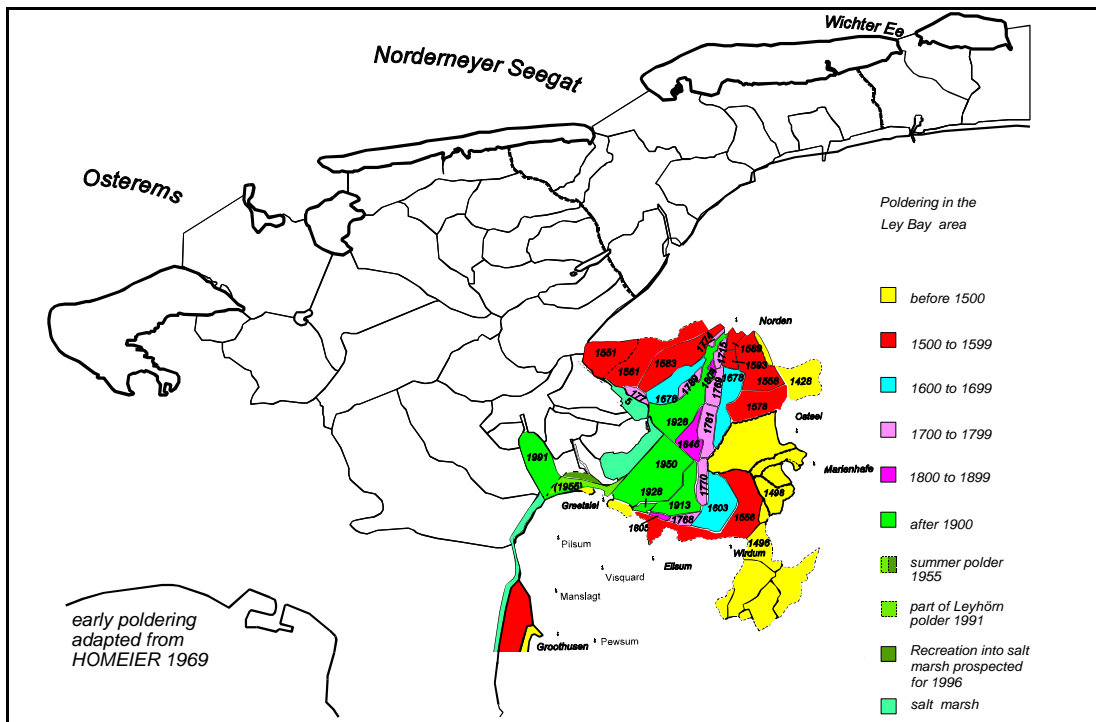


Figure 3. Partial enclosures of the Ley Bay during the last six centuries

Harle Bay

The Harle Bay already existed at the beginning of dyke construction at the end of the last century. It was silting up and the dyking of growing salt marshes is reported for the 12th and 13th century [HOMEIER 1969, 1979]. In the middle of the 14th century an unknown number of subsequently following storm surges caused the destruction of dyke lines and created erosion in the flooded areas. But the enlarged size of the tidal basin was not in tune with the dynamical equilibrium and in particular the higher intertidal areas silted up due to the absence of waves

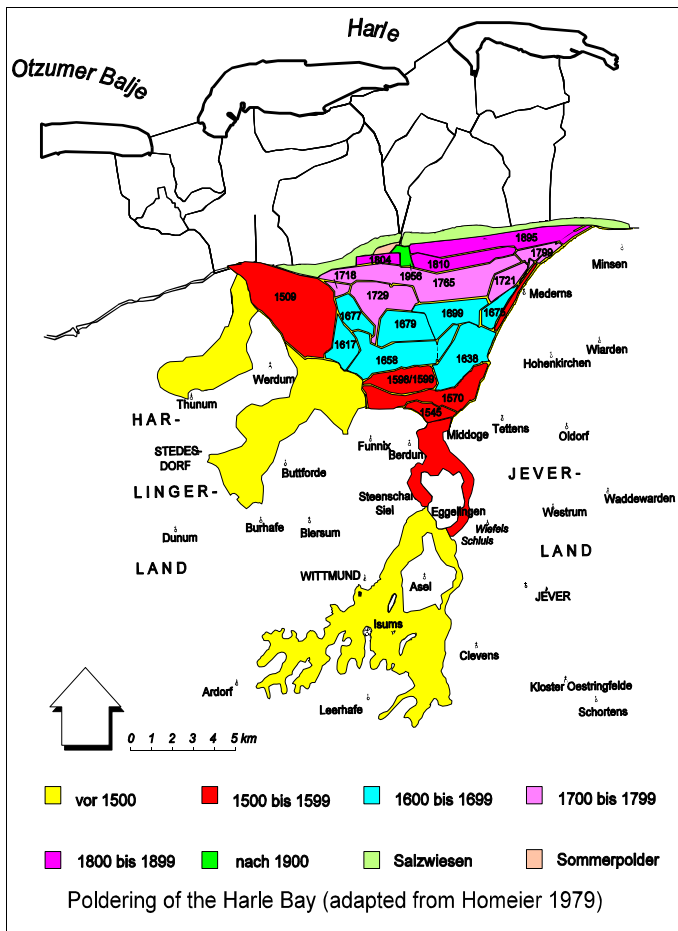


Figure 4. Partial enclosures of the Harle Bay

further increase of sedimentation, resulting reduction of tidal volume and again sedimentation until a new equilibrium stage was achieved [NIEMEYER 1991b]. In areas where only small storm surge bays had been created as i. e. g. in the basin of the tidal inlet Accumer Ee in the central part of the East Frisian Wadden Sea (fig. 1) morphodynamical changes during the last centuries have been less dramatic than in those where storm surge bays performed a quantitatively remarkable part of the total basin area.

Western East Frisian Wadden Sea

In comparison to its present total area of about 334 km² the basin of the tidal inlet Osterems has experienced a remarkable reduction of about 100 km² since the 14th century due to the numerous partial enclosures (fig. 3). Surprisingly the total basin area has nearly remained unchanged since 1650 (tab. 1) whereas more than 40 km² have been reclaimed in the Ley Bay during that period (fig. 5). This development and the morphodynamical processes in the remaining parts of the offshore areas must have substantially interacted. A comparison of the situations of 1650 and 1960 using the historical maps evaluated by HOMEIER [1962] makes evident that the basin of the tidal inlet Osterems has compensated nearly all its losses by an eastward extension of its watershed against the basin of the tidal inlet Norderneyer Seegat which can probably be explained by the remarkably larger tidal volume of the Osterems tidal basin. This process cannot be explained due to the direction of the littoral drift, because the migration of the tidal inlet Osterems [HOMEIER & LUCK 1977; STEPHAN 1994] is counterdirectional. This development is in tune with the increase of relative area and respectively tidal volume in the

with sufficient energy to prevent siltation and the subsequent growth of supratidal salt marshes. The nearly continuous silting up occurred since then was followed by partial enclosures of the emerged supratidal salt marshes. More than 50% of the bay area had already been reclaimed at the end of the 16th century and two hundred years later only small remnants of the formerly large Harle Bay existed which mostly were reclaimed until the end of the 19th century. The Harle Bay had disappeared totally and a closed straight coastline was established (fig. 4).

Morphodynamical impacts of storm surge bay enclosures

General remarks

The enclosure of medieval storm surge bays has led to the following consequences: reduction of basin area, of basin volume, of tidal basin volume and of ebb delta volume in order to provide the basin's requirements for sedimentation. All these changes provoked additionally changes of local wave climate in the basin leading to a

eastern part of its basin which performs nowadays its largest subsystem. These facts indicate strongly that the morphodynamical processes due to the migration of the tidal inlet Osterems (fig. 5) could be credited to the silting-up and consecutively reclamation by partial enclosures of the Ley Bay.

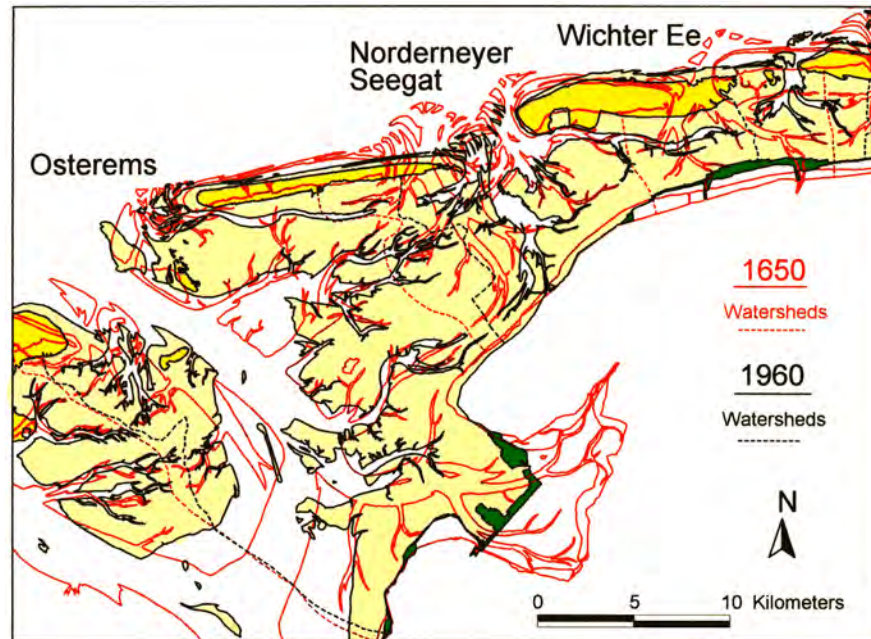


Figure 5. Morphological development of the tidal inlets Osterems, Norderneyer Seegat, Wichter Ee, of their basins and watersheds between 1650 and 1960 (reconstruction from HOMEIER [1962])

Indirectly also the eastern shift of the watershed between the Osterems and Norderneyer Seegat basins is remarkably influenced by that and not only a consequence of littoral drift. Even the migration of the tidal inlet Norderneyer Seegat must at least partly be regarded as a consequence of the consecutive reduction of the Ley Bay superimposing here littoral drift effects. This statement is contradictory to the qualitative migration models of LUCK [1977] for tidal inlets of the Norderneyer Seegat and Harle type basing on reconstructions of HOMEIER [1962, 1964] and being causally supplemented by NIEMEYER [1990] considering hydrodynamical impacts on ebb deltas and barrier islands. The explanation of migration processes by LUCK [1977] is still very useful in order to provide insight into processes which happened in the past but their cyclic character is doubtful due to regarding littoral drift as steering force of inlet migration. Considering the impact created by the areal reduction of the Ley Bay on primarily the shift of watershed between Osterems and Norderneyer Seegat basin and secondarily on the migration of the tidal inlet Norderneyer Seegat itself a continuation of inlet migration at the same scale could -even in the case of no human interference- not be expected because after the large areal reduction of the Ley Bay an important steering force has nearly disappeared.

The consequences of the migration of the Norderneyer Seegat for its ebb delta and respectively for the sediment balance on the beaches on the island of Norderney have been described as well as the measures to preserve the coast line and to combat erosion there [LUCK 1977; NIEMEYER 1990, 1991a; KUNZ 1991]. Moreover inlet migration and subsequent morphological changes have also had remarkable impacts on the adjacent mainland coastline [NIEMEYER 1990]: The gradual disappearance of the remnants of the former island of Buise and the reunification of the two inlets to a wider channel with wider spread swash bars in its ebb delta rendered

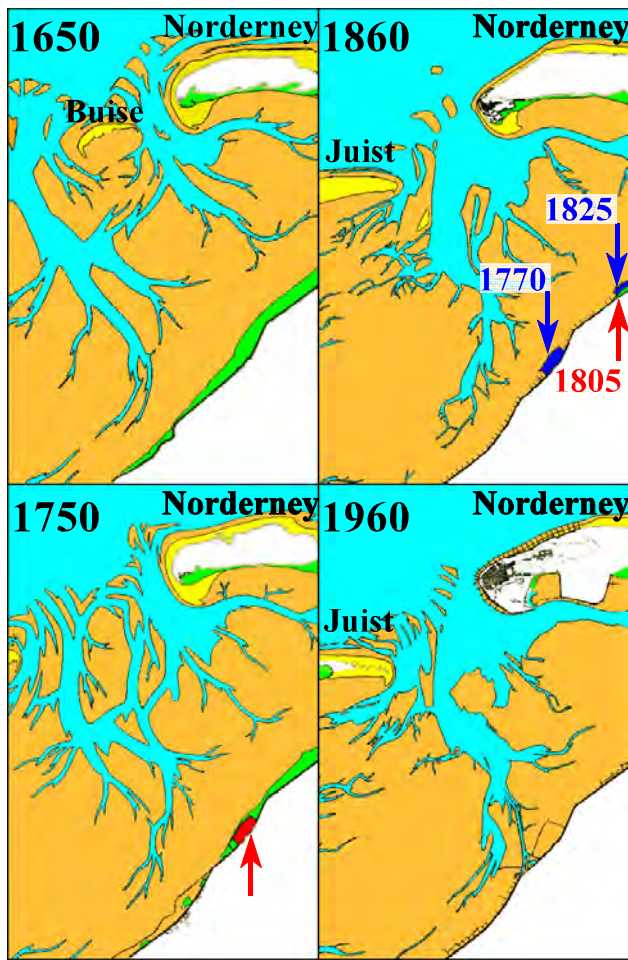


Figure 6. Impact of tidal inlet migration between Juist and Norderney in the period from 1650 to 1960 on the adjacent mainland coast (reconstruction from HOMEIER [1962])

the eastern part of the regarded area has lost shelter due to the morphological changes of the ebb delta and the inlet. The resulting effect is the total disappearance of salt marshes there and as well the destruction of the 1750 already existing polder and of a second one which had been erected at the beginning of the 19th century. Both were flooded during the storm surge of 1825 and had afterwards to be abandoned. Starting about 1860 the tidal inlet was successfully fixed by the construction of groynes ranging across the eastern slope of its deep channel.

The areal losses of the Osterems tidal basin have been compensated by an eastward shift of its watershed at the cost of that one of the Norderneyer Seegat. The same process repeated itself in the interaction of the basins of the Norderneyer Seegat and of the Wichter Ee (fig. 5): Again the basin with the larger volume shifted the watershed between both remarkably into eastern direction between 1650 and 1860. The western shore of the island of Baltrum experienced in the same period enormous erosion and moved more than 4 km eastward. Since the eastern watershed of the Wichter Ee tidal basin did not shift to the same extent into eastern direction as the western one the basin area was enormously reduced (tab. 1). The differences in the eastward shift of the western and the eastern watershed of the Wichter Ee tidal basin indicate also the impact of the partial enclosures in the Ley Bay on the morphodynamical processes of the tidal inlets and basins in its eastern neighbourhood.

as well possible the impact of higher wave energy up to the opposite mainland coast as the accompanying extension of sublittoral areas between the inlet and the coast (fig. 6). In 1650 there was a broad stretch of supratidal salt marshes in front of the mainland dykes. In 1750 the salt marshes in front of the mainland dyke of the Westermarsch had disappeared and a coastline retreat had become necessary after the dyke breaches during the storm surge of 1717. On the one hand the shadow effect of the remnants of the former island of Buisse was no longer effective. On the other had the migration of the inlet channels and of their tributaries led to the superposition of wave systems entering via Buissegat and Norderneyer Gat from the North Sea into that coastal area. Easter of this area the salt marshes in front of the dyke of the Linteler Marsch must have been sufficiently stable in order to encourage people to build a polder. In 1860 the inlets Buissegat and Norderneyer Gat merged to a one-inlet-system called Norderneyer Seegat. The consequences are primarily a less pronounced ebb delta with smaller shallows being spread wider. The higher concentration of tidal energy effects also a relative increase of sublittoral areas in the basin close to the inlet. Secondly this allows in tune with the wider inlet the input of higher wave energy into the basin upto the mainland coast. Particularly

Eastern East Frisian Wadden Sea

Another example of subsequent consequences of the enclosure of a medieval storm surge bay becomes evident regarding the tremendous relative reduction of the basin area of the tidal inlet Harle since the middle of the 14th century due to the land reclamation in the area of the former Harle Bay leading finally to its total enclosure. The reduction of basin area and corresponding tidal volume initialized consequently as well a decrease of cross-sectional area and width of the tidal inlet as of the seaward extension and volume of the ebb delta (fig. 7). This process was accompanied by an eastward migration of the tidal inlet Harle, an erosion and retreat of the eastern shore of the island of Wangeroog, a remarkable eastward extension of the island of Spiekeroog and a corresponding shift of the watershed between the tidal basins of the Otzumer Balje and Harle, whereas the eastern watershed of the Harle tidal basin did not move remarkably within the same period. A comparable eastward shift of the latter one was probably impossible because the neighbouring Jade estuary with its much higher tidal volume and resulting kinetic energy hampered such a reaction. Since also the watershed between the basins of the Accumer Ee and Otzumer Balje has migrated easterly to a much lesser extent than that one between the Otzumer Balje and the Harle, the basin area of the latter one experiences a large reduction while the Otzumer Balje basin's area increases significantly. Correspondingly the island of Spiekeroog enlengthened by more than 4 km or more than 80 % (fig. 7).

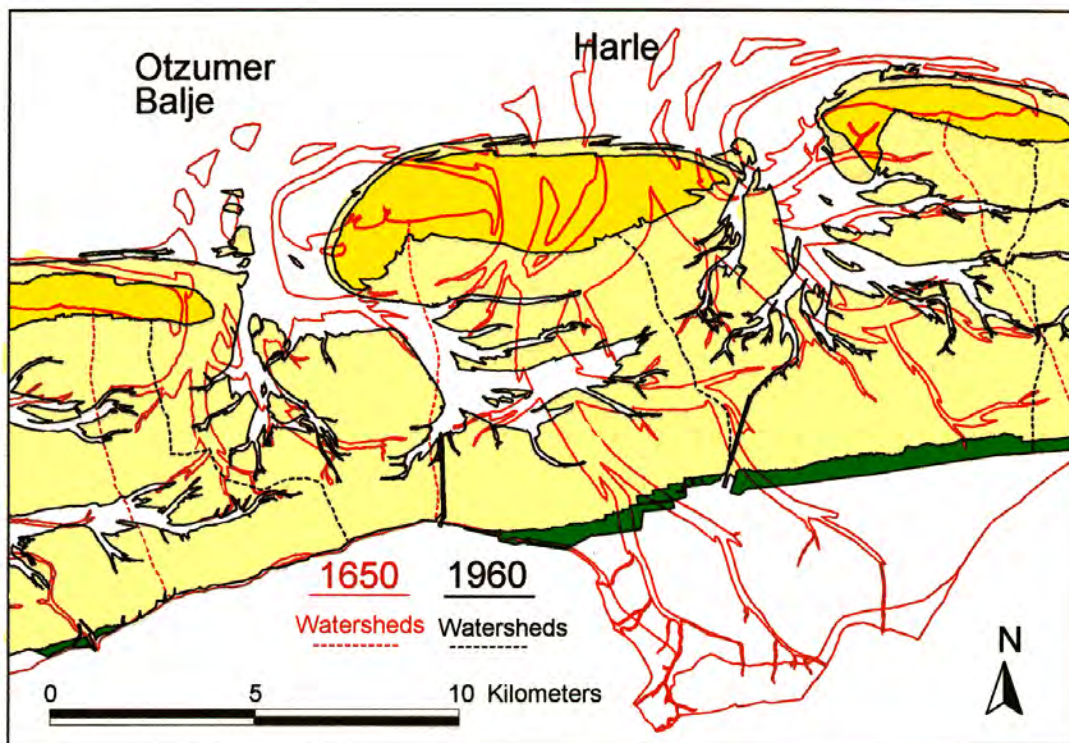


Figure 7. Morphological development of the tidal inlets Otzumer Balje and Harle, of their basins and watersheds between 1650 and 1960 (reconstruction from HOMEIER [1962])

This differences in inlet, ebb delta, island and migration are not explainable by littoral drift though not counterdirectional. But it is evident that the reduction of area and tidal volume of the Harle basin is intensively steered by the silting up of the Harle Bay. Therefore this must be regarded as the major steering impact for the enormous morphodynamical changes in this area.

Quantitative change of characteristic basin parameters

Total basin areas A_b

The total area of the tidal basins in the East Frisian Wadden Sea experienced a reduction of more than 13 % between 1650 and 1860 and afterwards fluctuated around a value of 85 % of the 1650 existing area (fig.8, tab. 1). The losses must mainly be credited to the reduction of the storm surge bays, particularly to that of Ley and Harle Bay with an reclaimed area of more than 80 km² during that period. Corresponding to the already described morphodynamical development of the western East Frisian Wadden Sea the basin areas of the Osterems and of the Norderneyer Seegat experienced maximal losses of about 10 % being later reduced to about 5 % whereas the basin area of the Wichter Ee was reduced by more than 55 % (fig. 8, tab. 1). The total reduction of the three basin areas is somewhat larger than the corresponding reduction of the Ley Bay between 1650 and 1960, but this could probably be explained by a phase shift of morphodynamical adaption to former silting up of bay areas.

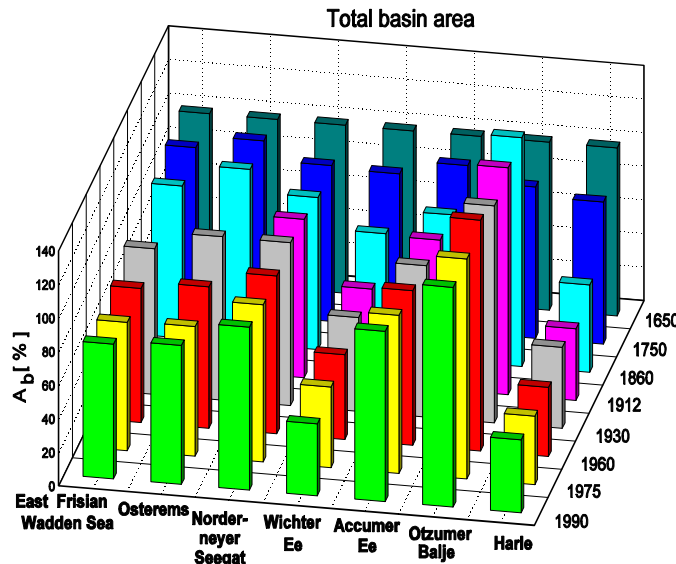


Figure 8. Relative development of total basin areas A_b (in percentages) in the East Frisian Wadden Sea

		1650	1750	1860	1912	1930	1960	1975	1990
East Frisian Wadden Sea	A_b [$10^6 \cdot m^2$]	835,00	806,37	755,54		723,83	666,28	637,72	669,54
	A_b [%]	100,00	96,57	90,48		86,68	79,79	76,37	80,18
Osterems		358,32	372,76	371,70		348,26	301,20	276,52	296,22
		100,00	104,03	103,73		97,19	84,06	77,17	82,67
Norderneyer Seegat		109,83	101,79	99,31	103,44	106,50	103,28	102,70	106,47
		100,00	92,67	90,42	94,18	96,96	94,04	93,51	96,94
Wichter Ee		53,93	49,16	38,93	30,27	30,10	27,20	25,93	23,09
		100,00	91,17	72,20	56,13	55,82	50,43	48,08	42,82
Accumer Ee		100,21	99,69	87,01	88,88	90,20	92,25	94,30	101,54
		100,00	99,47	86,83	88,69	90,01	92,05	94,10	101,32
Otzumer Balje		56,90	51,29	77,53	76,82	73,50	78,17	74,57	74,47
		100,00	90,14	136,25	135,00	129,17	137,38	131,04	130,87
Harle		155,80	131,68	81,06	66,37	75,27	64,18	63,70	67,75
		100,00	84,52	52,03	42,60	48,31	41,20	40,89	43,49

Tab. 1 Total basin areas 1650 - 1990

The basin area of the Accumer Ee has remained in the same order of magnitude independently from the enormous morphodynamical developments both in the western and eastern neighbourhood of that area. In the eastern East Frisian Wadden Sea the tidal basin area of the Otzumer Balje increased by about 30 % between 1650 and 1960. This increase was compensated by losses of basin area of the Harle of more than 45 % (fig.8, tab. 1). The total loss of area

for both basins is also higher than the correspondingly reclaimed areas in the Harle Bay. But here also the same explanation fits as for the western part of the East Frisian Wadden Sea. The area of partial enclosures was until the end of the 19th century only an indirect measure of long term silting up, because in that time dykes were only built on supratidal salt marshes which had been silted up earlier. In connection with the phase shift of morphodynamical adaption this quantitative differences must not necessarily be inconsistent with the basic idea. Moreover the phase shift of morphodynamical adaption of the seaward basin area to bay reduction becomes i. e. g. evident by the response of the Harle basin with a remarkable areal decrease until 1912 (fig. 8, tab. 1) whereas the most partial enclosures had already been carried out at the end of the 18th century (fig. 4).

Sublittoral and Intertidal basin areas A_{sl} and A_i

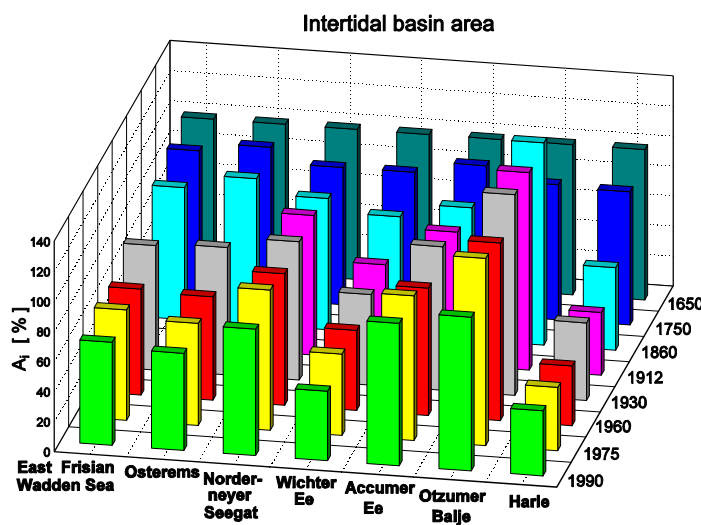


Figure 9. Relative development of intertidal basin areas A_i (in percentages) in the East Frisian Wadden Sea

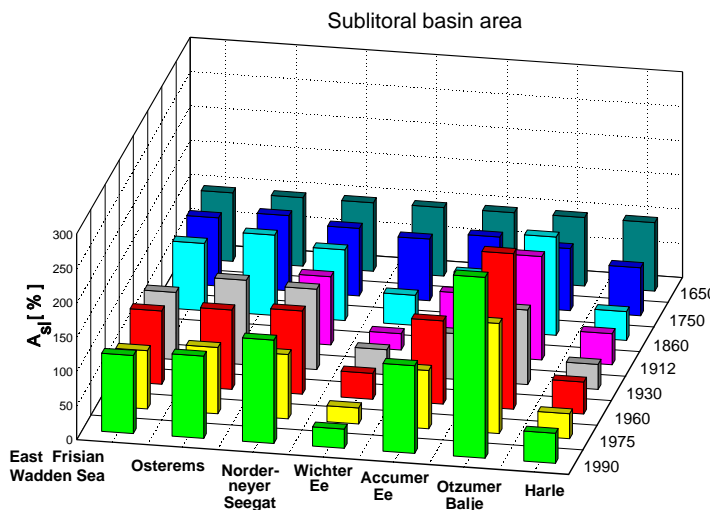


Figure 10. Relative development of sublittoral basin areas A_{sl} (in percentages) in the East Frisian Wadden Sea

The intertidal areas of the East Frisian Wadden Sea have both absolutely and relatively much more decreased (fig. 9, tab. 2) than the total basin areas (fig. 8, tab. 1). Correspondingly the sublittoral areas have as well absolutely as relatively increased (fig. 10, tab. 3). But this tendency is not uniform for all tidal basins: It is valid for those ones with as a small reduced total area like Osterems and Norderneyer Seegat, a nearly constant one like Accumer Ee or even enlarged one like Otzumer Balje. Contradictory in those basins which total area experienced reduction like those ones of the Wichter Ee and the Harle the tendency is different. In the Harle basin both intertidal and sublittoral areas have experienced nearly the same amount of relative reduction whereas in the Wichter Ee basin the sublittoral areas have been relatively more reduced than the intertidal ones (fig. 9, tab. 2; fig. 10, tab. 3). In total the tendency of reduction for the intertidal areas being evident until 1960 has been substituted by a fluctuation of less than 3 % since then (fig. 9, tab. 2) which is generally in tune with the development of the total basin areas (fig. 8, tab. 1). Contradictory the until 1930 rather stable figures for the sublittoral

		1650	1750	1860	1912	1930	1960	1975	1990
East Frisian Wadden Sea	A_b [$10^6 \cdot m^2$]	623,35	596,07	548,41		515,86	439,63	458,02	428,60
	A_i [%]	100,00	95,62	87,98		82,76	70,53	73,48	68,76
Osterems		242,28	245,48	235,76		205,60	166,85	164,30	156,81
		100,00	101,32	97,31		84,86	68,87	67,81	64,72
Norderneyer Seegat		88,69	80,95	77,54	82,35	81,65	77,65	82,90	74,61
		100,00	91,27	87,43	92,85	92,07	87,55	93,47	84,13
Wichter Ee		43,90	40,15	34,52	27,87	26,48	23,40	23,82	20,29
		100,00	91,45	78,64	63,48	60,32	53,31	54,26	46,22
Accumer Ee		80,52	79,95	70,88	71,30	77,00	68,32	77,56	76,34
		100,00	99,29	88,03	88,55	95,63	84,85	96,32	94,81
Otzumer Balje		46,86	42,19	63,15	61,70	62,60	55,39	58,40	47,96
		100,00	90,02	134,76	131,66	133,58	118,20	124,61	102,34
Harle		121,10	107,36	66,55	50,57	62,53	48,01	51,04	52,59
		100,00	88,66	54,96	41,76	51,63	39,64	42,15	43,43

Tab. 2: Intertidal basin areas 1650 - 1990

		1650	1750	1860	1912	1930	1960	1975	1990
East Frisian Wadden Sea	A_b [$10^6 \cdot m^2$]	211,63	210,29	207,13		207,97	226,65	179,92	240,93
	A_{sl} [%]	100,00	99,37	97,87		98,27	107,10	85,02	113,84
Osterems		116,04	127,28	135,94		142,66	134,35	112,22	139,41
		100,00	109,69	117,15		122,94	115,78	96,71	120,14
Norderneyer Seegat		21,14	20,84	21,77	21,09	24,85	25,64	19,80	31,86
		100,00	98,54	102,96	99,75	117,52	121,25	93,65	150,68
Wichter Ee		10,02	9,02	4,41	2,40	3,62	3,79	2,33	2,80
		100,00	89,94	44,00	23,94	36,12	37,84	23,25	27,94
Accumer Ee		19,69	19,74	16,13	17,58	13,20	23,93	16,74	25,20
		100,00	100,23	81,92	89,28	67,01	121,50	85,03	127,95
Otzumer Balje		10,04	9,10	14,37	15,12	10,90	22,77	16,17	26,51
		100,00	90,70	143,20	150,62	108,59	226,90	161,08	264,07
Harle		34,70	24,32	14,50	15,80	12,74	16,17	12,66	15,16
		100,00	70,10	41,79	45,55	36,73	46,62	36,49	43,69

Tab. 3: Sublittoral basin areas 1650 - 1990

basin areas tend to fluctuate more significantly since then (fig. 10, tab. 3). Partly this effect might also be caused by changes in the seaward boundary of the basins for the different surveys due to the chosen determination of the seaward inlet cross-section for computations.

Supratidal salt marsh areas A_{sm}

The interactions of hydro- and morphodynamics in the storm surge bays created favourable boundary conditions for the growth of supratidal salt marshes as described before. But these were more and more dyked by subsequent partial enclosures. The deceleration of silting-up due to the reduction of the bays' oversize effected primarily also a deceleration of salt marsh (fig. 3 + 4). Though only insufficient data are available for the time before 1650 the areal development of salt marshes from then still reflects that process (fig. 11, tab. 4): The total area of supratidal salt marshes in the East Frisian Wadden Sea has been reduced from 1650 to 1750 by about 20 % and then again until 1860 by another 12 %. The decrease between 1860 and 1930 has again decelerated to less than 5 % even followed by an increase of nearly 4 % until

1960. The subsequent reduction of about 5 % until 1975 has growth and secondarily in tunewith partial enclosures a reduction of existing salt marsh areas been a consequence of the enclosures of salt marshes by construction of new dykes due to the guidelines for coastal safety established after the catastrophic storm surge of 1962 seawardly of the old ones.

Regarding the tidal basins separately the developments do not reflect the same uniform tendency (fig. 11, tab. 4): The Osterems tidal basin has lost nearly 60 % of its supratidal salt marsh areas between 1650 and 1860, particularly due to the partial enclosures in the Ley Bay. But it regained about until 1975 about 20 %, particularly to salt marsh growth in the Ley Bay in spite of executed partial enclosures in the same period. The initial losses of salt marsh areas in the tidal basin of the Norderneyer Seegat have already been explained as a consequence of inlet migration and changes of local wave climate with a decrease of about 55 % from 1650 to 1750. But already between 1750 and 1860 the continuous losses (fig. 6) were overcompensated by salt marsh growth in other areas of the basin. Since then salt marshes areas have increased until 1975. The losses of supratidal salt marsh areas in the tidal basin of the Wichter Ee must particularly be regarded as a consequence of the enormous reduction of its total basin area which is also evident for the changes between 1650 and 1975. The pursued reduction of salt marshes in the tidal basin of the Accumer Ee since 1650 must be primarily credited to the seaward movement of dyke lines whereas the continuous growth of salt marsh areas in the tidal basin of the Otzumer Balje is particularly a consequence of the described extension of its total basin area since 1650.

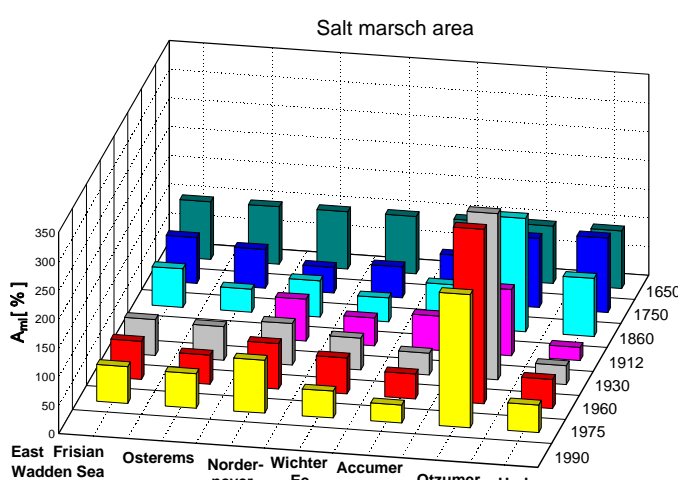


Figure 11. Relative development of salt marsh basin areas A_m (in percentages) in the East Frisian Wadden Sea

		1650	1750	1860	1912	1930	1960	1975
East Frisian Wadden Sea	$A_b [10^6 \cdot m^2]$	45,59	36,24	30,60		28,50	30,26	29,22
	$A_m [%]$	100,00	79,49	67,12		62,51	66,37	64,09
Osterems		16,96	11,47	6,82		9,93	8,65	10,23
		100,00	67,63	40,21		58,55	51,00	60,32
Norderneyer Seegat		5,85	2,61	3,70	4,26	4,23	4,65	5,38
		100,00	44,69	63,34	72,90	72,40	79,53	92,02
Wichter Ee		5,15	2,78	2,15	2,52	2,86	3,23	2,41
		100,00	53,95	41,71	48,88	55,56	62,74	46,84
Accumer Ee		6,74	5,46	4,90	4,06	2,54	2,92	2,11
		100,00	80,98	72,72	60,22	37,63	43,31	31,28
Otzumer Balje		2,10	2,52	4,14	2,42	6,06	6,37	4,87
		100,00	120,50	197,44	115,44	289,27	303,87	231,90
Harle		8,80	11,40	8,89	2,01	2,88	4,45	4,22
		100,00	129,57	101,09	22,80	32,69	50,58	48,01

Tab. 4: Salt marsh areas 1650 - 1975

The reduction after 1960 is an effect of the dyking of salt marshes. Between 1750 and 1912 salt marsh areas in the tidal basin of the Harle have as well decreased as the total basin area due to re-sedimentation and partial enclosures of the Harle Bay. Until 1960 then a certain growth appeared in tune with the stabilization of the tidal basin which only experienced a slight reduction after 1960 due to dyking of salt marshes.

Evaluation of tidal volumes

The parametrization of Wadden Sea areas in the framework of the project WADE was carried out in order to establish empirical relationships between these parameters describing morphodynamical equilibrium conditions. A parametrization of morphological parameters like areas must be insufficient for that purpose, the evaluation of hydrodynamical parameters is additionally necessary for reaching the aim. The most common hydrodynamical parameter used in empirical morphodynamical relationships is the tidal volume. The evaluation of tidal volumes for defined areas is no problem if detailed surveys or maps are available and the representative tidal high and low water peaks are known. But in the case of the reconstructed historical coastal morphology of 1650, 1750 and 1860 by HOMEIER [1962] there are only the contour lines of mean tidal high and low water and the border lines of the supratidal salt marshes available. Furthermore measurements of tidal water levels providing reliable data have been carried out in the East Frisian Wadden Sea since the end of the 19th century (fig. 14). Therefore the evaluation of tidal volumes for these dates requires extra efforts.

The substitution of complex tidal basin morphology by only mean high and low water contour lines has been exercised by WALTHER [1972] in order to avoid enormous computational efforts without the aid of modern computers:

$$V_T = TR @ (A_b + A_{sl}) / 2$$

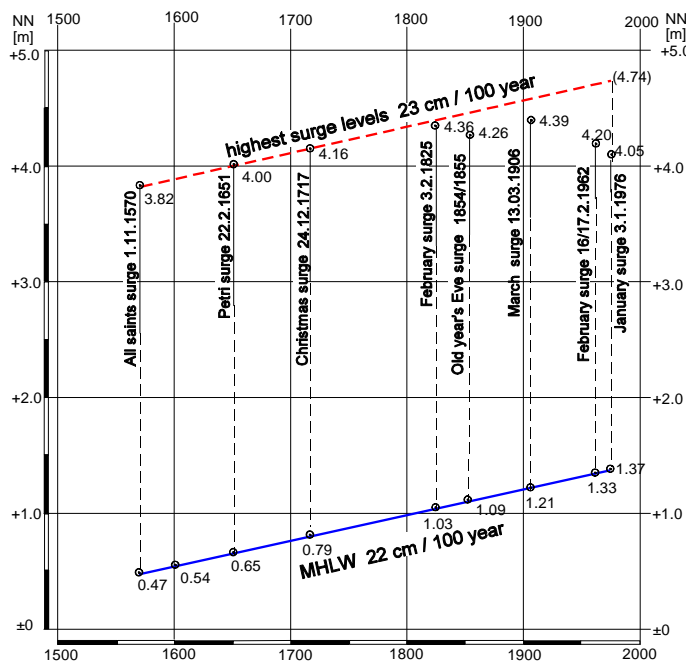


Figure 12. Reconstructed historical mean high tide and storm surge water levels and long-term trends, island of Wangeroog, tidal inlet Harle [LÜDERS 1977]

Since there is nothing reported about the accuracy of this method a calibration test for recent data sets was carried out with the data of all six East Frisian tidal basins from the surveys of 1960, 1975 and 1990. Surprisingly the deviation from data being evaluated with the aid of a GIS was on the average about 6 % (fig. 12) which is in the same or even in a lower order of magnitude as the measuring accuracy of data from hydrographic surveys. Based on these results the method of WALTHER [1972] is a suitable tool for the evaluation of tidal volumes for the situations of 1650, 1750 and 1860 for the reconstructed coastal morphology. In order to keep the data comparable the tidal volumes for the surveys since 1912 were also determined by the same method.

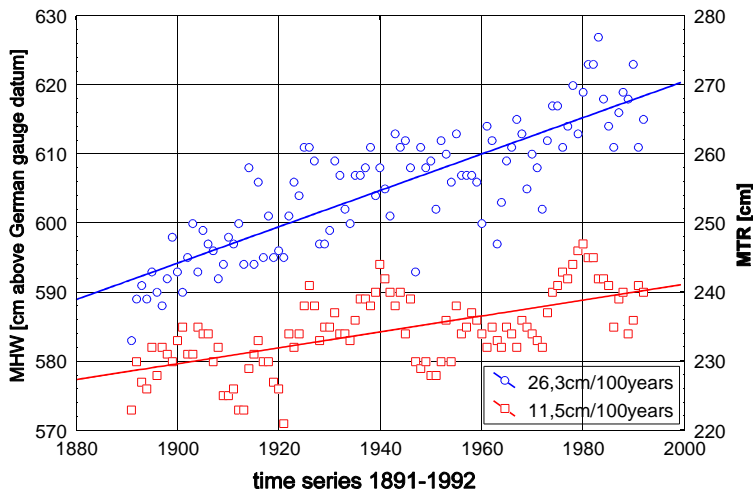


Figure 13. Yearly mean high water levels and tidal ranges since 1896 and corresponding mean trends, island of Norderney, tidal inlet Norderneyer Seegat

Beside the before mentioned data of tidal water levels there are also reconstruction of historical mean higher water and storm surge levels available. A very valuable data set has been elaborated by LÜDERS [1977] for the island of Wangerooge at the shore of the tidal inlet Harle (fig. 1) based on historical levellings being transferred to present datum and metric scale (fig. 13). These long-term data set has nearly the same rising velocity as that one being measured in the course of the last 100 years at the tidal gauge at the island of Norderney in the

tidal inlet Norderneyer Seegat (fig. 1 + 14). The measured data make also a parallel increase of tidal range with rising high water levels evident (fig. 14). Referring to the documented rise of high water levels since 1570 it is reasonable that the tidal range has increased since then by nearly the same order of magnitude as for the last century. Based on this assumption the tidal volumes for the morphological situations of 1650, 1750 and 1860 have been evaluated by taking into account an increase of tidal range between 1650 and 1900 of 10 cm per century (fig. 15, tab 5). This figure is used in order to consider the long-term tendency of tidal boundary conditions of the morphodynamical development in the investigation area. The evaluated tidal volumes are quantitative not very sensitive against a possible inaccuracy of ± 5 cm/century, the fluctuation of the tidal volumes is therefore less than 2,5 %.

The tidal volumes of the tidal basins in the East Frisian Wadden Sea have in total remained nearly constant over the regarding the long-term development. The increase of tidal range measured since the end of the 19th century (fig. 14) and expected to have also occurred with a

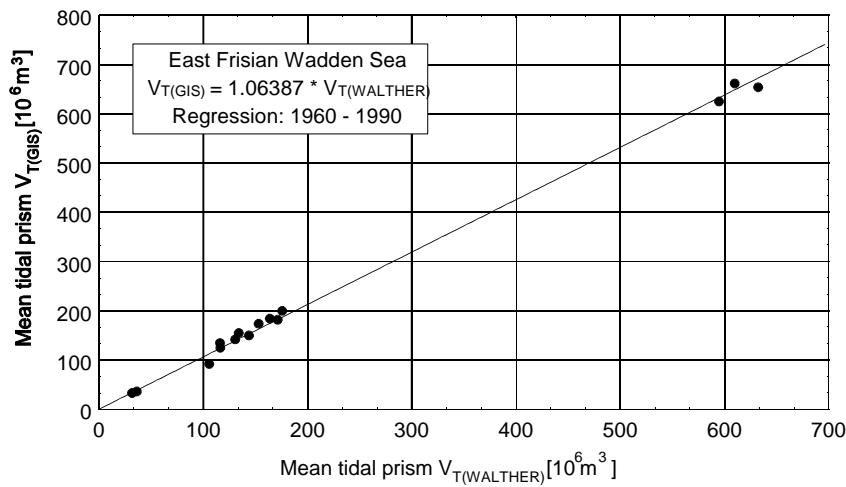


Figure 14. Comparison of tidal volumes computed with a GIS from detailed morphological maps and evaluated by the method of WALTHER [1972]

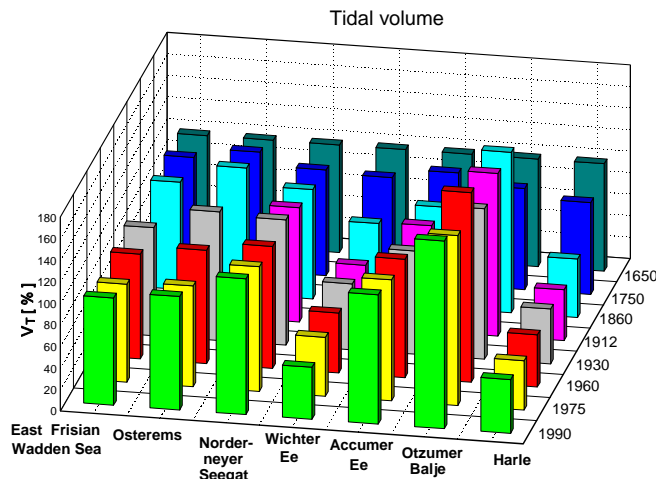


Figure 15. Relative development of tidal volumes (in percentages) of the tidal basins in the East Frisian Wadden Sea

similar coincidence to the rise of mean tidal high water since the 16th century (fig. 13) has compensated the reduction of basin areas. For the midterm development of the last decades with nearly stable total basin areas the tidal volume has not experienced a remarkable increase whereas the tidal range has also increased during this period (fig. 14); for 1975 even a significant reduction occurred (fig. 15, tab. 5) which can partly be explained by the reduction of the total basin areas (fig. 8, tab.1). According to the reduction of total areas the tidal volumes of the Wichter Ee and Harle

have decreased significantly. Correspondingly the tidal volume of the Otzumer Balje has increased overproportional in respect of other tidal basins. The Accumer Ee has in 1990 a tidal volume which is 20 % higher than 1650, whereas the total basin areas for both dates are nearly constant. The tidal volume of the Osterems has experienced remarkable fluctuation which are generally in tune with the development of its basin areas. That one of the Norderneyer Seegat has generally increased. The fairly reduction of its basin areas must have been compensated partly by the increase of tidal range. Furthermore the shape of the basin and the relation of intertidal and sublittoral areas might have been of importance.

		1650	1750	1860	1912	1930	1960	1975	1990
East Frisian Wadden Sea	$V_T [10^6 \cdot m^3]$	1135,35	1149,22	1131,64		1141,33	1105,40	1032,77	1133,23
	$V_T [\%]$	100,00	101,2	99,67		100,5	97,36	90,97	99,81
Osterems		498,08	550,04	583,79		594,01	524,83	466,48	524,93
		100,00	110,4	117,2		119,5	105,3	93,66	105,3
Norderneyer Seegat		134,25	131,82	136,22	142,58	156,30	152,12	155,58	169,45
		100,00	98,19	101,4	106,2	116,4	113,3	115,8	126,2
Wichter Ee		65,55	62,54	48,76	37,40	40,13	36,57	35,89	31,72
		100,00	95,54	74,39	57,06	61,22	55,79	54,75	48,39
Accumer Ee		131,90	137,34	123,78	129,35	126,66	145,22	148,25	158,42
		100,00	104,1	93,84	98,07	96,03	110,1	112,4	120,1
Otzumer Balje		76,98	72,48	114,88	116,30	107,61	135,77	121,58	134,29
		100,00	94,15	149,2	151,0	139,7	176,3	157,9	174,4
Harle		228,59	195,01	124,22	108,06	116,62	110,89	104,99	114,41
		100,00	85,31	54,34	47,27	51,02	48,51	45,93	50,05

Tab. 5: Tidal volumes of the East Frisian Wadden Sea tidal basins 1650 - 1990

Long term stability of empirical relations

The morphological changes in the East Frisian Wadden Sea [HOMEIER 1962, LUCK 1977] has decelerated enormously in the course since the middle of the last century and particularly since the beginning of this one. The fixing of four of the six inlets since the beginning of this

century and particularly the coincidentally nearly finished resedimentation and land reclamation in the areas of the medieval storm surge bays has effected that development. Therefore morphodynamical changes in the East Frisian Wadden Sea occur not only self-evidently on much lower time scales but also on smaller length scales leading to a morphodynamical quasi-equilibrium, which in the long run is expected to be only temporarily. But nowadays a mid-term dynamical equilibrium could be assumed which is expressed by a number of well-established semi-empirical relationships being evaluated on a data basis with sufficient density for that purpose. That method for a functional parametrization of morphodynamical processes has proved as a success for coastal research and for coastal engineering planning since decades [O'BRIEN 1931; WALTHER 1972; EYSINK 1979, 1991; NIEMEYER 1991]. One of the important relationships describing a morphodynamical equilibrium is that one between total basin area and tidal volume which has been introduced by EYSINK [1979] and was used in the framework of the Dutch coastal defense study as a tool for the estimation of the impacts of an accelerated relative sea-level rise.

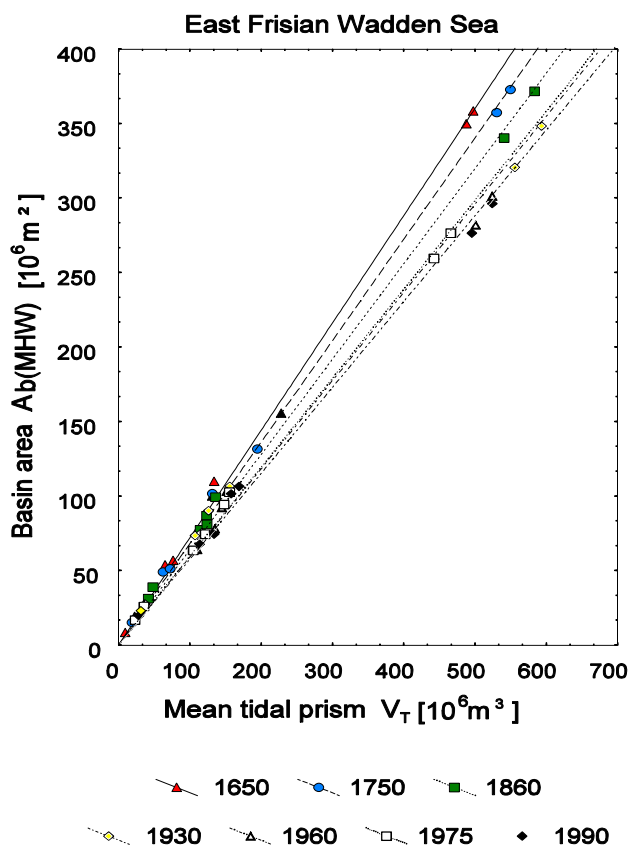


Figure 16. Correlation of total basin areas A_b and tidal volumes V_T since 1650

In order to get a deeper insight into those documented long-term morphodynamical processes occurring at the East Frisian coast since 1650 this relationship has also been adapted to the evaluated parameters being available for all situations from 1650 to 1990 beside that one of 1912 for which not a complete data set was available. Though the incorporated assumption of a dynamical equilibrium could not be assumed as valid for the situations between 1650 and 1860 the relation e. g. between tidal volumes and intake areas of the basins are for all situations rather strict (fig. 16). In respect of the experience gained from recent data [EYSINK 1979, 1991] this result is not trivial, because these data sets incorporate also a variation in tidal range due to its regional differences. Looking at the data sets from 1960, 1975 and 1990 including also the subsystems of the tidal basins for the same parametrization for the East Frisian Wadden Sea this effect is evident only for the larger values of 1990 (fig. 17). A first explanation of this discrepancy is the only use

of data for midterm developments: As tidal ranges varies to a much lesser extent than for the long-term time scale, statistical scattering is of the same or even bigger order of magnitude than the structural differences due to tidal range variation.

Further emphasis will be laid on finding a reliable explanation and detecting the mechanism steering that process. The solution to this problem is of high importance because these relations provide the basis for conceptual or empirical model like the Box-model of VAN DONGEREN & DE VRIEND [1994] being up to now the only promising tool for morphodynamical modelling of

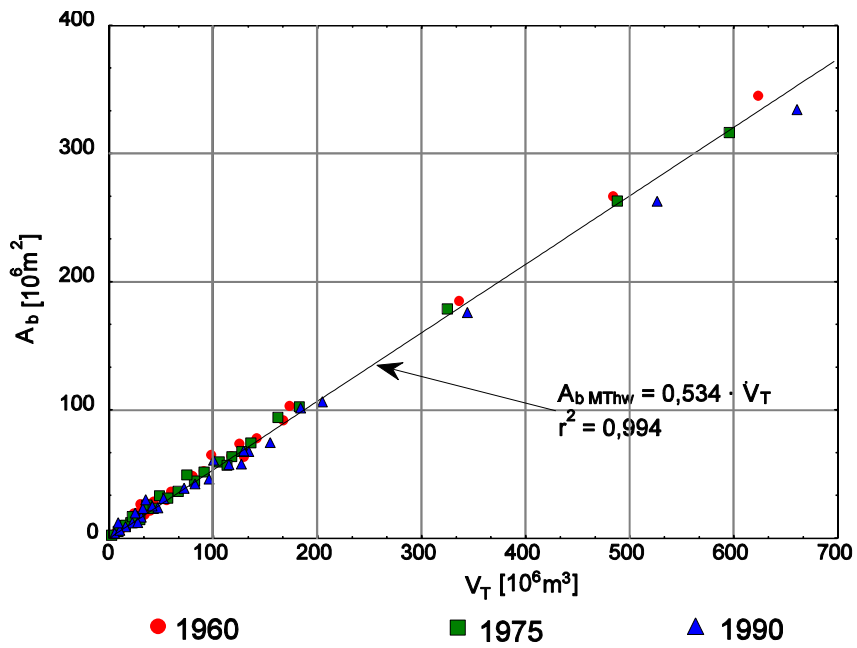


Figure 17. Correlation of basin areas and tidal volumes for the tidal basins and subsystems in the East Frisian Wadden Sea (surveys 1960, 1975, 1990).

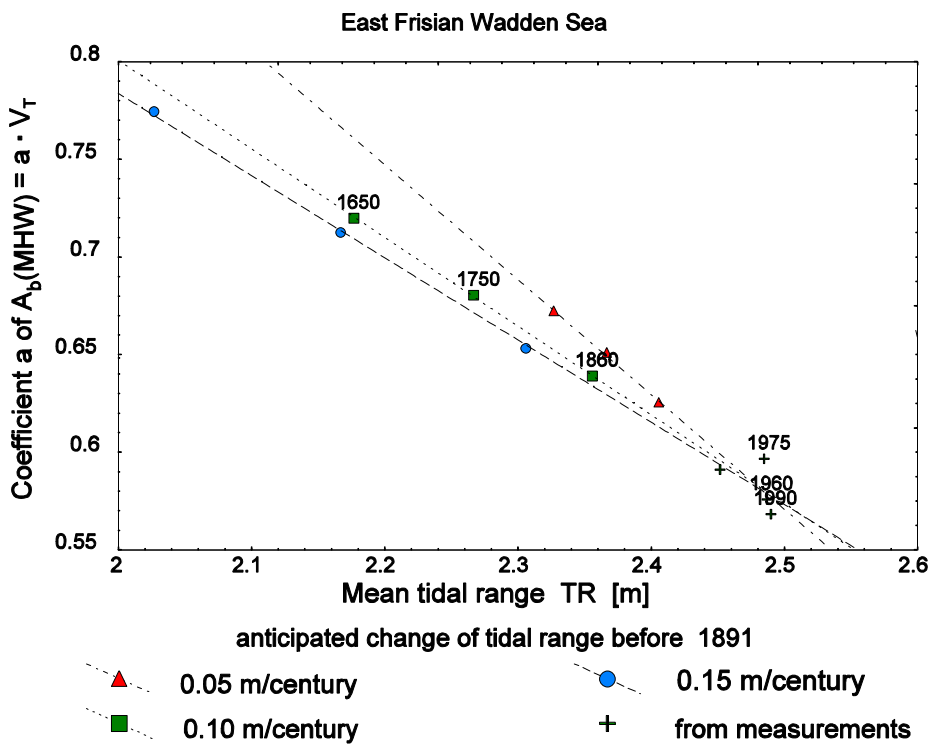


Figure 18. Correlation of the coefficient a from $A_b = a \cdot V_T$ with tidal range TR

future mid- and long-term development. A successful treatment will therefore deliver a valuable basis not only for current problems with structural erosion but also for the forecasting of prospected long-term morphodynamical processes due to changing boundary conditions like an expected acceleration of relative sea-level rise.

An obvious explanation would be a change of hydrodynamical boundary condition. Considering that possibility the changes of tidal range over the time were taken into account though no measured data before 1891 were taken into consideration and the figures for 1860, 1750 and 1650 were evaluated on the basis of an assumption. But this assumption is regarded as rather sound and in every case as a sufficient basis to look for indications for a qualitative change of empirical relationships for morphodynamics: The data reflect a pronounced correlation of the factor a of the relationship

$$A_b = a \cdot V_T$$

and tidal range TR (fig. 18). Obviously those correlations depend particularly on the anticipated change of tidal range before 1891. In order to estimate the effect of a misjudgement a variation of ± 5 cm per century is taken additionally into consideration. The result makes evident that the tendency of the correlation is still evident (fig. 18). Therefore it must be concluded that for long term investigations in the same area the variation of the tidal range must be taken into consideration in order to describe the relationship between total basin areas and tidal volumes with sufficient accuracy.

Conclusions

The resedimentation of storm surge bays at the East Frisian mainland coast has been a major steering impact of morphodynamical processes in five of the six tidal basins of the East Frisian Wadden Sea during the last centuries. As well the shifting of basin watersheds, the migration of inlets as the changes in size and position of the barrier islands can no longer only be credited to littoral drift. Furthermore they could not be regarded as a cyclic process which would have continued without the fixing of tidal inlets since the middle of the last century.

A reliable quantitative approximation of tidal volumes is also possible for the reconstructions of historical coastal morphology of Wadden Sea areas. The accuracy of these figures is sufficient for use in the framework of empirical relationships used for empirical and conceptual morphodynamical modeling. It has become evident that relationships being used for empirical or conceptual modeling which have been established for data sets covering only a period of a few decades or even less could not in every case be regarded as valid for long-term periods like centuries. This was demonstrated for the well known relationship of tidal basin areas and tidal volumes which is in the long run dependent on tidal range variations.

Acknowledgements

This work was carried out in the framework of the Dutch-German research project WADE (Wadden Sea Morphological Development in respect of an accelerated relative sea-level rise). The German part is sponsored by the GERMAN FEDERAL MINISTRY FOR RESEARCH AND TECHNOLOGY (BMFT) under contract no. MTK 0508. The author is very grateful to the assistance he got from colleagues of the CRS Section of Coastal Hydrodynamics: H. Alberts, R. Goldenbogen, T. Hartkens, R. Kaiser, W. Liebig, M. Puschmann and E. Schröder transferred the reconstructions of historical coastal morphology and recent maps into the GIS, extracted data and elaborated graphics. Finally it is urgently necessary to stress the fact that this kind of investigation was only possible on the basis of the reconstruction of historical coastal morphology being carried out successfully by the author's late colleague Hans HOMEIER between 1949 and 1980.

References

- EYSINK, W.D. [1979]:** Morphologie van de Waddenzee. Waterloopkundig Laboratorium, Rap. H 1336
- EYSINK, W.D. [1991]:** Morphologic response of tidal basins to changes. Proc. 22nd Int. conf. Coast. Eng. Delft, ASCE, New York
- HAYES, M.O. [1975]:** Morphology and sand accumulation in estuaries. **in:** L. E. Cronin (ed.): Estuarine Research, Vol. 2, Academic Press, New York
- HOMEIER, H. [1962]:** Historisches Kartenwerk 1:50000 der niedersächsischen Küste. Jber. 1961 Forsch.-Stelle f. Insel- u. Küstenschutz, Bd. 13
- HOMEIER, H. [1964]:** Beiheft zu : Niedersächsische Küste, Historische Karte 1:50 000 Nr. 5 .Forsch.- Stelle f. Insel- u. Küstenschutz
- HOMEIER, H. [1969]:** Der Gestaltwandel der ostfriesischen Küste im Laufe der Jahrhunderte. **in:** J. Ohling (Hrsg.): Ostfriesland im Schutze des Deiches, Bd.2. Eigenverlag, Deichacht Krummhörn
- HOMEIER, H. [1972]:** Beiheft zu : Niedersächsische Küste, Historische Karte 1:50 000 Nr. 4. Forsch.- Stelle f. Insel- u. Küstenschutz
- HOMEIER, H. [1979]:** Die Verlandung der Harlebucht bis 1600 auf der Grundlage neuerer Befunde. Jber. 1978 Forsch.-Stelle f. Insel- u. Küstenschutz, Bd. 30
- HOMEIER, H. & LUCK, G. [1977]:** Untersuchungen zur Nordstrandentwicklung von Borkum als Grundlage für den Inselerschutz. Jber. 1976 Forsch.-Stelle f. Insel- u. Küstenschutz, Bd. 28
- KRÜGER, W. [1911]:** Meer und Küste bei Wangeroog und die Kräfte die auf ihre Gestaltung einwirken. Zeitschr. f. Bauwesen, Jg. 1911
- KUNZ, H. [1991]:** Protection of the island of Norderney by beach nourishments, alongshore structures and groynes. Proc. 3rd Conf. Coast & Port Eng. i. Devel. Countr., Mombasa/Kenya
- LUCK, G. [1977]:** Inlet changes of the East Frisian islands. Proc. 15th Int. Conf. o. Coast. Eng. Honolulu, ASCE, New York
- LÜDERS, K. [1951]:** Die Entstehung der Ostfriesischen Inseln und der Einfluß auf den geologischen Aufbau der ostfriesischen Küste. **in:** Probleme d. Küstenforsch. i. südlich. Nordseegebiet, Bd. 5
- LÜDERS, K. [1977]:** Wangerooch hett'n hooge Toren, ... Jber. 1976 Forsch.-Stelle f. Insel- u. Küstenschutz, Bd. 30
- NIEMEYER, H.D. [1984]:** Hydrographische Untersuchungen in der Leybucht zum Bauvorhaben Leyhörn. Jber. 1983 Forsch.-Stelle f. Insel- u. Küstenschutz, Bd. 35
- NIEMEYER, H.D. [1990]:** Morphodynamics of tidal inlets. Civ. Eng. Europ. Course Prog. o. Cont. Educ. Coast. Morph., Syll. Delft Univ. o. Tech. Int.-Int. Civ. Eng.
- NIEMEYER, H.D. [1991a]:** Field measurements and analysis of wave-induced nearshore currents. Proc. 22nd Int. Conf. o. Coast. Eng. Delft, ASCE, New York
- NIEMEYER, H.D. [1991b]:** Case study Ley Bay: an alternative to traditional enclosure. Proc. 3rd Conf. Coast & Port Eng. i. Devel. Countr., Mombasa/Kenya
- O'BRIEN, M. P. [1931]:** Estuary tidal prisms related to entrance areas. ASCE, Civ. Eng., Vol. 1, No. 8
- STEPHAN, H.-J. [1994]:** Dünenabbrüche am Nordweststrand der Insel Borkum. Ber. Forsch.-Küste
- STREIF, H. [1994]:** Das ostfriesische Küstengebiet - Nordsee, Inseln, Watten und Marschen. Samml. geolog. Führer 57, Gebr. Borntraeger, Berlin/Stuttgart
- VAN DONGEREN, A. & DE VRIEND, H. [1993]:** A model of morphological behaviour of tidal basins. Coast. Eng., Vol. 22, Nos. 3,4
- WALTHER, F. [1972]:** Zusammenhänge zwischen der Größe der ostfriesischen Seegaten mit ihren Wattgebieten sowie den Gezeiten und Strömungen. Jber. 1971 Forsch.-Stelle f. Insel- u. Küstenschutz, Bd. 23



August 31 – September 05

Short Course on Morphodynamics

- **Ida Brøker**

Name - Date of Birth - Nationality Ida Brøker – 14 May 1958 - Denmark

Education Technical University of Denmark. MSc in Sediment Transport, 1982
Technical University of Denmark. Ph.D. in Sediment Transport, 1985

Present position Head of department for Coastal and Estuarine Dynamics, DHI

Key qualifications



Dr Brøker has a broad experience within sediment transport, sedimentation, morphological evolution in the coastal zone and shoreline management. She was employed at DHI in 1985 as a coastal engineer. She has been heavily involved in the development of DHI's numerical modelling tools for non-cohesive sediment transport and morphological evolution and has worked with numerous coastal projects world wide.

Dr Brøker is author or co-author of more than 40 papers on various aspects of sediment transport, morphodynamics in the coastal zone.

Dr. Brøker is a reviewer for the Journal of Geophysical Engineering and Coastal Engineering and an external examiner for MSc and Phd work.

Selected publications

Karsten Mangor, Ida Brøker, Dan Hasløv (2008): Water front developments in Harmony with nature. Terra et Aqua, number 111.

Brøker, I. 2008. The use of advanced numerical models to support the design of coastal structures. European Journal of Environmental and Civil Eng. *Revue Européenne de Génie Civil*. Vol 12 – No. 1-2.

Ida Brøker 2007: Human Interferences in Morphodynamics. Proceeding from IAHR Symposium on River, Coastal and Estuarine Morphodynamics; Twente, Holland.

Ida Brøker, Julio Zyserman, Erik Østergaard Madsen, Karsten Mangor, John Jensen: MORPHOLOGICAL MODELLING (2007): A tool for optimisation of coastal structures. Journal of coastal research, Vol. 23, Issue 5, Sept. 2007 pp 1148-1158.

Elfrink, B., Brøker, I. and Deigaard, R. 2000. Beach Profile Evolution due to Oblique Wave Attack. *ICCE 2000, 27th Int. Conf. on Coastal Eng., Sydney, July*.

Brøker, I., J.A. Zyserman and Per Roed Jakobsen: Thyborøn Coastal Investigations 1995.1996. New lessons from an old coastal problem. *ICCE'96, Florida, USA, 2-6 September 1996*.


Effects of coastal structures

-along sandy beaches
by
Ida Brøker, DHI


- Introduction by examples
- Coastal classification
- Various types of structures
 - Groynes
 - Shore –parallel breakwaters
 - Mega offshore schemes
- Structures on zero net sediment transport coast lines
- Structures on net sediment transport coastlines

Examples


Old coastal protection in Denmark...



Nearshore beach break waters



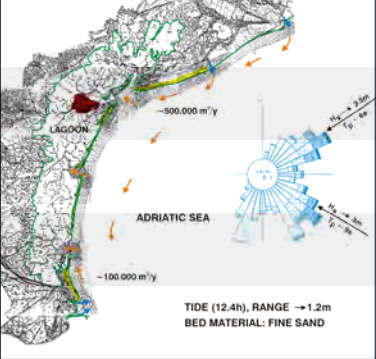
Groynes



Groynes, jetties, break waters

Examples

Jetties for regulation of tidal inlets, Venice



LAGOON
-500.000 m³/y
ADRIATIC SEA
-100.000 m³/y
TIDE (12.4h), RANGE → 1.2m
BED MATERIAL: FINE SAND

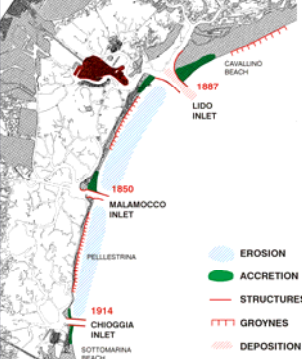
CONDITIONS BEFORE 1800

- Natural barrier island
- wide, low inlets
- equilibrium between supply from littoral drift and weak sea level rise
- lagoon with shallow mud flats, ell grass, deeper channels


Examples

Present conditions along the littorals

Natural beauty has been replaced by “engineered” beaches

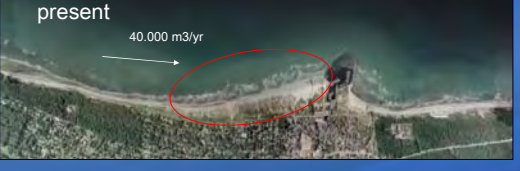


EROSION
ACCRETION
STRUCTURES
GROYNES
DEPOSITION





Harbour sedimentation – coastal impact

Example: Hornbæk harbour Denmark



present
40.000 m³/yr





1997

500 m

Coastal classification

Natural sandy beaches :

- Appearance determined by hydrographic conditions and geology
- Any interference with structures will cause a reaction in the form of a shoreline response

Reference: Karsten Mangor (2004): Shoreline management guidelines

Coastal classification

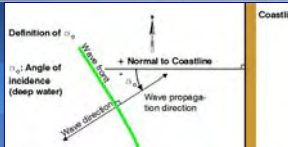
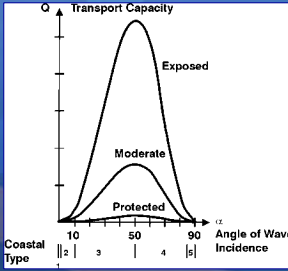
Consider:
Relatively long stretches of sandy beach (3-5 x width of surf zone)

Angle of pre dominant wave incidence:


1. Perpendicular
2. Nearly perpendicular, 1°-10°
3. Moderate oblique wave approach, 10°-50°
4. Very oblique wave approach, 50°-85°
5. Nearly coast parallel wave approach, >85°

Wave exposure

P. Protected, $H_{s, 12h/yr} < 1\text{ m}$
M. Moderately exposed, $1\text{ m} < H_{s, 12h/yr} < 3\text{ m}$
E. Exposed, $H_{s, 12h/yr} > 3\text{ m}$

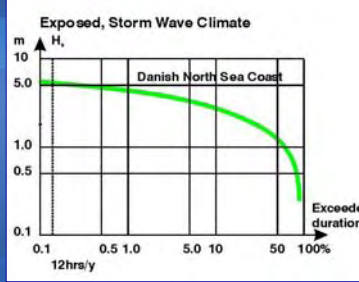



Coastal classification




Exposed, Storm Wave Climate

Danish North Sea Coast

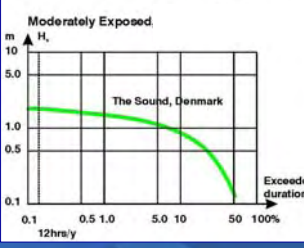


Coastal classification



Moderately Exposed

The Sound, Denmark



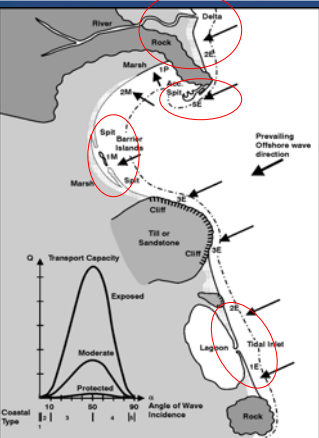
Coastal classification



Protected

2005 Mamzar beach

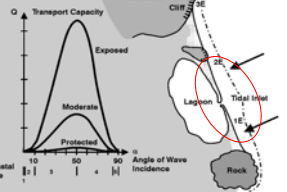
Coastal classification



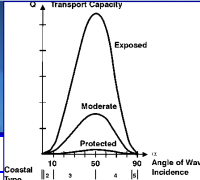
Delta stability depends on supply and exposure

Sand spits 5M-5E
• Very active!

Barrier islands, 1M-2E



Typical coastal characteristics

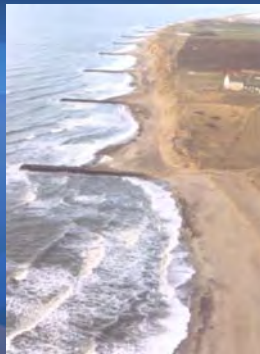


Coastal Type	Angle of Incidence (0° = shore normal)	Exposure	Main Coastal Characteristics
1P		Protected	Marshy
1M	0°	Moderate	Narrow stable sand beach, barrier isl., sand spits
1E		Exposed	Wide stable sand beach, barrier isl., sand spits
2P		Protected	Marshy
2M	1° < 10°	Moderate	Narrow stable sand beach, barrier isl., sand spits
2E		Exposed	Wide stable sand beach, barrier isl., sand spits
3P		Protected	Marshy
3M	10° - 50°	Moderate	Narrow unstable sand/shingle beach, cliff or dunes
3E		Exposed	Wide unstable sand/shingle beach, cliff or dunes
4P		Protected	Marshy
4M	50° - 85°	Moderate	Narrow unstable sand/shingle beach, cliff or dunes
4E		Exposed	Wide unstable sand/shingle beach, cliff or dunes, spits
5P		Protected	Marshy
5M	85° - 90°	Moderate	Sandy beach, accumulative land forms, spits
5E		Exposed	Sandy beach, accumulative land forms, spits

Groynes

Definition: Normally straight structures perpendicular to the beach, single or several in row in a groyne fields

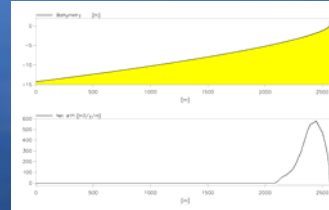
Works by blocking part of the littoral transport, their function highly dependent of coastal type. Causes downstream erosion



Function of Groyne Field

...depends on transport conditions

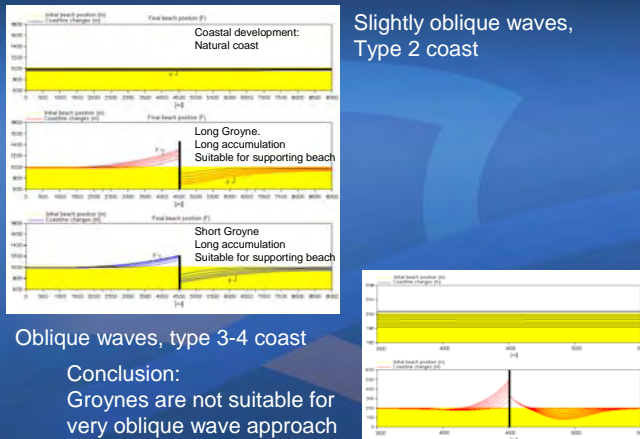
- Exposure decides width of transport zone
- Wave direction decides form of accumulation
- Groyne dimensions decides extent of interference
- Number of groynes decides length of protected area



Coastal profile

Transport distribution

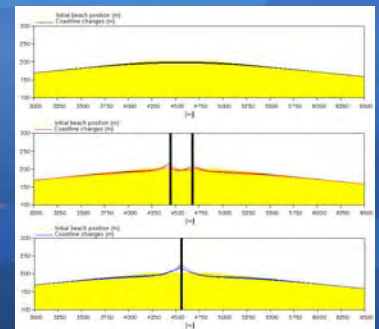
Groyne impact for different wave climates



Groyne impact for different wave climates

Groyne impact in a nodal area, zero net transport, with almost perpendicular wave approach and eroding coast

Conclusion: Groyne are not suitable for Type 1 coasts



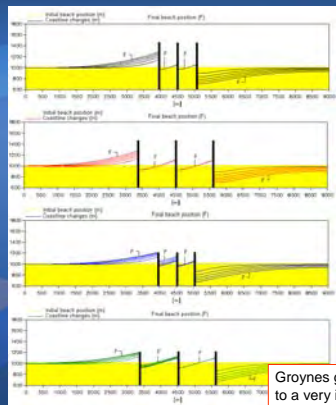
Groyne fields for a Type 2 Coast

Three long groynes spacing 500m

spacing 1100m

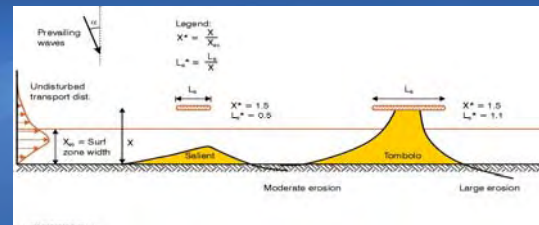
Three short groynes spacing 500m

spacing 1100m



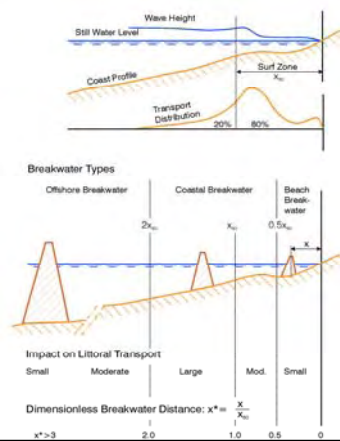
Groyne generally lead to a very irregular shoreline

Detached Breakwaters

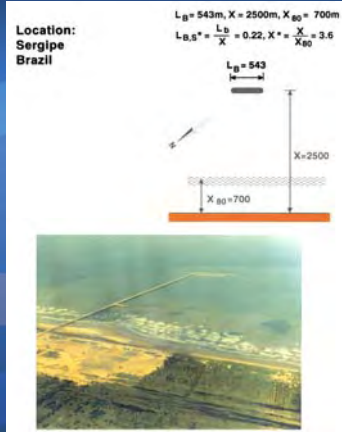


Rule of thumb for accumulation forms:
Salient when L_B is less than $0.6x$
Tombolo when L_B is greater than $0.9x$

Types of detached breakwaters



Offshore breakwater



Example from Sri Lanka, Negombo Coast. Protection Scheme

Coastal Breakwaters
Sand fill from Offshore Sources

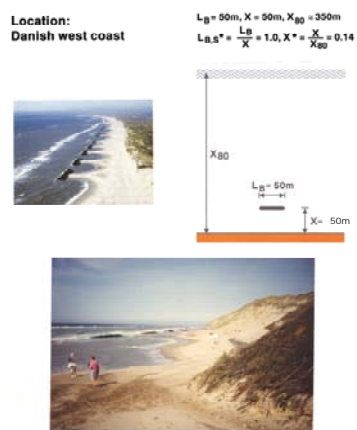
- Provides:
- Protection
 - Restoration of sandy beaches



Coastal Breakwater



Beach Breakwater



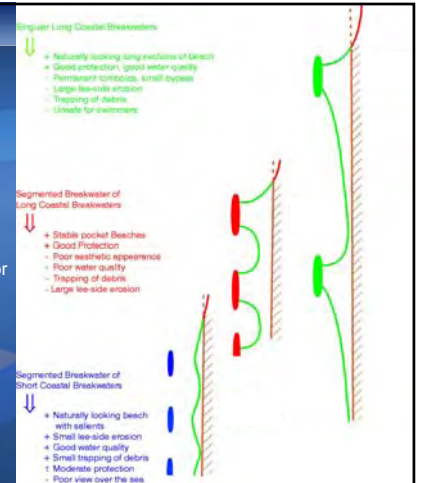
Sand accumulation characteristics for segmented breakwaters

Rules of Thumb:

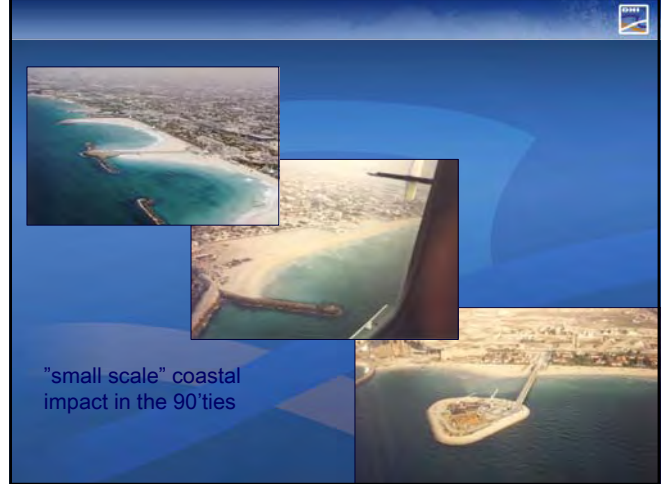
Breakwater most efficient for $X/X_{B0} = 1.1 - 1.6$

Tombolo formation for $L_B/X > 0.9$

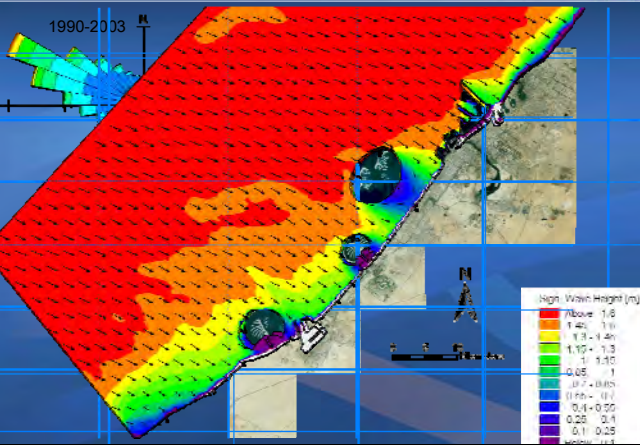
Salient formation for $L_B/X < 0.6$



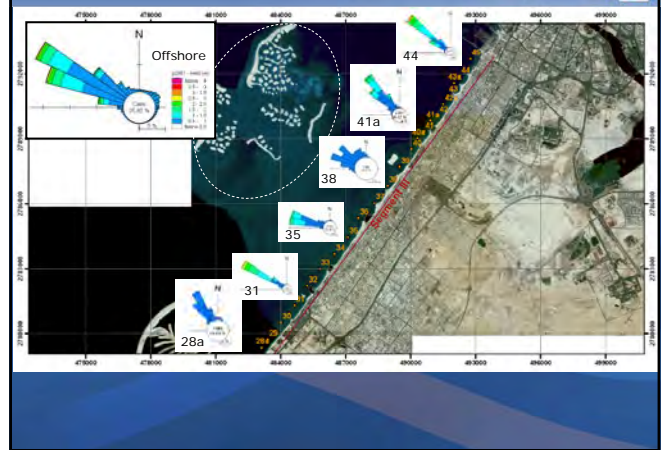
IMPACT from major schemes -example: Dubai



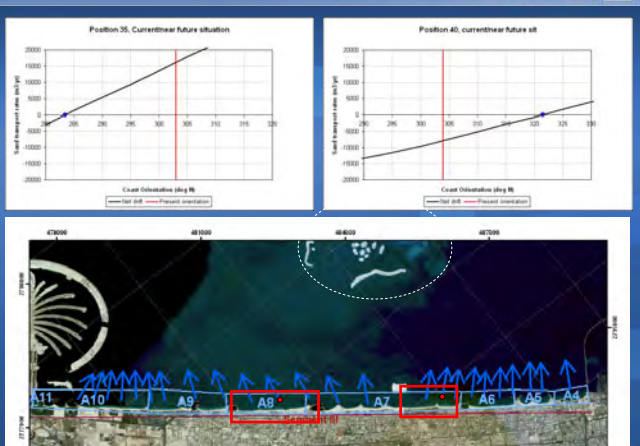
Wave transformation: Offshore wind/wave data via Nearshore Windwave Model to nearshore wave conditions



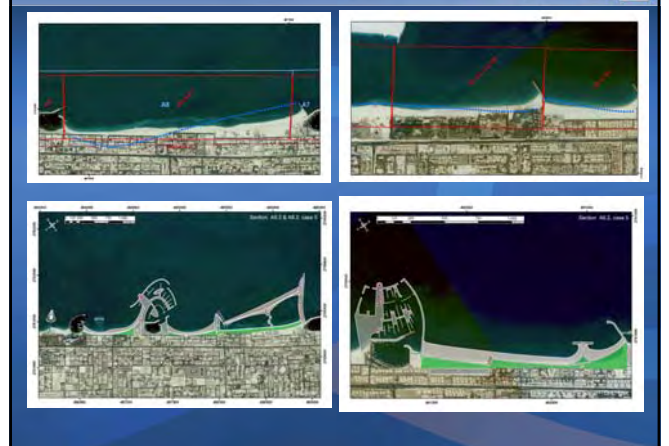
Wave transformation

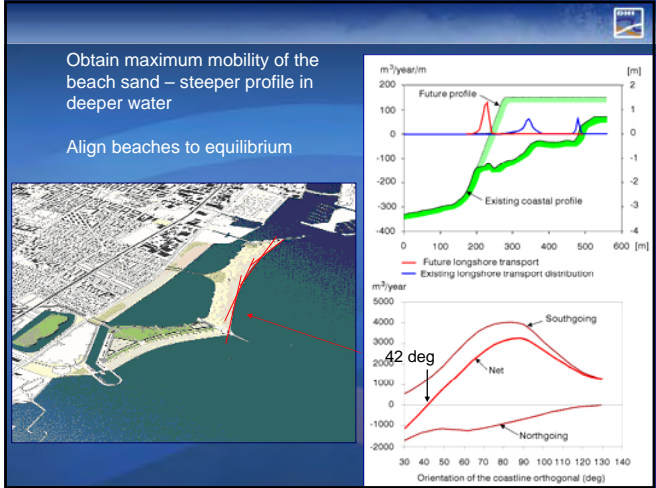
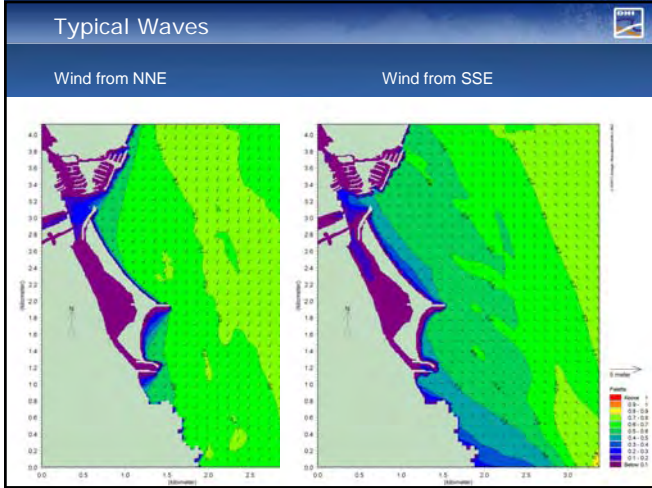
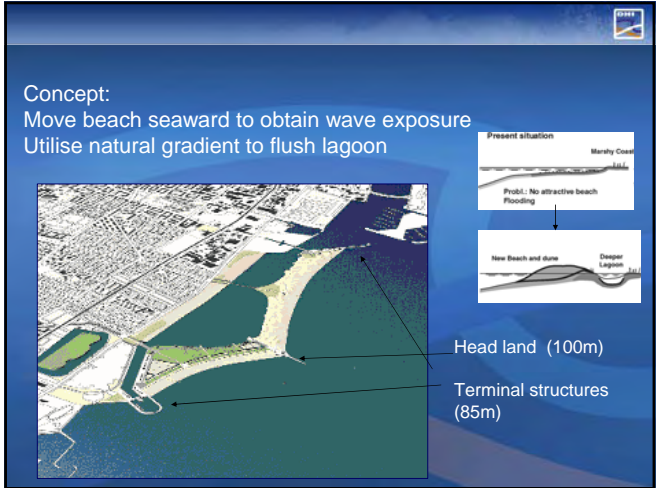
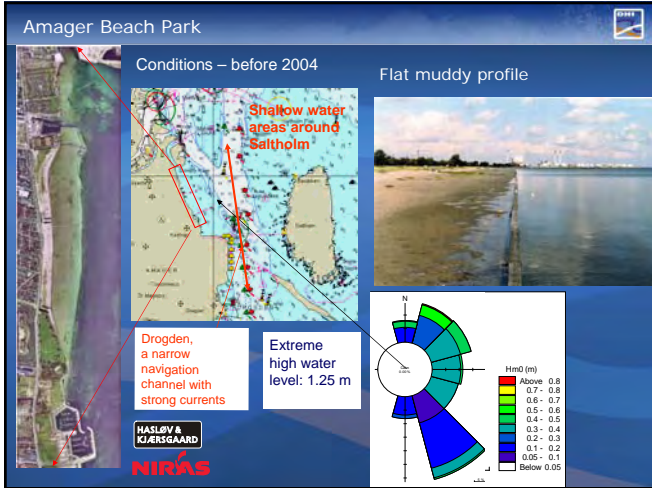
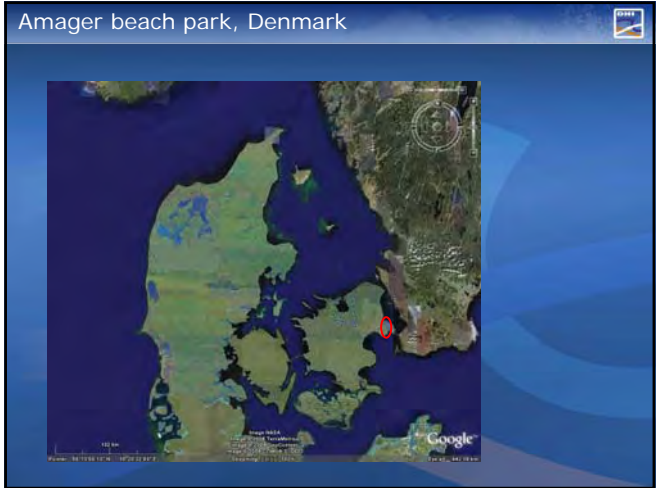
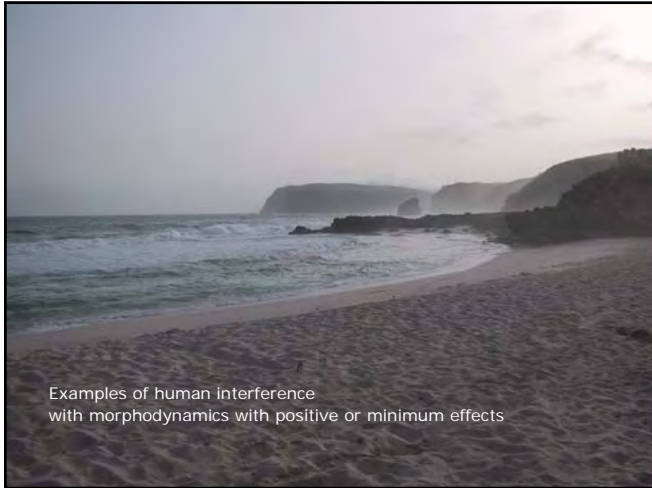


Sediment transport – equilibrium orientations



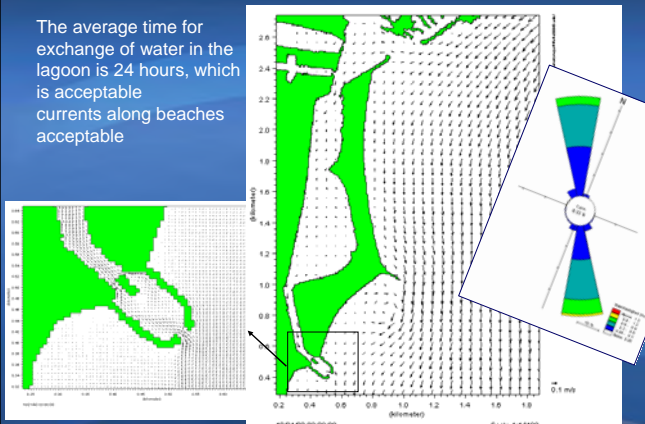
Potential shoreline evolution (20 years) – new schemes





Regional/local currents - flushing

The average time for exchange of water in the lagoon is 24 hours, which is acceptable currents along beaches acceptable



August 2005 – just after construction



Important understanding

Artificial beaches and lagoons obey the same rules as natural beaches and lagoons !

Good quality beaches are

- **always** exposed to waves
- Tidal range is moderate
- The water is clear and clean
- The beach material is medium to coarse sand
- But very exposed beaches are dangerous for bathing


Nice lagoons have

- Stable openings to the sea securing water exchange
- Good flushing in the entire lagoon
- Good water quality (minimum discharge of pollutants)
- Natural flora and fauna

note: Sandy beaches exist only if the lagoon is wide or semi open towards the sea


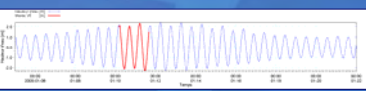
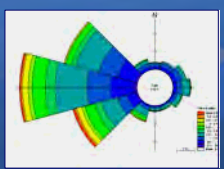
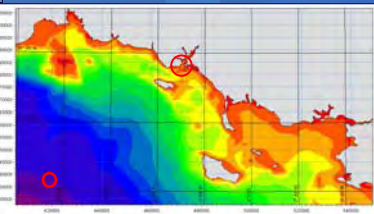



La Nourriguel






Hydrographic conditions

Pocket beaches with medium sand

Present conditions

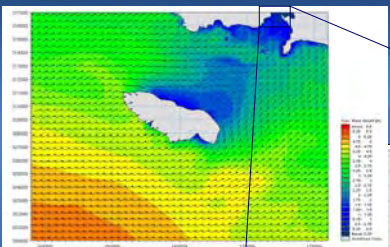
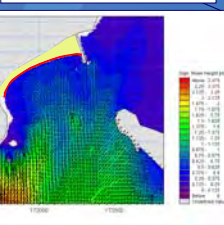




Bad weather ..

Regional and local waves

New artificial beach
Supported by headland
Aligned to dominant wave direction

Natural stable beach aligned to face the dominant waves





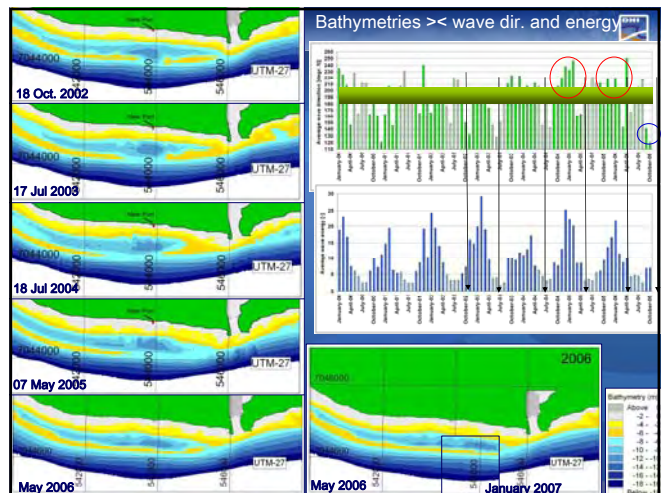
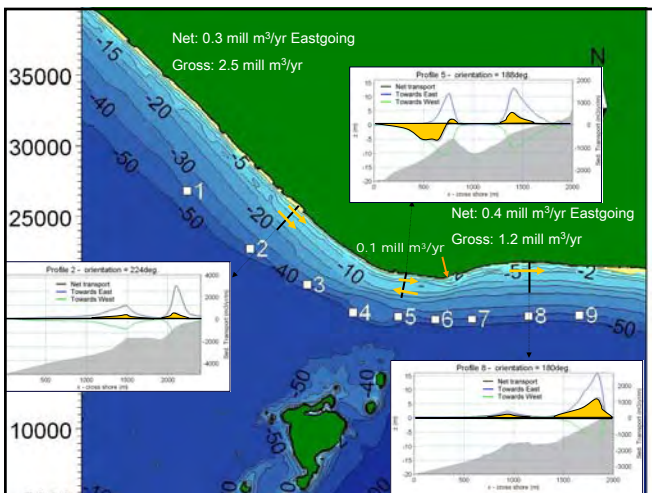
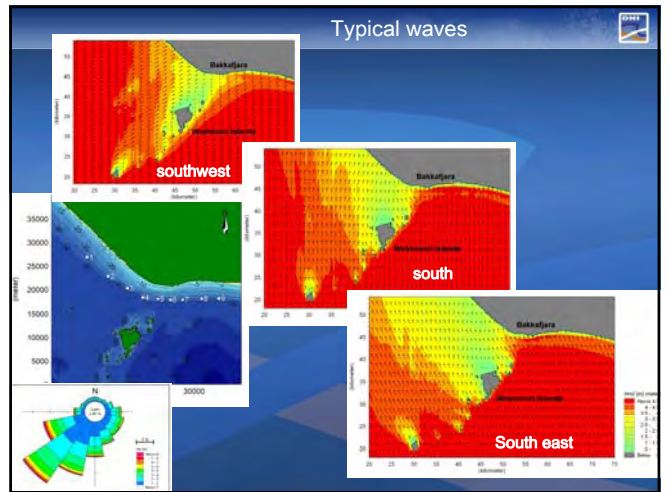
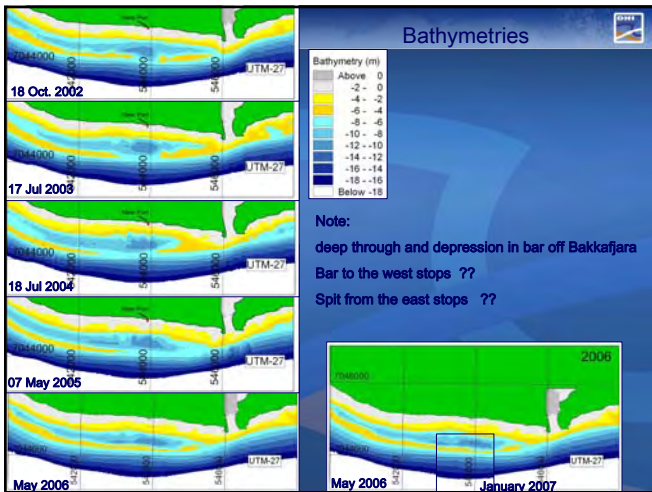
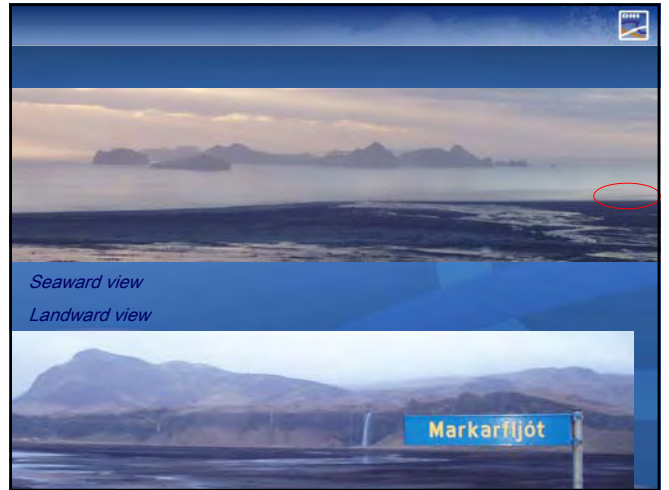
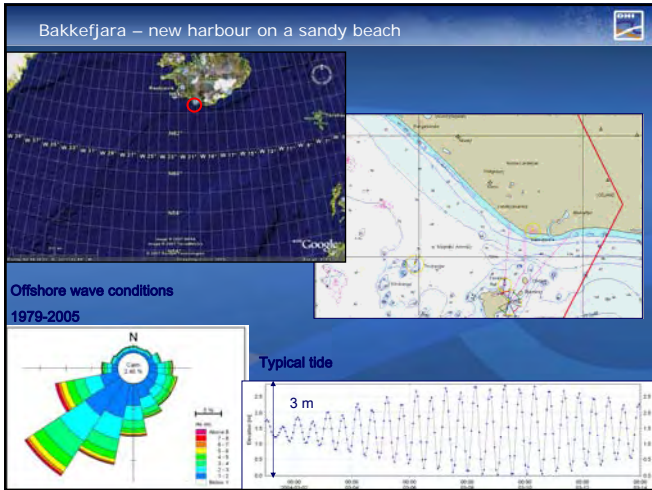
Present layout

Future layout

Wave, current and sediment transport modelling has supported the design of the future stable sandy beach and headland

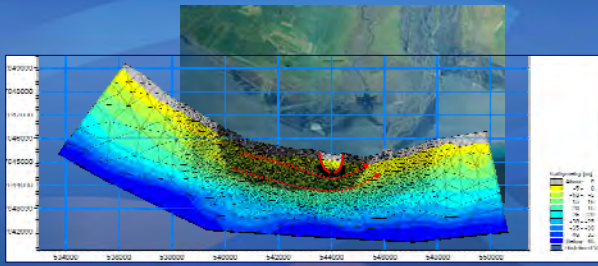
Sandy beach will dissipate wave energy before waves hit the wall

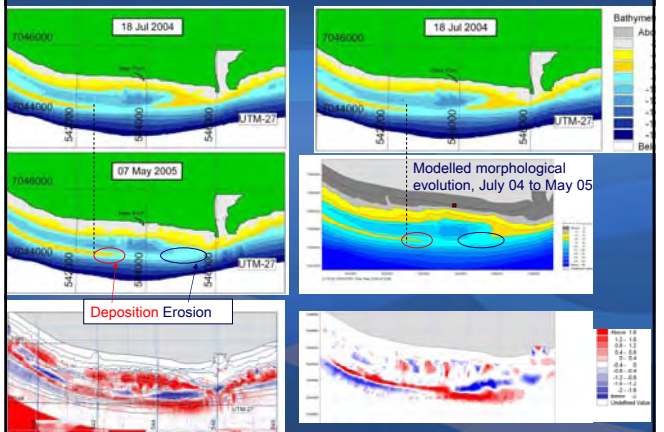


A harbour layout is needed which:

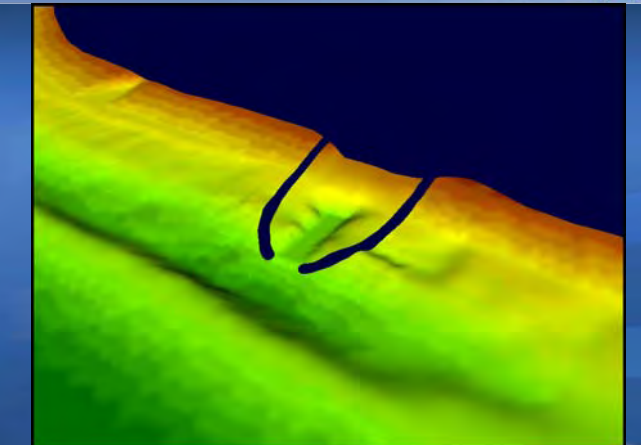
Results in minimum sedimentation and allows maximum natural by-pass and thereby minimum possible impact



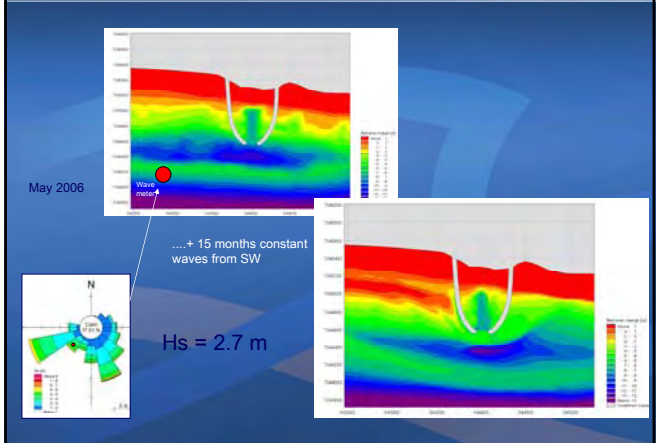
From the calibration/validation



Testing with morphological modelling



Equilibrium depth in front of the harbour



Understand nature - work with nature



Soft solutions - nourishment when possible



Tidal inlet:
Dredging and
artificial bypass

Maximum natural
sediment by-pass
harbour



Artificial beaches aligned to
the equilibrium orientation

Human interferences in morphodynamics

I. Brøker

DHI, Hørsholm, Denmark

ABSTRACT: The present paper discusses human interferences with the natural morphological development. Examples of negative impacts such as erosion, sedimentation or degradation of water quality in rivers, estuaries and coastal zones are presented. Further, examples are given, where human activities in sensitive environments have been successfully introduced. The examples are explained and documented using numerical models; however, emphasis in this paper is on the overall description of the morphodynamic processes.

1 INTRODUCTION

Over the past centuries increasing human activities have taken place along rivers, estuaries and coasts. Harbours are built with ever growing requirements to the water depth, rivers have been regulated to serve navigation purposes and provide fresh water for water supply, hydro power and prevent flooding and low lying land in estuaries have been reclaimed. Many projects have been initiated at times where the morphological processes and developments were not understood and in many cases not even thought of. Today consequences of human interferences are seen many places. Many negative effects could have been prevented had understanding and tools to do the analysis been available. Today engineers and planners work closely together in an attempt to in some cases make up for historical mistakes, or to combine the various requirements to the developments in the active coastal, riverine and estuarine environments and at the same time “work with nature” to make the most of the artificially created environment. The present paper shows examples of consequences of various activities in the morphodynamic environments as well as examples where modern planning and modern analysis tools have been applied to support the design of successful projects. The morphological consequences of sand mining and regulation of rivers, reclamation of land in estuaries, fixing of tidal inlets by structures, major structures in the coastal zone, land reclamations and harbours are discussed. Further, the paper shows an overview of the analysis necessary for the successful design of a harbour on a very exposed coastline and an artificial beach park. The analysis is supported by numerical modelling. The paper

therefore includes at the end a brief overview of the numerical tools applied.

2 MORPHODYNAMIC CONSEQUENCES OF VARIOUS ACTIVITIES

In this section effects on the morphology of various types of activities are discussed and illustrated by examples. The examples start in the “upstream” end with regulations of rivers and sand mining in rivers, continues with a brief introduction to projects in estuaries, in tidal inlets and ends with examples from the coastal zone.

2.1 *Sand mining and regulations of rivers*

Interventions in rivers take place all over the world where man need to control or use the natural resources. Interventions can be dams for collection of water for irrigation and water supply, dams for hydropower, dams for control of flooding along the lower parts of the river etc. etc. The regulations of rivers often led to unwanted effects and in previous time also unexpected negative side effects. Many of the World’s bigger rivers not only discharge water but carry loose material, stones, gravel, sand and fines from the hinterland down to the coastal zone. Some places large deltas have been built up by alluvial deposits which are eroded in the mountains or washed away by the rain on the ground and have been transported to the sea during heavy rain falls or melting of snow in the mountains. The coast lines and bed contours around a delta adjust in such a way that the wave action on the coastal zone transports the supplied material away to the adjacent beaches. Such coast lines are in a dynamic

equilibrium with a yearly supply of sand and therefore adjusted to an orientation of the coastline compared to the incoming waves, which corresponds to littoral drift away from the delta of the same order of magnitude as the supplied amount of material. Decrease in the supply has serious consequences. One of the most famous examples is the regulation of the Nile River, which was made to avoid floods, to improve irrigation and to provide hydropower. The regulations led to coastal erosion of up to 200 m/year at certain stretches due to lack of supply of sediment. The example presented in the following is taken from the southwest coast of Sri Lanka and is a part of the basic analysis for the development of shoreline management plans for the area.

The sand mining in and the supply from the catchments to three major rivers around Colombo have been quantified for the period 1976-2001, see Figure 1 for a location map. The result of the analysis and the deficit in supply to the coastal zone are presented in Table 1.

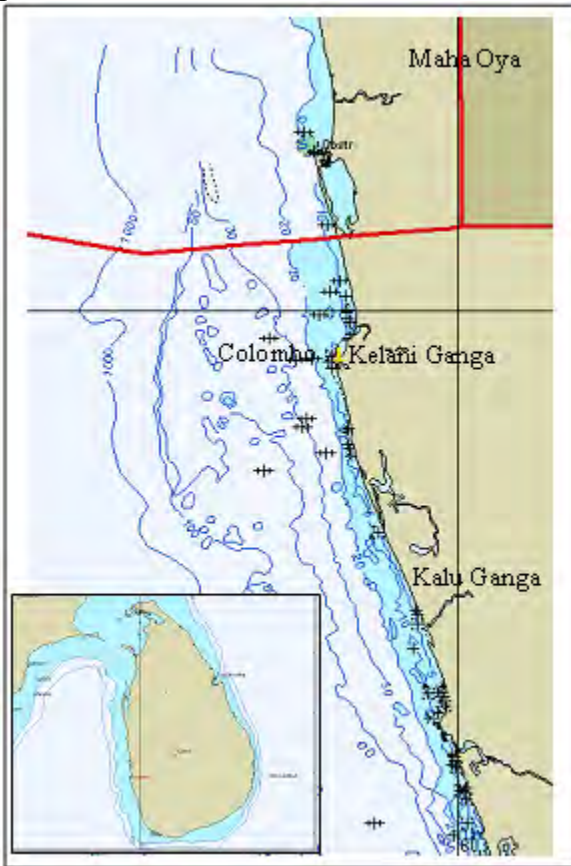


Figure 1. Location map, three major rivers in Sri Lanka.

Table 1. Sand mining, catchments supply and deficit in mill. m³ for the period 1976-2001.

River	Sand mining	Catchments Supply	Deficit
Maha Oya	23.0	5.0	18.0
Kelani Ganga	32.0	7.5	24.5
Kalu Ganga	12.0	10.0	2.0

The supply to the coastal stretch between the three rivers (approx. 100 km) has been reduced by 44.5 mill m³, which correspond to approx. 50% of the natural supply, due to sand mining.

The consequences of the sand mining have been the following:

Immediate effects:

- river bed degradation
- bank erosion

Long term effects:

- Coastal erosion
- Lowering of water table
- Increased saline intrusion

Bank erosion and coastal erosion in the area are shown in the photos in Figure 2.



Figure 2. Illustrations from Sri Lanka: upper photo: river bank erosion, lower photo: coastal erosion at the southwest coast.

2.2 Reclamation of land in estuaries

Through centuries estuaries and tidal lagoons have been placed where man has settled. Harbours have been built and the hinterland has been utilized more and more intensively for agriculture. Typically, estuaries include large shallow water areas, which can easily be reclaimed and turned into land. Estuaries are at the same time often morphologically very dynamic areas. The tidal inlets are in a state of dynamic equilibrium where the tidal exchange through the inlet is sufficient to flush the inlet area and maintain sufficient cross-section area to withstand backfilling of the inlet area by littoral drift along the open coast.

The mechanisms and the effect of changing the tidal prism by reclaiming land in the estuary are illustrated by an example from Portugal. Figure 3 shows the Obidos Lagoon on the very exposed west

coast of Portugal. The tidal range is 2.4 m and the gross littoral drift on the sandy Atlantic coastline is approx. 1 mill. m³/yr. In historical times the lagoon covered an area about 3 times larger than today and extended about 15 km inland compared to about 5 km today. The changes in tidal prism are due to mainly reclamations of shallow water areas. The result is a decrease in flushing capacity. The littoral drift from both sides is trapped in the inlet and is not flushed out by the tidal exchange.

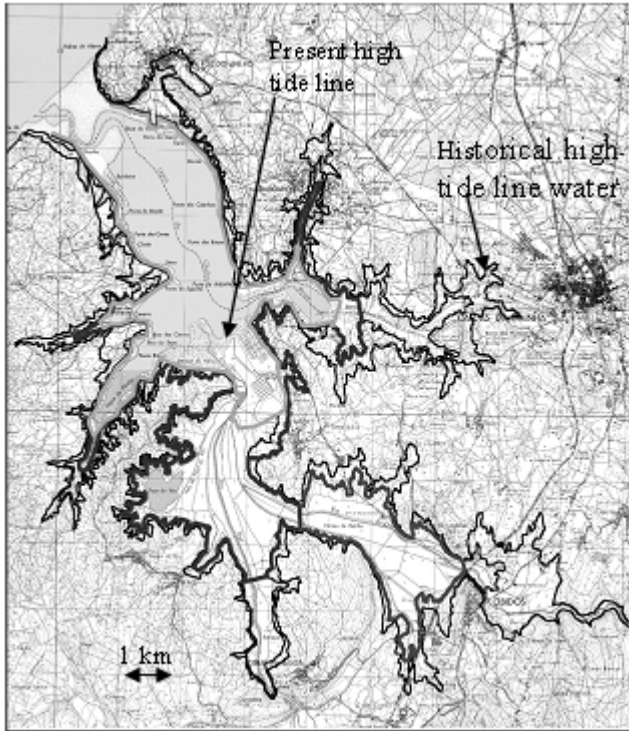


Figure 3. Obidos Lagoon, Portugal. Historical and present high tide lines.



Figure 4. The sand bar built up across the entrance to Obidos lagoon during severe northwesterly storms.

After the severe winter storms the lagoon may be completely separated from the Atlantic sea with the consequences that the lagoon is not navigable and the water quality of the lagoon is deteriorated. The photo in Figure 4 shows the sand bar built up across the entrance during a series of northwesterly storms.

2.3 Regulation of tidal inlets

Various interventions to prevent sedimentation in the entrance to Obidos lagoon were evaluated in connection with the restoration. One option was the construction of jetties to fix the entrance. This is a solution which has been chosen at numerous tidal inlets worldwide and is a measure to secure navigation into the lagoon. However, the impact on the morphology of the adjacent beaches can be dramatic and cause other problems. In case of Obidos the proposed jetties were not chosen because the impact on the adjacent beaches might get out of control. The Venice lagoon is a well-known example of fixed tidal inlets, see Figure 5.

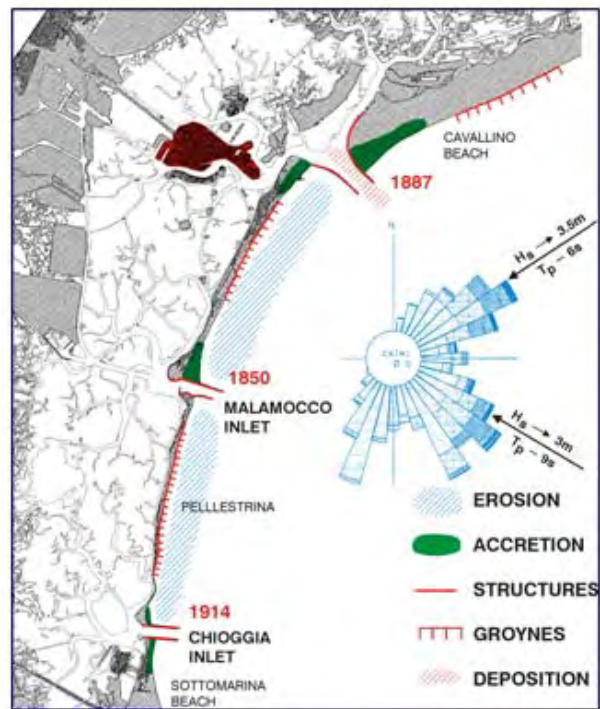


Figure 5. The Venice lagoon and the three inlets with the long jetties.

The jetties were constructed between mid eighteenth hundred and beginning of nineteenth hundred. The jetties were long, up till 4 km and with an inlet width up till 1 km. The littoral drift is northgoing south of the southern jetty and southgoing to the north of the northernmost jetty. The jetties blocked completely the littoral drift and during the years after construction the beach north of the northern jetty accreted by more than 2.5 km. At the time when the beach reached the tip of the northern jetty and sand started to bypass the jetties the offset in the coastline from updrift to downdrift of the northern inlet was about 3 km. The sand, which is not trapped inside the inlet, is deposited on ebb shoals and does not supply the downdrift beach. The central parts of the beaches between the three inlets have suffered from erosion since the construction of the jetties as sediment is either caught in the corners at the jetties or lost to offshore due to rip currents along the jetties. Huge protection schemes have

been established to fix the narrow sandy barrier islands. Clearly, the jetties have provided safe navigation, but at the same time introduced coastal erosion problems, which were probably not foreseen at the time of construction.

Grådyb, Denmark is an example of a tidal inlet placed between two sandy barrier islands facing the North Sea, where navigation has been secured not by hard structures but by dredging and maintenance of a navigation channel. A sediment trap is dredged on the north side of the channel and the trapped sand is moved artificially from the trap to the active nearshore zone on the downdrift site of the channel. The site is shown in Figure 6, which also shows the location of the sediment trap and the dredged channel. The water depth in the channel is maintained at 9.3 m with a minimum width of the channel of 200 m. The southgoing littoral drift is approx. 1 mill m^3/yr . This inlet is an example where a management solution has proven successful, which can be seen from the fact that the downdrift coastline has not suffered from erosion.



Figure 6. Grådyb inlet, at the Wadden Sea.

2.4 Major structures in the coastal zone, land reclamation and harbours

Many beautiful beaches which appear to be completely natural are actually the result of human activities in the coastal zone. One example is one of the most popular swimming beaches in Denmark, Hornbæk Beach on the northeast coast of Zealand, see Figure 7. In the late eighteenth century a small fishery port was built. The beach is sandy, with a littoral drift towards east of about $40,000 m^3/yr$. The little port was filled with sand shortly after construction and a sand filet built up on the updrift side. The main breakwater was extended a number of times until 1991 where the main breakwater was supplemented with a symmetrical downdrift breakwater. A very attractive natural looking beach has been built up during the 100 years since the first harbour was constructed, with a wide beach plane and sand dunes. However, it is all a result of human

interference. It is noted that the construction of the downdrift breakwater has actually reduced the dredging requirement to one third of what it was before the second breakwater was built and natural bypassing starts to take place, see the photo in Figure 7.

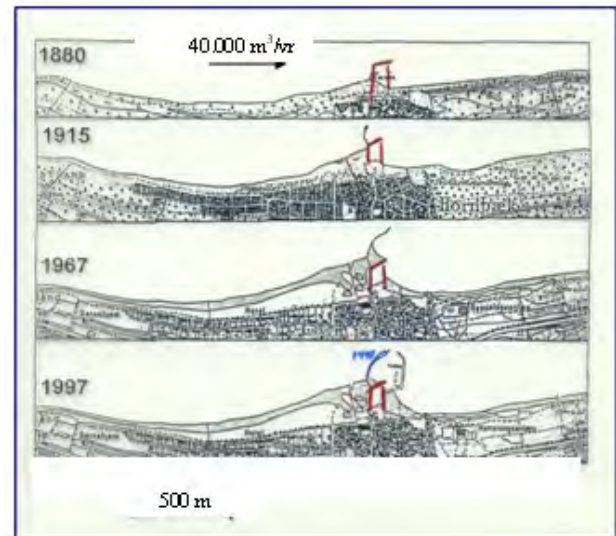


Figure 7. Location map, historical development of the coastline and the extension of the harbour. Oblique photo of the present harbour.

The next example of human interference with coastal morphodynamics is taken from Dubai, one of the fastest growing communities in the World. The natural coast is a straight sandy beach. The net littoral drift is northeast-going approx. $20-40,000 m^3/year$. Before the 90'ties the two major harbours, Jebel Ali and the Dubai Dry Docks and a number of small fishery ports were the only structures along the otherwise open sandy coast. The fishery ports

extended to 4-5 m of water depth and the coastline adjusted between the small harbours, which suffered from siltation. In the beginning of the 90'ties a shore parallel breakwater, a T-groyne and a curved breakwater were constructed as part of the enhancement of the recreational values of the Dubai coast to the south of the Dry Docks. Figure 9 shows the rapid response of the coastline to these structures: a tombolo developed behind the breakwater and sand was pushed to the corners of the T-groyne and the curved breakwater. The construction of Palm Jumeirah was initiated around the turn of the century. Since then The World Islands have been built and the two other palms are underway, see Figure 8. The consequences for the original coastline have been dramatic: The very big offshore structures have changed the nearshore wave climate to the extent where the littoral drift has changed direction along long stretches and the equilibrium orientations of the beaches have changed from about 10° anticlockwise turning compared to the original coastline to between 20° anticlockwise and 10° clockwise to the original coastline, see Figure 10. New coastal schemes must be developed along the entire frontage to accommodate the big changes to the nearshore wave conditions.

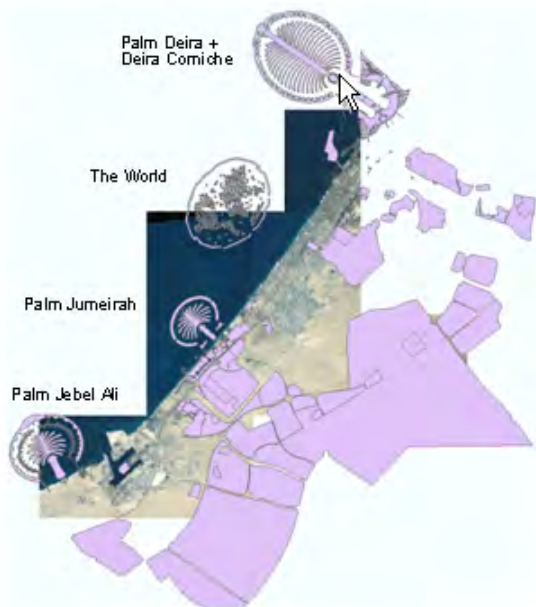


Figure 8. Sketch of the land reclamations along the Dubai coastline.



Figure 9. Shore parallel breakwaters and a small fishery port approx. 10 years after construction.



Figure 10. New equilibrium coastlines in the lee of The World Islands between the Palm Jumeirah and Dubai Dry Docks.

3 INVESTIGATIONS FOR A HARBOUR ON AN EXPOSED COAST, BAKKAFJARA, ICELAND

Westmann Islands is a group of islands about 5 nautical miles south of the south coast of Iceland. Bakkafjara is a location on Iceland immediately west of one of the outflows from melting of a glacier during spring and summer which supplies about 1 mill. m^3/yr fines and about 100,000 m^3/yr sand to the coastal zone. The offshore wave conditions are characterized by high waves that have been measured up to 16.7 m, see Figure 11. The river mouth and delta vary strongly from year to year. Storms from southeasterly directions push the river mouth to the west whereas southwesterly waves push the mouth to the east. The delta grows during periods of melting of the glacier. The tide is

semidiurnal with a maximum range of 3 m. The sediment in the coastal zone and on the beach plane is medium sand with d_{50} between 0.1 and 0.50 mm.

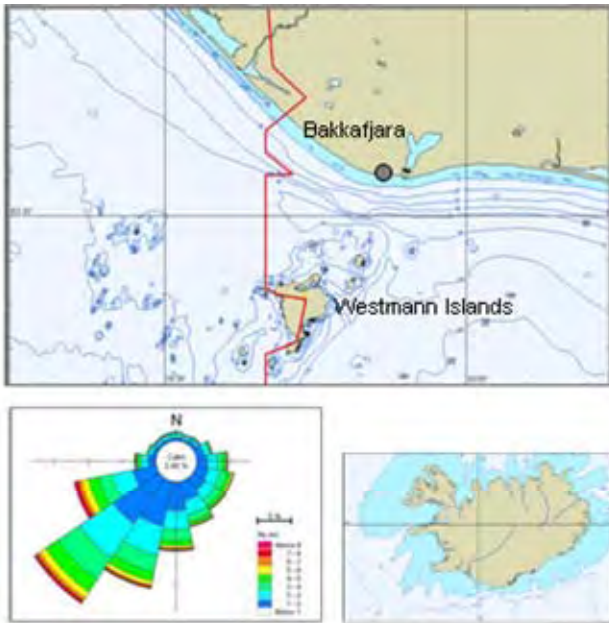


Figure 11. The location of Bakkafjara on the south coast of Iceland, illustration of the offshore wave statistics.

The preliminary location of the new harbour was selected based partly on analysis of the nearshore wave conditions, which showed that the Westmann Islands provide some shelter for the rough wave conditions along the coastline, and partly on the local fishermen's experience: off Bakkafjara there is almost "always" a deep trough and a depression in the bar, see Figure 12. The purposes of comprehensive hydraulic studies were

- To understand the physical processes, which determine the location of the depression in the bar
- To optimize the harbour layout to have minimum impact on the overall morphology and minimum siltation

The river mouth is known to be highly dynamic. A guiding wall will be established east of the harbour to avoid migration to the west of the river mouth. The stability of the river is therefore not part of the present study. Five measured bathymetries are shown in Figure 12. The depression in the bar and the trough are clearly seen. Further it appears that a well developed bar with a water depth of less than 6 m exists on the west side of the planned harbour location whereas the coast to the east of the river has got no bar.

The hydraulic studies have been initiated by transformation of the offshore wave conditions to the nearshore. Two examples of wave fields and the influence of the Westmann Islands on the nearshore wave conditions are shown in Figure 13.

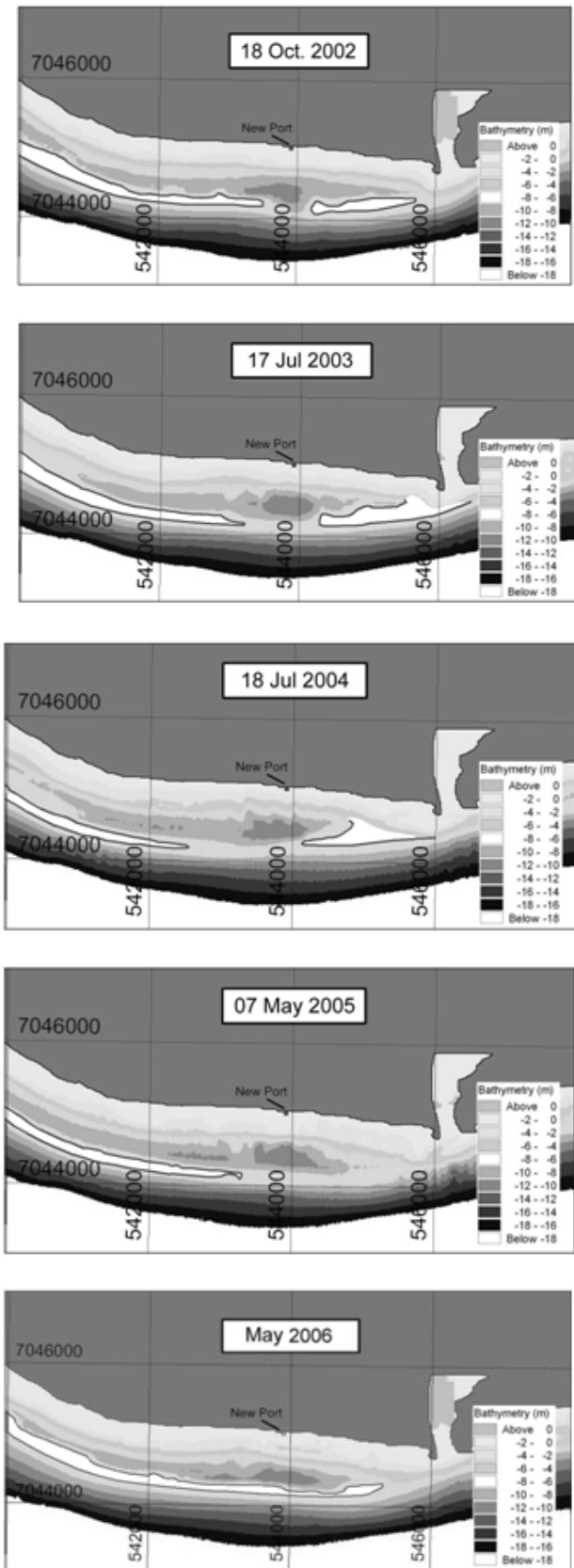


Figure 12. Bathymetries measured between October 2002 and May 2006. (6 m contour line highlighted).

Offshore wave data are available from hindcast studies starting in 1959. Littoral drift corresponding to the average wave conditions has been calculated using the assumption of long and uniform beach profiles. The overall sediment budget indicated a net eastward littoral drift west of the harbour location of approx. 300,000 m³/yr and approx. 400,000

m³/yr to the east of the harbour and the river. The river supplies in average 100,000 m³/yr of sand to the coastal zone.

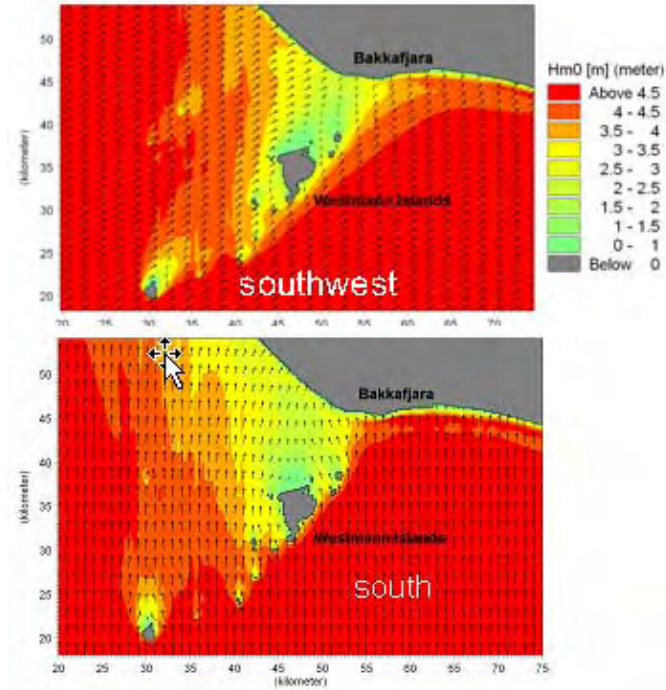


Figure 13. Results from the wave transformation study.

The distribution along the coastal profile of the littoral drift is, however, interesting: to the west of the harbour the littoral drift is eastgoing on the bar as well as along the inner part of the profile. To the east of the river the littoral drift is concentrated along the inner part of the profile as a significant breaker bar has not developed here. At the location of the harbour the net littoral drift is eastgoing on the inner part of the profile and westgoing on the breaker bar. This sediment transport pattern is due to the effect of the Westmann Islands on the waves. The most common southwesterly waves lead to eastgoing littoral drift along the entire stretch, but the eastgoing transport capacity decreases from west to east as one moves into the zone sheltered by the Westmann Islands. The most severe waves come from southeast. These waves pass behind the Westmann Islands and push the net littoral drift on the outer bar to the west. During years of dominant waves from southwest the western breaker bar will grow towards the east. During years of severe easterly waves the tip of the western breaker bar will be pushed back towards west. The calculated average distributions of littoral drift are shown in Figure 14 for three sections. The bathymetrical measurements show years where a “spit” has developed from the delta towards west, see Figure 12, and other years where the spit is non-existing. The spit develops after the growth of the delta during spring and summer followed by severe waves from southeasterly directions. It appears that the growth of the spit is dependent both on the supply of sand from the river and a long period of persistent southeasterly waves.

Analysis of littoral drift capacity during the period 1979-2006 has shown that no continuous event, or series of storms, has led to westgoing transport at the location of the delta of more than 500,000 m³, which corresponds to a few hundred metres of spit formation. The eastgoing littoral drift is more common and many events are registered where the littoral drift on the outer bar east of the harbour exceeded 150,000 m³. As seen in Figure 12 the outer bar has almost closed off the depression of the bar during the last few years. However, analysis of a long time series for average wave energy and direction of average offshore wave energy, see Figure 15

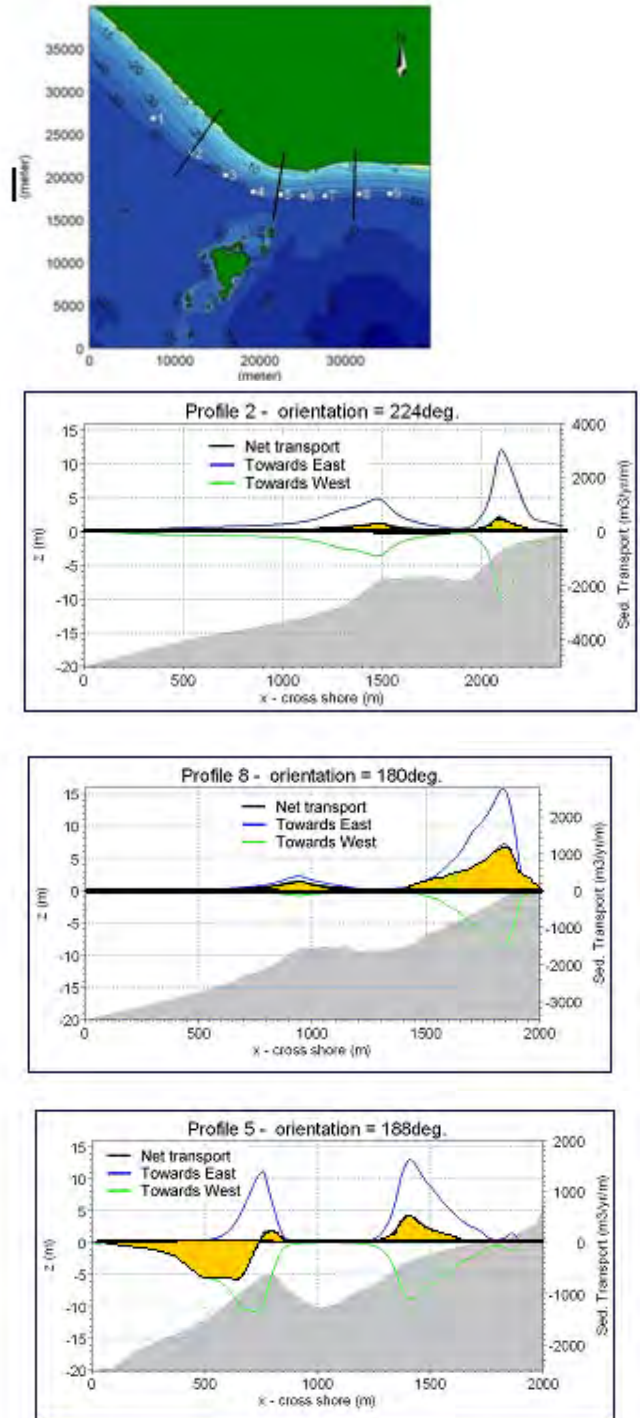


Figure 14. Average littoral drift and the distribution along the coastal profiles at locations west of, at and east of the planned harbour.

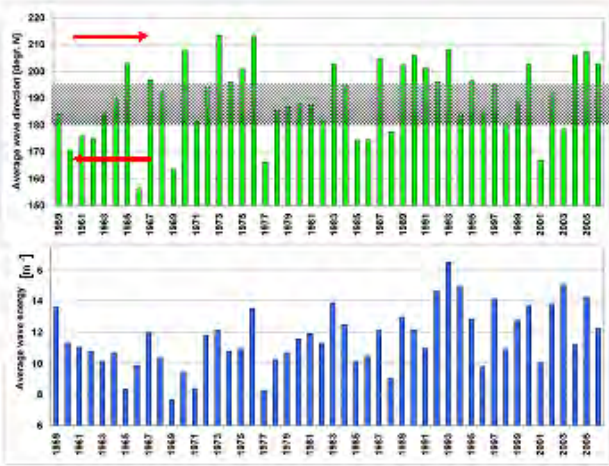


Figure 15. Average offshore wave energy direction and wave energy, 1959-2006. Eastgoing littoral drift at Bakkafjara for $dir > 195^\circ$ and westgoing for $dir < 180^\circ$.

clearly indicate that this is not the most common situation. In the past years there has been a series of years with high energy from southwesterly directions which led to lengthening of the bar from west towards east. Figure 16 shows the details of the variation of the two determining parameters wave energy and average wave energy direction during the period of intensive measurements. Figure 12 and Figure 16 can be compared and it appears that the dynamic behaviour of the depression can be explained. The risk of having to dredge through the outer bar has been evaluated and found acceptable for the project. It is noted that the required navigation depth is 6 m.

The planned harbour extends approx 700 m from the shoreline out to the present 8 m depth contour and is located at the deep trough. The morphological impact of the harbour on the trough and the adjacent nearshore bathymetry as well as the expected equilibrium depth in front of the harbour have been tested and optimised by a morphological modelling complex. The model complex reproduced currents due to tide and waves, wind generated waves, and sediment transport due to depth integrated currents, wave orbital motion, turbulence due to wave breaking, see a brief description in Section 5. Examples of results are presented in Figure 17. The upper panel shows the bathymetry measured May 2006 and the harbour layout. The second panel shows the modelled bathymetry after 200 days with constant severe waves from southwest, corresponding to a wave height of 3.7 m at 15 m of water depth off the site. It appears that the trough is not being back-filled but a sand feature will develop in front of the harbour. Due to the streamlined shape and the narrow entrance the majority of the sand will bypass the harbour and it appears that the impact on the adjacent coastline is very small. The bathymetry will adjust to a depth in front of the harbour which allows the sand migrating on the inner part of the coastal profile from the west towards the harbour to

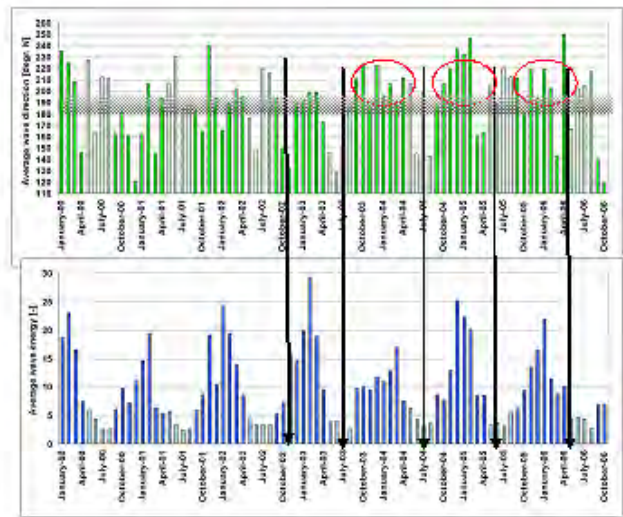


Figure 16. Average offshore wave energy direction and wave energy, 2000-2006.

bypass. The third panel in Figure 17 shows a close-up around the entrance. The development in water depth is shown in the fourth panel in Figure 17. The water depth in front of the harbour is seen to stabilise at around 6 m. The two lower panels in Figure 17 illustrate the development around the entrance in case the angle between the two main breakwaters is changed from 40° to 65° . The equilibrium depth is seen to be slightly deeper, more than 7 m in this case. Several combinations of wave directions and height have been modelled to support the design of the harbour. Further, the sedimentation of sand in the fore-harbour due to eddy exchange has been estimated as well as the sedimentation of fines during the periods where the adjacent river discharges large amounts of fine sediments.

The results selected for presentation in this paper illustrate the strength of the combination of analysis of the coastal environment, quantification of littoral drift for understanding of the overall processes and the detailed analysis of the processes around the new harbour for optimising the layout with regards to impact and sedimentation.

4 A SUCCESSFUL BEACH PARK, AMAGER BEACH PARK, DENMARK

Amager beach is located out to the Sound in Copenhagen, Denmark. The problem at this site is that the existing beach is of a poor quality (muddy shoreface) due to the lack of wave exposure. The site is only moderately exposed and the existing beach is further protected due to a very shallow shoreface, see Figure 18. A new beach park was recently built at this location. The project includes 2 km of new beaches and is located less than 10 km from the Copenhagen city centre. The main concept for the new beach park has been to move the beaches seaward beyond the shallow shoreface and thereby providing the highest possible wave exposure, which, however, is still moderate. The new beaches have been constructed on an island and a new lagoon (deepened) has been excavated between the island and the old shoreline. As the beach park is located near the gorge section of the Sound between Denmark and Sweden, there is always a good gradient on the water surface in the area of the beach park. This situation has been utilised to generate good flushing in the lagoon by making two openings, one at the northern and one at the southern end. The wave climate at the site is characterised by having two main directions, i.e. NE and SE, see Figure 18, which is due to the shelter provided by the island located just opposite of the site. This situation has been utilised to create two sections of beaches separated by a headland, one facing towards the NE and one facing towards the SE. The headland provides shelter at the NE facing beach for waves from the SE and shelter at the SE facing beach for waves from the NE, respectively, see Figure 19. The layout can be seen in and Figure 20.

The exact equilibrium shapes of the two beaches have been established based on modelling of a large number of wave conditions. The equilibrium orientations, i.e. orientations of zero net transport were calculated in a number of points along the coastlines. Finally, the shapes of the beaches were fitted to the series of equilibrium orientations. The length of the central headland is one of the parameters which were optimised through this process. The flushing of the lagoon was quantified by a depth-integrated hydrodynamic model. The average flushing time is about 24 hours, which will secure a good water quality. An aerial photo of the new beach park just after finalisation of the civil works is presented in Figure 20.

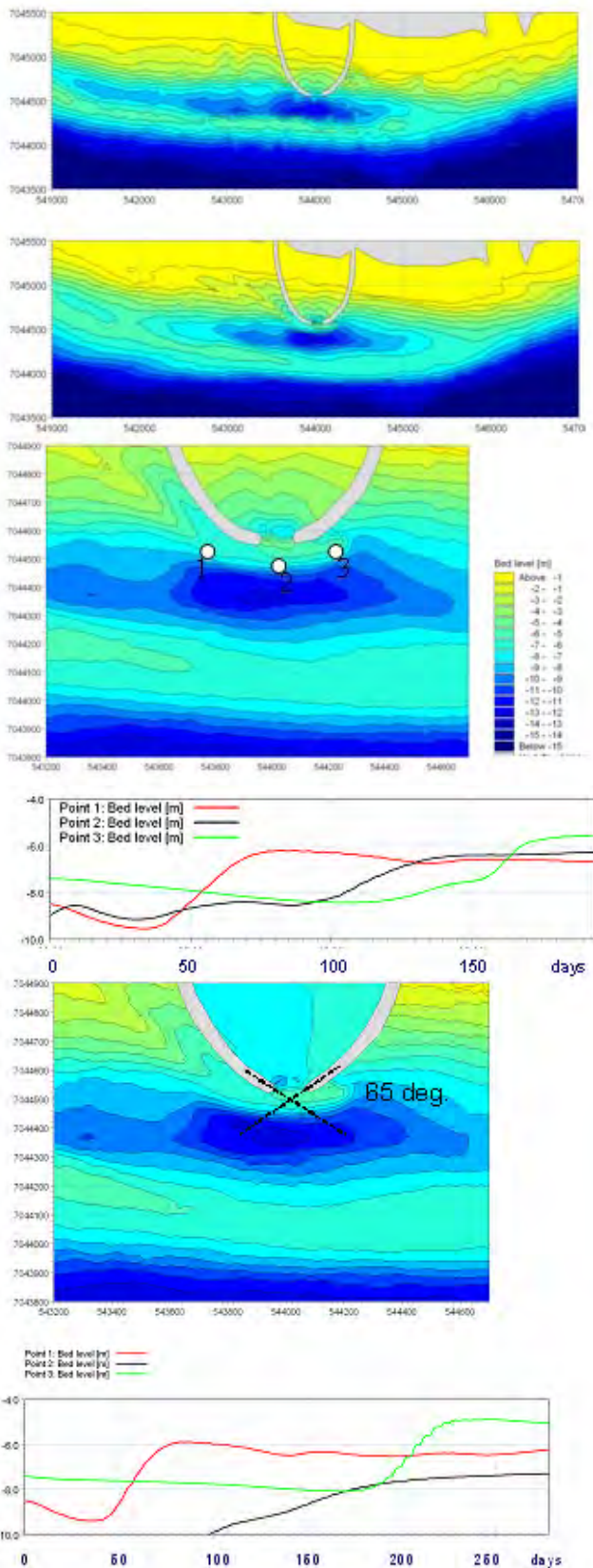


Figure 17 Upper panel: initial bathymetry, second panel: modelled bathymetry after 200 days of constant wave action and tide, third panel: close-up around the harbour entrance, fourth panel: morphological changes at three points off the harbour (see third panel), fifth and sixth panels: similar to third and fourth, but with an angle of 65° between the breakwaters compared to 40° .

5 BRIEF OVERVIEW OF APPLIED NUMERICAL MODELLING TOOLS

Over the past decades, numerical models have increasingly become support tools to shoreline management and design of coastal structures. The tools applied in the present paper are all developed at DHI and comprise:

- Littoral drift and shoreline evolution models suited for relatively uniform sandy beaches, which, given proper input on variability of the wave conditions along the shore and with time, cast light over the large-scale shoreline developments.
- 2-dimensional (in plan) wave and hydrodynamic models for the detailed study of waves and flow fields on complex bathymetries and in the vicinity of coastal structures.
- Quasi 3-dimensional model for sediment transport.
- Coastal area morphological modelling tool to appraise the short- to medium-term morphological response of the coast to for example coastal structures, harbours, shoreface nourishments etc.

The littoral drift and shoreline evolution model includes wave transformation, longshore wave driven currents, longshore and cross-shore sediment transport, shoreline evolution and coastal profile evolution. The bed contours are assumed to be parallel and quasi-uniform in the longshore direction and the waves and currents are considered to be quasi-stationary. These two basic assumptions limit the use of the tool to cases of long and uniform sandy beaches and cases where the shoreline evolution is the result of the overall gradients in the longshore sediment transport capacity. On the other hand, due to these assumptions, long coastal stretches can be covered over long time spans and the complex is a fast tool for calculation of equilibrium orientations of coast lines. See for instance Fredsøe and Deigaard (1992).

The two-dimensional so-called area model consists of a series of modules capable of simulating different wave-related, current and sediment transport processes. The following modules are currently most used for coastal morphological studies:

Wave models: still the very advanced wave models which include all important processes in the coastal zone are not fast enough to be applied in practical cases where many different wave conditions have to be considered. Very efficient wind wave models are, however, available and are excellent tools when diffraction is not a dominant process, Holthuijsen et al. (1989). Wave models based on the parabolic approximation to the mild-slope equation, Kirby (1986) have proven to be useful for smaller areas in the order of magnitude 10 by 10 km. Both models account for the effects of shoaling, refraction, breaking, directional spreading and bed friction. The mild slope models further include

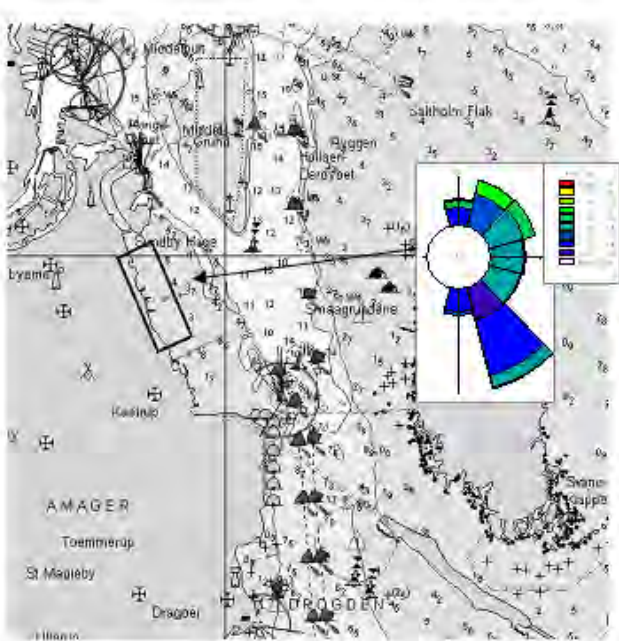


Figure 18 Amager Beach, Copenhagen, Denmark. Moderately exposed site with a protected beach due to a shallow shoreface.

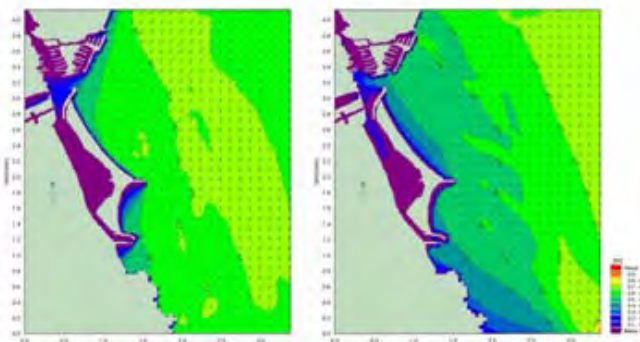


Figure 19. Modelling of wave patterns from the two main directions NE and SE.



Figure 20 Aerial photo of Amager Beach Park, which consists of the following main elements: island with terminal structures north and south and a separating headland between the northern and southern beaches and a lagoon.

partial diffraction and forward scattering, whereas the wind wave models include growth and decay of short-period waves and the effects of current may be included. In both types, the dissipation of wave energy due to breaking is parameterised. A much used approach is the model of Battjes and Janssen (1978).

The hydrodynamic model calculates the flow field from the solution of the depth-integrated continuity and momentum equations, Abbott (1979). In addition to wind and tide, the forcing terms may include the gradients in the radiation stress field as calculated by the wave module of the morphological modelling system. The currents and the mean water level are calculated on a bed evolving at a constant rate equal to $\partial z/\partial t$ as calculated by the sediment transport module.

The non-cohesive sediment transport model is used to calculate the transport rates of graded sediment and the rates of bed level change $\partial z/\partial t$ under the combined action of waves and current. The transport model for sand is an intra-wave period sediment transport model which calculates the total (bed load + suspended load) transport rates of non-cohesive sediment. The model accounts for the effects of waves propagating at an arbitrary angle to the current, breaking/unbroken waves, uniform/graded bed sediment, plane/ripple covered bed when calculating the local rates of total load transport, see e.g. Fredsøe (1984) and Deigaard et al. (1986). The model includes a quasi-3-dimensional description of the flow and the sediment transport, as described in Elfrink et al. (2000). Use of this approach allows calculation of net sediment transport rates both in the longshore and cross-shore directions.

Morphological modelling complex. The three above-mentioned models, waves, hydrodynamics and sediment transport are combined into a morphological modelling system, see Johnson et al (1994) and Johnson and Zyserman (2002). The model complex is developed both in a finite difference scheme which uses rectangular grids as well as a complex which uses a fully flexible grid, triangles.

6 CONCLUSIONS

The paper shows examples of negative consequences of human interference with morphodynamics as well as examples of projects where understanding of the processes and the quantification of the processes by advanced numerical modelling tools have led to successful projects.

The optimal use of numerical models can briefly be characterised as follows:

- Perform basic hydraulic studies utilising existing data and regional numerical models.

- Develop concepts for schemes by utilising the basic information on processes and the concept of "work with nature".

- Utilise detailed numerical models to optimise the hydraulic and coastal performance of the schemes including optimisation through minimisation of negative impacts.

7 ACKNOWLEDGEMENTS

The author has drawn on experience from various studies undertaken by the coastal and estuarine experts at DHI over the past 25 years.

The studies at Bakkafjara, Iceland have been undertaken as a collaboration between DHI and Eng. Gisli Viggósson, Siglingastofnun, Iceland.

8 REFERENCES

- Abbott M.B. 1979. *Computational hydraulics, elements of the theory of free surface flows*. Pitman, London.
- Battjes, J.A. and Janssen J.P.F.M. 1978. "Energy loss and set-up due to breaking of random waves". *Procs. of the 16th Int. Conf. On Coastal Engineering*, ASCE, 569-587.
- Brøker Hedegaard, Ida, Mangor, Karsten and Lintrup, Morten J. 1993: "Modelling of sediment transport in connection with tidal inlets". *Int. Colloquium and Exposition on Computer Applications in Coastal and Offshore Engineering (ICE-CACOE '93)*, Kuala Lumpur, Malaysia, June 14-16, 1993.
- Deigaard, R., Fredsøe, J. and Brøker Hedegaard, I. 1986. "Suspended sediment in the surf zone". *J. Waterway, Port, Coastal and Ocean Engineering*, 112 (1), ASCE, 115-128.
- Deigaard, R.; Fredsøe, J., and Brøker, I. (1986). "Mathematical model for littoral drift". *Journal of Waterway, Port, Coastal and Ocean Eng.*, ASCE, Vol. 112, No. 3, pp. 351-369.
- Elfrink, B., Brøker, I. and Deigaard, R. 2000. "Beach profile evolution due to oblique wave attack". *Procs. of the 27th Int. Conf. on Coastal Eng.*, ASCE, 3021-3034.
- Fredsøe J. 1984. "The turbulent boundary layer in combined wave-current motion". *Journal of Hydr. Eng.*, 110(8), ASCE, 1103-1120.
- Fredsøe J, Deigaard R. 1992. *Mechanics of coastal sediment transport*. World Scientific. Advanced series on ocean engineering
- Holthuijsen, L.H., Booij, N. and Herbers, T.H.C. 1989. "A prediction model for stationary, short-crested waves in shallow water with ambient currents". *Coastal Engineering*, 13, 23-54.
- Johnson, H.K.; Brøker, I.; and Zyserman, J.A. 1994. "Identification of some relevant processes in coastal morphological modelling". *Proceedings of the 24th International Conference on Coastal Engineering*, ASCE, 2871-2885.
- Johnson, H.K. and Zyserman, J.A. 2002. "Controlling spatial oscillations in bed level update schemes". *Coastal Engineering*, 46, 109-126.
- Kirby, J.T. 1986. "Rational approximations in the parabolic equation method for water waves". *Coastal Engineering*, 10, 355-378.
- Mangor, K. 2004. *Shoreline Management Guidelines*, DHI Water & Environment, 232p.

- Sørensen, T.; Fredsøe J.; Roed Jakobsen, P.(1996) *History and heritage of coastal engineering in Denmark* pp 103-141 ISBN 0784401969
- Vieira, José Rodrigues and Foster, Tom: Recovering the Óbidos Lagoon. An integrated management approach. *Med-coast*, 24-27 October 1999, Tarragona, Spain.

KARSTEN MANGOR, IDA BRØKER AND DAN HASLØV



WATERFRONT DEVELOPMENTS IN HARMONY WITH NATURE

ABSTRACT

The main development theme in many coastal countries is to utilise the attractiveness of water in a broad context. The emphasis has shifted from coastal protection to the development of coastal communities, with coastal resorts along existing coastlines. Waterfront developments as such are considered to be artificial pieces of new nature. The artificial beaches and lagoons, however, do not know that they are artificial. Consequently, these landscape elements will follow the natural marine and coastal processes resulting from the characteristics of the hydrodynamic forces on the coastal sediments, flushing and pollution loading to which they are exposed following construction. Therefore, understanding the prevailing natural processes responsible for creating attractive waterfront, beach and lagoon environments as a basis for the design of well-functioning artificial coastal and marine elements is essential.

This article focuses on providing a basic understanding of how to develop well-functioning coastal and offshore developments with regard to the hydraulic issues – for some the most desired elements in the modern waterfront developments, beaches

and lagoons. Design guidelines for *artificial beaches* and for *artificial lagoons* will be presented as well as guidelines for *recreational and landscape elements of coastal developments*. A holistic design of the new Amager Beach Park in Copenhagen is presented as an example of how a successful collaboration between the coastal engineer and the architect can lead to a sustainable new coastal landscape. Finally, a new type of offshore development scheme is presented, where the main idea is the development of an exposed crescent-shaped bay with a high quality beach, which could form the backbone for development of a coastal promenade. All photographs accompanying this article are by DHI or Hasløv & Kjærsgaard.

INTRODUCTION

The art in developing waterfront projects is to utilise the possibilities provided at a specific site to the benefit of the project, i.e., to integrate the possibilities provided by the marine environment with the demands of society. The art is to perceive

Above, Attractive natural, beaches such as the Skaw Spit in Denmark benefit from the natural wave action that keeps them clean and sandy.

the marine forces, such as waves and tides, as external opportunities to be used to maintain high quality artificial beaches and lagoons, contrary to the traditional approach of perceiving these external forces as problem generators, against which protection is required. The article is divided in the following sections:

- Characteristics of natural landscape elements
- Design guidelines for artificial beaches
- Design guidelines for artificial lagoons
- Landscape elements of coastal and offshore developments and their hydraulic design
- Example of beach park development
- Presentation of a new concept for an offshore development scheme

CHARACTERISTICS OF NATURAL LANDSCAPE ELEMENTS

Characteristics of natural beaches

Attractive and safe recreational beaches are always characterised by their exposure to moderate wave action, the tide is micro to moderate (tidal range < ~1.5 m), clean and transparent water, no rock outcrops, well sorted medium sand and minimal amounts of natural and artificial debris.



Figure 1. Other examples of attractive natural beaches with exposure to waves. Left: NW Mediterranean coast in Egypt. Right: Sunset Beach in Dubai, UAE.

Examples of attractive natural beaches are presented in Figure 1. These beaches are all characterised by their exposure to waves, their clean beach sand and their clean water. The type and colour of the sand is different, but all types are natural beach sand of great beauty and recreational value. The exposed beaches have a sandy and clean appearance owing to the wave action which prevents settlement of fine sediments and organic matter. However, there are also many examples of good quality beaches along coasts, where the water contains high amounts of suspended sediments, at least during the rainy season and/or during rough weather. This is, e.g., the situation along Malaysia’s East coast

and along Sri Lanka’s entire coastline. These beaches also remain clean and sandy, because they too are exposed to waves.

Natural beaches develop differently when they are lacking wave exposure. This is clearly seen in the examples presented in Figure 2 and Figure 3. These examples of exposed and protected natural beaches demonstrate that wave exposure is of paramount importance for the type of natural beach which develops in an area.

Clearly, one of the main hazards in relation to developing attractive artificial sandy beaches is lack of wave exposure. Lack of wave exposure on an artificial beach will

allow settlement of suspended matter on the seabed and on the beach, also in cases where the beaches have been built of clean sand. This will, with time, lead to the seabed being covered with a layer of soft sediment. Though this is a natural process, it is the main reason for poor quality of beaches found in protected environments. Such beaches feel muddy when walking on them, which is unattractive for recreational beaches.

Characteristics of natural lagoons

Natural lagoons are attractive from a recreational point of view owing mainly to the open water body they offer and not their beaches, which are normally of poor

Figure 2. Beaches lacking wave exposure. Left: Beach in a natural lagoon in the UAE, which suffers from algae and deposition of fine sediments. Right: “Beaches” in Dubai Creek.





KARSTEN MANGOR

holds a MSc from the Technical University of Denmark, 1972. He has worked for over 30 years with DHI in the fields of coastal hydraulics, shoreline and environmental management and waterfront developments. He is author of the book, "Shoreline Management Guidelines" and is chairman of the PIANC CoCom Working Group 2 on Best Practices for Coastal Stabilization Methods. He is presently Chief Engineer for Shoreline Management at DHI.



IDA BRØKER

obtained her PhD in sediment transport in 1985 at the Technical University of Denmark and joined DHI immediately after. She has been heavily involved in the development of DHI's numerical modelling tools for non-cohesive sediment transport and morphological evolution in the coastal zone and in numerous coastal studies worldwide. She is head of Coastal and Estuarine Dynamics Department at DHI.



DAN BORGEN HASLØV

is a partner in Hasløv & Kjærsgaard I/S, Architects and Planners, Copenhagen K, Denmark, and has wide experience in coastal zone planning as well as in planning and design in the fields of urban development, tourism, coastal rehabilitation and maritime facilities at local, regional and national levels.

quality. Coastal lagoons are characterised by the following elements:

- One or more so-called tidal inlets which connect the lagoon and the sea.
- Tidal exchange of water between the lagoon and the sea known as the tidal volume.
- Rich flora, such as sea grass beds, mangroves and meadows.
- Rich fauna such as mussel banks, nursery areas for many fish species and rich bird life.
- The openings are sometimes stable and sometimes suffering from sedimentation; this is dependent on the balance between the tidal range and the wave exposure.
- The lagoon environment is protected and is therefore often characterised by the settlement of fines, which in many cases leads to the formation of mudflats.

These natural conditions offer the following attractions:

- Protected water environment, which are traditionally used by coastal societies as a natural location for communities based on natural harbour facilities.
- Possibilities for a great number of commercial activities such as fishing, hunting, aquaculture, location for water intakes/outlets of different kinds and salt production for example.
- Recreational activities such as water sports, navigation in protected waters, fishing, bird watching and so on.

On the other hand, however, these communities as well as the many associated activities in the lagoons also contribute to the high risk of impacts on the lagoons, such as:

Figure 3. Examples of correlation between type of beach and wave exposure. Below left: Location "Map", North Beach in Doha, Qatar. Note, the southern part is protected by an island and associated reefs and has a muddy tidal flat beach (photo lower right) whereas the northern part is exposed and has a sandy beach (photo upper right).





Figure 4. Above: Marsa Matrouh Lagoon, NW Mediterranean coast of Egypt; red dot is photo location for photos below. Lower left: Semi-exposed sandy beach looking towards NW. Lower right: semi-exposed beach towards SE.

- Pollution leading to degradation of the water quality and associated degradation of flora and fauna.
- Installation of sluices leading to changes in the salinity and such.
- Reclamations leading to changes in the tidal volume.
- Regulation of inlets and dredging of navigation channels leading to changes in the tidal volume, which may lead to local erosion or general siltation.
- Navigation, which may lead to pollution and erosion and other impacts.

An example of an attractive lagoon environment is the semi-open Marsa Matrouh lagoon located at the NW Mediterranean coast of Egypt (Figure 4). This lagoon offers

attractive sandy beaches because of the wide opening towards the sea, which allows some wave penetration and good water quality. The breaking waves over the reef and shoals ensure a good exchange of waters.

DESIGN GUIDELINES FOR ARTIFICIAL BEACHES

The most important landscape elements in many waterfront developments are *attractive sandy beaches*. An artificial beach is the construction of a new beach by the supplying of sand, so-called beach fill. The design requirements for a good quality recreational beach are outlined below.

Beach exposure to waves

A beach will be exposed to waves in order to obtain a good quality beach. However, a recreational beach should not be too exposed, as this endangers bathing safety. This means that there are two opposing requirements:

- A certain degree of exposure to ensure a self-cleaning beach.
- The exposure should not be too great in order to ensure safe bathing conditions.

In order to safeguard an attractive sandy beach the yearly wave exposure should be moderate to exposed, which means that the significant wave height ($H_{s, 12hr}$), which is exceeded 12 hours per year, should be higher than 1.0 m. This consistent movement of the sand during rough conditions by the wave action is what naturally maintains a nice sandy beach and shoreface by preventing settlement of the content of fines, which are often present in seawater, on the beach and shoreface. Furthermore, the wave exposure prevents sea grasses from growing on the shoreface.

The difference between two artificial beaches in a beach park in the UAE area, where the first beach is exposed to waves and the second beach is a protected lagoon beach, can be seen clearly in Figure 5.

No internationally agreed criteria exist as related to wave height relative to safe bathing conditions. Bathing safety is mainly related to the occurrence and type of breaking waves and the wave-generated currents in the breaking zone. These conditions are discussed below.

Breaking waves

Spilling breakers are often associated with the formation of bars and rip currents, which can carry both adults and children out into deep water. This situation is typical for strong wind and storm conditions at sandy (ocean) coasts. Plunging waves are dangerous because the violent breaking can hit a person who is swimming. Plunging breakers typically occur on ocean coasts with moderate wave conditions, such as under monsoon and trade wind conditions on coasts with relatively coarse sand. Based on the above, obviously ocean coasts are



Figure 5. Left: An exposed artificial beach in the UAE is a nice clean beach owing to the wave action. Right: At an artificial beach in an artificial lagoon in the UAE, note the muddy seabed, which is caused by the lack of wave exposure. The lack of freshness can be clearly seen.

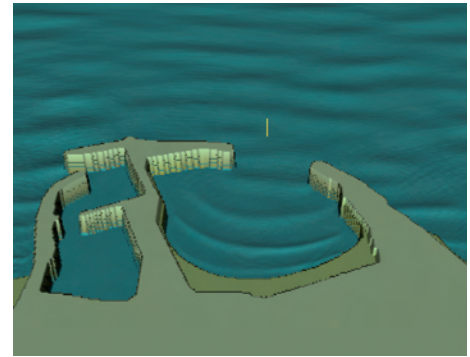


Figure 6. Modelled wave conditions at an artificial beach in Alexandria, Egypt. The design is made by DHI, Hasløv & Kjærsgaard and ECMA.

the most dangerous. However, if an upper limit for wave heights were to be recommended in relation to safe bathing conditions, an estimated criterion will be $H_s < 0.8-1.2$ m during the swimming season. The low limit is valid for long period waves (swell) and the high limit for steep waves (wind waves). This means that protective measures are required if a site is more exposed during the bathing season than given in the above rough criteria, e.g. in the form of specially designed coastal structures.

Rip currents generated as a result of the presence of coastal structures can also be very dangerous. This danger occurs because during a storm situation waves will be partially sheltered behind the coastal structure, but in the same area strong currents, which can carry poor swimmers out into deep water, will arise owing to eddy formation. Such areas with partial shelter provided by coastal structures generate a false sense of safety and such arrangements should consequently be avoided.

The principle of providing safe partial shelter and shoreline stability at an exposed coast is presented in Figure 6, which shows a project for an artificial beach and a marina in Alexandria, Egypt:

- Large breakwaters provide partial shelter; the width of the opening has been adjusted to provide suitable wave exposure to fulfil the requirements of moderate exposure for securing a good beach quality and semi-sheltered conditions for providing safe swimming conditions.

- The beach is designed to be stable under the resulting wave conditions, and a nice curved shape is obtained by the diffracting waves.
- No dangerous rip currents are created because of the long distance between the breakwaters and the beach and because of the equilibrium shape of the beach.

Minimum wave exposure

A recreational beach should have an active profile out to a water depth of about 2.0 m relative to low tide. This recommendation of a depth of 2.0 m relative to low tide results from the requirement that swimmers walking on the seabed should experience an attractive clean sandy seabed without deposition of fines, which causes a muddy seabed. The clean and active seabed is ensured by the requirement that the active coastal profile should extend out to a water depth of 2.0 m, that is, $d_l \geq 2.0$ m or in terms of wave height: $H_{s,12hly} \geq 1.0$ m. This means that the seabed out to this water depth will regularly be exposed to waves which will prevent fine sediments from settling on the shoreface. Furthermore, the growth of sea grasses will also be prevented.

If the natural shoreface does not allow these requirements to be fulfilled, e.g., if the shoreface is shallower than the equilibrium profile, then two possibilities may fulfil the requirements:

- The beach is shifted seaward.
- The existing coastal profile is excavated to accommodate the equilibrium profile.

Beach exposure in relation to tidal range

A certain tidal range and storm-surge activity will cause a wide beach. However, a tidal flat may develop if the mean spring tidal range is much larger than the yearly average breaker wave height H_b . A high tidal range may also cause a danger to bathers. Thus, a good quality recreational beach is normally characterised with a micro to moderate tidal regime, which means a tidal range smaller than approx 1.5 m.

Beach plan form

The beach should be stable in plan form (horizontally) in order to ensure minimum maintenance. This means that the orientation of the beach must be perpendicular to the direction of the prevailing waves, or in other words, the orientation of the beach will be in the equilibrium orientation, which is the orientation providing net zero littoral transport. This often leads to the requirement of supporting coastal structures for stabilising the beach in an orientation, which is different from the natural orientation of the coastline in the area of interest.

At an exposed beach with oblique wave attack, the supportive coastal structures for an artificial beach should be designed to fulfil the following conditions:

- Provide support for a stable lateral shape of the beach and prevent loss of sand out of the artificial beach area.
- Provide partial protection against wave action.

- Must not lead to dangerous currents near the beach.
- Structures will have a streamlined form to minimise trapping of floating debris.
- All coastal structures should also have recreational functions.

Beach profile form

The beach profile should be stable, which means that a beach will be built in the form of the equilibrium profile. A beach adjusts to the equilibrium profile in the active littoral zone. The shape of the profile is mainly dependent of the grain size characteristics of the sand. The equilibrium shape, Dean’s Equilibrium Profile, follows the shape $d = A x^{2/3}$ where d is the depth in the distance x from the shoreline, both d and x in metres. A is Dean’s constant, which is dependent on the grain size of the sand according to the directions given in Table I.

The equilibrium profile concept is valid only for the active littoral zone, i.e., out to the Closure Depth d_c . As a rule of thumb $d_c \sim 2H_{s, 12hr}$ can be used for normal wind waves.

Beach fill material

The beach fill material for artificial beaches should fulfil the following criteria in order to provide a high quality recreational beach:

- Characteristics of the fill sand should be similar to that of the natural sand in the area if the new artificial beach is connected to an existing beach, however, as a rule slightly coarser.
- Sand should be medium, i.e., $0.25 \text{ mm} < d_{50} < 0.5 \text{ mm}$, preferably coarser than 0.3 mm , which minimises wind loss.
- Minimum content of fines, i.e., silt content less than 1-2%.
- Gravel and shell content less than 3%.
- Well-sorted sand, $u = d_{60}/d_{10}$ less than 2.0.
- Colour shall be white, light grey or yellow/golden.
- No content of organic matter.
- Thickness of sand layer will be at a minimum 1 m, preferably thicker.

The reason for the requirement for the beach sand to be medium, well-sorted sand with minimum content of fines is discussed below. If this requirement is not fulfilled, i.e., if the sand is graded (the opposite of



Figure 7. Examples of anoxic conditions and the formation of hydrogen sulphide at protected artificial beaches. Left: Dark substance suspended in the water when seabed at shallow water is disturbed, artificial beach in lagoon environment at the Egyptian NW coast. Right: Dark substance at beach in artificial lagoon in the Red Sea.



Figure 8. Artificial beaches with too much coarse material. Left: Beach Park in Copenhagen. Section where the content of gravel and pebble is too high. Right: Artificial beach in the UAE where the content of shells and coral debris is too high.

well sorted) with some content of fines, the permeability is low, which means that the beach will drain very slowly at falling tide. This implies that the beach will be wet at all times and will have a tendency to be swampy, and thereby unpleasant to walk on. This criterion is especially important for artificial beaches built at protected locations, as there will not be enough wave action to wash the fine sediments out of the beach. Furthermore, algae may grow on the beach, which makes it greenish in colour and un-aesthetic. Finally, in such environments the beach will attract beach crabs and their pellets. Especially at protected sites, the use of clean sand with zero

content of organic matter is important, because the combination of lack of wave exposure and content of organic matter may lead to anoxic conditions resulting in formation of hydrogen sulphide, which causes a bad smell and dark colouring of the sand (see examples in Figure 7).

The requirement for a small content of gravel and coarse fractions is important for the quality of the beach surface as the action of the waves will wash away the fine fractions leaving the beach armoured with the coarse fractions. Such a beach surface is unpleasant to walk on (see examples in Figure 8).

Table I. Correlation between mean grain size d_{50} in mm and the constant A in Dean’s Equilibrium profile equation. For typical beach sand.

d_{50}	0.20	0.25	0.30	0.50
A	0.080	0.092	0.103	0.132

Clearly, from the examples in Figures 7 and 8, the use of very good quality fill sand for the construction of artificial recreational beaches is very important.

DESIGN GUIDELINES FOR ARTIFICIAL LAGOONS

The most important landscape elements in many coastal development schemes are attractive tidal lagoons. Such lagoons provide an attractive protected marine environment – but also major technical challenges. Design guidelines for elements of artificial lagoons are discussed below.

Lagoon mouth and channel sections

The stability of tidal inlets is a science in itself, which is not be discussed in detail here. Suffice it to say that at littoral transport coasts the stability of tidal inlets is a major issue, which means that careful studies are needed. The required cross sections will be dependent on the tidal volume in the lagoon. No specific criteria can be given. However, the cross section area of mouth and channel sections of artificial lagoons should be large enough that peak tidal current velocities are less than ~ 0.8 m/s. The width and depth should also be designed according to guidelines for safe navigation if the lagoon is to accommodate boating by motor and sailing yachts.

Open water body

The main purpose of introducing artificial lagoon and channel elements is to add attractive landscape elements adjacent to an urban development area. The lagoon may be designed to accommodate water sports, navigation and swimming, but swimming in a lagoon will never be as attractive as in the sea. The most important function is to provide the inherent attraction of water to an area which does not have this in its native condition. The lagoon therefore should be properly designed as an important landscape element.

A requirement for maintaining good water quality is the proper flushing of the lagoon. Flushing can be expressed in terms of a characteristic “flushing time” T_{50} , which is the time it takes before 50% of the water in the lagoon system has been exchanged with clean water from the sea outside the lagoon during a design scenario. The design scenario should be a calm and warm period, as this is most critical for flushing and water quality. No required criteria are specified for the flushing time. An acceptable flushing time for a natural lagoon will normally be 5–7 days but the flushing time for artificial recreational lagoons should preferably be shorter.

Under many conditions, more than one opening is recommended in order to accommodate sufficient flushing;

sometimes forced flushing circulation by gates or additional pumping may be required. Other rules of thumb are:

- Water depths shall not be larger than 3–4 m.
- There must be no local depressions in the seabed.
- There must be no discharge of pollutants to the lagoon, such as sewage, storm water, brine, cooling water, pesticides and nutrients.

The above-mentioned flushing guidelines are imperative for obtaining good bathing conditions. Fulfilment of international bathing water quality standards must be ensured, e.g. the EU Standard, Ref. /2/.

Perimeters

Normally it is difficult to obtain a good quality beach inside a lagoon for the reasons discussed in the previous section. The following guidelines should be followed to obtain the best possible lagoon beaches if lagoon beaches are embarked on despite the above “warnings”:

Figure 9. Pictures from Amager Beach Park, Copenhagen. Right: Middle pier functions as terminal structure for the two beach sections and as viewing and bathing facility. Below: Seawall along the southern beach section has multiple functions: Coast protection, separation between promenade and beach and sitting furniture.





Figure 10. Aerial photo of Amager Beach Park, Copenhagen (courtesy of Jan Kofod Winther), which consists of the following main elements: Island with terminal structures north and south and a separating headland between northern and southern beaches and a lagoon. Designed by DHI, Hasløv and Kjærsgaard and NIRAS.

- Use only high standard beach sand as explained under the design guidelines for beaches.
- Construct the desired beach profile from the beginning.
- Build only beaches at exposed locations in “large” lagoons with dimensions preferable > 2–5 km and water depth not less than 2 m.
- Build only beaches if the amount of suspended substances in the lagoon water is very small, say in the order of less than 5–10 mg/l.

It is strongly advised to consider other alternatives than beaches inside lagoons.

LANDSCAPE ELEMENTS OF COASTAL AND OFFSHORE DEVELOPMENTS

The recreational and landscaping requirements in relation to design of the marine elements of waterfront developments are discussed below.

The characteristic elements are:

- Beaches
- Other types of shoreline perimeters
- Landscape behind the shoreline perimeter
- Lagoon areas/body lines

Far too many coastal projects are developed without a clear understanding and respect for the natural hydraulic and coastal processes which are decisive for the overall layout of the marine elements of a development. Consequently, many projects are developed without a clear idea of which layouts are feasible and of how the different elements can support each other.

This may lead to unsuitable shoreline perimeter solutions of poor quality and consequently major expenses for maintenance – often resulting in poor results.

The planning process for a waterfront development should consequently ensure a balance between the objectives of the developer and the possibilities that the

specific development site offers in terms of artificial marine elements, taking environmental impacts into consideration. The main objectives of the developer, being a public authority or a private company, are typically some of the following:

- Enhancing of economic development possibilities in an area.
- Expanding the length of water perimeter through establishment of artificial water bodies.
- Developing recreational and service facilities.
- Providing balanced public and private access.
- Providing sandy beaches and other shoreline perimeter types.
- Establishing optimum internal functionality and causing minimum environmental impacts.

These objectives must be balanced against the possibilities and constraints offered by the natural conditions in the development area: Where can beaches be located and

how should they be orientated? How can good flushing and water quality be ensured in artificial lagoons and so on? These conditions are already discussed in the previous sections where design guidelines for artificial beaches and artificial lagoons are presented.

It is especially important to ensure that necessary coastal structures are planned and designed as multifunctional facilities. Examples of such layouts could be:

- A terminal structure is designed as a viewing headland.
- A groyne structure is designed as a headland which can be utilised for recreational facilities.
- A lagoon opening can be designed as a marina.
- A seawall can be designed as an integrated part of the beach furniture (see Figure 9).

Landscaping principles for the layout of artificial beaches should focus on as long and uninterrupted beach sections as possible, with a minimum number of structures, as this will enhance the natural appearance of a beach section.

An integrated plan based on workable marine elements will make it possible for developers and planners to create unique and sustainable coastal developments where the possibilities and requirements of nature are utilised optimally according to the needs of society.

AN EXAMPLE OF A SUCCESSFUL BEACH PARK DEVELOPMENT

A new beach park was recently built in Copenhagen using the principle of making the new beaches exposed to waves by moving them out to deep water thereby avoiding the shelter provided by the existing shallow shoreface. An aerial photo of the new beach park just after finalisation

Figure 11. Recreational activities in Amager Beach Park, Copenhagen. Upper: Beach activities. Lower: Kayaking and kite surfing on the Lagoon; the beach islandis in the background (courtesy Adrian Saly).

of the civil works is presented in Figure 10. The main wave directions at the site are NE and SE, which have been utilised to make two sections of beach separated by a headland, one facing towards NE and one facing towards SE. Note the Y-shape of the headland structure providing a smooth transition between the structure and the beaches, which secures minimum trapping of floating seaweed and debris in the transition areas. The new beaches have been constructed on an island and a new lagoon (excavated) has been built between the island and the old shoreline. There is always a good current just off the beach park as it is located in the Sound, the strait between Denmark and Sweden, where the water exchange between the Baltic and the North Sea takes place. This results in a good flushing of the lagoon.

The beach park has been very well received by the residents of Copenhagen and in an opinion poll it was nominated as the best beach in the Copenhagen area. It has also received a reward from the "Society for the beautification of the Capital", and people are enjoying all the facilities in the park (see Figure 11).

A NEW CONCEPT FOR AN OFFSHORE DEVELOPMENT SCHEME

A new concept for an offshore development plan utilising the principles presented in this article has been developed by DHI and Hasløv & Kjærsgaard, Planners and Architects, Copenhagen. The plan is universal because it can be implemented at any location where a coastal development is



needed and where wave exposure is present. The plan has been created under the motto, "Work with Nature", meaning that the wave exposure at the site should be considered a valuable natural gift, to be utilised for developing a significant recreational facility, namely a high-quality exposed beach.

The centre of the plan is the unique half-moon-shaped ocean bay providing an excellent sandy beach. The plan thus offers the possibility for developing an extremely high quality urban beach which can be equipped with an attractive cornice along which most of the important recreational and leisure functions of the new city can be developed, such as promenades, retail downtown areas, advanced apartment schemes, hotels, marine sport facilities, entertainment facilities, parks and other amenities.



Figure 12. "The Universe" concept for an offshore development scheme. Artist's impression of the beach in "The Universe" and a possible concept for a marina. © DHI and Hasløv & Kjærsgaard. All rights reserved.

CONCLUSIONS

It is clearly crucial for a successful design of beach and lagoon elements in waterfront developments that the hydraulic, coastal and environmental aspects are included in the planning from the earliest planning stage. The design of these elements has to follow the "rules of nature", which imposes certain restrictions on the design. The main issues to observe are:

Artificial beaches:

- Good quality recreational beaches should be moderately exposed to waves; they should be orientated towards the direction of the prevailing waves to be stable and terminal structures should be constructed to prevent loss.
- Artificial beaches should be constructed by good quality beach sand: medium, i.e. $0.25 \text{ mm} < d_{50} < 0.5 \text{ mm}$, well sorted, attractive colour, minimum content of fines and minimum content of coarse fractions and no content of organic matter.
- Coastal structures adjacent to beaches should be designed so that no dangerous currents are generated.

Artificial lagoons:

- High water quality standards should be ensured in recreational lagoons; the "flushing time" T_{50} should be better than 5 to 7 days, which may require special precautions.
- The lagoon mouths should be stable and free of sedimentation.
- Water depths should be between 2 m and 4 m.
- There must be no local depressions in the seabed.
- There must be no discharge of pollutants to the lagoon, such as sewage, storm water, brine, cooling water, pesticides and nutrients.

Waterfront developments in general:

- A thoroughly planned location and layout of the urban elements integrating recreational demands with the natural dynamics of artificial beaches and lagoons are important.
- Coastal structures should also have recreational functions.

REFERENCES


- Amager Beach Park, Copenhagen, 2003–05. Technical reports (Coastal hydraulics, landscaping, detailed design and EIA) for Amager Beach Park I/S by DHI, Hasløv & Kjærsgaard, Planners and Architects, and NIRAS, Consulting Engineers and Planners.
- Directive 2006/7/EC of the European Parliament and of the Council of 15 February 2006 concerning the management of bathing water and repealing Directive 76/160/EEC.
- Mangor, Karsten, 2004. *Shoreline Management Guidelines*. Published by DHI Water & Environment, ISBN 87-981950-5-0.
- Mangor, Karsten, 2005. *Successful Waterfront Developments – Work with Nature*. Keynote Speech at ArabianCoast 2005, Dubai, UAE.



August 31 – September 05

Short Course on Morphodynamics

- **Tim J. Chesher**

NAME - DATE OF BIRTH - NATIONALITY:	Tim J Chesher – April 15, 1965 - English
EDUCATION:	MBA University of Reading BSc Physics and Meteorology, University of Reading
PRESENT POSITION	Group Manager, Coasts and Estuaries Group, HR Wallingford
KEY QUALIFICATIONS:	 <p>Tim Chesher joined HR Wallingford in 1988 working as a project scientist in the Tidal Engineering Department with principal focus on 2D and 3D hydrodynamic and transport modelling for consultancy in relation to coastal developments (power plants, barrages, ports, and terminals). He transferred into the Marine Sands group led by Professor Richard Soulsby and was one of the principal scientists involved in developing the HR Wallingford coastal area morphodynamic modelling suite, PISCES and was heavily involved in the MAST G6M and G8M European Collaborative Research Programmes. Thereafter Tim transferred into the Maritime Group of HR Wallingford and spent most of his time in consultancy projects worldwide with key focus on sediment transport and sedimentation studies. Tim is now Group Manager for the Coasts and Estuaries Group which comprises approx 25 graduate scientists and engineers working primarily in the field of coastal sediment transport, sedimentation and dredging, and coastal defence.</p>
PUBLICATIONS	<p>Selection of recent journal publications</p> <p>Numerical Approaches for 1D morphodynamic modelling. Judson, J, Damgaard J, Dodd N, Chesher, TJ, Cooper AJ (2005). Coastal Engineering 52 pp691-707.</p> <p>Evaluation of coastal area modelling systems at an estuary mouth. Sutherland J, Walstra DJR, Chesher TJ, van Rijn LC and Southgate HN (2004). Coastal Engineering 51 pp119-142.</p> <p>Evaluation of coastal area modelling systems at an estuary mouth. Sutherland J, Walstra DJR, Chesher TJ, van Rijn LC and Southgate HN (2004). Coastal Engineering 51 pp119-142.</p> <p>Morphodynamic modelling of rip channel growth. Damgaard J, Dodd N, Hall L, and Chesher TJ (2003). Coastal Engineering, 45 pp199-221.</p>

Siltation Studies

Tim Chesher, HR Wallingford



Lecture structure

Basics of sedimentation

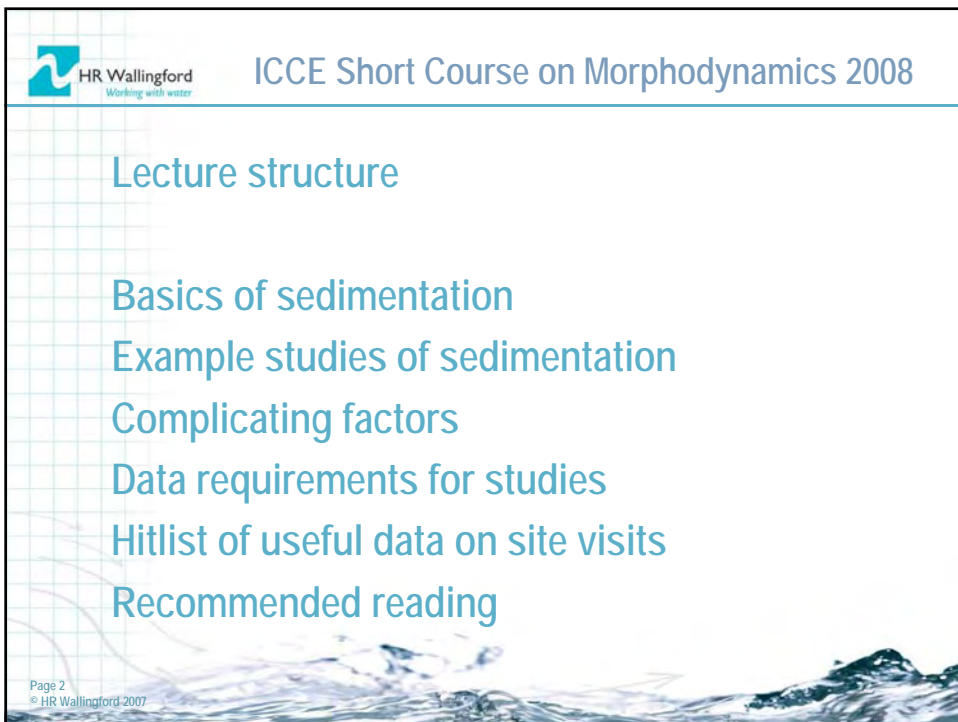
Example studies of sedimentation

Complicating factors

Data requirements for studies

Hitlist of useful data on site visits

Recommended reading



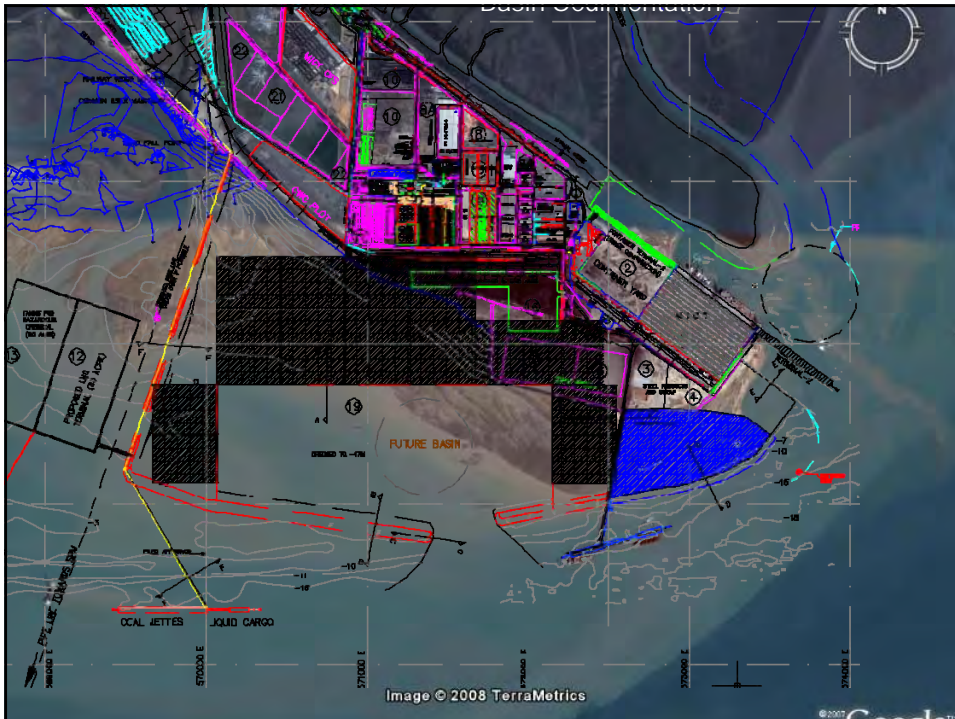
Basics of Sedimentation

Definition: sand, silt, mud depositing

Where?: Intake channels, approach channels, basins, locks and docks, harbours, marinas, ports, pipeline trenches, one-off access channels, etc

Why study? – design (new build)

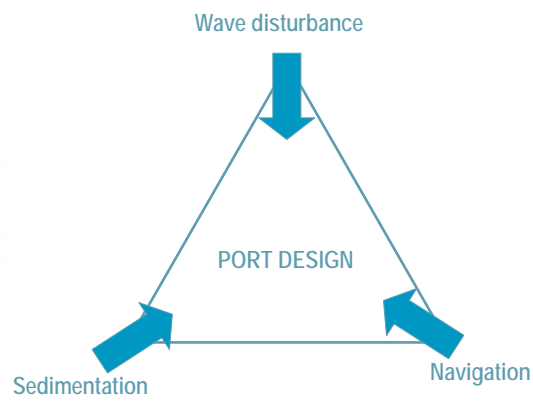
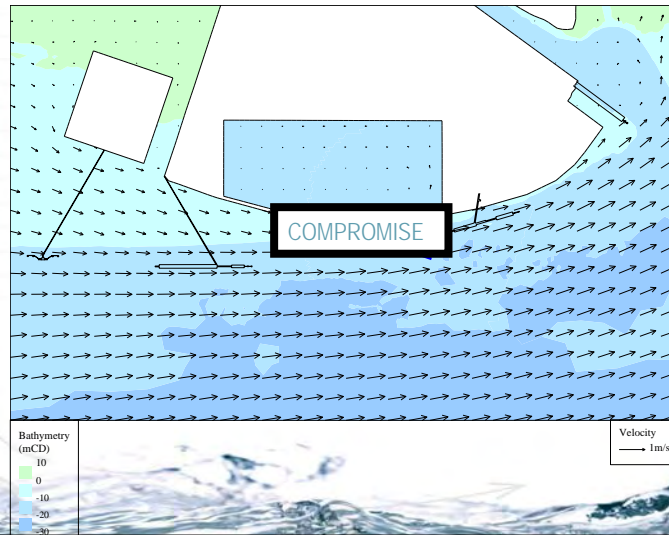
- impact assessment (new build)
- problem solving (existing)



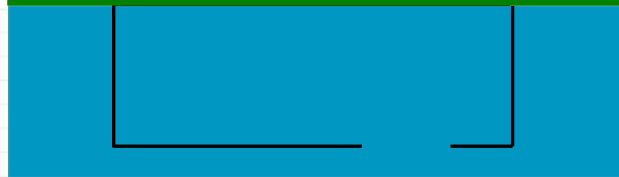
Wave disturbance

Sedimentation

Navigation



Basic infill of a basin

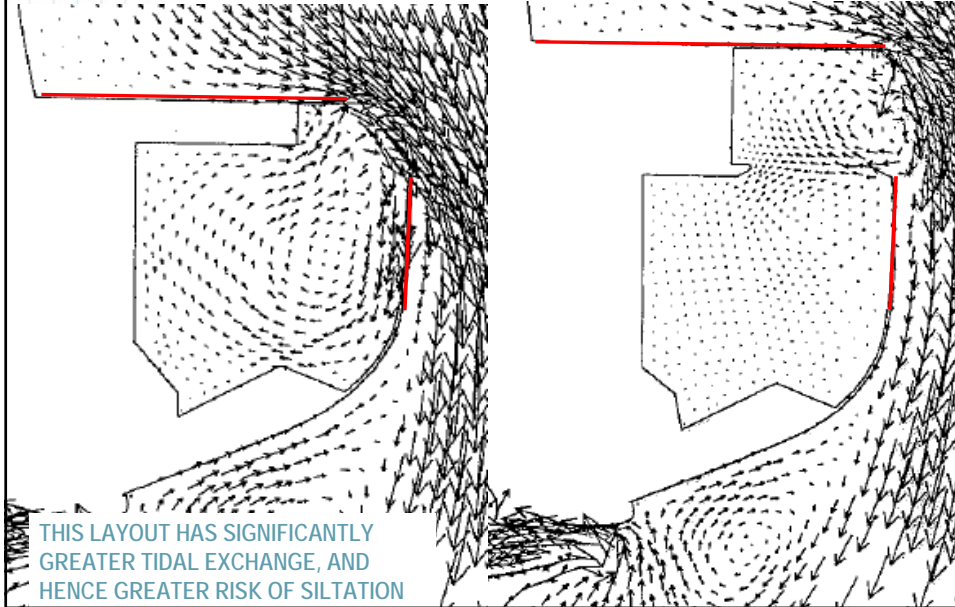


Tide range = Xm
Area of basin = Ym^2
Volume of water entering = Zm^3
Outside concentration = 100-1000mg/l
Settling velocity = 0.05-2mm/s
Residence time ~6hrs

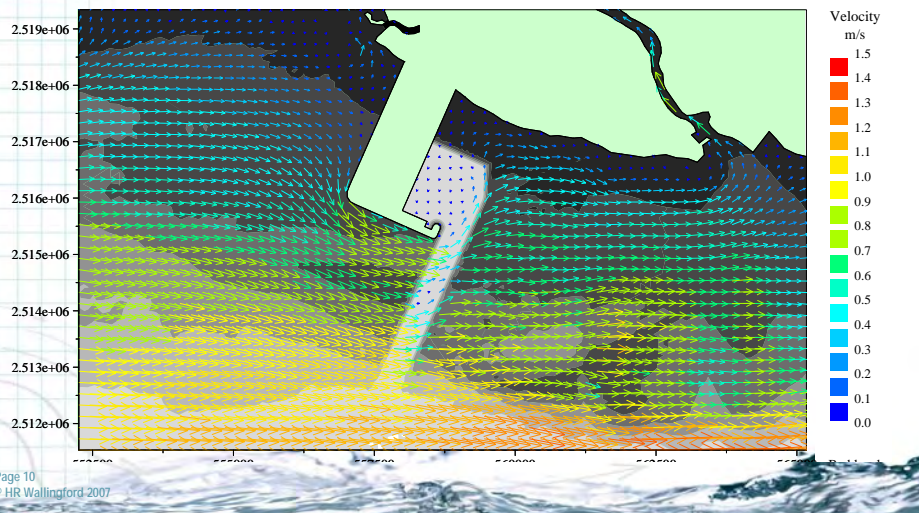
} "trapping efficiency" = $E\%$

Volume of sediment per tide = A to Bm^3 /tide
Tidal variations, concentration variations, etc → Estimate of infill

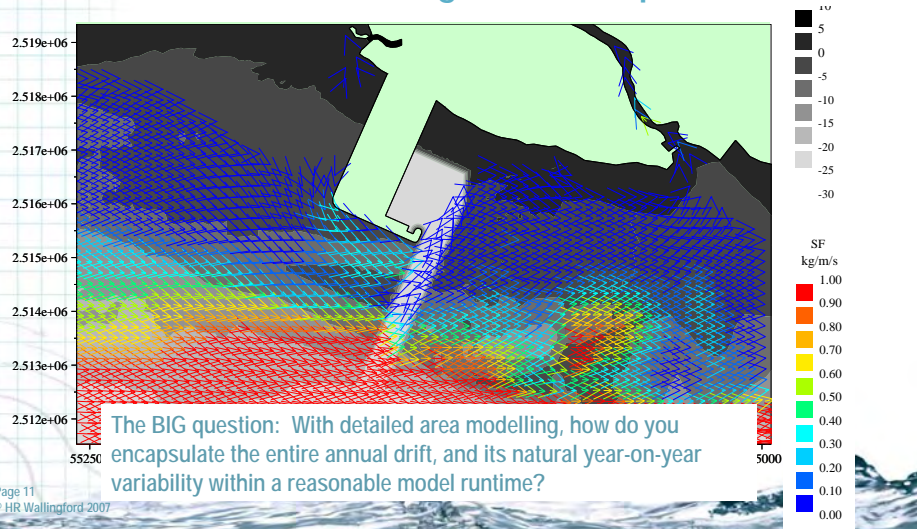




Sedimentation causing coastal impact



Sedimentation causing coastal impact



Approach channel sedimentation

Modern 2D/3D flow and sediment transport models can deal with many of the processes

Issues of importance include:

- Normal or oblique current angle (to channel)
- The effects of lag
- Gravity (changing transport pathways)
- Density effects
- Effects of waves on stability
- Geotechnical (slumping)

See Lean G, HR Wallingford (1980) for concise summary of the above processes

Straightforward tidal infill (change in transporting capacity)

APPROACH CHANNEL SEDIMENTATION

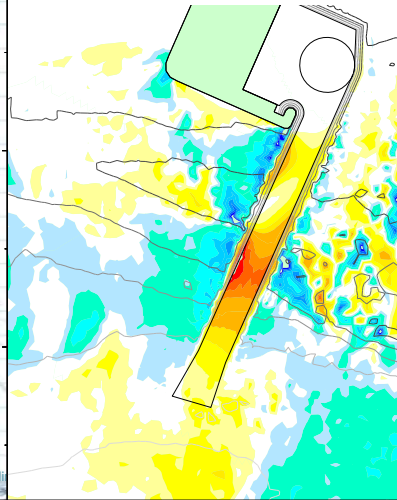
What are the uncertainties?

2.5175e+06

2.515e+06

2.5125e+06

Page 13
© HR Wall



Complicating factors (1). Waves

test3_lyrlongswell
Peak period: 14s
Swan and Artemis (5p5d)

Wave reflections enhance the transport rate
AND thereby degrade the channel slope

2517000

2516500

2516000

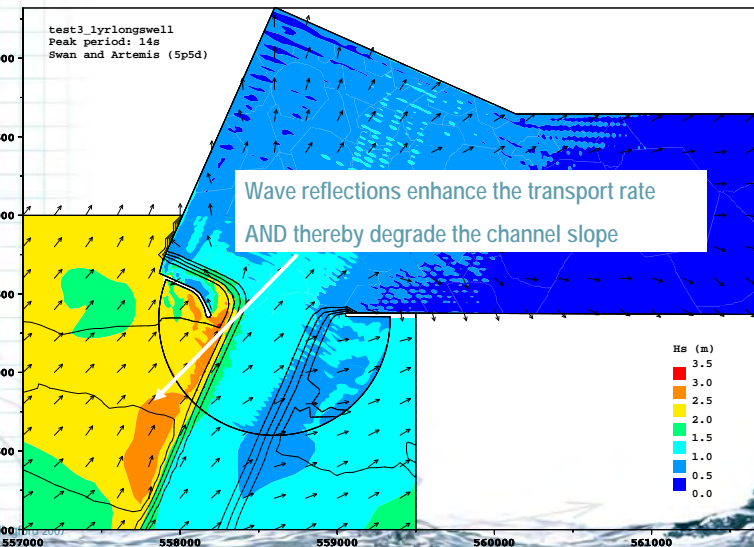
2515500

2515000

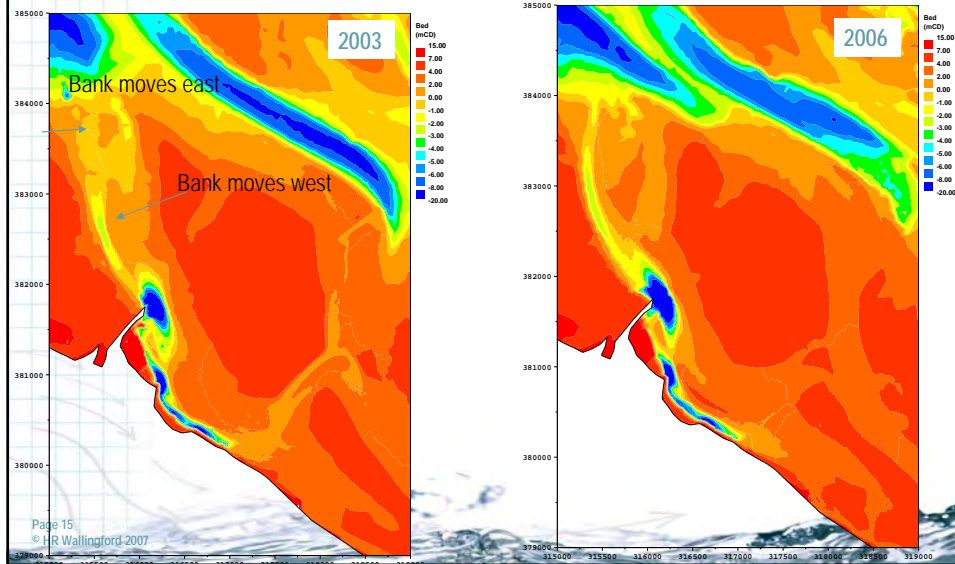
2514500

Page 14
© HR Wall

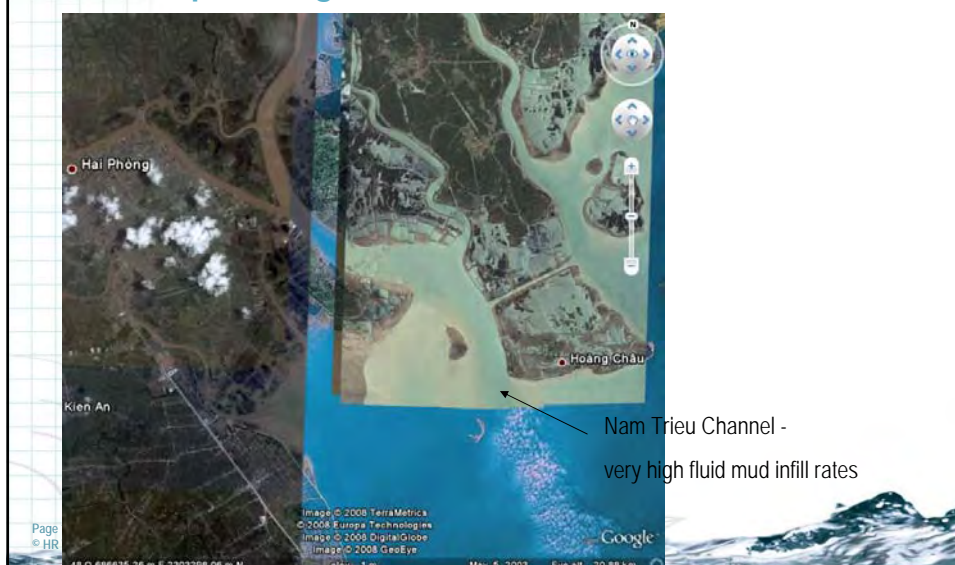
2514000



Complicating factors (2) Bank migration



Complicating factors (3) Fluid mud

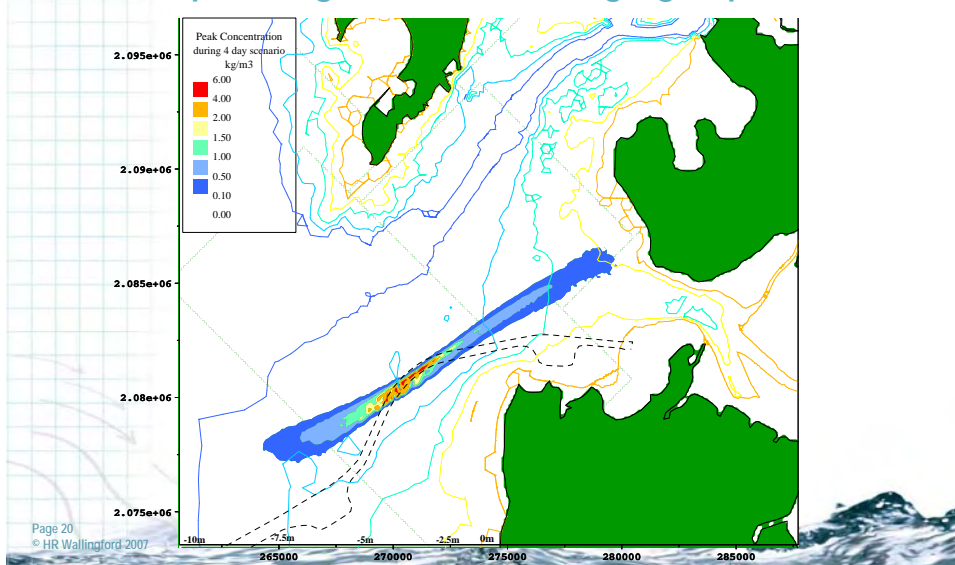




Complicating factors (5) Littoral drift



Complicating factors (6) Dredging deposition



Other influencing factors:

- Limitation in source
- Dredging
- Barriers (barrages, CDW, bubble curtain)
- Ship motion

Data

Requirements versus what the clients *may think* they have:

- Bathymetry – covering the entire area you are going to model
- Bathymetry change – repeat surveys, over long enough periods
- Dredging records. Precise details (e.g. disposal volumes (only) are of little use)
- Tidal levels
- Waves. Ideally offshore and local, climates or time series
- Current metering for calibration (together with tidal levels), fixed station, ADCP, float tracking (beware problems)
- Seabed sediments. Grain size distribution, spatial variability and limitations in supply, temporal variability
- Suspended sediment. Concentrations (synoptic with currents, waves), grain size distribution, variability (NB measurements are seldom made when its most *interesting*)

IF POSSIBLE, REVIEW THE DATA AT THE EARLIEST OPPORTUNITY, AND LONG BEFORE YOU EMBARK ON MODELLING

Site visits – things to watch out for

Greenfield sites:

- Know the tidal conditions before you go
- See if you can find out about wave climate
- Is it muddy or sandy?
- What does the coastal morphology tell you? Drift direction?
- Where is the source of the sediment (sand, mud)?
- Are there any natural obstructions nearby to confirm the drift?
- What do the locals (fishermen, etc) say? (NB can be counterproductive)
- Can you make any measurements (orange float tracks, bed grab sampling)
- Sensitive receptors (impact)

Brownfield site or nearby activity (in addition to the above):

- Are there similar “schemes” nearby?
- Do nearby schemes confirm (or otherwise) the drift?
- Are there any repeat surveys or dredging records (NB dredging records take many forms)
- What were the stakeholder concerns in the case of other developments?

(Some) recommended literature

- Deigaard and Fredsoe. River, Coastal and Estuarine Morphodynamics (ISBN: 3540418393) , pages: 61-92, 2001, Springer Verlag
- Soulsby RL. Dynamics of Marine Sands. Thomas Telford.
- Fredsoe J, Sedimentation of River Navigation Channels *Journal of the Hydraulics Division*, Vol. 104, No. 2, February 1978, pp. 223-236
- Lean GH, Estimation of Maintenance Dredging for Navigation Channels. HR Wallingford (1980)

(starting with the above will spawn many other articles)



Short Course on Morphodynamics

● Dano Roelvink

August 31 – September 05

NAME - DATE OF BIRTH -
NATIONALITY:

J.A. (Dano) Roelvink – May 10, 1959 - Dutch

EDUCATION:

PhD Civil Engineering, Delft University of Technology
MSc Civil Engineering, Delft University of Technology

PRESENT POSITION

Professor of Coastal Engineering and Port Development, UNESCO-IHE
(0.8) and Senior Specialist Coastal Morphology, Deltares (0.2)

KEY

QUALIFICATIONS:



Prof. Roelvink has 25 years of experience in coastal engineering and research. He has participated as team member and as project manager in a number of major consultancy projects related to coastal morphology. He has managed the development of the Delft3D model system for two- and three-dimensional simulation of waves, currents, water quality, ecology and morphodynamics, and has heavily contributed to development of the morphological part of this system. He has been actively involved in the EU-sponsored MaST-G6M and MaST-G8M, SASME, COAST3D and DELOS research projects on coastal morphodynamics. His field of expertise is in coastal hydrodynamics and morphodynamics modelling, in one, two or three dimensions. In 1993 he obtained a PhD-degree at Delft University of Technology, based on a thesis on the effect of surf beats on coastal profiles. He has published numerous articles on coastal hydraulics and morphodynamics in international journals and conference proceedings, and he has been a part-time Associate Professor at Delft University of Technology from 1990-2005 and presently holds an honorary Professorship there. He has been Delft Hydraulics' principal investigator in the discipline of morphology and is a strong proponent of international scientific cooperation with various parties in order to further the state-of-the-art in morphodynamic modelling and has set up collaborative projects with the US Geological Survey, the US Office of Naval Research and the Army Corps of Engineers. He currently leads the development of XBeach, an open-source model for storm impacts

PUBLICATIONS Selection of recent journal publications

- 2008 Ap van Dongeren, Nathaniel Plant, Anna Cohen, Dano Roelvink, Merrick Haller and Patricio Catalan. Beach wizard: nearshore bathymetry estimation through assimilation of model computations and remote observations. In Press, Coastal Engineering
- 2008 van der Wegen, M., Z. B. Wang, H. H. G. Savenije, and J. A. Roelvink (2008), Long-term morphodynamic evolution and energy dissipation in a coastal plain, tidal embayment, *J. Geophys. Res.*, 113, F03001, doi:10.1029/2007JF000898.
- 2008 van der Wegen, M., and J. A. Roelvink (2008), Long-term morphodynamic evolution of a tidal embayment using a two-dimensional, process-based model, *J. Geophys. Res.*, 113, C03016, doi:10.1029/2006JC003983.
- 2007 Ilic, S., van der Westhuysen, A.J., Roelvink, J.A, Chadwick, A.J. Multidirectional wave transformation around detached breakwaters. *Coastal Engineering*, Volume 54, Issue 10, October 2007, Pages 775-789.
- 2007 Ruessink, B. G.; Kuriyama, Y.; Reniers, A. J. H. M.; Roelvink, J. A.; Walstra, D. J. R. Modeling cross-shore sandbar behavior on the timescale of weeks. *J. Geophys. Res.*, Vol. 112, No. F3, F03010 DOI:10.1029/2006JF000730
- 2006 Elias, E.P.L., Cleveringa, J., Buisman, M.C., Stive, M.J.F. and Roelvink, J.A. (2006). Field and model data analysis of sand transport patterns in Texel Tidal Inlet (the Netherlands). *Coastal Engineering*, 53 (5-6), 505-529.
- 2006 Roelvink, J.A. Coastal morphodynamic evolution techniques. *Coastal Engineering* Volume 53, Issues 2-3, February 2006, Pages 277-287
- 2005 Elias, J.P.L., M.J.F. Stive and J.A. Roelvink. Impact of back-barrier changes on ebb-tidal delta evolution. *Journal of Coastal Research*, Special Issue no. 42, pp. 460-476
- 2004 Aarninkhof, S. G. J.; Ruessink, B. G.; Roelvink, J. A. Nearshore subtidal bathymetry from time-exposure video images. *J. Geophys. Res.*, Vol. 110, No. C6, C06011 10.1029/2004JC002791
- 2004 G.R. Lesser, J.A. Roelvink, J.A.T.M van Kester, G.S. Stelling, Development and Validation of a Three-dimensional Morphological Model
Coastal Engineering, Volume 51, Issues 8-9, October 2004, Pages 883-915

Modelling of geological processes

Prof. Dano Roelvink
UNESCO-IHE Institute for Water Education (0.8)
Deltares (0.2)
Delft University of Technology (0.0)

Modelling in support of geology

- **Using process models as morphological facility**
- **Testing geological hypotheses**
- **Underpinning of simpler model concepts**
- **Pushing limits of simulation duration**
- **Modelling extreme events**

Typical timescales

- Adaptation of beach profile – one storm
- Behaviour rip-current cells –days-months
- Bar profile behaviour – 1-10 years
- Channel/shoal cycles: 1-100 years
- Tidal banks – hundreds of years
- Delta formation: 10-10000 years

Purpose of prediction/simulation

- $t < T_{mor}$ - absolute prediction sometimes possible, estimating impacts of human interference feasible
- $t > T_{mor}$, in a system that tends to equilibrium: predict equilibrium states
- $t \gg T_{cycle}$ – absolute prediction impossible or at least very uncertain; purpose is to represent natural behaviour, natural variability

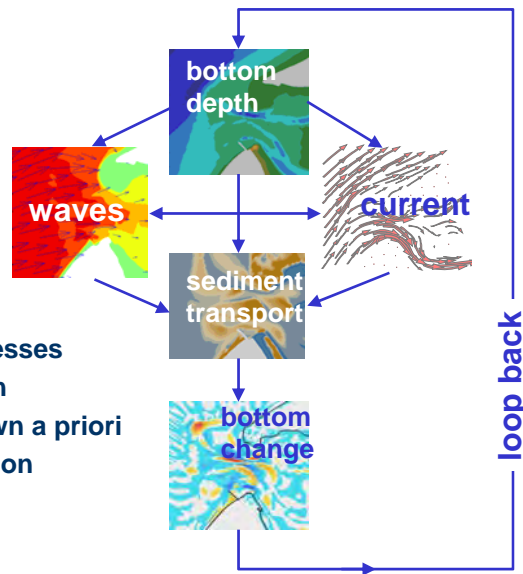
Types prediction-models

- **Behaviour models where equilibrium is forced: coastline models (coastline parallel to wave crests), Asmita (basin-relations), Estmorph (equilibrium channels and shoals)**
- **Process-based models where equilibrium follows from balance of forces/transport contributions**
- **Hybrid models, where process-based models are used but a certain behaviour is forced**

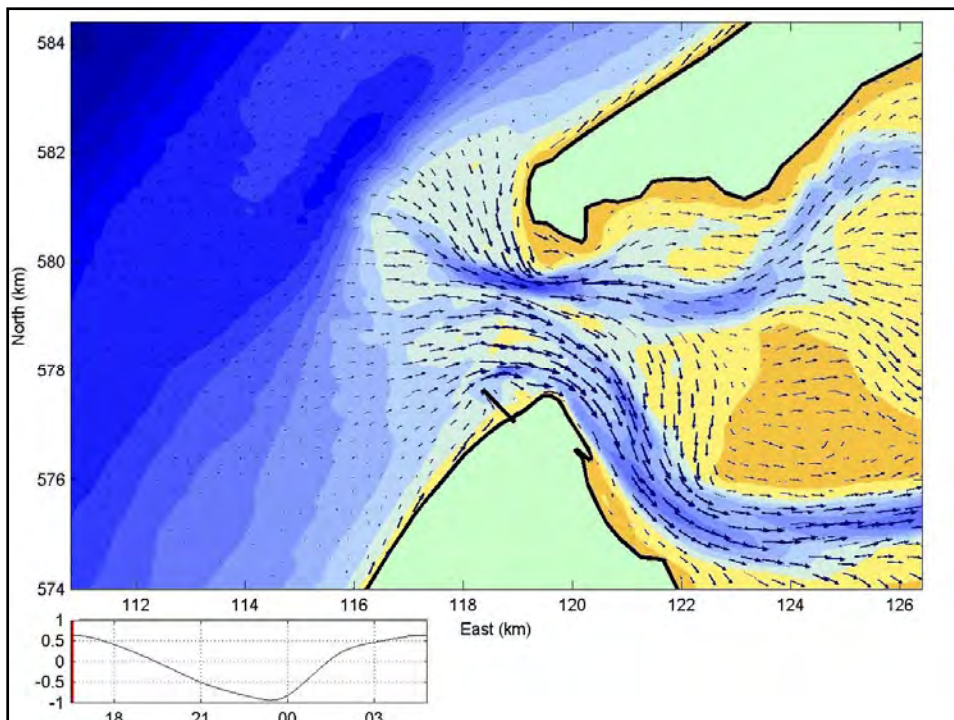
Main challenges

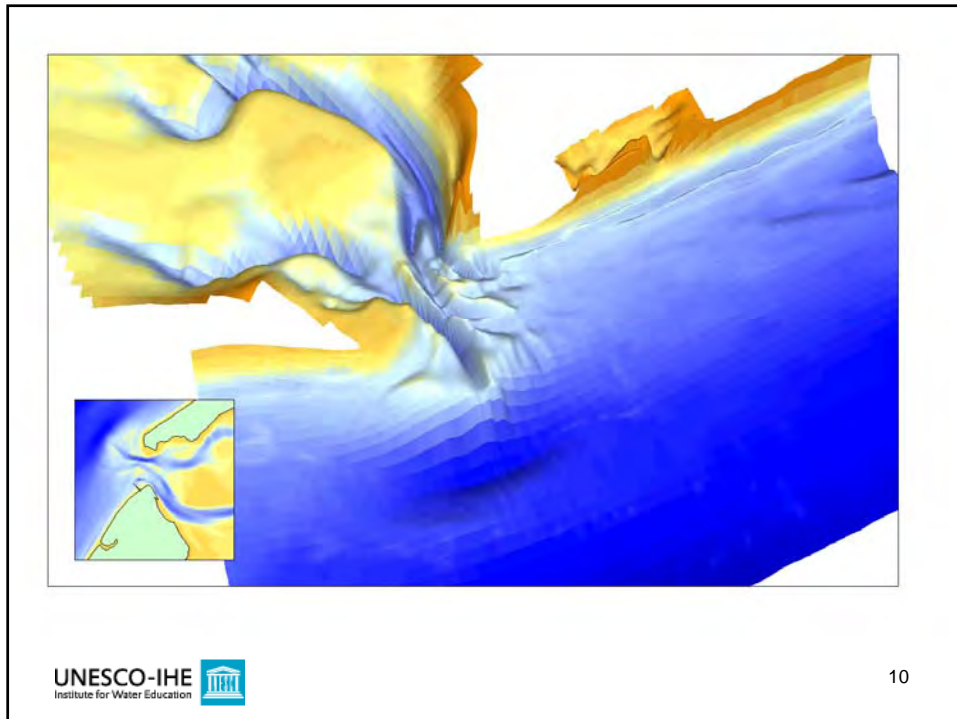
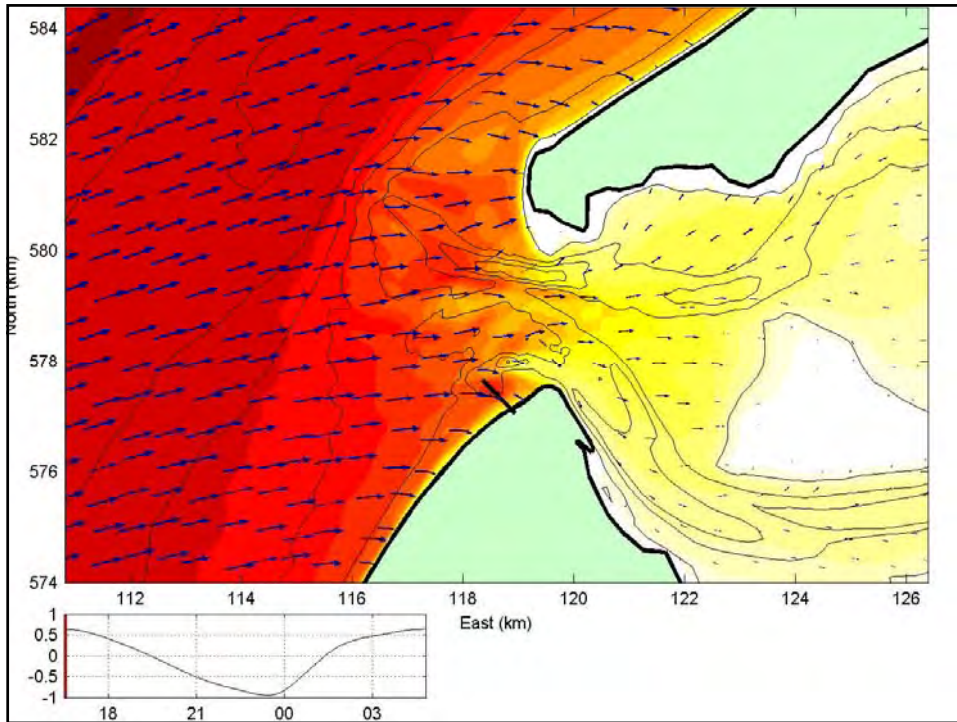
- **Forced equilibrium:**
 - Will the relation remain valid under changed circumstances
 - What are the underlying processes
 - What determines the time-scales
- **Process-based:**
 - What kind of equilibrium circumstances does the model tend to
 - How can I influence that
 - How can I simulate towards relevant time-scales
- **Hybrid:**
 - What approximations are sensible
 - What are sensible rules of behaviour

Process-based, area models



- simulate basic processes
- 'upscaling' approach
- equilibrium not known a priori
- detailed representation



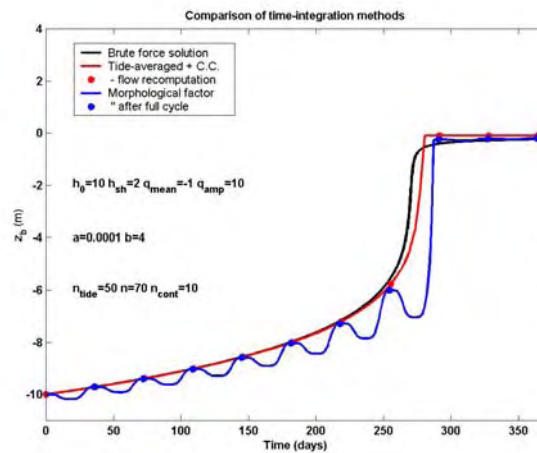


Elongated tide approach

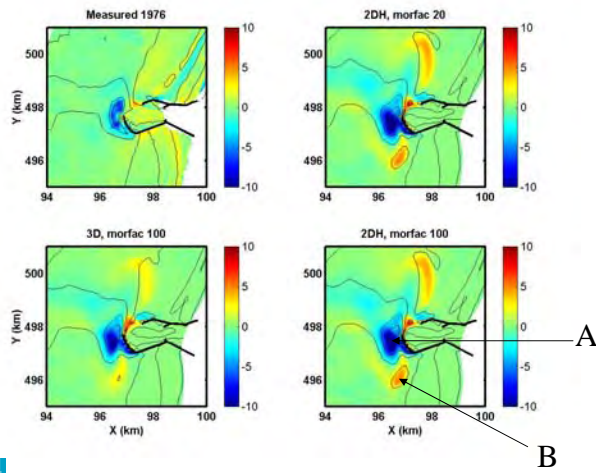
- Compute transport fields at each flow timestep
- Compute bottom changes
- Multiply by morphological factor
- Update bathymetry
- Continue

$$\Delta z_b = \int_0^{nT} \frac{\partial z_b}{\partial t} dt \approx \int_0^T n \frac{\partial z_b}{\partial t} dt$$

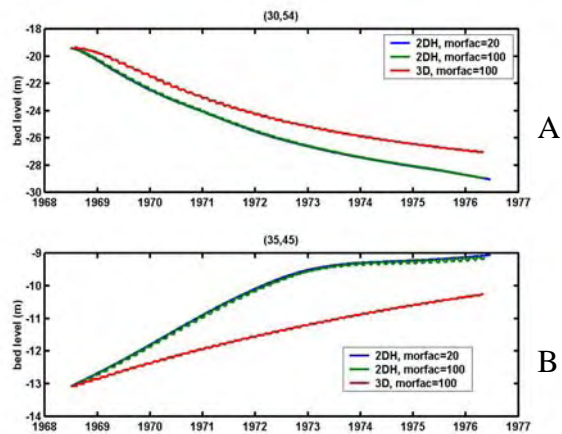
Comparison: morphological factor vs brute force



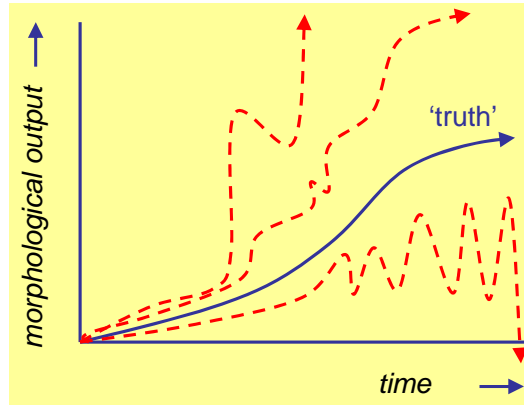
Real-life case: IJmuiden Harbour



Time-evolution of bed level

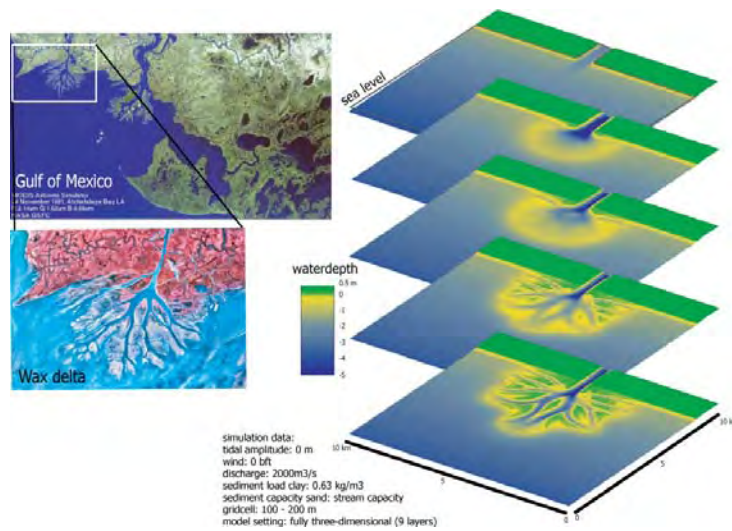


Beyond our lifetime



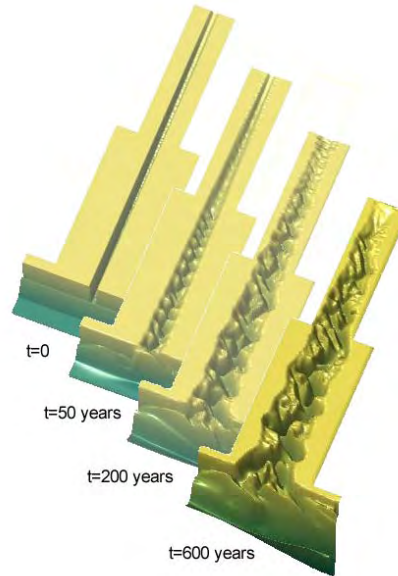
Morphosceptics' view of bottom-up models

Geological application: Wax delta



Long-term behaviour of estuaries

- Given coastline and tidal boundaries, can we predict channel shapes, cross-section?
- Does equilibrium exist?

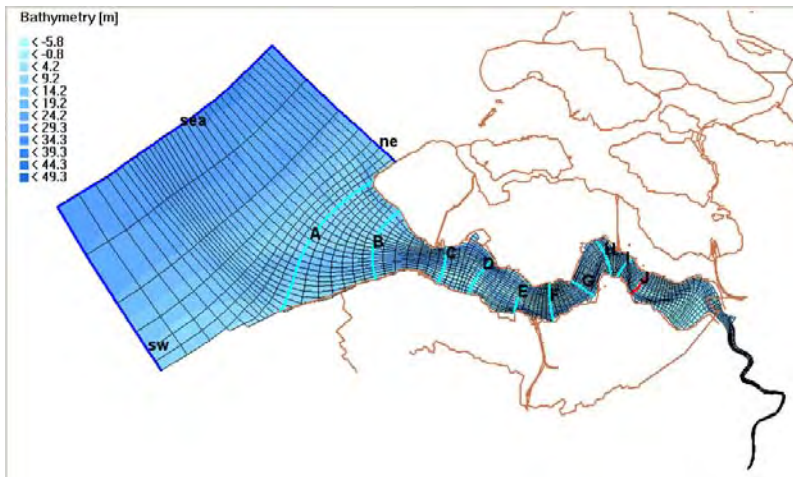


Western Scheldt

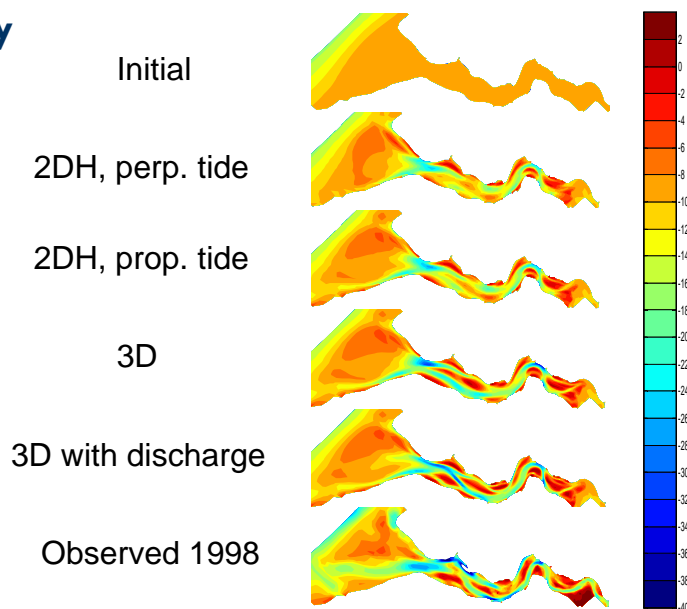
- What determines present channel configuration
 - history?
 - present outline?
 - tidal forcing?
 - Schelde discharges?
- Simple model setup
 - 1 sediment size
 - flat initial bathymetry
 - present coastline fixed
 - Single tide, M2+M4+M6
 - 2DH, 3D and 3D with high discharge



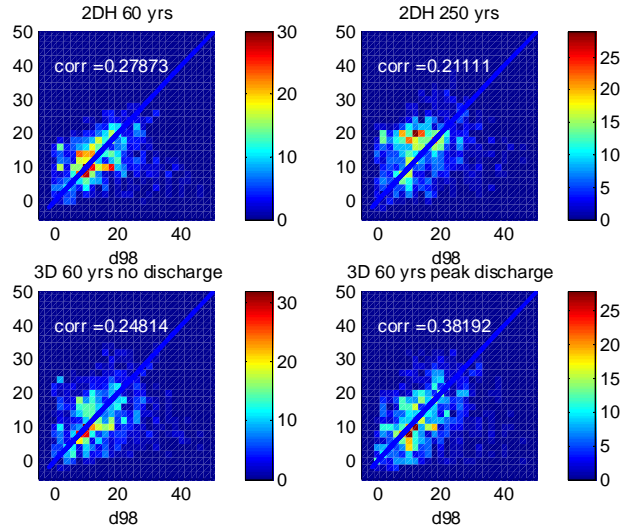
Westerschelde grid



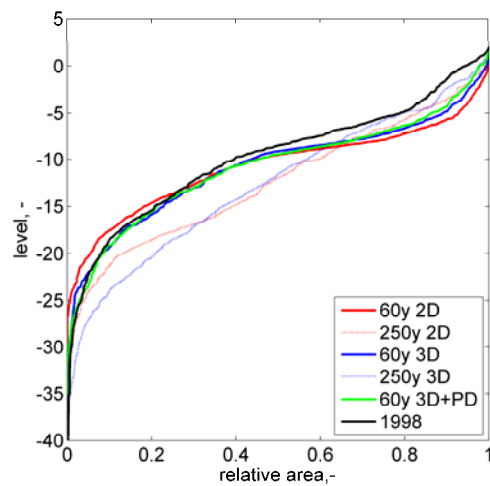
Bathymetry after 60 years



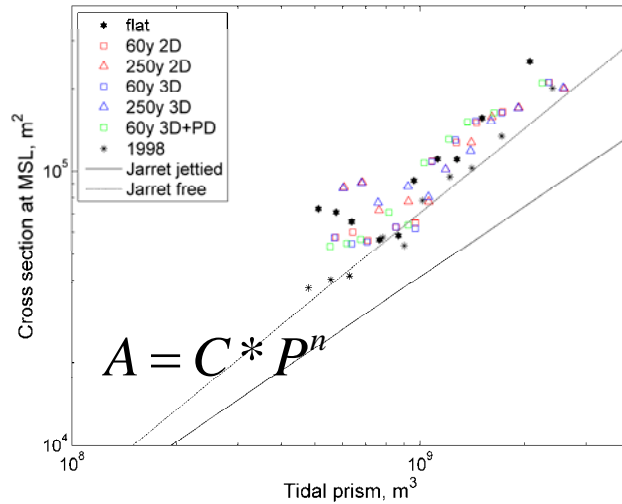
Correlation observed-simulated bathymetry



Hypsometry



Jarrett



Conclusions large-scale modeling

- A lot of natural behavior is captured in really simple physics (2DH tidal flow plus simple transport formula)
- A number of empirical relationships are reproduced
- Long-term, process based simulations do not necessarily get out of hand and even show some skill
- For modelling 'the real thing' we need more processes (waves, wind, variable sediments)

ICCE 08: Short course. Jørgen Fredsøe: A SHORT CURRICULUM VITAE



Nationality Danish

Education Technical University of Denmark, Copenhagen, 1971. MSc in Civil Engineering.
Technical University of Denmark, Copenhagen, 1974. Ph.D. in Civil Engineering.
Dr.Tech, 1984. Title of Thesis: Sediment Transport in Current and Waves.

Key topics Coastal, River and Offshore Engineering.

Employment record

Year	Firm	Position and responsibilities
2007-date	DHI Denmark (Coastal Engineering and Ports & Offshore Technology)	Consultant. Flow and sediment transport in harbour, coastal, and river engineering.
1986-date	Institute of Hydrodynamics and Hydraulic Engineering. Technical University of Denmark.	Professor in Marine Hydraulic Engineering.
1975-2002	DHI Water & Environment (former DHI)	Consultant.
1979-1984	LICconsult, Consulting Engineers, Denmark	Partner of the firm.
1979	Iowa Institute of Hydraulic Research, Iowa City, USA	Visiting researcher.

BOOKS

2002 Sumer, M.B. and Fredsøe, J.: "Mechanics of scour in the marine environment". World Scientific.

1997 Sumer, M.B. and Fredsøe, J.: "Hydrodynamics around cylindrical structures". World Scientific.

1992 Fredsøe, J. and Deigaard, R.: "Mechanics of coastal sediment transport". World Scientific.

ICCE 08: a short list of literature used in the lecture “small scale morphodynamics” given by Jørgen Fredsøe

Instability, steady current:

[SEDIMENT RIPPLES AND DUNES](#)

ENGELUND F, FREDSOE J

ANNUAL REVIEW OF FLUID MECHANICS Volume: 14 Pages: 13-37, 1982.

Instability, oscillatory flow:

[SEA RIPPLE FORMATION - THE TURBULENT BOUNDARY-LAYER CASE](#)

FOTI, E; BLONDEAUX, P

COASTAL ENGINEERING Volume: 25 Issue: 3-4 Pages: 227-236 JUL 1995.

[SAND RIPPLES UNDER SEA WAVES .1. RIPPLE FORMATION](#)

BLONDEAUX, P

JOURNAL OF FLUID MECHANICS Volume: 218 Pages: 1-17 SEP 1990.

Fully developed bedforms, steady current:

[Calculation of dune morphology](#)

Tjerry S, Fredsoe J

JOURNAL OF GEOPHYSICAL RESEARCH-EARTH SURFACE Volume: 110, Issue: F4 Article Number: F04013, NOV 30 2005.

[SHAPE AND DIMENSIONS OF STATIONARY DUNES IN RIVERS](#)

FREDSOE, J

JOURNAL OF THE HYDRAULICS DIVISION-ASCE Volume: 108 Issue: 8 Pages: 932-947, 1982.

The stability of a sandy river bed.

J. Fredsøe. In: Issues and directions in Hydraulics, Edited by Nakato and Ettema. Pages: 99-113. Balkema, Rotterdam.1996.

Sand dunes in unidirectional flow at low Froude numbers, PART I: Model description and dune development . S.L. Niemann, J. Fredsøe and N.G. Jacobsen Submitted for possible publication, ASCE, HY DIV.

Fully developed bedforms, oscillatory flow:

[A particle model of rolling grain ripples under waves](#)

Andersen, KH

PHYSICS OF FLUIDS Volume: 13 Issue: 1 Pages: 58-64 Published: JAN 2001.

How to calculate the geometry of vortex ripples.

Andersen, KH and J. Fredsøe
Coastal Sediments, Long Island. Pages: 78-93, 1999.

Flow resistance:

[The wave plus current flow over vortex ripples at an arbitrary angle](#) ,

Andersen KH, Faraci C, COASTAL ENGINEERING Volume: 47 Issue: 4 Pages: 431-441 Published: FEB 2003

[Wave plus current over a ripple-covered bed](#)

Fredsøe J, Andersen KH, Sumer BM, COASTAL ENGINEERING Volume: 38 Issue: 4 Pages: 177-221 Published: DEC 1999.

Small scale morphodynamics



Jørgen Fredsøe
DTU MEK

Small scale bed forms

- Rolling grain ripples
- Vortex ripples
- Mega ripples

What is a small scale

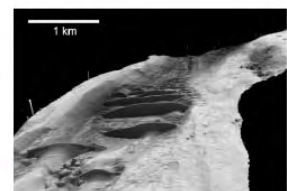
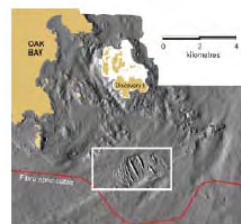
- Sandgrain
- Small scale bed forms
- Beach cusps
- Bars, rips
- Undulations
- coastlines



ripples

- Longterm modelling: you don't need to go into detail.
- Right??

Megaripples





Megaripples



- Description
- Importance
- Why are they formed
- Fully developed bedforms

Tidal ripples



Importance

- Hydrodynamics: roughness
- Sediment transport: increased suspended sediment and modification of net transport.
- Changes in available depth



Biology??



Steady current:

Ripples, geometry related to grain size
Dunes: related to flow depth

Waves:

Rolling grain ripples: related to grain size
Vortex ripples: related to orbital motion.

Model testing



Where is net transport important?

- Profile modeling



Soil properties important

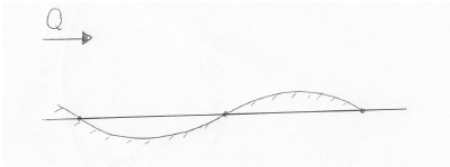


Morphodynamic modelling of bed forms: Tools:

- Continuity equation $\frac{\partial q}{\partial x} = -\frac{\partial h}{\partial t}$
- Sediment transport formula $\Phi = 8(\theta - \theta_c - \mu \frac{\partial h}{\partial x})^{3/2}$
- Flow description

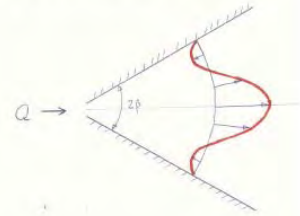
1. Why are bedforms formed?

- instability



Diverging

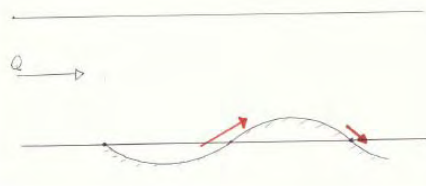
- Diffuser flow
- No bl-characteristics
- Low bed shear stress: disappear around $\beta=4.3$ degrees



Properties of converging and diverging flow

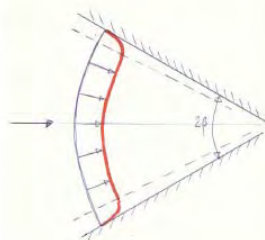
- Boundary layer
- Diffuser (jet-like)
- Unsteady

Instability - steady flow



converging

- Boundary layer properties:
- High shear
- Thin thickness



Wave length

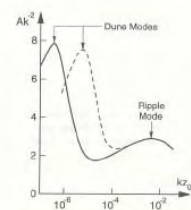
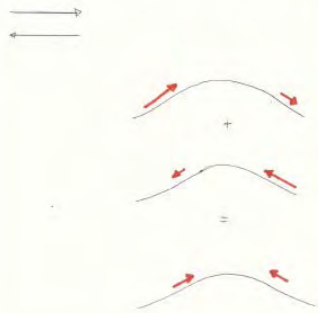


Figure 6. Variation in amplification factor A with wave number k. Note that z_0 = bed roughness, —: $Dz_0 = 10^2$, and - - - : $Dz_0 = 10^1$. [After Richards (1989)].

Instability – unsteady flow



Migrating front



E. Foti, P. Blondeaux / Coastal Engineering 25 (1995) 227–236

233

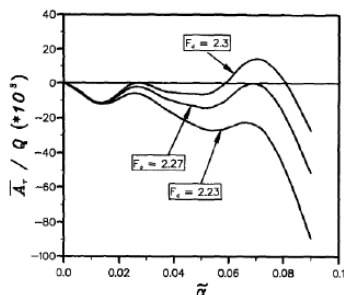


Fig. 1. Amplification rate (\dot{A}/\dot{Q}) of the bottom perturbation versus the dimensionless ripple wavenumber $\tilde{\alpha} = 2\omega\theta^*/U_*' = 2\pi\gamma/2\pi\omega^*/U_*'$ ($R_d = 450$; $Re = 45000$).

Here the sediment Reynolds number R_d and the sediment Froude number F_d , are defined in terms of the sediment size d^*

$$R_d = \frac{U_*' d^*}{\nu}; \quad F_d = \frac{U_*'}{[(s-1)gd^*]^{1/2}}$$

$$\frac{\partial q}{\partial x} = \frac{dq}{d\theta} \frac{d\theta}{dx} \quad \theta = \tau_b / (\rho g (s-1)d)$$

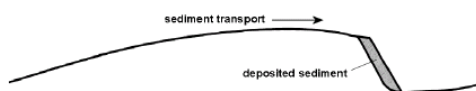
$$\theta \sim V^2 \quad V(D-h) = q$$

$$\theta = \theta_{top} \left[\frac{D-H/2}{D+H/2-h} \right]^2$$

$$\frac{d\theta}{dx} = \frac{2\theta}{D-H/2} \frac{\partial h}{\partial x}$$

2. Further development: Steady current. A simple non-linear model

- Sandwave is a migrating front.



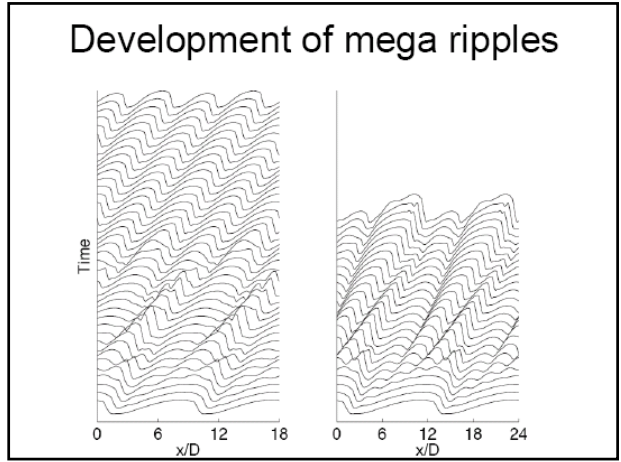
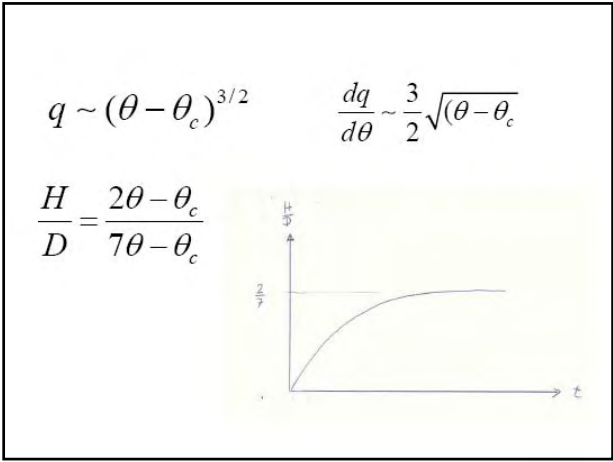
$$a = q_d / H \quad \frac{dH}{dt} = \frac{\partial h}{\partial t} + a \frac{\partial h}{\partial x}$$

$$\frac{dH}{dt} = \frac{\partial h}{\partial t} + a \frac{\partial h}{\partial x}$$

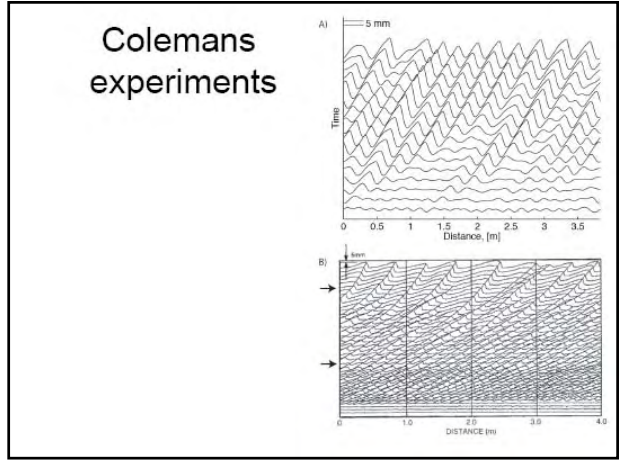
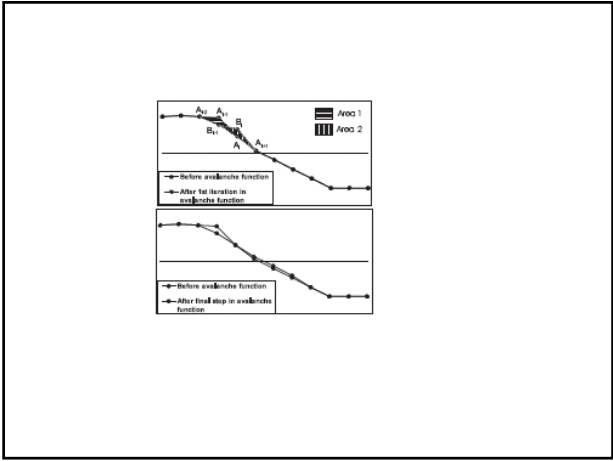
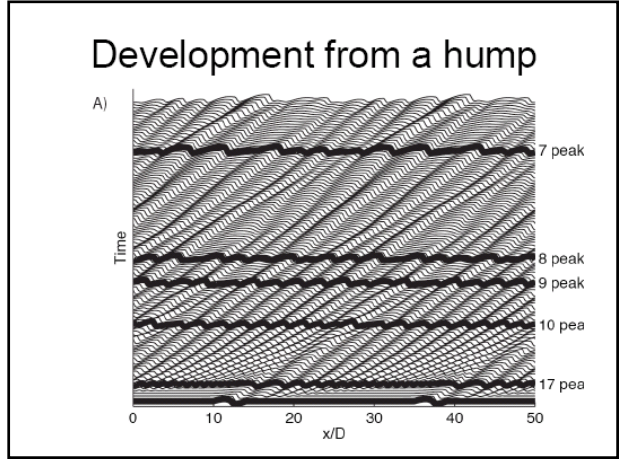
$$a = q_d / H$$



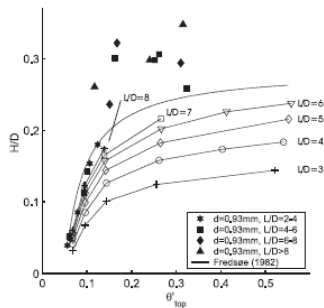
$$\frac{dH}{dt} \left[-\frac{dq}{d\theta} \frac{2\theta}{D-H/2} + q_d / H \right] \frac{\partial h}{\partial x} \approx \left[-\frac{dq}{d\theta} \frac{2\theta H}{D-H/2} + q_d \right] / L$$



- ### 3. Steady current, advanced modelling
- Sediment transport formula
 - Flow description: turbulence model ($k-\omega$).



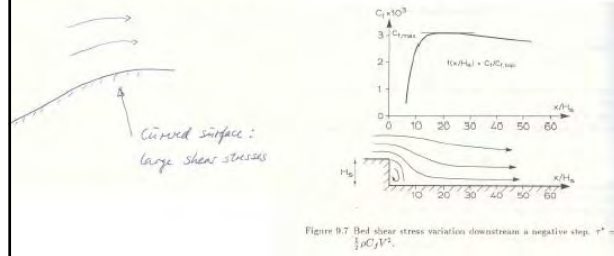
Height predicted by turbulence model: curvature effects



$$\text{Equilibrium: } \frac{q}{q_{top}} = \frac{h}{H}$$

Tjerry and jf 2005

jf 1982



Still not possible to calculate final shape of small scale current ripples and windblown ripples



4. Nonlinear development Oscillatory flow

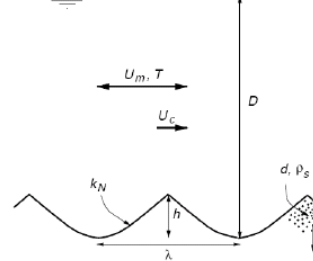
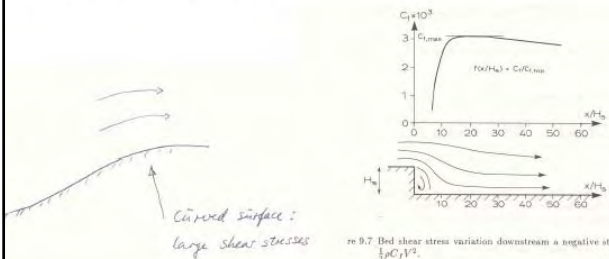


Figure 1.3: The dimensional quantities appearing in the ripple problem

$$\frac{q}{q_{top}} = \frac{h}{H}$$

• Tjerry and jf 2005



Nielsen plot

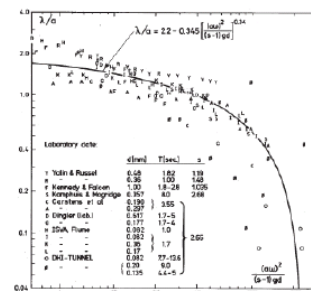


Figure 6.1: The average wavelength for a number of experiments, collected by Nielsen (1979).

Oscillatory flow: simple model.

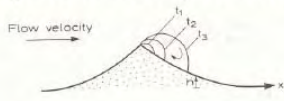
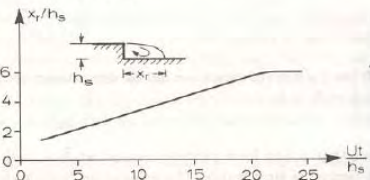


Figure 10.4 Development of separation bubble downstream of ripple crest. $t_1 < t_2 < t_3$.



Andersen 2001: rolling grain ripples



Figure 3.2. Each particle has a shadow zone extending a length a_s/d_s in the upstream direction (left). Right: The function f is used to describe how a particle is slowed down when it enters the shadow zone of another particle. Δx is the distance between two neighbouring ripples. The example shown here is a time in the wave period when the flow is from the left to the right.

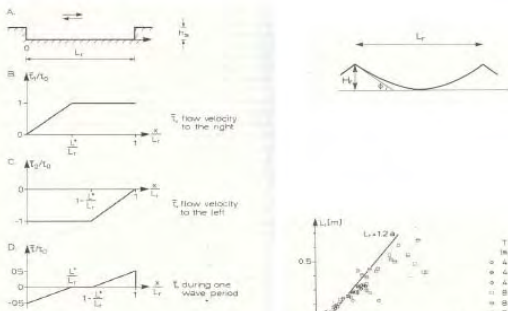


Figure 18.7 Mean bed shear distribution in a hole for the case $T/2 < 8h_s/(a_s U)$ and $L^* > 12 h_s$. L^* is defined in Eq. 18.5.

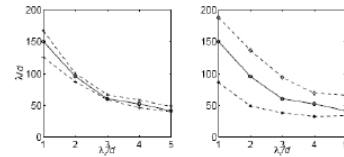


Figure 3.7. The average length between the rolling grain ripples at equilibrium. The basic example is shown with the full line: $a_s/d_s = 35$ and $a_b/d_b = 10.0$. To the left, the value of a_s/d_s is varied, for plots $a_b/d_b = 20$, crosses $a_b/d_b = 50$. To the right a_b/d_b is varied: stars $a_s/d_s = 7$, diamonds $a_s/d_s = 13$.

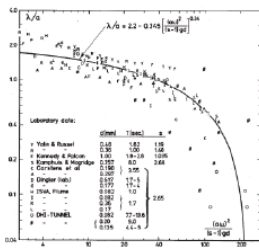
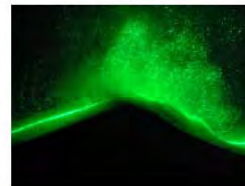


Figure 5.1. The average wavelength for a number of experiments, collected by Nielsen (1979).

Suspended sediment tend to smoothen out ripples



Oscillatory flow:

Advanced modelling

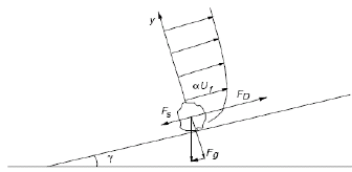
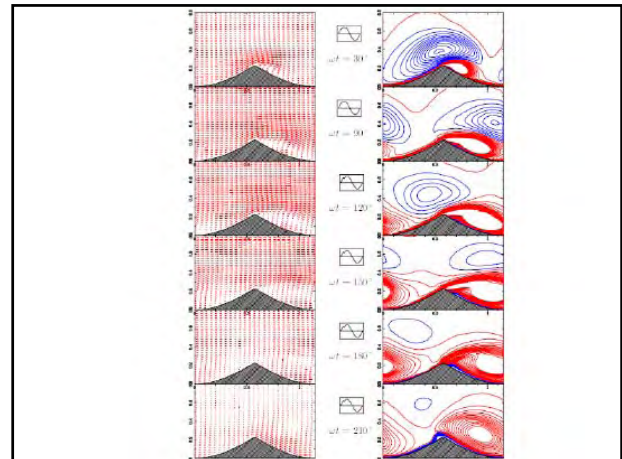


Figure 2.6: The forces acting on a single grain on a sloping bed

Circulation cell calculated by a k- ω model

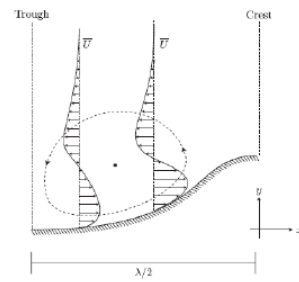


Figure 1.2: Sketch of the recirculation cell over half a ripple length.

Bed load at large slopes

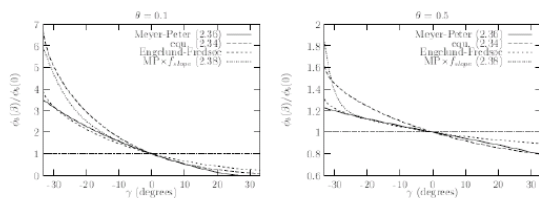


Figure 2.8: The bed load calculated for different slopes and at small shear stress (left) and high shear stress (right). The bed load have been divided with the bed load at a flat bed to make a facilitate an easier comparison of the slope effect alone.

Creation of new ripples

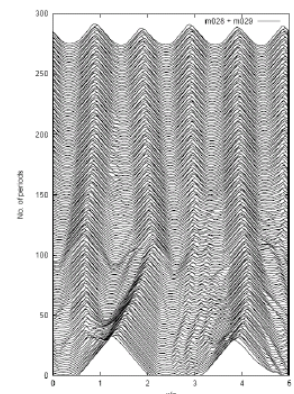


Figure 0.4: The evolution of a ripple profile over long time, showing the creation of new ripples. This profile is drawn several times each plotted on the movement.

annihilation

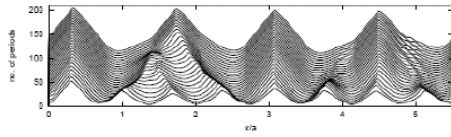


Figure 6.5: The evolution of a ripple profile showing the process of annihilation ($\theta' = 0.15$, $w_s/U_{*m} = 0.070$).

Equilibrium Requirement: $\int_0^T q dt = 0$

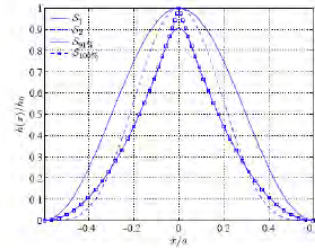


Figure 3.2: Four of the bed shapes with heights relative to h_0 .

Shape dominated by slope

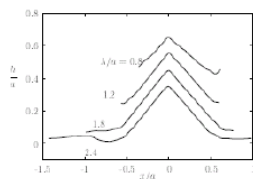
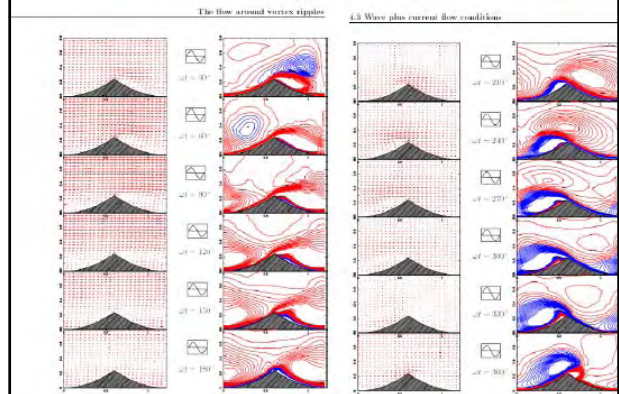


Figure 6.7: The equilibrium profiles for ripples varying lengths. The profile with $\lambda/a = 2.4$ is not in equilibrium – the flat piece develops into a new ripple (test case W1).

5. Waves plus current



Intra wave description

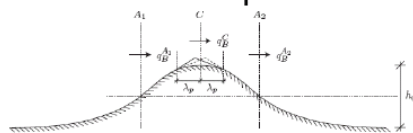


Figure 4.1: Sketch of the entire ripple profile with a perturbation on top of the crest. The size of the perturbation is based on the sediment transport averaged over one half wave period.

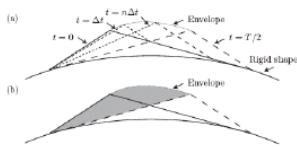


Figure 4.2: Sketch of the dynamic perturbation on top of some rigid shape. (a) Principal movement of the perturbation profile. The time is local in terms of the near-bed velocity and not the free stream velocity. (b) The shaded area is the volume moved each half period.

Suspended sediment over ripples

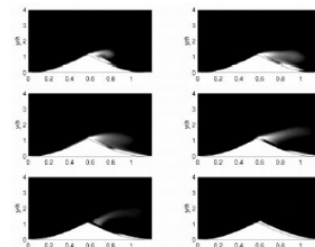
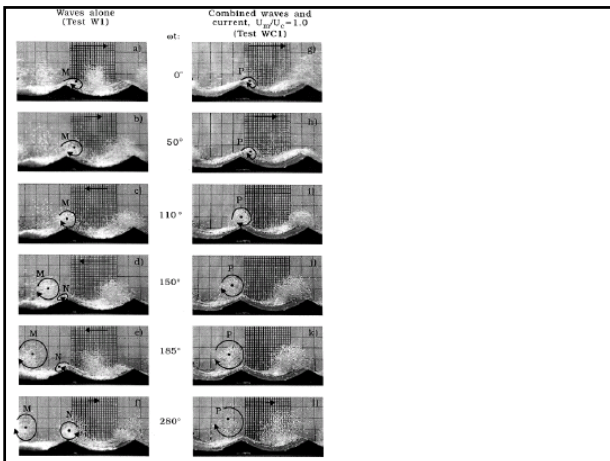


Figure 5.4: The transport of suspended sediment over a ripple at six azimuths ($\phi = 0^\circ$ to 210°). The flow is the same as in figure 4.4. The scale shows the log of the concentration of suspended sediment; the lighter the higher concentration of sediment (test case W2, $\lambda/a = 1.2$, $\theta' = 0.15$, $w_s/U_{*m} = 0.185$).



Roughness to the current

- A.: plane bed

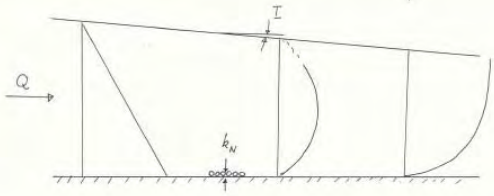
$$\tau = \rho g I (D - y) \quad v_i = \kappa U_f y (1 - y/D) \quad \frac{U}{U_f} = \frac{1}{\kappa} \ln \left(\frac{y}{k_n} \right)$$

Sediment transport against the current

6. Bed Roughness:

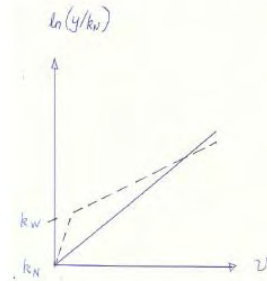
- Current: k_n
- Current plus waves: k_w
- Current plus waves plus ripples ??

Roughness felt by the current



$$\tau = \rho g I (D - y) \quad v_i = \kappa U_f y (1 - y/D) \quad \frac{U}{U_f} = \frac{1}{\kappa} \ln \left(\frac{y}{k_n} \right)$$

Apparent wave roughness



Wave boundary layer

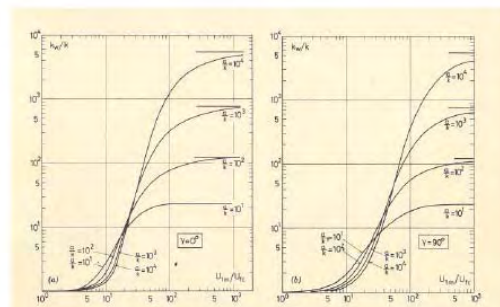
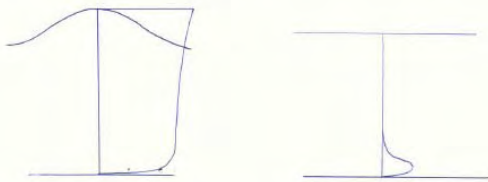


FIG. 7.—Variation in k_w/k with U_{1m}/U_c for Different Values of a/k : (a) $\gamma = 0^\circ$; (b) $\gamma = 90^\circ$

Change in turbulence and velocity profile due to waves

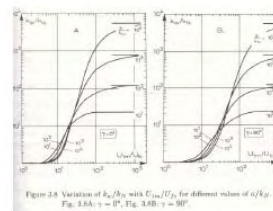
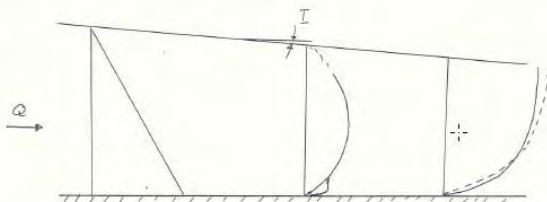
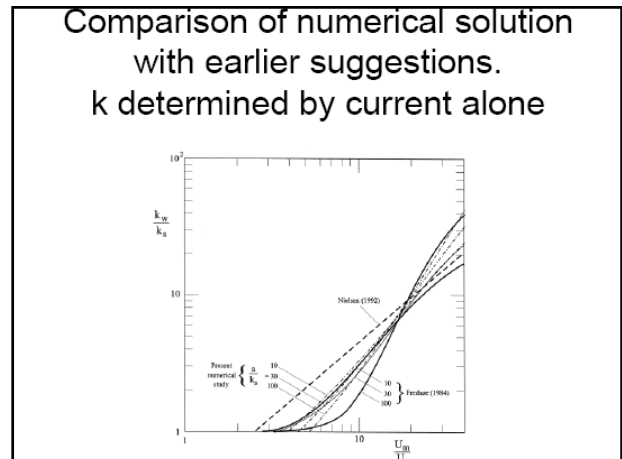
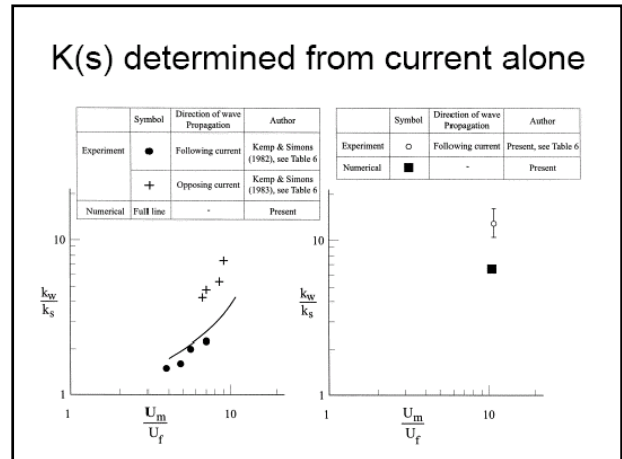
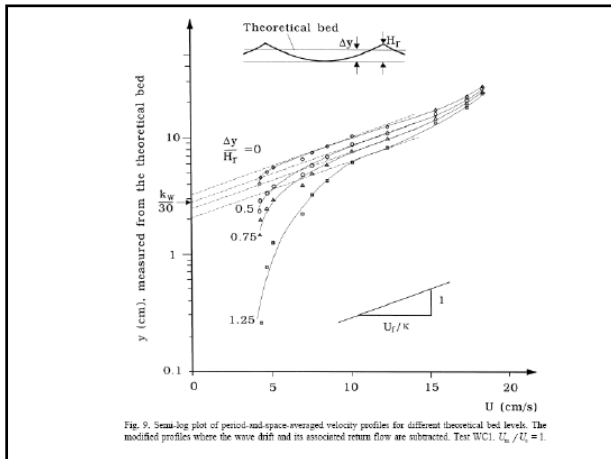
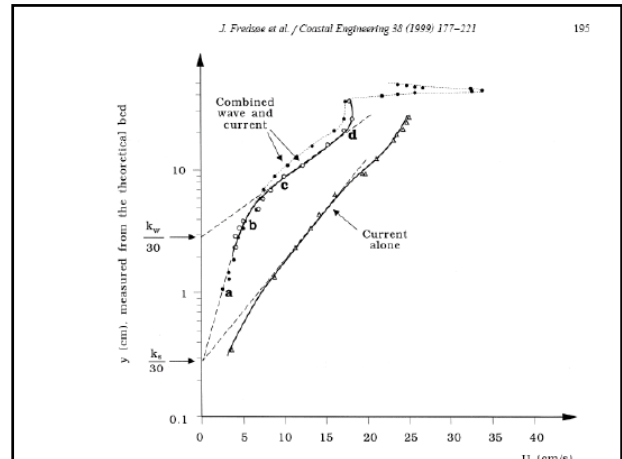
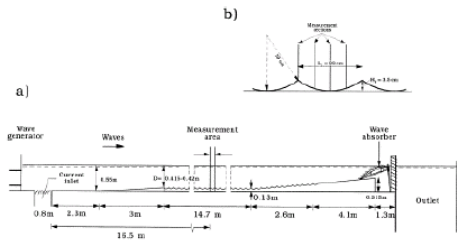
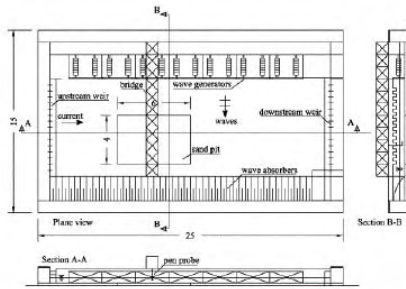


Figure 2A Variation of k_w/k_w with U_{1m}/U_c for different values of a/k_w . Fig. 2.AA: $\gamma = 0^\circ$, Fig. 2.AB: $\gamma = 90^\circ$.

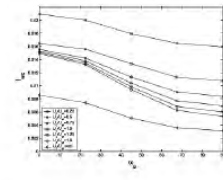
Flume tests, JF et al 1999.



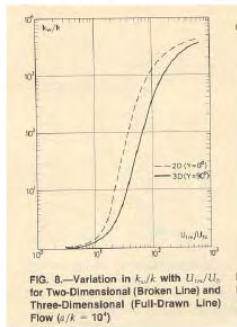
Andersen and Faraci 2003



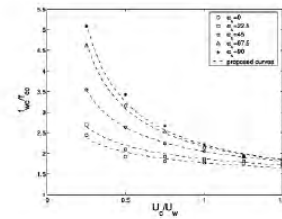
The wave plus current friction due to combined wave plus current over the rippled bed as a function of the mean current direction α .



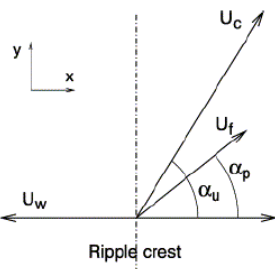
3D effects plane bed: larger roughness in 2D.



The wave plus current friction normalize with the current-only friction as a function of the current strength.



Ripples parallel with wave front: 2D formulation



Waves plus current

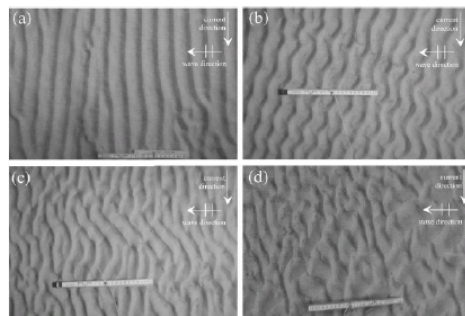


Fig. 2. Different types of ripple patterns: (a) regular (test no. 26, $U_c/U_w = 0.13$); (b) wavy (test no. 21, $U_c/U_w = 0.5$); (c) segmented (test no. 22, $U_c/U_w = 0.9$); (d) irregular (test no. 8, $U_c/U_w = 1.5$). The size of the ruler is 20 cm.

6. Some conclusions

- The progress in numerical modelling is extremely fast, open foam.
- Difficult to model current ripples, ripples in mud, silt and clay.
- You need to incorporate small scale in large scale modelling



August 31 – September 05

Short Course on Morphodynamics

- **Andreas Malcherek**

P R O F . D R . - I N G . A N D R E A S M A L C H E R E K

PERSONALS

Born: June 5th 1962
in: München (Munich)
nationality: German

EDUCATION

1968 – 1972 Primary School, Bremerhaven
1972 – 1980 Secondary School, Bremerhaven
December 1980 Abitur

1981 – 1984 Study of Physics, University of Hamburg
1984 – 1988 Study of Physics, Universität of Göttingen
Mai 1988 Diploma (M.Sc.) in Physics
1990 – 1996 Ph.D. Student at the Institute for Fluid Mechanics,
University of Hannover
Mai 1995 Ph.D. (Promotion Dr.-Ing.), Grade A
January 2001 Habilitation in Hydromechanics

CIVIL SERVICE

1988 – 1990 Man and Nature Institute Verden and
Orthopedical Clinic Hessisch-Lichtenau

PROFESSIONAL CAREER

1990 – 1996 Scientific Employee at the
Institute for Fluid Mechanics, Hannover University
1991 Exchange Scientist at the EDF, Paris, Chatou
1996 – 2004 Scientific Employee at the BAW Federal Waterways
Research and Engineering Institute, Germany, Hamburg

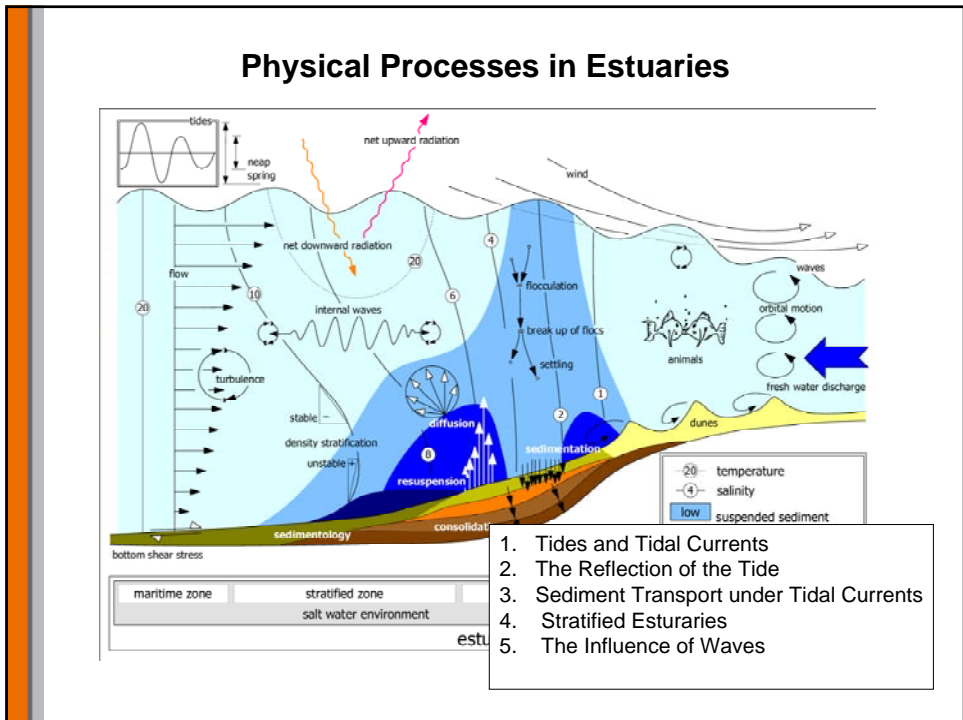
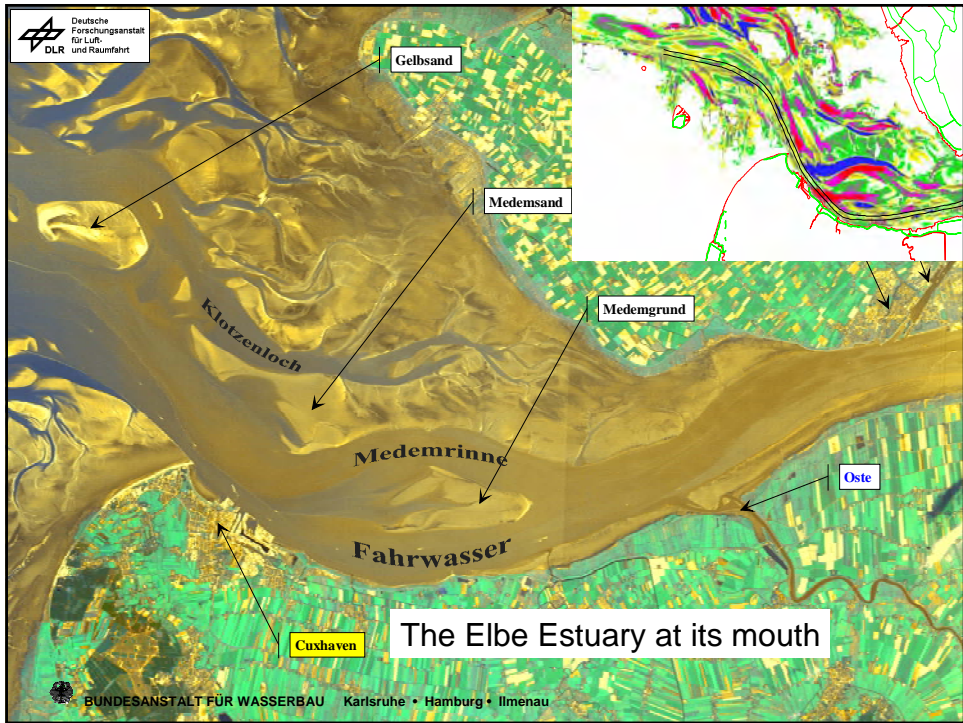
December 2004 Professorship for Hydraulic Engineering at the
University of the German Armed Forces, Munich

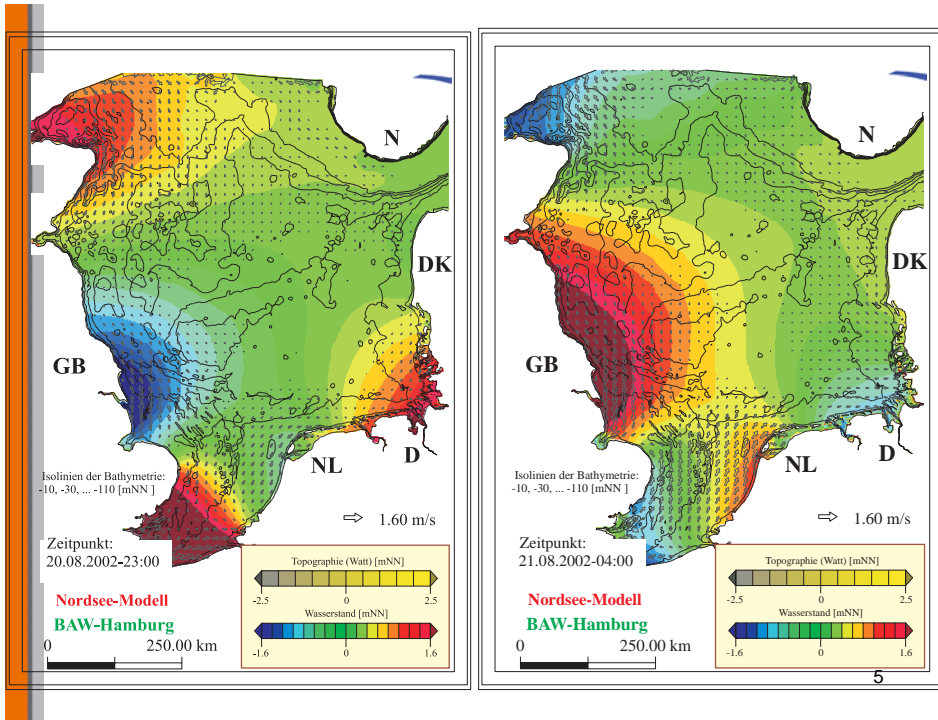
The Morphodynamics of Estuaries

Prof. Dr.-Ing. Andreas Malcherek
Institute for Water Sciences
University of the German Armed Forces München

Who am I?

1962 born in München
1980 High school diploma in Bremerhaven
1987 Master in Physics in Göttingen
(Max-Planck-Institute for Fluid Dynamics)
1995 Ph.D. in Civil Engineering
Prof. Dr.-Ing. W. Zielke, Hannover University
1996 Federal Waterways and Research Institute (BAW), Hamburg
2001 Habilitation in Hydromechanics
Since Dez. 2004 Professor for Hydraulic Engineering,
University of the German Armed Forces, München





Shallow Water Theory of the Tidal Wave

Free Surface Wave

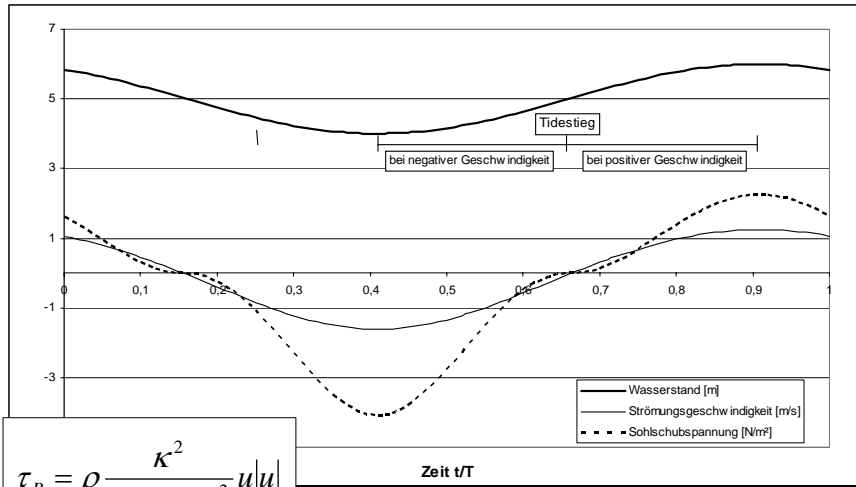
$$z_s(x, t) = \bar{z}_s + A \sin(kx - \omega t)$$

Momentum Equation

$$\frac{\partial u}{\partial t} = -g \frac{\partial z_s}{\partial x}$$

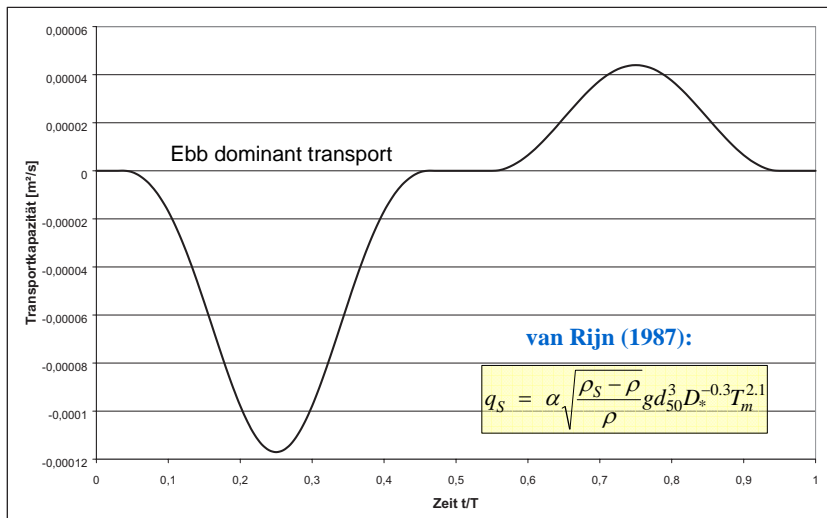
Velocity under Wave

$$u(x, t) = A \sqrt{\frac{g}{h}} \sin(kx - \omega t)$$



$$\tau_B = \rho \frac{\kappa^2}{\left(\ln \frac{12h}{k_s}\right)^2} u|u|$$

Bed Shear Stress under Tidal Wave

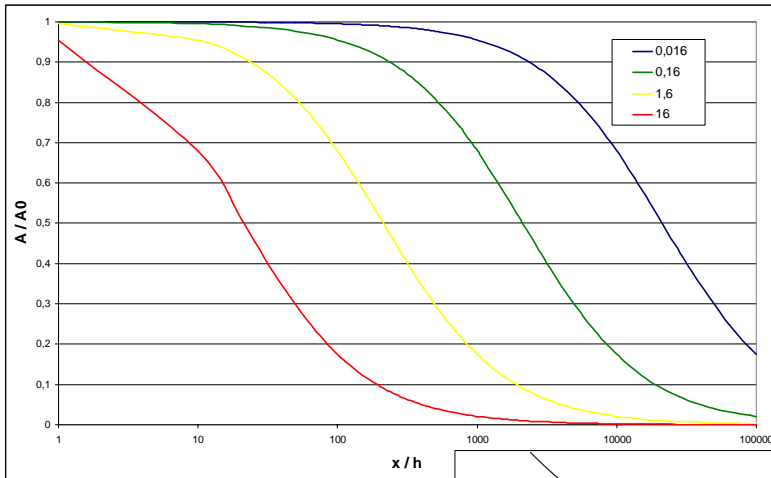


van Rijn (1987):

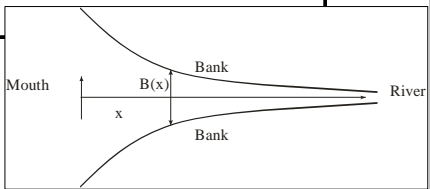
$$q_s = \alpha \sqrt{\frac{\rho_s - \rho}{\rho}} g d_{50}^3 D_*^{-0.3} T_m^{2.1}$$

Bed Load Transport Capacity under Tidal Wave

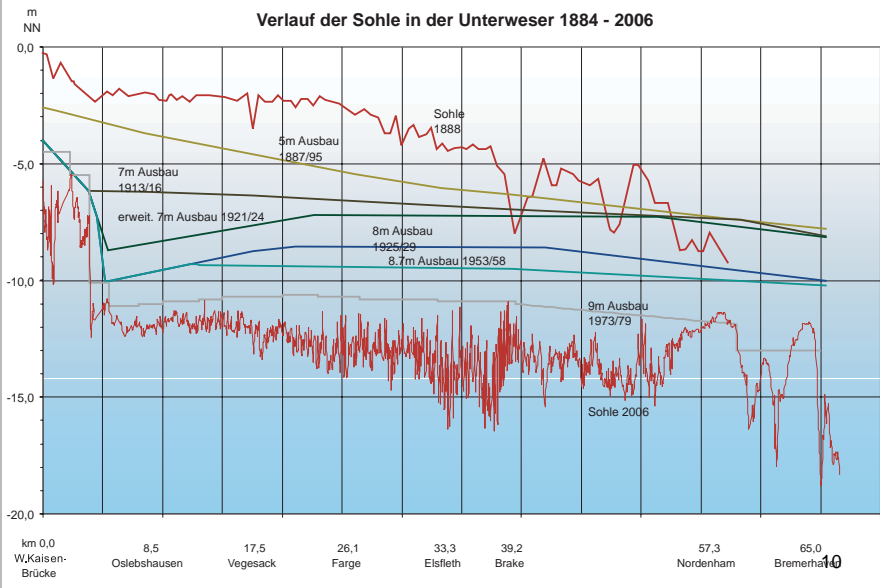
Tidal Wave Damping in an Estuary



$$\frac{A(\Delta x)}{A_0} = \left(1 + \frac{\lambda}{24\sqrt{2}} \frac{A_0}{h} \frac{\Delta x}{h} \right)^{-1}$$



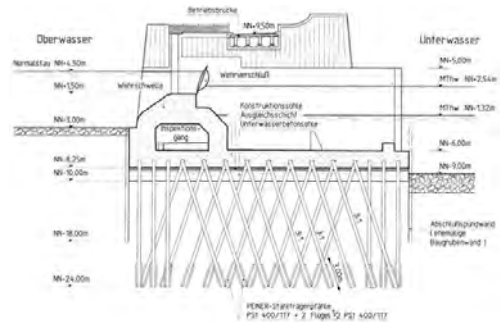
Channel Deepening



Stopping the Tidal Influence: Tidal Weirs

Length L of Tidal Influence:

$$\frac{L_1}{L_2} = \frac{h_1}{h_2}$$

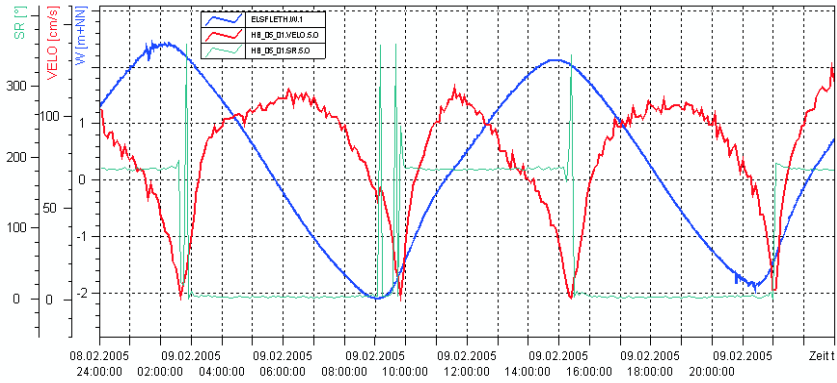


Tidal Reflection (without damping)

$$z_s(x, t) - \overline{z_s} = A(\sin(kx - \omega t) + \sin(-kx - \omega t)) = -2A \cos(kx) \sin(\omega t)$$

$$u(x, t) = A\sqrt{\frac{g}{h}}(\sin(kx - \omega t) - \sin(-kx - \omega t)) = A\sqrt{\frac{g}{h}} \sin(kx) \cos(\omega t)$$

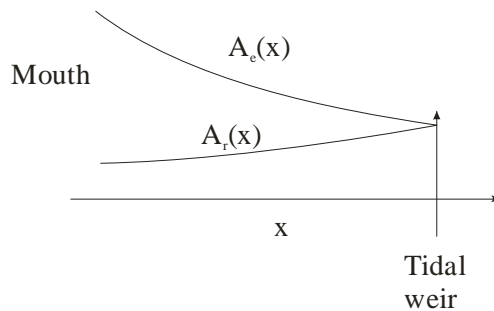
1. Amplitudes are doubled
2. Velocity nodes: No flow velocity
3. Free surface elevation nodes
4. 90° phase shift between velocity and tidal elevation



Tidal Elevation, Velocity and Flow Direction at Weser Gauge Elsfleth

13

Tidal Reflection including Damping

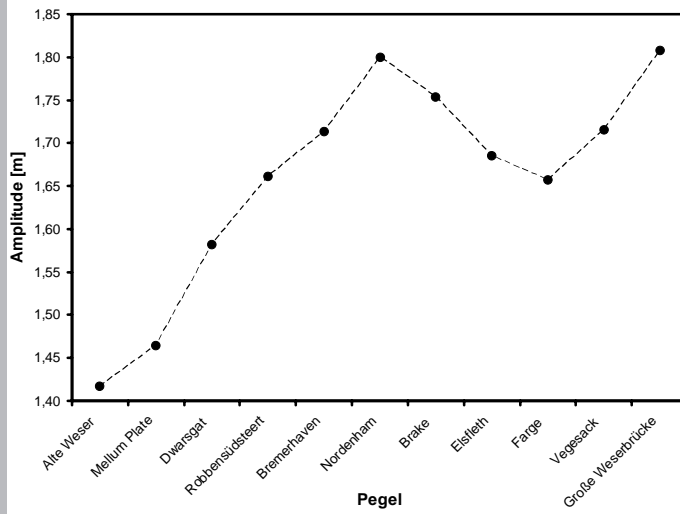


$$z_S(x, t) = \bar{z}_S + A_e(x) \sin(kx - \omega t) + A_r(x) \sin(-kx - \omega t)$$

$$u(x, t) = \sqrt{\frac{g}{h}} (A_e(x) \sin(kx - \omega t) - A_r(x) \sin(-kx - \omega t))$$

14

M2 Amplitude along the Weser

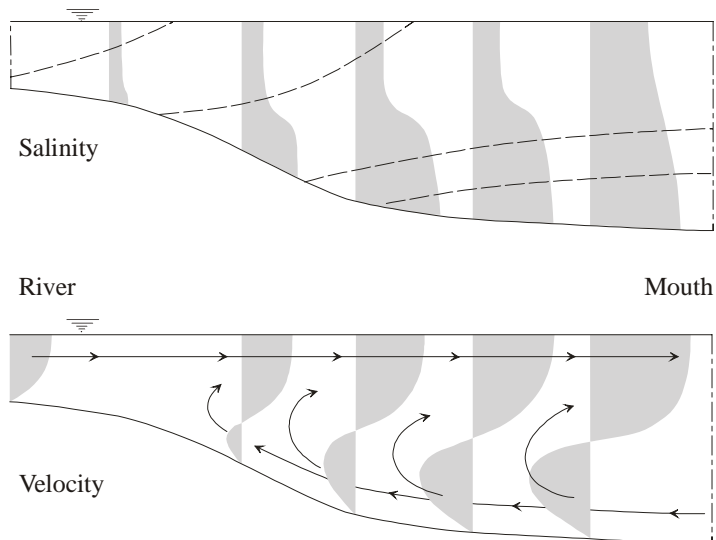


Reduction of Sediment Flushing

Microtidal Estuaries in the Baltic Sea



Circulation Patterns in Stratified Estuaries



Classification of Estuaries with Respect to Stratification

Estuary Number (Harleman & Abraham)

$$E = \frac{P_T F_0^2}{Q_F T}$$

$E < 0.005$ Stratified Estuary
 $0.005 < E < 0.2$ Partially Mixed Estuary
 $E > 0.2$ Well Mixed Estuary

Examples: Weser Estuary: $E = 0.25$
 Warnow Estuary $E = 0.0022$

19

Morphology of Stratified Estuaries

- Wave Climate
- Flushing by Fresh Water
- Near Bed Intrusion of Coarser Material by Circulation Pattern
- Outflow of Fine Sediments at the Free Surface

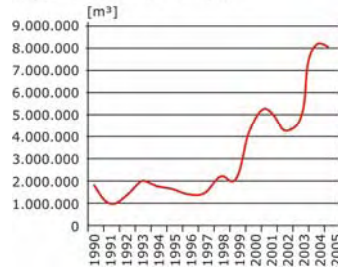


20

Phenomena Related with Cohesive Suspended Sediment Transport

- Turbidity (Maximum)
- Mud Formation
- (Harbour) Siltation

Baggermenge (Schlick-Sediment)

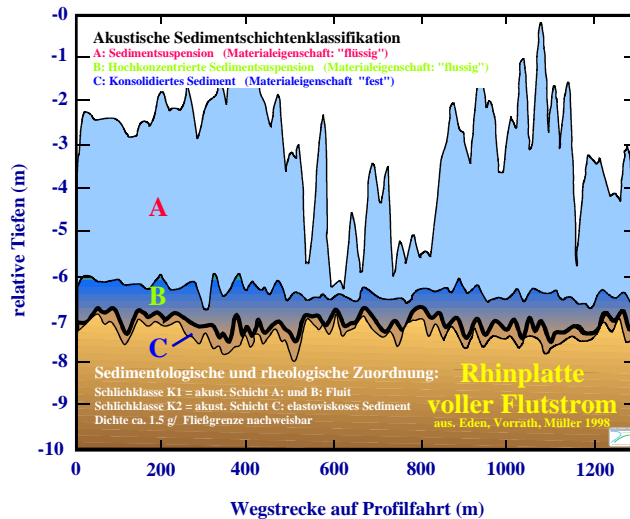


Volume of dredged sediments in Ports of Hamburg (HPA)



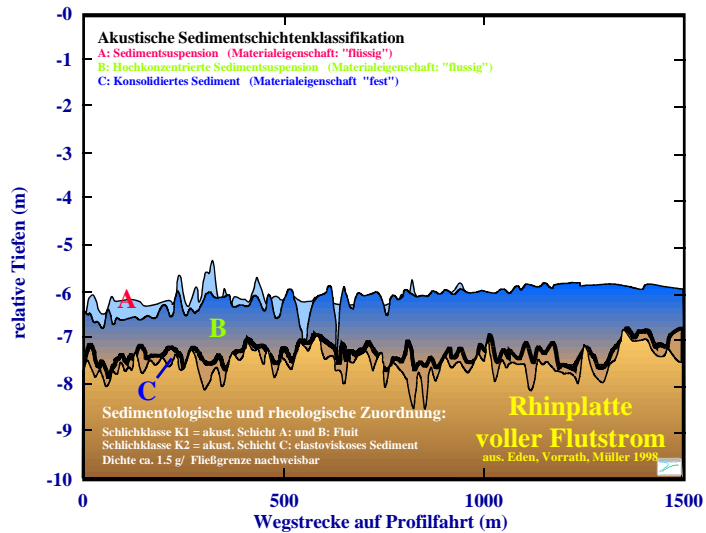
21

Acoustic Profile during full Ebb Flow



22

Accoustic Profile during Slack Water



23

Process Classification Depending on Concentration

C	Medium	Vertical movement	Horizontal Transport	Rheology	Turbulence
<1g/l	Suspension	Free settling	Advection	Newton	No influence
>1g/l	HCS	Hindered Settling	Advection	Newton	damped
>10g/l	Fluid Mud	Hindered Settling	Shear flow	Visco-plastic	none
>250g/l	Consolidated bed	Consolidation	none	Plastic-elastic	none

24

Changes of State

From /to	Suspension	Mud	Soil
Suspension	-	Settling	Deposition
Mud	Entrainment	-	Consolidation
Soil	Erosion	Fluidisation Liquefaction	-

25

Suspended Matter Concentration Elbe Estuary

Run01 - Laengsprofil

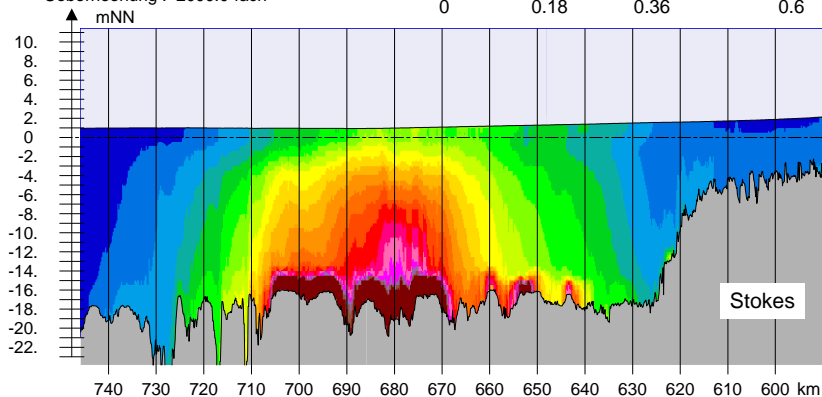
Zeitraum: 11.05.2002-16:40 bis 25.05.2002-23:30

0 25.00 50.00 km

Ueberhoehung : 2000.0-fach

mittlerer Schwebstoffgehalt (Mit)
sum of all fractions
kg/m³

0 0.18 0.36 0.6



Profil : Laengsprofil Tideelbe TRASSE

26

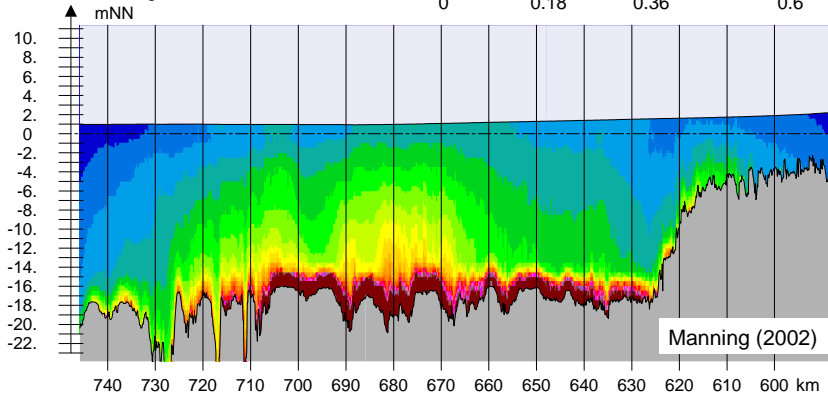
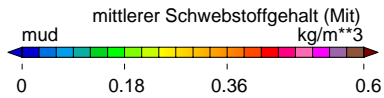
Suspended Matter Concentration Elbe Estuary

Run04 - Laengsprofil

Zeitraum: 11.05.2002-16:40 bis 25.05.2002-23:30

0 25.00 50.00 km

Ueberhoehung : 2000.0-fach



Profil : Laengsprofil Tideelbe TRASSE

27

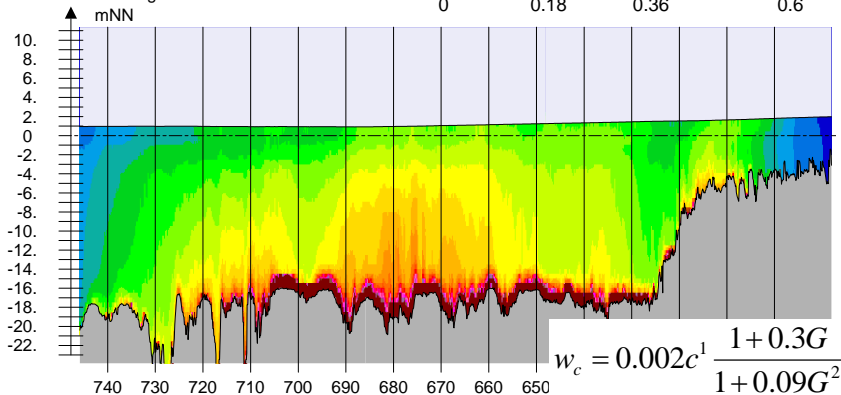
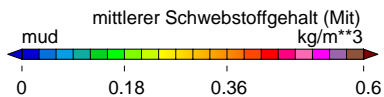
Suspended Matter Concentration Elbe Estuary

Run06b

Zeitraum: 11.05.2002-16:40 bis 25.05.2002-23:30

0 25.00 50.00 km

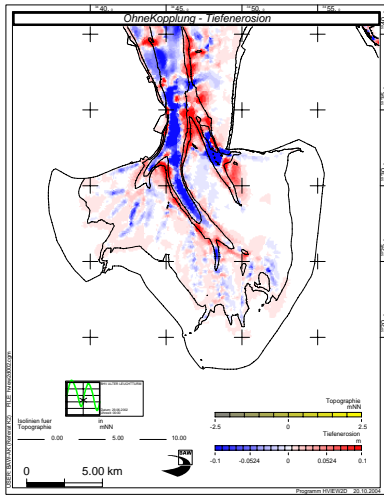
Ueberhoehung : 2000.0-fach



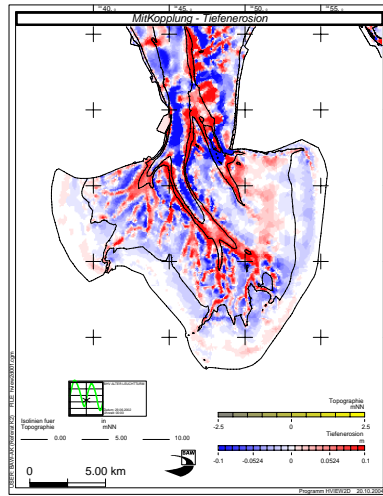
Profil : Laengsprofil Tideelbe TRASSE

28

The Effect of Waves ... on the bed evolution



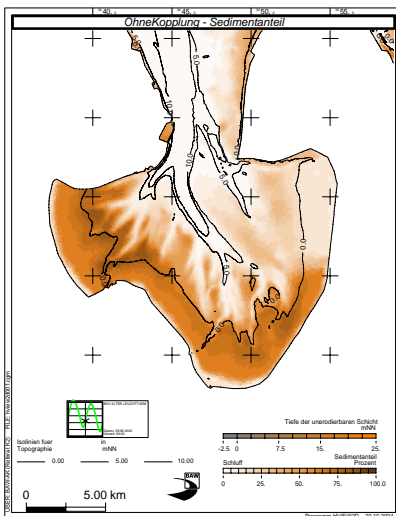
With waves



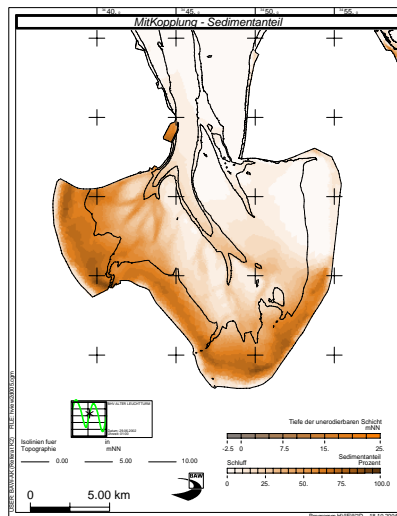
without waves

29

The Effect of Waves ... on the silt contents



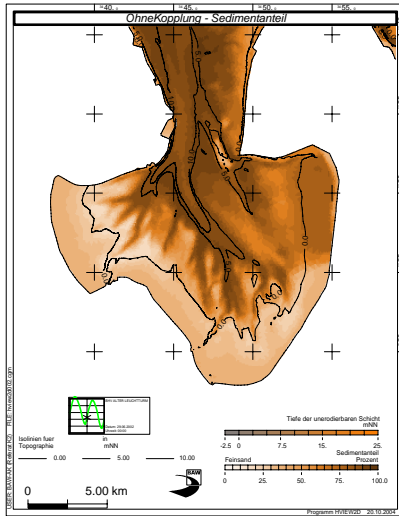
With waves



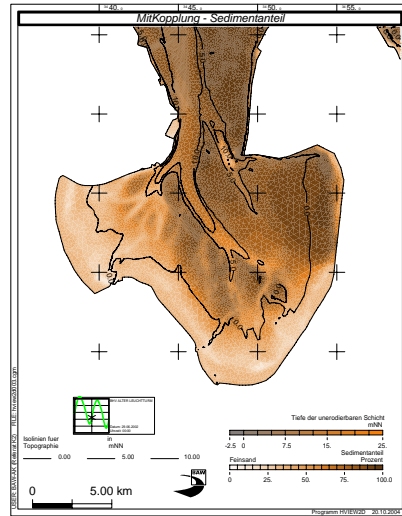
without waves

30

The Effect of Waves ... on the fine sand contents



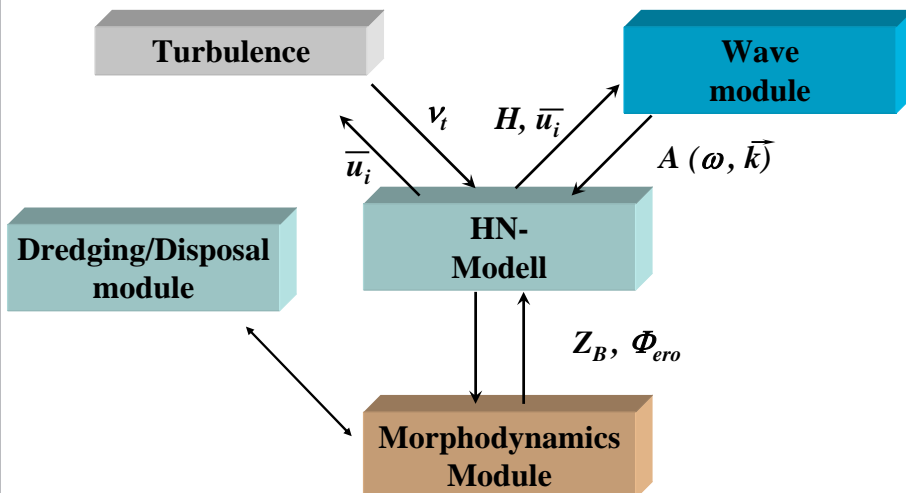
With waves



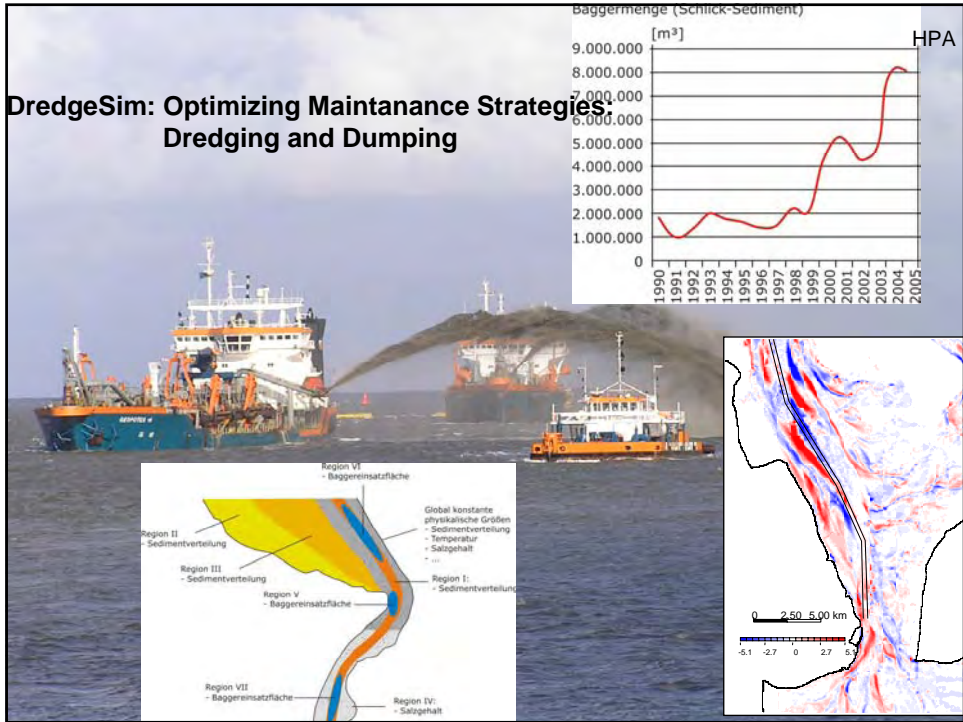
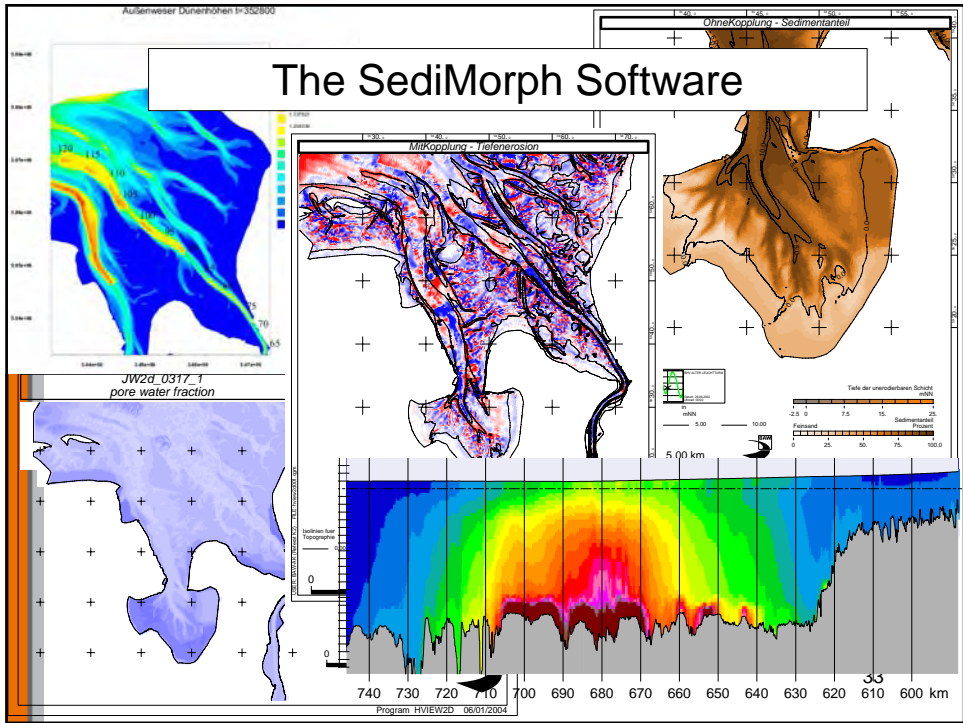
without waves

31

Simulation of Estuarine Morphodynamics using Modular Systems



32





August 31 – September 05

Short Course on Morphodynamics

- **Chris Sherwood**

Christopher R. Sherwood, 05 July 1954, U.S.A.

Research oceanographer, Coastal and Marine Geology,
U. S. Geological Survey, Woods Hole, Massachusetts, U.S.A

Chris Sherwood received an A.B. in Economics and Environmental Studies at Bowdoin College, Maine in 1976, an M.S. and Ph.D. in Geological Oceanography at the University of Washington, Seattle in 1982 and 1995.

His first job was as an oilwell mudlogger and wellsite geologist. After his M.S., he worked as a project oceanographer for a consulting firm in Alaska, and as a research scientist at the Pacific Northwest National Laboratory, in Richland and Sequim, Washington, focusing on marine environmental problems. His dissertation work included measurements and a model of suspended-sediment transport on the California continental shelf. He spent three years in Australia, working as a research scientist for the Commonwealth Scientific and Industrial Research Organisation (CSIRO) in Hobart, Tasmania, before returning to the U.S. to work for the U.S. Geological Survey. Sherwood is the USGS leader and co-principal investigator of the Community Sediment-Transport Modeling System (CSTMS), a project funded by the National Oceanographic Partnership Program to develop an open-source model for coastal oceanography, sediment transport, and morphodynamics. He is active in the American Geophysical Union and was co-chair of the Ocean Sciences 2008 Meeting, held in Orlando, Florida last March.



Butman, B., C. R. Sherwood, and P. S. Dalyander (2008) Northeast storms ranked by wind stress and wave-generated bottom stress observed in Massachusetts Bay, 1990-2006, *Continental Shelf Research*, 28(10-11): 1231-1245, DOI: 10.1016/j.csr.2008.02.010.

Condie, S. A., and C. R. Sherwood (2006) Sediment distribution and transport across the continental shelf and slope under idealized wind forcing, *Progress In Oceanography*, 70: 255-270, doi:10.1016/j.pocean.2005.07.003.

Haidvogel, D. B., H. Arango, W. P. Budgell, B. D. Cornuelle, E. Curchitser, E. Di Lorenzo, K. Fennel, W. R. Geyer, A. J. Hermann, L. Lanerolle, J. Levin, J. C. McWilliams, A. J. Miller, A. M. Moore, T. M. Powell, A. F. Shchepetkin, C. R. Sherwood, R. P. Signell, J. C. Warner, and J. Wilkin (2008) Ocean Forecasting in Terrain-following Coordinates: Formulation and Skill Assessment of the Regional Ocean Modeling System, *Journal of Computational Physics*, 2008: 3595-3624, 10.1016/j.jcp.2007.06.016.

Lacy, J. R., C. R. Sherwood, D. J. Wilson, T. A. Chisholm, and G. R. Gelfenbaum (2005) Estimating hydrodynamic roughness in a wave-dominated environment with a



August 31 – September 05

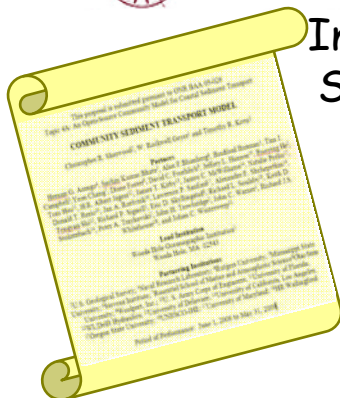
Short Course on Morphodynamics

- **Chris Sherwood**

- high-resolution acoustic Doppler profiler, *Journal of Geophysical Research*, 110, C06014.
- Lee, H. J., C. R. Sherwood, D. E. Drake, B. D. Edwards, F. Wong, and M. Hamer (2002) Spatial and temporal distribution of contaminated, effluent-affected sediment on the Palos Verdes margin, southern California, *Continental Shelf Research*, 22(6-7): 859-880.
- Rinehimer, J. P., C. K. Harris, C. R. Sherwood, and L. P. Sanford (2007) Sediment consolidation in a muddy, tidally-dominated environment: model behavior and sensitivity, *Proceedings of the Estuarine and Coastal Modeling Conference*, in press.
- Sherwood, C. R., J. W. Book, S. Carniel, L. Cavaleri, J. Chiggiato, H. Das, J. D. Doyle, C. K. Harris, A. W. Niedoroda, H. Perkins, P.-M. Poulain, J. Pullen, C. W. Reed, A. Russo, M. Sclavo, R. P. Signell, P. Traykovski, and J. C. Warner (2004) Sediment dynamics in the Adriatic Sea investigated with coupled models, *Oceanography*, 17(4): 58-69.
- Sherwood, C. R., D. E. Drake, P. L. Wiberg, and R. A. Wheatcroft (2002) Prediction of the fate of p,p'-DDE in sediment on the Palos Verdes shelf, California, USA, *Continental Shelf Research*, 22(6-7): 1025-1058.
- Sherwood, C. R., J. R. Lacy, and G. Voulgaris (2006) Shear velocity estimates on the inner shelf off Grays Harbor, Washington, U.S.A., *Continental Shelf Research*, 26(17/18): 1995-2018, doi:10.1016/j.csr.2006.07.025.
- Signell, R. P., S. Carniel, J. Chiggiato, I. Janekovic, J. Pullen, and C. R. Sherwood (2008) Collaboration tools and techniques for large model datasets, *Journal of Marine Systems*, 69: 154-161, doi:10.1016/j.jmarsys.2007.02.013.
- Warner, J. C., C. R. Sherwood, and W. R. Geyer (2007) Sensitivity of estuarine turbidity maximum to settling velocity, tidal mixing, and sediment supply, in Maa, J. P.-Y., L. P. Sanford, and D. H. Schoellhammer, eds., *Estuarine and Coastal Fine Sediment Dynamics*: Amsterdam, Elsevier, 355-376.
- Warner, J. C., C. R. Sherwood, R. P. Signell, C. K. Harris, and H. G. Arango (2008) Development of a three-dimensional, regional, coupled wave, current, and sediment-transport model, *Computers & Geosciences*, 34: 1284-1306, doi:10.1016/j.cageo.2008.02.012.
- Wiberg, P. L., and C. R. Sherwood (2008) Calculating wave-generated bottom orbital velocity from surface wave parameters, *Computers & Geosciences*, 34: 1243-1262, doi:10.1016/j.cageo.2008.02.010.



National Oceanographic Partnership Program
Promoting Partnerships for the Future of Oceanography



Introduction to the Community Sediment-Transport Modeling System

Christopher R. Sherwood
U.S. Geological Survey

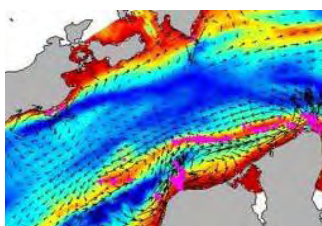
Presented by Dano Roelvink
ICCE 2008 Morphodynamics Short Course
2 September 2008, Hamburg, Germany



<http://www.cstms.org>



What are we trying to do?



Signell, 2007

- Coupled models: Meteorological + Hydrodynamics + Sediment Transport + Bed Stratigraphy + Morphodynamics
- Improved parameterizations for sediment processes
- Model tests and evaluation
 - Regression tests
 - Simple cases: analytical, lab, and process evaluation
 - Real-world applications
- Model tools - Grid generation, I/O preparation, Visualization
- Distribution, documentation, training

How are we doing it?



The daydreams of cat herders

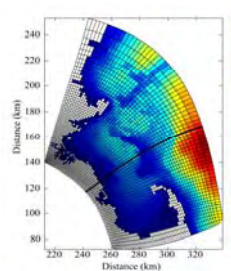
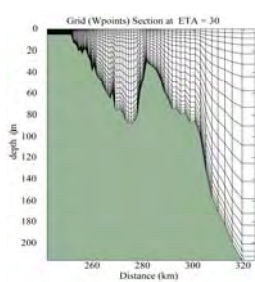
Copyright © 2002 David Farley, d-farley@ibiblio.org
http://ibiblio.org/Dave/drfun.html

- Building on an existing model
- MIT/X open-source license
- Collaboration tools: Subversion, Trac, Wiki, WebEx, Winmerge
- Entraining unfunded collaborators

Regional Ocean Modeling System



- Free surface, hydrostatic ocean model w/ time-splitting
- Finite-difference 3D Reynolds-averaged Navier-Stokes equations
- Horizontal orthogonal curvilinear Arakawa C grid
- Vertical stretched terrain-following “S” coordinates
- Wide range of advection schemes: (e.g. 3rd-order upstream-biased, 4th-order)
- Wide range of open boundary conditions: (e.g. Radiation, clamped, nudged)
- Multiple vertical mixing schemes (LMD/KPP, MY2.5, Ri-based, constant)

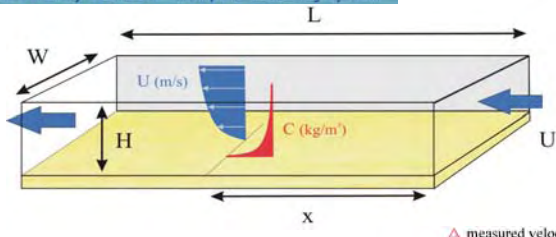


- Biological modules (NPDZ, ECOSIM)
- Model adjoint for data assimilation
- Surface and bottom boundary layer models
- Parallel Fortran 90 code in MPI and OpenMP
- Runs on Unix, Mac, and Windows; notebook PC to massive clusters.

CSTMS

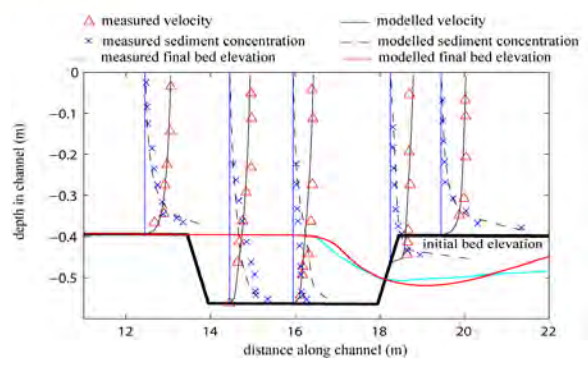
Community Sediment Transport Modeling System

Test Cases



- Steady channel flow
- 1-D sediment

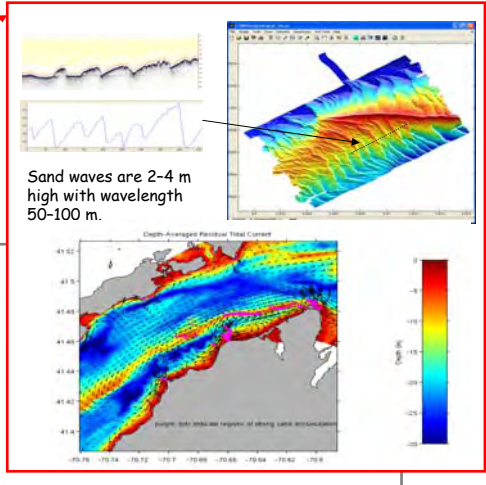
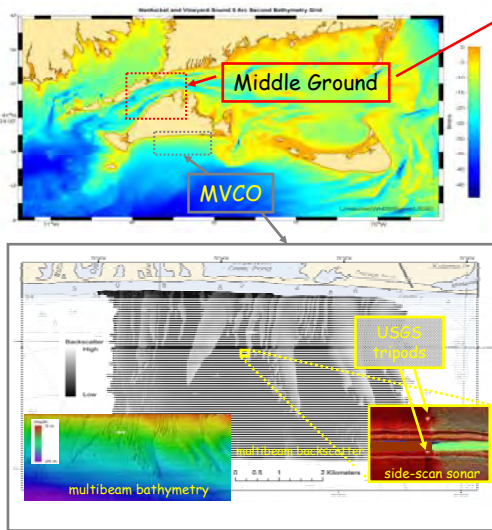
- Flume comparison
- Tidal inlet
- Estuary



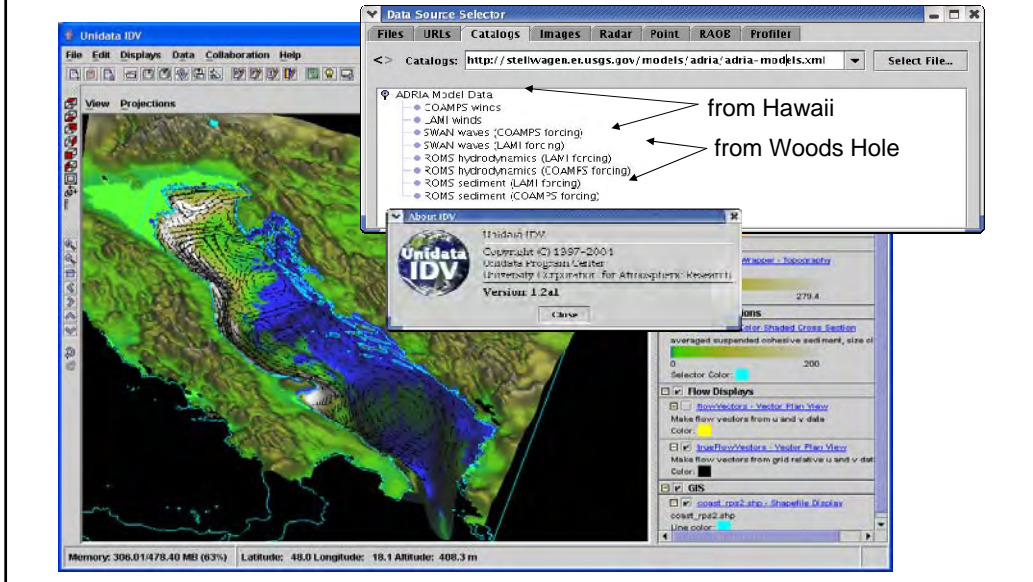
CSTMS

Community Sediment Transport Modeling System

Demo Applications



Visualization Tools via Standards: IDV



What have we accomplished?

- New turbulence submodel
- Better advection scheme
- Bedload, suspended load, stratigraphy
- Coupled wave model, wave-driven circulation
- Wetting/drying
- Composite grids
- Cohesive sediment and mixed sediment
- Time-dependent bedforms
- NOPP funding for 18 partner institutions
- Open-source license
- Web-based collaboration tools
- ESMF coupling
- Documentation
- Standards
- Test cases
- Applications

<http://www.cstms.org>



How can I participate in CSTMS?

- Register as a ROMS user; indicate "research interest" in CSTMS
- Use Subversion to download the code
- Build it and run it on a Windows laptop, using Cygwin and gfortran
- Coupled applications will run on a dual-core PC.
- Larger applications run efficiently on Linux clusters
- Get a branch in the CSTMS repository
- Maintain your own modified code there
- Allow everyone or selected collaborators to view it
- Merge the code with the Trunk in your branch, provide a test case, and Hernan Arango will port it to the Trunk

*Attend workshops in Grenoble (October 2008)
or Sydney (March 2009)*

<http://www.cstms.org>

Development of a three-dimensional, regional, coupled wave, current, and sediment-transport model[☆]

John C. Warner^{a,*}, Christopher R. Sherwood^a, Richard P. Signell^a, Courtney K. Harris^b, Hernan G. Arango^c

^aUS Geological Survey, Coastal and Marine Geology Program, Woods Hole, MA 02543, USA

^bVirginia Institute of Marine Science, Gloucester Point, VA 23062, USA

^cInstitute for Marine and Coastal Sciences, Rutgers-The State University of New Jersey, New Brunswick, NJ 08901, USA

Received 5 September 2006

Abstract

We are developing a three-dimensional numerical model that implements algorithms for sediment transport and evolution of bottom morphology in the coastal-circulation model Regional Ocean Modeling System (ROMS v3.0), and provides a two-way link between ROMS and the wave model Simulating Waves in the Nearshore (SWAN) via the Model-Coupling Toolkit. The coupled model is applicable for fluvial, estuarine, shelf, and nearshore (surfzone) environments. Three-dimensional radiation-stress terms have been included in the momentum equations, along with effects of a surface wave roller model. The sediment-transport algorithms are implemented for an unlimited number of user-defined non-cohesive sediment classes. Each class has attributes of grain diameter, density, settling velocity, critical stress threshold for erosion, and erodibility constant. Suspended-sediment transport in the water column is computed with the same advection–diffusion algorithm used for all passive tracers and an additional algorithm for vertical settling that is not limited by the CFL criterion. Erosion and deposition are based on flux formulations. A multi-level bed framework tracks the distribution of every size class in each layer and stores bulk properties including layer thickness, porosity, and mass, allowing computation of bed morphology and stratigraphy. Also tracked are bed-surface properties including active-layer thickness, ripple geometry, and bed roughness. Bedload transport is calculated for mobile sediment classes in the top layer. Bottom-boundary layer submodels parameterize wave–current interactions that enhance bottom stresses and thereby facilitate sediment transport and increase bottom drag, creating a feedback to the circulation. The model is demonstrated in a series of simple test cases and a realistic application in Massachusetts Bay.

© 2008 Elsevier Ltd. All rights reserved.

Keywords: Sediment transport; Nearshore modeling; Three-dimensional numerical model; Model coupling

1. Introduction

1.1. Community modeling approach

Models for transport and long-term fate of particles in coastal waters are essential for a variety of applications related to commerce, defense, public

[☆] <http://www.unidata.ucar.edu/software/netcdf/>.

*Corresponding author. Tel.: +1 508 457 2237; fax: +1 508 457 2310.

E-mail addresses: jwarner@usgs.gov (J.C. Warner), csherwood@usgs.gov (C.R. Sherwood), rsignell@usgs.gov (R.P. Signell), ckharris@vims.edu (C.K. Harris), arango@marine.rutgers.edu (H.G. Arango).

health, and the quality of the marine environment. There exists a need to develop a sediment-transport model that is freely available, well tested, widely accepted, and applicable to a variety of coastal settings.

We are using a community approach to develop the model as a tool for both research and practical applications. The need and value for this approach was elucidated in a community sediment-transport modeling workshop (Sherwood et al., 2002). A community effort enables us to include a broad range of processes and scales, more than would be feasible for individuals or small groups. We have started with a model that is being used and developed actively by a large research community. We are incorporating proven methodologies from other models such as ECOMSed, EFDC, COHERENS, and Delft3D. Scientists and engineers may contribute to the model according to their expertise, and users (including scientists from other disciplines, students, resource managers, engineers, and operational personnel) may draw from well-tested, state-of-the-art algorithms. Incorporation of alternative parameterizations for similar processes allows us to compare them in identical frameworks. Collaborative work on a community model helps identify key research and modeling issues, and efficiently focus research efforts, minimizing duplication and preventing critical components from being overlooked. Wide use and broad participation in model development, along with extensive testing and peer review, will produce a robust model that can serve the scientific community.

1.2. Regional oceanographic modeling system (ROMS)

Our eventual goal is to produce a sediment model that may be coupled in a flexible way to any of a number of hydrodynamic modules. To reach this goal, we started with a specific model so we could develop sediment-transport algorithms in the context of a completely functional framework. The advancements we are making and the algorithms that we are developing are linked integrally, for now, with the Regional Ocean Modeling System (ROMS). ROMS is a numerical coastal ocean circulation model that includes several submodels that simulate, for example, sea ice, biological processes, and sediment transport. For each application, different components of the model are included or excluded via C-preprocessor (cpp)

directives defined in an include file (*cppdefs.h*). This ensures that memory is allocated only as needed, and that only relevant computational algorithms are compiled, creating a more efficient executable file.

The ROMS community interacts through internet, publications, and annual meetings. Revised versions of model code, reports of bugs, and solutions to problems are posted on-line at the ROMS website. Most model inputs and output files, including those relevant for sediment-transport calculations, are written using the NetCDF data architecture (<http://www.unidata.ucar.edu/software/netcdf/>) in a format compliant with climate and forecast (CF) metadata conventions (<http://www.unidata.ucar.edu/software/netcdf/conventions.html>). This allows users to capitalize on existing visualization and processing tools that have been and are continuing to be developed by various communities, and encourages documentation of model runs via metadata embedded in input and output files. The code is written in modular Fortran90 and runs in serial mode or on multiple processors using either shared- or distributed-memory architectures (OpenMP or MPI). These characteristics made ROMS an ideal starting point for our development of a community sediment-transport model.

1.3. Objective

This paper describes the implementation in ROMS of a sediment-transport model, new bottom-boundary layer routines, a bed model to track morphology and stratigraphy, wave-current interaction, and coupling of ROMS to the surface wave model Simulating Waves Nearshore (SWAN). The coupled system is distributed as ROMS v3.0. Here we provide background information about ROMS, details of the new sediment algorithms, methods for two-way coupling of ROMS to SWAN, and several examples that demonstrate specific capabilities of the modeling system.

The model is continually evolving, and this description represents a snap-shot of current capabilities and algorithms. Our plan is to eventually extract the sediment-transport components and provide them as separate modules. Our long-term objectives are to expand the modeling system to include effects of cohesive sediments, couple with Boussinesq phase-resolving wave models, add submodels for wave runup on the beach, and include submodels for detailed fluid mechanics and particle interactions near the bed.

2. Circulation and wave model framework

2.1. Hydrodynamic model

ROMS is a three-dimensional, free surface, terrain-following numerical model that solves finite-difference approximations of the Reynolds-averaged Navier–Stokes (RANS) equations using the hydrostatic and Boussinesq assumptions (Chassignet et al., 2000; Haidvogel et al., 2000) with a split-explicit time stepping algorithm (Shchepetkin and McWilliams, 2005; Haidvogel et al., 2007). It uses a horizontal curvilinear Arakawa C grid and vertical stretched terrain-following coordinates (see Section 2). ROMS has a flexible structure that allows choices for many of the model components, including options for advection schemes (second order, third order, fourth order, and positive definite), turbulence submodels, and boundary conditions. It includes bottom- and surface-boundary layer submodels, air-sea fluxes, surface drifters, a nutrient-phytoplankton-zooplankton model, and a fully developed adjoint model for computing model inverses and data assimilation. Momentum, scalar advection, and diffusive processes are represented using transport equations. The density field is determined from an equation of state that accounts for temperature, salinity, and suspended-sediment concentrations. In this paper, the term constant refers to values that are time-invariant, and the term uniform refers to values that do not vary in space. The governing Eqs. (1)–(5) are presented in flux form, in Cartesian horizontal coordinates and sigma vertical coordinates. For curvilinear grids, additional metric terms appear (Haidvogel et al., 2000) that are not shown here. A complete list of variables is given in Table 1. The momentum equations are:

$$\begin{aligned} & \frac{\partial(H_z u)}{\partial t} + \frac{\partial(u H_z u)}{\partial x} + \frac{\partial(v H_z u)}{\partial y} + \frac{\partial(\Omega H_z u)}{\partial s} - f \\ H_z v = & -\frac{H_z}{\rho_0} \frac{\partial p}{\partial x} - H_z g \frac{\partial \eta}{\partial x} - \frac{\partial}{\partial s} \left(\overline{u'w'} - \frac{v}{H_z} \frac{\partial u}{\partial s} \right) \\ & - \frac{\partial(H_z S_{xx})}{\partial x} - \frac{\partial(H_z S_{xy})}{\partial y} + \frac{\partial S_{px}}{\partial s} \end{aligned} \quad (1)$$

$$\begin{aligned} & \frac{\partial(H_z v)}{\partial t} + \frac{\partial(u H_z v)}{\partial x} + \frac{\partial(v H_z v)}{\partial y} + \frac{\partial(\Omega H_z v)}{\partial s} + f \\ H_z u = & -\frac{H_z}{\rho_0} \frac{\partial p}{\partial y} - H_z g \frac{\partial \eta}{\partial y} - \frac{\partial}{\partial s} \left(\overline{v'w'} - \frac{v}{H_z} \frac{\partial v}{\partial s} \right) \\ & - \frac{\partial(H_z S_{yx})}{\partial x} - \frac{\partial(H_z S_{yy})}{\partial y} + \frac{\partial S_{py}}{\partial s} \end{aligned} \quad (2)$$

$$0 = -\frac{1}{\rho_0} \frac{\partial p}{\partial s} - \frac{g}{\rho_0} H_z \rho \quad (3)$$

with continuity as

$$\frac{\partial \eta}{\partial t} + \frac{\partial(H_z u)}{\partial x} + \frac{\partial(H_z v)}{\partial y} + \frac{\partial(H_z \Omega)}{\partial s} = 0 \quad (4)$$

and scalar transport:

$$\begin{aligned} & \frac{\partial(H_z C)}{\partial t} + \frac{\partial(u H_z C)}{\partial x} + \frac{\partial(v H_z C)}{\partial y} + \frac{\partial(\Omega H_z C)}{\partial s} \\ & = -\frac{\partial}{\partial s} \left(\overline{c'w'} - \frac{v_\theta}{H_z} \frac{\partial C}{\partial s} \right) + C_{source} \end{aligned} \quad (5)$$

where u , v , and Ω are the mean components of velocity in the horizontal (x and y) and vertical (s) directions respectively; the vertical sigma coordinate $s = (z - \eta)/D$ ranges from $s = -1$ at the bottom to $s = 0$ at the free surface; z is the vertical coordinate positive upwards with $z = 0$ at mean sea level; η is the wave-averaged free-surface elevation; D is the total water depth $D = h + \eta$; h is the depth below mean sea level of the sea floor; H_z is the grid-cell thickness; f is the Coriolis parameter. An overbar indicates a time average, and a prime (') indicates a fluctuating turbulent quantity. Pressure is p ; ρ and ρ_0 are total and reference densities for seawater; g is acceleration due to gravity; ν and ν_θ are molecular viscosity and diffusivity; C represents a tracer quantity (for example, salt, temperature, and suspended-sediment); C_{source} are tracer source/sink terms; and a function $\rho = f(C)$ is required to close the density relation. These equations are closed by parameterizing the Reynolds stresses and turbulent tracer fluxes as

$$\begin{aligned} \overline{u'w'} &= -K_M \frac{\partial u}{\partial z}, & \overline{v'w'} &= -K_M \frac{\partial v}{\partial z}, \\ \overline{\rho'w'} &= -K_H \frac{\partial \rho}{\partial z} \end{aligned} \quad (6)$$

where K_M is the eddy viscosity for momentum and K_H is the eddy diffusivity. Eddy viscosities and eddy diffusivities are calculated using one of five options for turbulence-closure models in ROMS: (i) Brunt-Väisälä frequency mixing in which mixing is based on the stability frequency; (ii) a user-provided analytical expression such as a constant or parabolic shape; (iii) the K -profile parameterization (Large et al., 1994), expanded to include both surface and bottom-boundary layers by Durski et al., 2004; (iv) Mellor-Yamada level 2.5 (MY2.5) method (Mellor and Yamada, 1982); and (v) the generic length-scale (GLS) method (Umlauf and Burchard,

Table 1
List of symbols

Symbol	Description	Dimensions
A_b	Wave orbital excursion amplitude	m
A_R	Wave roller area	m ²
C	Tracer (temperature, salt, or suspended-sediment concentration)	°C, salinity, or kg m ⁻³
C_{dBF}	Bedform drag coefficient	–
C_{source}	Tracer source/sink term	C units ms ⁻¹
D	Total water depth	m
D_{50}	Median grain diameter	m
	Wave energy	m ³ s ⁻²
E_s	Erosion source term	kg m ⁻² s ⁻¹
E_0	Erosion rate for each sediment class	kg m ⁻² s ⁻¹
$F_{CC} F_{CS} F_{SS} F_{SC}$	Hyperbolic functions	–
H_z	Grid cell thickness	m
K_H	Eddy diffusivity	m ² s ⁻¹
K_M	Eddy viscosity	m ² s ⁻¹
L	Wave length	m
N	Wave action density	m ³ s ⁻¹
N_{bed}	Number of bed layers	–
Q_b	Fraction of breaking waves	–
R_z	Wave roller shape function	–
S_w	Wave energy source/sink term	m ³ s ⁻²
$S_{px} S_{py}$	Vertically varying vertical radiation stresses	m ² s ²
$S_{xx} S_{xy} S_{yx} S_{yy}$	Vertically varying horizontal radiation stresses	m ² s ²
$\overline{S_{xx}} \overline{S_{xy}} \overline{S_{yx}} \overline{S_{yy}}$	Vertically integrated horizontal radiation stresses	m ² s ²
T	Near-bottom average wave period	s
T^*	Ratio of τ_{wc}/τ_{ce}	–
C	Wave celerity	m s ⁻¹
c_x	Wave celerity x -direction	m s ⁻¹
c_y	Wave celerity y -direction	m s ⁻¹
c_g	Wave group celerity	m s ⁻¹
c_θ	Wave celerity in directional (θ) space	m s ⁻¹
c_σ	Wave celerity in frequency (σ) space	m s ⁻¹
c'	Turbulent concentration	°C, salinity, or kg m ⁻³
d_0	Wave orbital diameter	m
f	Coriolis parameter	s ⁻¹
f_w	Wave friction factor	–
g	Gravity	m s ⁻²
k	Wave number (= 1/wave length)	m ⁻¹
k_b	Bottom roughness length	m
k_x	Wave number in x -direction	m ⁻¹
k_y	Wave number in y -direction	m ⁻¹
$k_1 k_2$	Active layer thickness coefficients	–
m	Index for each sediment class	–
p	Pressure	N m ⁻²
q_{bl}	Bedload transport rate	kg m ⁻² s ⁻¹
q_{blx}	Bedload transport rate in x -direction	kg m ⁻² s ⁻¹
q_{bly}	Bedload transport rate in y -direction	kg m ⁻² s ⁻¹
q_{bl_slope}	Bedload slope factor	–
s	Vertical sigma coordinate	–
s	Specific gravity	–
t	Time	s
u	Velocity x -direction	m s ⁻¹
u_b	Bottom orbital velocity	m s ⁻¹
u_*	Friction velocity	m s ⁻¹
u_{*c}	Friction velocity due to currents	m s ⁻¹
u_{*wc}	Friction velocity due to combined waves and currents	m s ⁻¹
u'	Turbulent velocity x -direction	m s ⁻¹
u_s	Vertically varying stokes velocity x -direction	m s ⁻¹

Table 1 (continued)

Symbol	Description	Dimensions
\bar{u}	Depth-integrated velocity x -direction	m s^{-1}
\bar{u}_s	depth-integrated stokes velocity x -direction	m s^{-1}
V	Velocity y -direction	m s^{-1}
v'	Turbulent velocity y -direction	m s^{-1}
v_s	Vertically varying stokes velocity y -direction	m s^{-1}
\bar{v}	Depth-integrated velocity y -direction	m s^{-1}
\bar{v}_s	Depth-integrated stokes velocity x -direction	m s^{-1}
w'	Turbulent velocity s -direction	m s^{-1}
w_s	Sediment settling velocity	m s^{-1}
x	Horizontal direction	m
y	Horizontal direction	m
z	Vertical elevation	m
z_a	Active layer thickness	m
z_0	Total bottom roughness length	m
z_{oN}	Grain size bottom roughness	m
z_{oST}	Sediment transport bottom roughness	m
z_{oBF}	Bedform bottom roughness	m
z_{oMIN}	Minimum bottom roughness	m
z_r	Reference elevation for BBL	m
Φ	Non-dimensional bedload transport rate	–
$\vec{\Phi}$	Bedload transport vector in direction of and direction perpendicular to currents	–
Φ_{\parallel}	Bedload transport vector in direction of currents	–
$\Phi_{\parallel 1}, \Phi_{\parallel 2}$	Bedload transport quantities in direction of currents	–
Φ_{\perp}	Bedload transport vector in direction perpendicular to currents	–
Ω	Vertical velocity s -direction	s^{-1}
α	Roller parameter	–
β	Local bed slope	–
γ	Wave height to water depth ratio	–
γ_w	Wave asymmetry factor	–
γ_1	Linear drag coefficient	–
γ_2	Quadratic drag coefficient	–
δ_{wbl}	Wave boundary layer height	m
η	Wave averaged free surface elevation	m
η_r	Ripple wave height	m
θ	Wave direction	radians
θ_m	Shields parameter (uses τ_m)	–
θ_{sf}	Shields parameter (uses τ_{sf})	–
$\theta_{sf\parallel}$	Shields parameter (uses τ_{sf} in direction of currents)	–
$\theta_{sf\perp}$	Shields parameter (uses τ_{sf} in direction perpendicular to currents)	–
$\vec{\theta}_{sf}$	Shields parameter vector in direction of and direction perpendicular to currents	–
θ_c	Critical shields parameter (uses τ_{ce})	–
$\vec{\theta}$	Directional shields parameter	–
κ	von Kármán's constant (0.41)	–
λ_r	Ripple wave length	m
ρ	Density	kg m^{-3}
ρ_0	Reference density	kg m^{-3}
ρ_s	Sediment density	kg m^{-3}
ρ_{water}	Water density	kg m^{-3}
ν	Kinematic viscosity	$\text{m}^2 \text{s}^{-1}$
ν_0	Tracer kinematic diffusivity	$\text{m}^2 \text{s}^{-1}$
σ	Wave frequency (relative to currents)	s^{-1}
τ_{bx}	Bottom stress x -direction	$\text{m}^2 \text{s}^{-2}$
τ_{by}	Bottom stress y -direction	$\text{m}^2 \text{s}^{-2}$
τ_c	Bottom stress due to currents alone	$\text{m}^2 \text{s}^{-2}$
τ_{ce}	Bottom critical erosion stress	$\text{m}^2 \text{s}^{-2}$
τ_m	Mean bottom stress due to combined waves + currents	$\text{m}^2 \text{s}^{-2}$
τ_{sx}	Surface stress x -direction	$\text{m}^2 \text{s}^{-2}$

Table 1 (continued)

Symbol	Description	Dimensions
τ_{sy}	Surface stress y -direction	$m^2 s^{-2}$
τ_{sf}	Total skin friction bottom stress, (maximum combined wave + current)	$m^2 s^{-2}$
τ_{sfm}	Skin friction component due to form drag	$m^2 s^{-2}$
τ_w	Bottom stress due to waves alone	$m^2 s^{-2}$
τ_{wc}	Combined bottom stress due to waves and currents	$m^2 s^{-2}$
ϕ	Sediment bed porosity	–
ϕ_m	Friction angle of sediment	degrees

2003) as implemented by Warner et al. (2005) that also includes the option for surface fluxes of turbulence kinetic energy due to wave breaking. The wide choice in turbulence closures facilitates evaluation of the effects of turbulence parameterizations on model results (for example, see Wijesekera et al., 2003; Li et al., 2005).

We have modified ROMS to include physical processes that are important in nearshore regions by adding radiation-stress terms to the momentum equations based on Mellor (2003, 2005) where a vertical coordinate transformation and phase averaging are used to derive interacting current and surface gravity wave equations. We neglect the momentum transfer term that correlates wind-induced surface pressure fluctuations and wave slope because methods to incorporate these processes are still being developed. The horizontal radiation-stress terms (on the rhs of Eqs. (1) and (2)) are

$$\begin{aligned}
 S_{xx} &= kE \left[\frac{k_x k_x}{k^2} F_{CS} F_{CC} + F_{CS} F_{CC} - F_{SS} F_{CS} \right] \\
 &\quad + \frac{k_x k_x}{k} \frac{c^2}{L} A_R R_z \\
 S_{xy} &= S_{yx} = kE \left[\frac{k_x k_y}{k^2} F_{CS} F_{CC} \right] + \frac{k_x k_y}{k} \frac{c^2}{L} A_R R_z \\
 S_{yy} &= kE \left[\frac{k_y k_y}{k^2} F_{CS} F_{CC} + F_{CS} F_{CC} - F_{SS} F_{CS} \right] \\
 &\quad + \frac{k_y k_y}{k} \frac{c^2}{L} A_R R_z
 \end{aligned} \tag{7}$$

where the terms in brackets are the traditional momentum flux terms due to the waves (Mellor, 2003, 2005), and the last term is due to the surface roller (Svendsen, 1984; Svendsen et al., 2002), with a vertical distribution expressed as

$$R_z = 1 - \tanh \left(\frac{2s}{\gamma} \right)^4 \tag{8}$$

where R_z vertically distributes the additional stress term due to the roller as an exponentially function decaying with depth and γ is the ratio of wave height to water depth ($\gamma = H_s/D$), H_s is the significant wave height, k is the wavenumber ($k = 2\pi/L$ where L is wavelength), k_x and k_y are the wavenumber components in the x and y directions and c is the wave-propagation speed, computed as

$$c = \frac{\sigma}{k} = \sqrt{\frac{g}{k} \tanh kD} \tag{9}$$

where σ is the wave frequency ($\sigma = 2\pi/T$, where T is wave period). The two options available for determining the roller area (A_R) are (1) to obtain A_R directly from the wave model or (2) compute A_R based on a formulation from (Svendsen, 1984):

$$A_R = \frac{\alpha}{\sqrt{2}} H_s L Q_b \tag{10}$$

where α is a parameter with value 0.06, and Q_b is the fraction of breaking waves.

The vertical radiation-stress terms (last term on the rhs of Eqs. (1) and (2)) are:

$$\begin{aligned}
 S_{px} &= (F_{CC} - F_{SS}) \left[\frac{F_{SS}}{2} \frac{\partial E}{\partial x} + F_{CS}(1+s)E \frac{\partial(kD)}{\partial x} \right. \\
 &\quad \left. - EF_{SS} \coth(kD) \frac{\partial(kD)}{\partial x} \right] \\
 S_{py} &= (F_{CC} - F_{SS}) \left[\frac{F_{SS}}{2} \frac{\partial E}{\partial y} + F_{CS}(1+s)E \frac{\partial(kD)}{\partial y} \right. \\
 &\quad \left. - EF_{SS} \coth(kD) \frac{\partial(kD)}{\partial y} \right]
 \end{aligned} \tag{11}$$

where the vertical structure functions in Eqs. (7) and (11) are:

$$\begin{aligned}
 F_{SS} &= \frac{\sinh(kD(1+s))}{\sinh kD} & F_{CS} &= \frac{\cosh(kD(1+s))}{\sinh kD} \\
 F_{SC} &= \frac{\sinh(kD(1+s))}{\cosh kD} & F_{CC} &= \frac{\cosh(kD(1+s))}{\cosh kD}
 \end{aligned} \tag{12}$$

and $E = gH_s^2/16$ is the wave energy. The terms in Eqs. (12) provide wave-induced stresses in the momentum equations that decay with depth.

The momentum expressions derived by Mellor (2003, 2005) yield equations with mean (wave-phase averaged) velocities in a Lagrangian reference frame. The Lagrangian and Eulerian reference frames are related by the Stokes velocities u_s and v_s in the x and y directions, computed as

$$\begin{aligned} u_s &= \frac{2k_x}{c} \frac{\cosh 2kD(1+s)}{\sinh 2kD} \left(E + \frac{DgA_R}{L} \right), \\ v_s &= \frac{2k_y}{c} \frac{\cosh 2kD(1+s)}{\sinh 2kD} \left(E + \frac{DgA_R}{L} \right) \end{aligned} \quad (13)$$

where the last terms in the parentheses are the roller contributions. Stokes velocities are subtracted from Lagrangian velocities to maintain a consistent Eulerian reference frame for the entire model dynamics.

ROMS solves the equations with a mode-splitting technique (described in detail by Haidvogel et al., 2007) that requires depth-integrated momentum equations. Including the radiation-stress terms, these are:

$$\begin{aligned} \frac{\partial(D\bar{u})}{\partial t} + \frac{\partial(\bar{u}D\bar{u})}{\partial x} + \frac{\partial(\bar{v}D\bar{u})}{\partial y} - fD\bar{v} \\ = -D \frac{\partial p}{\partial x} + \tau_{sx} - \tau_{bx} - \frac{\partial \overline{S_{xx}}}{\partial x} - \frac{\partial \overline{S_{xy}}}{\partial y} \end{aligned} \quad (14)$$

$$\begin{aligned} \frac{\partial(D\bar{v})}{\partial t} + \frac{\partial(\bar{v}D\bar{u})}{\partial x} + \frac{\partial(\bar{v}D\bar{v})}{\partial y} + fD\bar{u} \\ = -D \frac{\partial p}{\partial y} + \tau_{sy} - \tau_{by} - \frac{\partial \overline{S_{xy}}}{\partial x} - \frac{\partial \overline{S_{yy}}}{\partial y} \end{aligned} \quad (15)$$

and continuity is

$$\frac{\partial \eta}{\partial t} + \frac{\partial(D\bar{u})}{\partial x} + \frac{\partial(D\bar{v})}{\partial y} = 0 \quad (16)$$

where the horizontal radiation-stress terms (Phillips, 1969; Mellor, 2003, 2005) with roller contributions based on Svendsen (1984) and Svendsen et al. (2002) are:

$$\begin{aligned} \overline{S_{xx}} &= E \frac{c_g}{c} \frac{k_x k_x}{k^2} + E \left(\frac{c_g}{c} - \frac{1}{2} \right) + \frac{k_x k_x}{k^2} \frac{c^2 A_R}{L} \\ \overline{S_{xy}} &= \overline{S_{yx}} = E \frac{c_g}{c} \frac{k_x k_y}{k^2} + \frac{k_x k_y}{k^2} \frac{c^2 A_R}{L} \\ \overline{S_{yy}} &= E \frac{c_g}{c} \frac{k_y k_y}{k^2} + E \left(\frac{c_g}{c} - \frac{1}{2} \right) + \frac{k_y k_y}{k^2} \frac{c^2 A_R}{L} \end{aligned} \quad (17)$$

where the group speed, c_g , is

$$c_g = \frac{\partial \sigma}{\partial k} = \frac{c}{2} \left(1 + \frac{2kD}{\sinh(2kD)} \right) \quad (18)$$

The depth-integrated velocities are also expressed in a Lagrangian reference frame and are related to the Eulerian reference frame by the depth-integrated Stokes velocities \bar{u}_s and \bar{v}_s , with:

$$\bar{u}_s = \frac{k_x E}{ckD} + \frac{k_x}{k} \frac{gA_R}{cL}, \quad \bar{v}_s = \frac{k_y E}{ckD} + \frac{k_y}{k} \frac{gA_R}{cL} \quad (19)$$

The Stokes velocities are subtracted from the Lagrangian velocities to maintain a consistent Eulerian reference frame in the model and for the output.

2.2. Wave model

The modification of the momentum equations to include the effects of surface waves requires information on basic wave properties such as wave-energy, propagation direction, and wavelength. Other algorithms, such as the bottom-boundary modules and turbulence submodels may also require wave information such as wave period, bottom orbital velocity, and wave-energy dissipation rate. These quantities are obtained from SWAN (Booij et al., 1999). SWAN is a wave-averaged model that solves transport equations for wave action density N (energy density divided by relative frequency):

$$\frac{\partial N}{\partial t} + \frac{\partial c_x N}{\partial x} + \frac{\partial c_y N}{\partial y} + \frac{\partial c_\sigma N}{\partial \sigma} + \frac{\partial c_\theta N}{\partial \theta} = \frac{S_w}{\sigma} \quad (20)$$

where c_x and c_y are the propagation velocities in the x and y directions, σ is the relative frequency, and θ is the wave direction. SWAN accounts for shoaling and refraction through dependent variations in c_x and c_y . The term S on the right-hand side is a source/sink term representing effects of wind-wave generation, wave breaking, bottom dissipation, and nonlinear wave-wave interactions. SWAN also can account for diffraction, partial transmission, and reflection. Specific formulations for wind input, bottom stress, whitecapping, wave-wave interactions, etc. are described in detail in Booij et al. (2004). SWAN can be run separately and the output used to force the hydrodynamic and sediment routines (one-way coupling). Alternatively, SWAN can be run concurrently with the circulation model with two-way coupling, whereby currents influence

the wave field and waves affect the circulation (see Section 2.4).

2.3. Model domains

ROMS is discretized in horizontal dimensions with curvilinear orthogonal Arakawa *C* grid (Arakawa, 1966) with $\xi(x-)$ and $\eta(y-)$ coordinates (Fig. 1). Grid-cell centers are termed ρ points and are the locations of tracer concentrations, water depth, and sea level. Velocities are computed on the grid-cell faces. The grid can be rectilinear with constant or varying grid spacings, or curvilinear to allow focusing of the mesh to specific areas, for example to accommodate land-sea boundaries. The model also allows land-sea masking to identify regions of dry areas. The model uses a stretched vertical *s*-coordinate system, which are similar to sigma coordinates with additional flexibility: the layers need not be a fixed percentage of the water column (see Haidvogel et al., 2000). Vertical resolution can be adjusted to allow increased resolution near the surface and bottom boundaries. The bed model comprises a user-defined number of layers that extend vertically into the sea floor. See Section 3.2 for a detailed description.

ROMS and SWAN must both use the same grid in our current implementation. The grid may be curvilinear. SWAN depths must coincide with ROMS ρ -points. ROMS has wetting and drying capabilities. The algorithm identify cells with water depths less than a user-specified value, and prevents outward flux of water from those cells, a process called cell flux blocking (Casulli and Cheng, 1992). Flux of water onto cells is always permitted. The same minimum depth can be specified in SWAN to exclude those points during wave computations.

2.4. Model coupling

We used the Model-Coupling Toolkit (MCT; <http://www-unix.mcs.anl.gov/mct/>; Larson et al., 2005; Jacob et al., 2005) to couple ROMS with SWAN (Warner et al., in press). MCT is an open-source software library, distributed as a set of Fortran90 modules for constructing a coupled model system from individual component models. Each component model has its own grid and runs on its own set of processors. The MCT provides protocols for decomposition and allocation of model grids among different processors, efficient transfer of data fields between the different models,

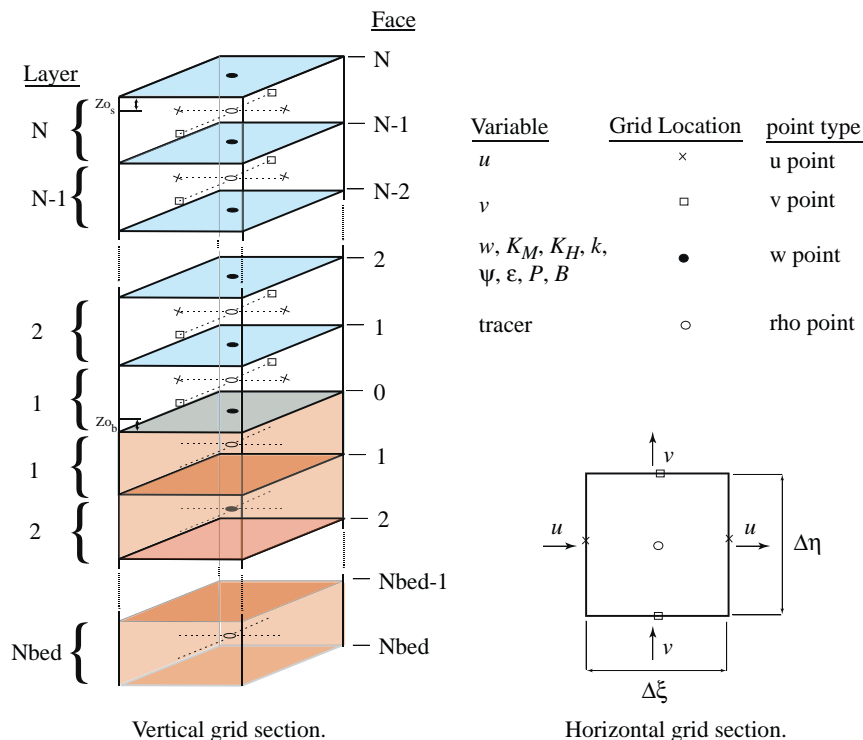


Fig. 1. A vertical section of the ROMS grid showing water column and bed layers.

and interpolation algorithms for the data fields that are transferred. SWAN sends to ROMS arrays of wave height, wavelength, average wave periods at the surface and near the bottom, wave-propagation direction, near-bottom orbital velocity, and wave-energy dissipation rate. ROMS provides to SWAN arrays of water depth, sea-surface elevation, and current velocity. Data exchange between SWAN and ROMS occurs at user-defined synchronization intervals. The frequency of data exchange depends on the application. If the exchanged fields fluctuate rapidly, more frequent synchronization is required. However, data exchange increases run time, so experience is required to determine the optimum synchronization interval for each application.

3. Sediment algorithms and implementation

3.1. Sediment classes

The model is capable of representing an unlimited number of user-defined sediment classes. Each class has fixed attributes of grain diameter, density, settling velocity, critical shear stress for erosion, and erodibility constant. These properties are used to determine bulk properties of each bed layer. Two classes of sediments (non-cohesive and cohesive) are included in the model framework, but the algorithms governing cohesive sediment dynamics are still being developed and are not discussed here.

3.2. Sediment bed

The sediment bed is represented by three-dimensional arrays with a user-specified, constant number of layers beneath each horizontal model cell (Fig. 1). Each cell of each layer in the bed is initialized with a thickness, sediment-class distribution, porosity, and age. The mass of each sediment class in each cell can be determined from these values and the grain density. The age property tracks the time that deposition last occurred in that layer. The bed framework also includes two-dimensional arrays that describe the evolving properties of the seabed, including bulk properties of the surface layer (active-layer thickness, mean grain diameter, mean density, mean settling velocity, mean critical stress for erosion) and descriptions of the subgrid-scale morphology (ripple height and wavelength). These properties are used to estimate bed roughness in the bottom stress calculations. The bottom stresses are then used by the sediment routines to determine

resuspension and transport, providing a feedback from the sediment dynamics to the hydrodynamics.

The bed layers are modified at each time step to account for erosion and deposition (Fig. 2) and track stratigraphy. At the beginning of each time step, an active-layer thickness z_a is calculated based on the relation of Harris and Wiberg (1997):

$$z_a = \max[k_1(\tau_{sf} - \overline{\tau_{ce}})\rho_0, 0] + k_2 D_{50} \quad (21)$$

where τ_{sf} is bottom skin-friction stress due to combined maximum wave and current interaction; τ_{ce} is the critical stress for erosion; and the overbar indicates this is averaged over all sediment classes; D_{50} is the median grain diameter of surface sediment; and k_1 and k_2 are empirical constants (values of 0.007 and 6.0, respectively). The thickness of the top bed layer has a minimum thickness equivalent to z_a . If the top layer is thicker than z_a , no action is required. If the top layer is less than z_a thick, then the top layer thickness is increased by entraining sediment mass from deeper layers until the top layer thickness equals z_a . If sediment from deeper than the second layer is mixed into the top layer, the bottom layer is split, enforcing the constant number of layers and conserving sediment mass.

Each sediment class can be transported by suspended-load and/or bedload (described in Sections 3.3 and 3.4). Suspended-load mass is exchanged vertically between the water column and the top bed layer. Mass of each sediment class available for transport is limited to the mass available in the active layer. Bedload mass is exchanged horizontally between the top layers of the bed. Mass of each sediment class available for transport is limited to the mass available in the top layer.

Suspended-sediment that is deposited, or bedload that is transported into a computational cell, is added to the top bed layer. If continuous deposition results in a top layer thicker than a user-defined threshold, a new layer is provided to begin accumulation of depositing mass. The bottom two layers are then combined to conserve the number of layers. After erosion and deposition have been calculated, the active-layer thickness is recalculated and bed layers readjusted to accommodate it. This step mixes away any very thin layer (less than the active-layer thickness) of newly deposited material. Finally the surficial sediment characteristics, such as D_{50} , ripple geometry, etc., are updated and made available to the bottom stress calculations.

Active layer thickness (Harris and Wiberg, 1997).

$$z_a = k_1(\tau_{sf} - \tau_{ce}) + k_2 D_{50}$$

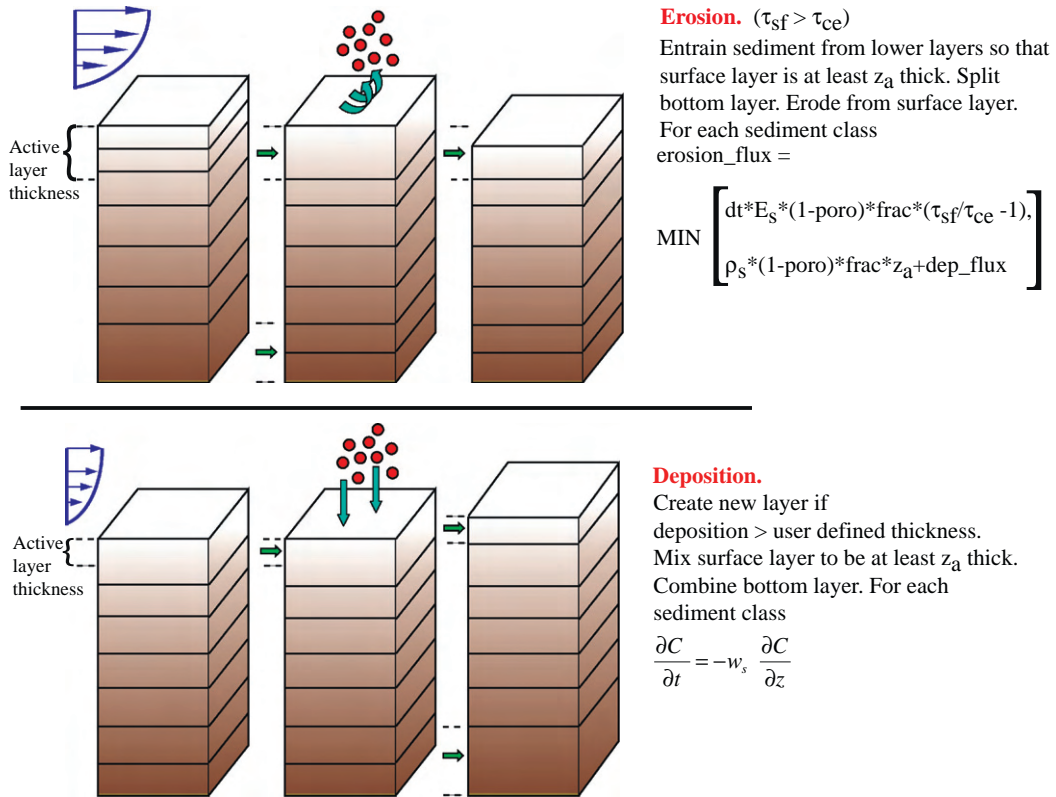


Fig. 2. Distribution of vertical layers in bed model. During erosion top layer thickness is increased to meet active layer thickness. Deposition creates a new layer if timing and thickness criteria are met. Total number of layers must be constant, often requiring a merge or splitting of bottom cells.

3.3. Suspended-sediment transport

Temperature, salinity, and sediment suspended in the water column are transported by solving the advection–diffusion equation (5). However for suspended-sediment, an additional source/sink term is added for vertical settling and exchange with the bed as

$$C_{source,m} = -\frac{\partial w_{s,m} C_m}{\partial s} + E_{s,m} \quad (22)$$

where $w_{s,m}$ is the vertical-settling velocity (positive upwards), $E_{s,m}$ is the erosion source (defined below), and m equals one through the number of classes. The model solves each term of Eq. (5) independently, in the sequence: vertical settling, source/sink, horizontal advection, vertical advection, vertical diffusion, and finally horizontal diffusion. Separation of these calculations has practical advantages

because it allows (1) reuse of the routines for advection and diffusion of water-column tracers, (2) use of high-order numerical schemes for vertical settling, and (3) formulation of the flux conditions to ensure conservation of sediment in both bottom sediments and the water column.

The vertical advection algorithm includes a piecewise parabolic method (Colella and Woodward, 1984) and a weighted essentially non-oscillatory (WENO) scheme (Liu et al., 1994). This method integrates depositional flux over multiple grid cells, so it is not constrained by the CFL criterion. Zero-flux boundary conditions are imposed at the surface and bottom in the vertical diffusion equation. The source or sink term in the advection equation represents the net of downward settling and upward flux of eroded material and is only applied to the bottom computational cell. Erosional flux is parameterized following Ariathurai and Arulanandan

(1978) as

$$E_{s,m} = E_{0,m}(1 - \phi) \frac{\tau_{sf} - \tau_{ce,m}}{\tau_{ce,m}}, \quad \text{when } \tau_{sf} > \tau_{ce,m} \quad (23)$$

where E_s is the surface erosion mass flux ($\text{kg m}^{-2} \text{s}^{-1}$), E_0 is a bed erodibility constant ($\text{kg m}^{-2} \text{s}^{-1}$), ϕ is the porosity (volume of voids/total volume) of the top bed layer, and m is an index for each sediment class. The erosional flux for each sediment class is also limited by the availability of that class in the top layer of the bed model.

3.4. Bedload transport

This version of ROMS implements two methods for computing bedload transport: (1) the Meyer-Peter Müller (1948) formulation for unidirectional flow and (2) the formulae of Soulsby and Damgaard (2005) that accounts for combined effects of currents and waves. The formulae depend on the characteristics of individual sediment classes, including size D , density ρ_s , specific density in water $s = \rho_s/\rho$, and critical shear stress τ_c . Non-dimensional transport rates Φ are calculated for each sediment class and converted to dimensional bedload transport rates q_{bl} using

$$q_{bl} = \Phi \sqrt{(s-1)gD_{50}^3 \rho_s} \quad (24)$$

These are horizontal vector quantities with directions that correspond to the combined bed-stress vectors.

3.4.1. Meyer-Peter Müller

The Meyer-Peter Müller (1948) formulation is

$$\Phi = \max[8(\theta_{sf} - \theta_c)^{1.5}, 0] \quad (25)$$

where Φ is the magnitude of the non-dimensional transport rate for each sediment class, θ_{sf} is the non-dimensional Shields parameter for skin stress

$$\theta_{sf} = \frac{\tau_{sf}}{(s-1)gD_{50}} \quad (26)$$

$\theta_c = 0.047$ is the critical Shields parameter, and τ_{sf} is the magnitude of total skin-friction component of bottom stress computed from

$$\tau_{sf} = (\tau_{bx}^2 + \tau_{by}^2)^{0.5} \quad (27)$$

where τ_{bx} and τ_{by} are the skin-friction components of bed stress, from currents alone or the maximum wave-current combined stress, in the x and y directions. These are computed at cell faces (u and

v locations) and then interpolated to cell centers (ρ points). The bedload transport vectors are partitioned into x and y components based on the magnitude of the bed shear stress as

$$q_{blx} = q_{bl} \frac{\tau_{bx}}{\tau_{sf}}, \quad q_{bly} = q_{bl} \frac{\tau_{by}}{\tau_{sf}} \quad (28)$$

3.4.2. Soulsby and Damgaard

The Soulsby and Damgaard (2005) formulae account for the combined effects of mean currents and asymmetrical waves on bedload flux. Their formulations are based on numerical integration, over a wave cycle, of the non-dimensional transport equation

$$\vec{\Phi} = \max \left[A_2 \theta^{0.5} (\theta_{sf} - \theta_c) \frac{\vec{\theta}_{sf}}{\theta_{sf}}, 0 \right] \quad (29)$$

where $\vec{\Phi}$ and $\vec{\theta}_{sf}$ are vectors with components in the direction of the mean current and in the direction perpendicular to the current, e.g., $\vec{\Phi} = (\Phi_{\parallel}, \Phi_{\perp})$, $\vec{\theta}_{sf} = (\theta_{sf\parallel}, \theta_{sf\perp})$, $\theta_{sf} = |\vec{\theta}_{sf}|$, θ_c is the critical Shields parameter (i.e. Eq. (26) with τ_{ce}), and $A_2 = 12$ is a semi-empirical coefficient. The implementation of this method requires computation of transport rates in the directions parallel and perpendicular to the currents as

$$\Phi_{\parallel} = \max[\Phi_{\parallel 1}, \Phi_{\parallel 2}] \quad (30)$$

where

$$\Phi_{\parallel 1} = A_2 \theta_m^{0.5} (\theta_m - \theta_c) \quad (31)$$

$$\Phi_{\parallel 2} = A_2 (0.9534 + 0.1907 \cos 2\phi) \theta_w^{0.5} \theta_m + A_2 (0.229 \gamma_w \theta_w^{1.5} \cos \phi) \quad (32)$$

$$\Phi_{\perp} = A_2 \frac{0.1907 \theta_w^2}{\theta_w^{3/2} + 1.5 \theta_m^{1.5}} (\theta_m \sin 2\phi + 1.2 \gamma_w \theta_w \sin \phi) \quad (33)$$

where θ_m is the mean Shields parameter (i.e. Eq. (26) with τ_m) and τ_m is

$$\tau_m = \tau_c \left(1 + 1.2 \left(\frac{\tau_w}{\tau_w + \tau_c} \right)^{1.5} \right) \quad (34)$$

and τ_c is the bottom stress from the currents only, τ_w is the bottom stress from the waves only calculated in the bottom-boundary layer routines (see below). The asymmetry factor γ_w is the ratio between the amplitude of the second harmonic and the amplitude of the first harmonic of the oscillatory

wave stress. Following the suggestion of Soulsby and Damgaard (2005), we estimate the asymmetry factor using Stokes second-order theory (e.g., Fredsøe and Deigaard, 1992) and constrain it to be less than 0.2. The non-dimensional fluxes (Eqs. (30) and (33)) are rotated into x and y directions using the directions for mean current and waves and dimensionalized with Eq. (24) to yield values for q_{blx} and q_{bly} for each sediment class.

3.4.3. Bed slope

Computed bedload rates are modified to account for local bed slope following Lesser et al. (2004) with a bed slope term:

$$q_{bl_slope} = \frac{\tan \varphi_m}{(\tan \varphi_m - \tan \beta) \cos \beta} \quad (35)$$

where the local bed slope $\beta = \tan^{-1}(dz/dx_x)$ is evaluated for each direction of transport with a positive value of dz/dx_x in the downslope direction, and where φ_m is the friction angle of the sediment (taken as 33°). The bedload magnitudes are then multiplied by q_{bl_slope} .

3.4.4. Bedload numerics

Bedload fluxes are computed at grid-cell centers and limited by the availability of each sediment class in the top layer. Fluxes are translated to cell faces using a simple upwind approach (e.g., Lesser et al., 2004): the bedload flux at each cell face is set to the bedload rate at the upwind cell center. Flux differences are then used to determine changes of sediment mass in the bed at each grid cell.

3.5. Morphology

The bed model accounts for changes in sea floor elevation resulting from convergence or divergence in sediment fluxes. These morphological changes can have significant influence on flow and transport when they are larger than a few percent of the water depth. The morphological changes are accounted for by equating the bottom-boundary condition of the vertical velocity to the rate of change of elevation of the sea floor. This method is completely mass conserving and retains tracer constancy preservation.

A morphological scale factor is also provided to allow an increased rate of morphological change, which can be useful for simulating evolution over long time periods. Strategies for morphological updating are described by Roelvink (2006). In our

implementation, bedload fluxes, erosion, and deposition rates are multiplied by a scale factor. A scale factor with a value of one has no effect, and values greater than one accelerate the bed response. For bedload transport, the scale factor is multiplied against the bedload transport rates. For suspended-load transport, the scale factor multiplies the exchange of sediment (erosive or depositional flux) at the bed-water interface. The magnitude of sediment concentrations in the water column are not modified—just the exchange rate to and from the bed. For both bedload and suspended load, sediment is limited in availability as described previously, based on the true amount of sediment mass (not multiplied by the scale factor). This morphological scale factor method works well for systems with unlimited sediment in the bed. However, it can generate extra sediment in systems with limited supplies of bed sediment. This occurs when the amount of sediment to be eroded is limited by the amount available and application of the morphological scale factor cannot remove the scaled amount of sediment from the bed. Subsequent deposition does place a scaled amount of sediment on the bed thus creating new mass in the bed. Other approach (Lesser et al., 2004) is to limit the amount of sediment fluxed to the water column in these situations. This gives unrealistically low sediment concentrations, but conserves bed sediment.

3.6. Sediment density effects

Effects of suspended sediment on the density field are included with terms for the weight of each sediment class in the equation of state for seawater density as

$$\rho = \rho_{water} + \sum_{m=1}^{N_{sed}} \frac{C_m}{\rho_{s,m}} (\rho_{s,m} - \rho_{water}). \quad (36)$$

This enables the model to simulate processes where sediment density influences hydrodynamics, such as density stratification and gravitationally driven flows.

3.7. Bottom stress calculations

Reynolds stresses, production and dissipation of turbulent kinetic energy, and gradients in velocity and suspended-sediment concentrations vary over short vertical distances, especially near the bed, and

can be difficult to resolve with the vertical grid spacing used in regional-scale applications. ROMS provides algorithms to parameterize some of these subgrid-scale processes in the water column and in the bottom-boundary layer (BBL). Treatment of the BBL is important for the circulation model solution because it determines the stress exerted on the flow by the bottom, which enters the Reynolds-averaged Navier–Stokes equations as a boundary conditions for momentum in the x and y directions:

$$K_M \frac{\partial u}{\partial s} = \tau_{bx}, \quad K_M \frac{\partial v}{\partial s} = \tau_{by} \quad (37)$$

Determination of the BBL is even more important for the sediment-transport formulations because bottom stress determines the transport rate for bedload and the resuspension rate for suspended sediment, as discussed in Sections 3.3 and 3.4.

ROMS implements either of two methods for representing BBL processes: (1) simple drag-coefficient expressions or (2) more complex formulations that represent the interactions of wave and currents over a moveable bed. The drag-coefficient methods implement formulae for linear bottom friction, quadratic bottom friction, or a logarithmic profile. The other, more complex methods, implement some of the many wave-current BBL models (e.g., Jonsson and Carlsen, 1976; Smith, 1977; Grant and Madsen, 1979; Madsen, 1994; Styles and Glenn, 2000) and couple them with calculations of bottom roughness. ROMS offers three methods that implement slightly different combinations of algorithms for the wave-current interactions and moveable bed roughness. The first method (*sg_bbl*) is based on the wave-current algorithm and the ripple geometry and moveable bed roughness of Styles and Glenn (2000, 2002). The second method (*mb_bbl*) uses efficient wave-current BBL computations developed by Soulsby (1995) in combination with sediment and bedform roughness estimates of Grant and Madsen (1982), Nielsen (1986) and Li and Amos (2001). These algorithms and an example of their use on the Southern California continental shelf are described by Blaas et al. (2005). The third method (*ssw_bbl*) implements either the wave-current BBL model of Madsen (1994) or that of Styles and Glenn (2000) along with moveable bed routines proposed by Wiberg and Harris (1994); Harris and Wiberg (2001). The differences in approach among these routines are small, but they can produce significantly different results. After reviewing the

simple drag-law approach, we discuss *ssw_bbl* in detail.

The linear and quadratic drag-coefficient methods depend only on velocity components u and v in the bottom grid cell and constant, spatially-uniform coefficients γ_1 and γ_2 specified as input:

$$\tau_{bx} = (\gamma_1 + \gamma_2 \sqrt{u^2 + v^2})u \quad (38)$$

$$\tau_{by} = (\gamma_1 + \gamma_2 \sqrt{u^2 + v^2})v \quad (39)$$

where γ_1 is the linear drag coefficient and γ_2 is the quadratic drag coefficient. The user can choose between linear or quadratic drag by setting one of these coefficients to zero. The bottom stresses computed from these formulae depend on the elevation of u and v (computed at the vertical mid-elevation of the bottom computational cell). Therefore, in this s -coordinate model, the same drag coefficient will be imposed throughout the domain even though the vertical location of the velocity is different.

The logarithmic formulation assumes that flow in the BBL has the classic vertical logarithmic profile defined by a shear velocity u_* and bottom roughness length z_0 as

$$|u| = \frac{u_*}{\kappa} \ln\left(\frac{z}{z_0}\right) \quad (40)$$

where speed $|u| = \sqrt{u^2 + v^2}$, friction velocity $u_* = \sqrt{|\tau_{bx}| + |\tau_{by}|}$, z is the elevation above the bottom (vertical mid-elevation point of the bottom cell), $\kappa = 0.41$ is von Kármán's constant, and z_0 is a constant (but possibly spatially varying) bottom roughness length (m). Kinematic stresses are calculated as:

$$\tau_{bx} = \frac{\kappa^2 u \sqrt{u^2 + v^2}}{\ln^2(z/z_0)} \quad (41)$$

$$\tau_{by} = \frac{\kappa^2 v \sqrt{u^2 + v^2}}{\ln^2(z/z_0)} \quad (42)$$

The advantage of this approach is that the velocity and the vertical elevation of that velocity are used in the equation. Because the vertical elevation of the velocity in the bottom computational cell will vary spatially and temporally, the inclusion of the elevation provides a more consistent formulation.

More complex routines are required to simulate BBL processes in the presence of waves and mobile sediment. The short (order 10-s) oscillatory shear of wave-induced motions in a thin (a few cm) wave-boundary

layer produces turbulence and generates large instantaneous shear stresses. The turbulence enhances momentum transfer, effectively increasing the coupling between the flow and the bottom and increasing the frictional drag exerted on the mean flow, averaged over many wave periods. The large instantaneous shear stresses often dominate sediment resuspension and enhance bedload transport. Sediment transport can remold the bed into ripples and other bedforms, which present roughness elements to the flow. Bedload transport can also induce drag on the flow, because momentum is transferred to particles as they are removed from the bed and accelerated by the flow. Resuspended sediments can cause sediment-induced stratification and, at high concentrations, change the effective viscosity of the fluid.

The BBL parameterization implemented in ROMS requires inputs of velocities u and v at reference elevation z_r , representative wave-orbital velocity amplitude u_b , wave period T , and wave-propagation direction θ (degrees, in nautical convention). The wave parameters may be the output of a wave model such as SWAN or simpler calculations based on specified surface wave parameters and should represent the full spectrum of motion near the bed (cf. Madsen, 1994; Wiberg and Sherwood, this issue). Additionally the BBL models require bottom sediment characteristics (median grain diameter D_{50} , mean sediment density ρ_s , and representative settling velocity w_s); these are based on the composition of the uppermost active layer of the bed sediment during the previous time step. Bed stresses associated with mean current above the wave-boundary layer τ_b , wave motions τ_w , and maximum vector sum of the two τ_{wc} from the previous time step are used as initial estimates for the next time level.

The procedure for bottom-boundary layer calculations in `ssw_bbl` is as follows:

- (1) Ripple height η_r and wavelength λ_r are calculated using information from the previous time step and the Malarkey and Davies (2003) implementation of the Wiberg and Harris (1994) formulation, which is valid for wave-dominated conditions. They approximate ripple wavelength as $535D_{50}$ and ripple steepness as

$$\frac{\eta_r}{\lambda_r} = \exp \left[-0.095 \left(\ln \left(\frac{d_0}{\eta_r} \right) \right)^2 + 0.442 \left(\ln \left(\frac{d_0}{\eta_r} \right) \right) - 2.28 \right] \quad (43)$$

where $d_0 = u_b T / \pi$ is the wave-orbital diameter. When transport stage is below the threshold for sediment transport ($T^* = \tau_{wc} / \tau_{ce} < 1$), ripple dimensions from the previous time step are retained.

- (2) Roughness lengths associated with grain roughness z_{0N} , sediment transport z_{0ST} , and bedform roughness length (ripples) z_{0BF} are estimated as

$$z_{0N} = 2.5D_{50}/30 \quad (44)$$

$$z_{0ST} = \alpha D_{50} a_1 \frac{T^*}{1 + a_2 T^*} \quad (45)$$

$$z_{0BF} = a_r \eta_r^2 / \lambda_r \quad (46)$$

where the sediment-transport coefficients are $\alpha = 0.056$, $a_1 = 0.068$, and $a_2 = 0.0204 \ln(100D_{50}^2) + 0.0709 \ln(100D_{50})$ (Wiberg and Rubin, 1989) with the bedform roughness D_{50} expressed in meters, and where a_r is a coefficient that may range from 0.3 to 3 (Soulsby, 1997). Grant and Madsen (1982) proposed $a_r = 27.7/30$ but we use as a default value $a_r = 0.267$ suggested by Nielsen (1992). The roughness lengths are additive, so subsequent BBL calculations use $z_0 = \max[z_{0N} + z_{0ST} + z_{0BF}, z_{0MIN}]$, where z_{0MIN} allows setting a lower limit on bottom drag (default $z_{0MIN} = 5e^{-5}$ m).

- (3) Initial estimates of (kinematic) bottom stresses based on pure currents $\tau_c (= \tau_b)$ and pure waves τ_w ($\tau_b = 0$) are made as follows.

$$\tau_c = \frac{(u^2 + v^2)\kappa^2}{\ln^2(z/z_0)} \quad (47)$$

and $\tau_w = 0.5f_w u_b^2$, where f_w is the Madsen (1994) wave-friction factor, which depends on the ratio of the wave-orbital excursion amplitude to the bottom roughness length A_b/k_b , where $A_b = u_b T / (2\pi)$ and $k_b = 30z_0$:

$$f_w = \begin{cases} 0.3, & A_b/k_b \leq 0.2 \\ \exp(-8.82 + 7.02(A_b/k)^{-0.078}), & 0.2 < A_b/k_b \leq 100 \\ \exp(-7.30 + 5.61(A_b/k)^{-0.109}), & A_b/k_b > 100 \end{cases} \quad (48)$$

- (4) The pure currents and pure wave limits are used as initial estimates for calculations towards consistent profiles for eddy viscosity and velocity between z_0 and z_r , using either the model of Madsen (1994) or Stiles and Glenn (2000). Both

of these models assume eddy viscosity profiles scaled by $u_{*wc} = \sqrt{\tau_{wc}}$ in the wave-boundary layer (WBL) and $u_{*c} = \sqrt{\tau_b}$ in the current boundary layer, calculated as

$$K_M = \begin{cases} \kappa u_{*wc} z, & z < \delta_{wbl} \\ \kappa u_{*c} z, & z > \delta_{wbl} \end{cases} \quad (49)$$

where δ_{wbl} is the thickness of the WBL, which scales as $u_{*wc} T / (2\pi)$. τ_{wc} represents the maximum vector sum of wave- and current-induced stress, but the τ_b is influenced by the elevated eddy viscosity in the WBL, and must be determined through an iterative process. The shape and elevation of the transition between these profiles and other details differ among the two models, but both the models of Madsen (1994) or Styles and Glenn (2000) return values for the horizontal vectors τ_b , τ_w , and τ_{wc} . The parameter τ_b is the mean (over many wave periods) stress used as the bottom-boundary condition in the momentum equations, and τ_{wc} is the maximum instantaneous stress exerted over the bottom by representative waves and currents.

- (5) When ripples are present, τ_{wc} is a combination of form drag, which does not directly contribute to sediment transport, and skin friction, which does. The next step in the BBL calculations is to estimate the skin-friction component of τ_{wc} using the ripple dimensions and a bedform drag-coefficient approach (Smith and McLean, 1977; Wiberg and Nelson, 1992), as follows.

$$\tau_{sfm} = \tau_{wc} \left[1 + 0.5 C_{dBF} \frac{\eta_r}{\lambda_r k^2} \left(\ln \frac{\eta_r}{(z_{0N} + z_{0ST})} - 1 \right)^2 \right]^{-1} \quad (50)$$

where $C_{dBF} \approx 0.5$ is a bedform drag coefficient for unseparated flow (Smith and McLean, 1977).

- (6) Finally, because shear stress varies between ripple crests and troughs, an estimate of the maximum shear stress at the crests τ_{sfm} is calculated for use in sediment-transport algorithms as

$$\tau_{sf} = \tau_{sfm} \left(1 + 8 \frac{\eta_r}{\lambda_r} \right) \quad (51)$$

In summary, the more advanced BBL routines calculate current and wave-boundary layer bottom stresses under the combined influence of wave, currents, and mobile sediments. These stresses directly influence flow near the bottom

and act as agents for sediment resuspension and bedload transport.

4. Examples

In this section we provide four examples that highlight the capabilities of the sediment-transport model. Example 1 demonstrates the ability of the model produce a classic suspended-sediment profile and illustrates the effect of varying vertical grid resolution and turbulence submodels. Example 2 demonstrates the morphology component of the model in a simulation of a lab experiment with a migrating trench. Example 3 demonstrates the impact of dynamic coupling for wave–current interactions at a tidal inlet. Example 4 is a realistic application with complex bathymetry that demonstrates transport and sorting of multiple sediment classes.

4.1. Example 1: Steady uniform open-channel flow

Example 1 exercises the models ability to simulate vertical profiles of suspended-sediment concentrations (no bedload) with varying vertical grids and turbulence closures. The simulation represents suspended-sediment transport for steady horizontally uniform flow in a straight rectangular channel, modified slightly from Warner et al. (2005). The channel is placed on a constant slope of 4×10^{-5} m/m and a depth-mean velocity of 1 m s^{-1} is imposed at both the upstream and downstream ends. The water-surface elevation is allowed to vary along the length of the channel. Radiation conditions for the free surface and 3D momentum at both ends allow waves to propagate out of the domain. An unlimited supply of sediment is available in the bed. Additional details are listed in Table 2.

Numerical simulations of vertical suspended-sediment profiles can be sensitive to the number and placement of vertical grid levels. As the number of vertical grid levels increases, the gradient of suspended-sediment near the bed is better resolved. Effects of changing the number of vertical levels and resolution are evaluated using the k – ϵ turbulence closure. The number of vertical levels is varied with values of 10, 20, 40, and 80 evenly spaced cells, and 10 and 20 cells using the stretching parameters of $\theta_s = 3$, $\theta_b = 1$, and $T_{cline} = 0$ (see Haidvogel et al., 2000). Vertical profiles of suspended-sediment converge with 40 or more evenly spaced cells (Fig. 3).

Table 2
Model parameters for test case 1—open-channel flow

Model parameter	Variable	Value
Length, width, depth	$Xsize, Esize, depth$	10 000, 100, 10 m
Number of grid spacings	Lm, Mm, Nm	100, 10, 20 (+ variable)
Bottom roughness	Zob	0.0053 m
Time step	dt	30 s
Simulation steps	$Ntimes$	5000
Settle velocity	w_s	1.0 mm s ⁻¹
Erosion rate	E_0	5 × 10 ⁻⁵ kg m ⁻² s ⁻¹
Critical stresses	τ_{ce}	0.05 N m ⁻²
Porosity	ϕ	0.90
Bed slope	S_0	4 × 10 ⁻⁵
Inflow/outflow boundary condition	\bar{u}	1 m s ⁻¹

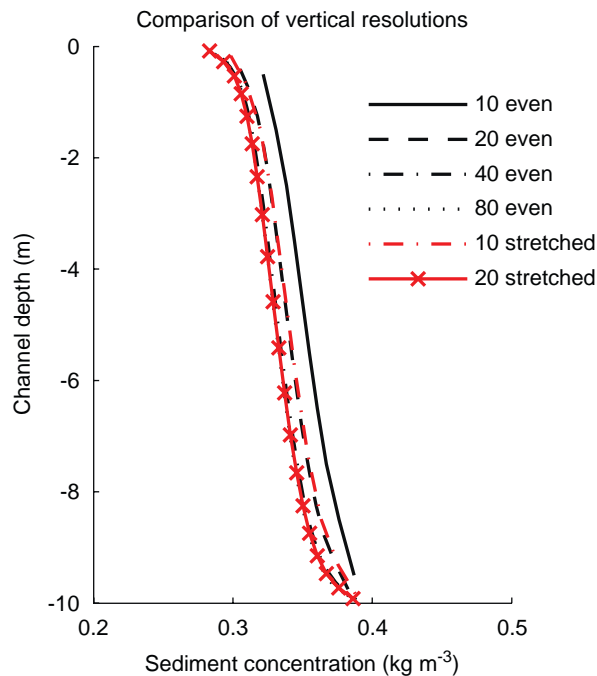


Fig. 3. Effect of vertical resolution on computed profiles of sediment concentration. Increasing the number of evenly distributed cells shows convergence to a steady profile. Simulation with 20 levels using increased boundary layer resolution is consistent with simulation using 80 evenly distributed layers.

The same profile can be obtained with 20 levels when the vertical stretching parameters are used to increase resolution near the bed (Fig. 3).

Simulations with different turbulence closures produce significantly different profiles of velocity, eddy diffusivity, and sediment concentration (Fig. 4). Results were obtained with the two-

equation k-ε closure, the original Mellor and Yamada (1982) level 2.5 closure (MY25) and an analytical expression (ANA) obtained by stipulating a parabolic shape to the eddy viscosity profile:

$$K_M = \kappa u_* z \left(1 - \frac{z}{D}\right) \quad (52)$$

where u_* is the friction velocity, z is the distance above the bed, and D is the water depth (10 m). The friction velocity is calculated by substituting the log law ($u(z)/u_* = 1/\kappa \ln(z/z_0)$) into the depth-mean flow equation and integrating over the entire depth of flow, yielding

$$u_* = \frac{\kappa \bar{u}}{\ln(D/z_0) - 1 + z_0/D} \quad (53)$$

where \bar{u} is the depth-mean velocity, and parameters in Table 2 produce $u_* = 0.0625 \text{ m s}^{-1}$. The eddy diffusivity in the model is determined from the turbulent Prandtl number (Pr ; ratio of eddy viscosity/eddy diffusivity) and, for neutrally stable flow, $Pr = 0.39/0.49 = 0.80$ (Kantha and Clayson, 1994; Warner et al., 2005). Therefore the algebraic eddy diffusivity is $K_H = K_M/0.80$ (Table 3).

The slope of the free surface should equal the bottom slope in steady uniform open-channel flow, producing a momentum balance of

$$\tau/\rho = u_*^2 = g \frac{\partial \eta}{\partial x} D \quad (54)$$

This theoretical balance is $(0.0625 \text{ m s}^{-1})^2 = (9.81 \text{ m s}^{-2})(0.00004)(10 \text{ m})$. The modeled balance depends on the calculated bottom shear stress and, therefore, on the details of the turbulence closure. The free-surface slopes generated using ANA and k-ε are very nearly equal to 4×10^{-5} so Eq. (54) holds with approximately the values calculated above. The slope calculated using the MY25 is closer to 3×10^{-5} , which balances u_* of 0.0544 m s^{-1} . The reduced shear near the bed with MY25 is apparent in the velocity profiles and results in less mixing and lower sediment concentrations (Fig. 4). This behavior is a result of the wall function used in the original MY25 closure, but results consistent with ANA and k-ε can be obtained using the alternative wall function proposed by Blumberg et al. (1992); see Warner et al. (2005).

4.2. Example 2: Trench migration

This example tests the sediment-transport components of bedload (Meyer-Peter Müller formulation),

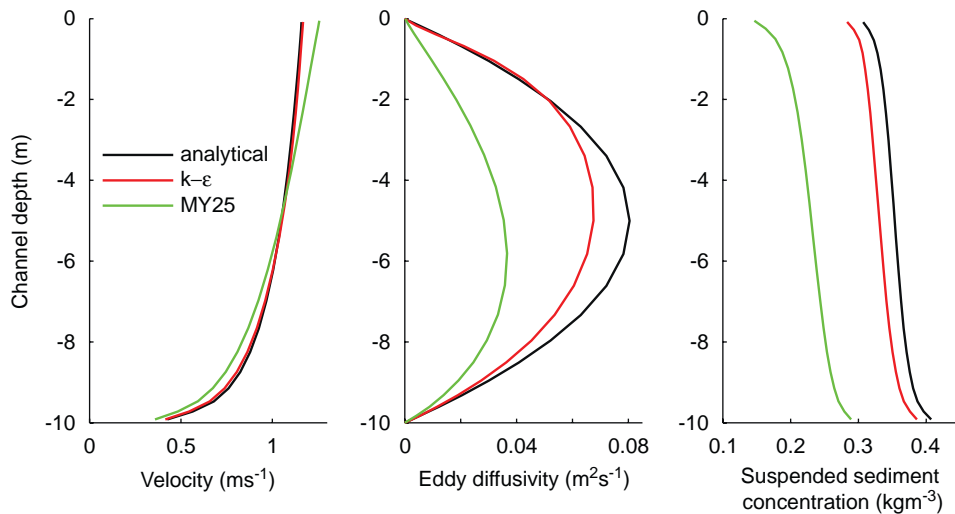


Fig. 4. Vertical profiles of velocity, eddy diffusivity, and sediment concentration for three of turbulence closure options of analytical parabolic expression, $k-\epsilon$, and MY25. Simulations used 20 vertical stretched levels.

Table 3
Results for open-channel flow test case

	$\partial\eta/\partial x$	u^* (m^2s^{-2})
Calculated	$4.00\text{e}-5$	0.0625
ANA	$4.21\text{e}-5$	0.0643
$k-\epsilon$	$3.98\text{e}-5$	0.0626
MY25	$3.00\text{e}-5$	0.0544

suspended-sediment load, and morphologic evolution by simulating the laboratory experiment of van Rijn (1987), also described in van Rijn (1993). The experimental and model setup (Table 4) consist of flow along a 30-m straight channel with a vertical depression (trench) incised in the mobile sand bed (Fig. 5). The bed material is well-sorted fine sand ($D_{50} = 140\ \mu\text{m}$). Flow is steady with a depth-mean velocity of $0.51\ \text{m s}^{-1}$. In the model simulations, flow and suspended-sediment are allowed to reach steady state before morphologic evolution is initiated, there is an unlimited supply of available sediment, and the $k-\epsilon$ turbulence-closure model is used.

As the flow travels into the deeper water of the trench, flow velocity and bottom stress decrease. Sediment begins to settle out of suspension, and bedload transport converges, so sediment accumulates at the upstream end of the trench. At the downstream end of the trench, erosion occurs as depth decreases, flow accelerates, and transport diverges. The trench migrates in the direction of the

flow (left to the right in Fig. 5) as the upstream end is filled, and the downstream end eroded.

Computed and observed velocity and suspended-sediment profiles at five locations, and the initial and final bed elevations are compared in Fig. 5. The velocity profiles are in good agreement with the measurements. The deceleration of near-bottom flow in the middle of the trench is captured well. Suspended-sediment profiles at the upstream and downstream ends match the observations but, in the trench, calculated concentrations of suspended-sediment deviate slightly from the observed profiles. At the end of the simulation, the modeled trench has migrated as far as the observed trench, but has not filled as much (compare red and blue lines in Fig. 5).

4.3. Example 3: Tidal inlet wave–current coupled system

This example demonstrates wave–current coupling and includes wave-induced forcing by the radiation-stress terms. The domain is a rectangular basin 15 km in width and 14 km long, with a uniform initial depth of 4 m (Table 5). The northern, western, and eastern edges are open with radiation boundary conditions. Along the center of the domain is a wall with a centered 2 km wide inlet. The model is forced by oscillating the water level on the northern edge with a tidal amplitude of 1 m. Waves are also imposed on the northern edge with a wave height of 1 m, directed to the south with a

period of 10 s. The model is run with two configurations: (1) one-way coupled with wave information passed to the circulation model and (2) two-way fully coupled. The model hydrodynamics were simulated for a period of 2 days with a morphologic scale factor of 10, simulating a 20-day period.

In the one-way coupled system, wave heights evolve to a steady state, decreasing southward toward the inlet and showing no effect from the

inlet currents (Fig. 6). At the peak of the ebb tide the combined wave–current bottom stresses are maximum near the location of maximum currents. Bathymetric evolution produces a flood and a larger ebb shoal. By contrast, the two-way coupled model results show greatly increased wave heights in front of the inlet as the approaching wave interacts with an opposing current. The increased wave heights create combined bottom stresses that are greater than the one-way coupled system, and the peak bottom stresses are located near the maximum wave heights. The morphology evolves a stronger ebb shoal due to the higher stresses and the shoal is displaced slightly further seaward.

Table 4
Model parameters for test case 2—migrating trench

Model parameter	Variable	Value
Length, width, depth	$Xsize,$	30, 0.5, 0.39 m
	$Esize,$	
	$depth$	
Number of grid spacings	Lm, Mm, Nm	300, 4, 20
Bottom roughness	Zob	0.000833 m
Time step	dt	0.05 s
Simulation steps	$Ntimes$	30 000 initial (no morphology), 12 000 with morphology
Morphology factor	$morph_fac$	0 for initial, 90 for morph
Settle velocity	w_s	11.0 mm s ⁻¹
Erosion rate	E_0	0.35×10^{-2} kg m ⁻² s ⁻¹
Critical stresses	τ_{cd}, τ_{ce}	0.11 N m ⁻²
Porosity	ϕ	0.40
Bed slope	S_0	4×10^{-4}
Inflow/outflow boundary condition	\bar{u}	0.51 m s ⁻¹

4.4. Example 4: Evolution of surficial sediment distribution in Massachusetts Bay

Here we highlight the sediment-transport capabilities of the model and its ability to simulate the transport of a mixed grain size bed and the evolution of the sea floor sediment grain size distribution. A detailed description is provided in Warner et al. (in press). In this simulation the sediment bed was initialized with 10 vertical levels with the top 6 layers at 0.01 m thick and the bottom 4 at 0.10 m thick. All layers had a porosity of 0.50 and initial spatially-uniform distributions of sediments with 7 equal fractions of grain size ranging from 7 phi (fine silt) to 1 phi (coarse sand) with

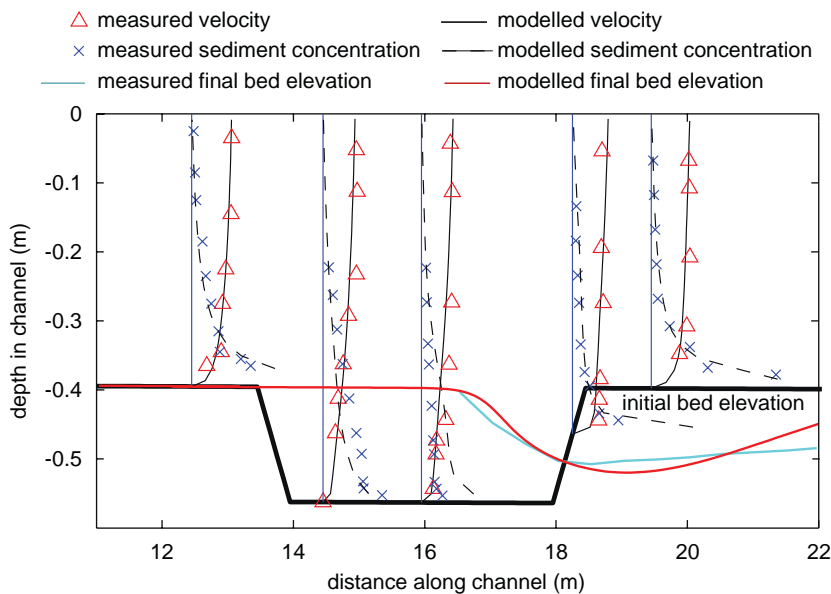


Fig. 5. Migrating trench test case showing initial (black line), final measured (cyan), and final modeled (red) bed elevations. Vertical profiles of measured and modeled suspended-sediment concentration and velocity are compared.

Table 5
Model parameters for test case 3—tidal inlet

Model parameter	Variable	Value
Length, width, depth	$Xsize, Esize, depth$	15,000, 14,000, 4.0 m
Number of grid spacings	Lm, Mm, Nm	75, 70, 10
Bottom roughness	z_{ob}	0.015 m
Time step	dt	10 s
Simulation steps	$Ntimes$	17280 steps (2 day)
Morphology factor	$morph_fac$	10 (= 20 day scaled simulation)
Settle velocity	w_s	11.0 mm s^{-1}
Erosion rate	E_0	$5 \times 10^{-3} \text{ kg m}^{-2} \text{ s}^{-1}$
Critical stresses	τ_{cd}, τ_{ce}	0.10 N m^{-2}
Porosity	ϕ	0.50
Bed thickness	bed_thick	10.0 m
Northern edge tide	A, T_t	1.0 m, 12 h
Northern edge wave height	H_{sig}	2 m
Northern edge wave period	T	10 s
Northern edge wave direction	θ	From 0°

critical shear stresses ranging from 0.022 to 0.27 Pa respectively. The simulation had a tidal forcing with 7 main constituents along the open boundary. After a spin-up time period, forcing with realistic wind stress and wave fields were imposed to simulate an 8-day December 1992 storm. This storm was repeated 10 times with an intervening 1-day period to allow sediment to settle out of the water column. The model time step was 30 seconds and hourly results were saved.

The repeating storm simulation generated realistic patterns of bottom stress, sediment resuspension, and bathymetric change (Fig. 7). The instantaneous bottom stress (maximum combined wave/current) at the peak of storm activity is greatest in the shallow water along the coastline and on the crest of Stellwagen Bank, coinciding with locations of increased bottom orbital velocities from the wave model (Fig. 7). Stresses are lower in Stellwagen Basin where the near-bottom wave currents are attenuated in the deep water, and in Cape Cod Bay because the Cape shelters the Bay from waves from the northeast. Along the western shore of

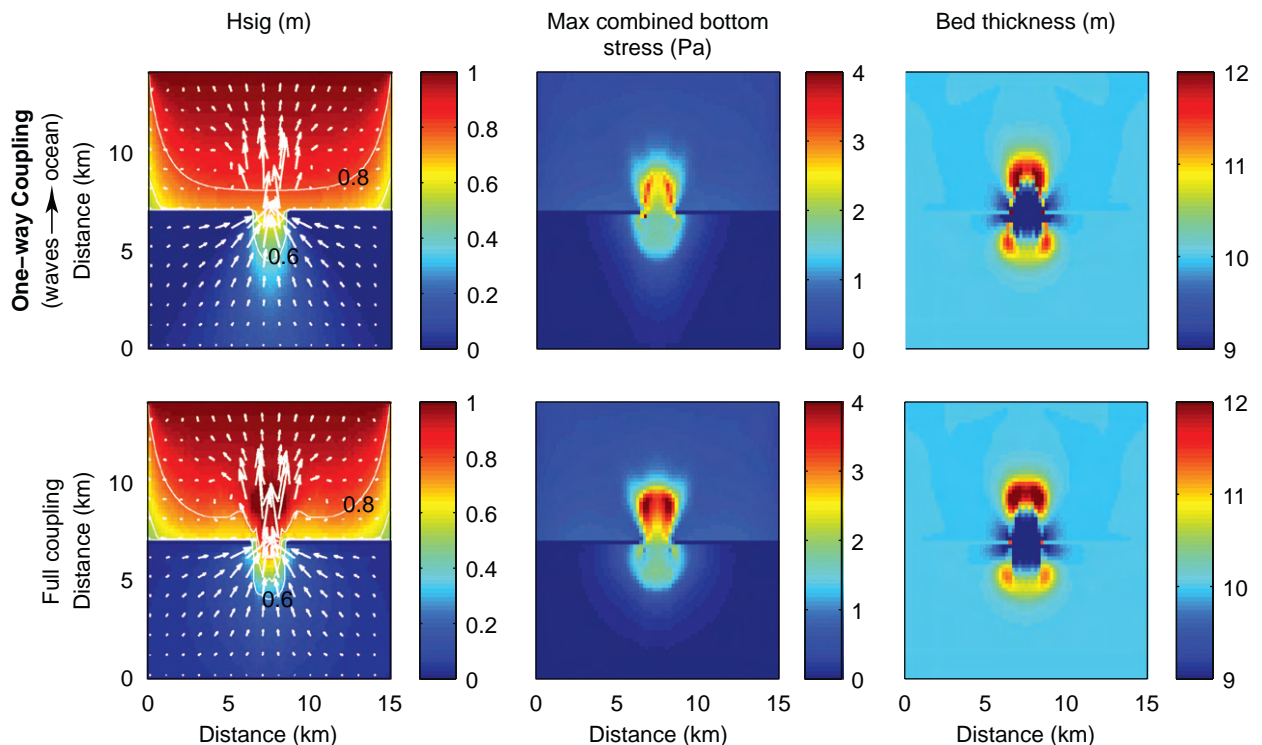


Fig. 6. Tidal inlet test case. Comparison of significant wave height, bottom stress, and bed thickness for a one-way coupled simulation (wave parameters sent to ocean model) to a fully coupled simulation (wave parameters to ocean model and ocean data to wave model). See text for full data transfer description. For the fully coupled system, wave heights show effect of currents, maximum bottom stress is enhanced due to increased wave heights, and bed thickness develops a stronger flood shoal than the one-way coupled system.

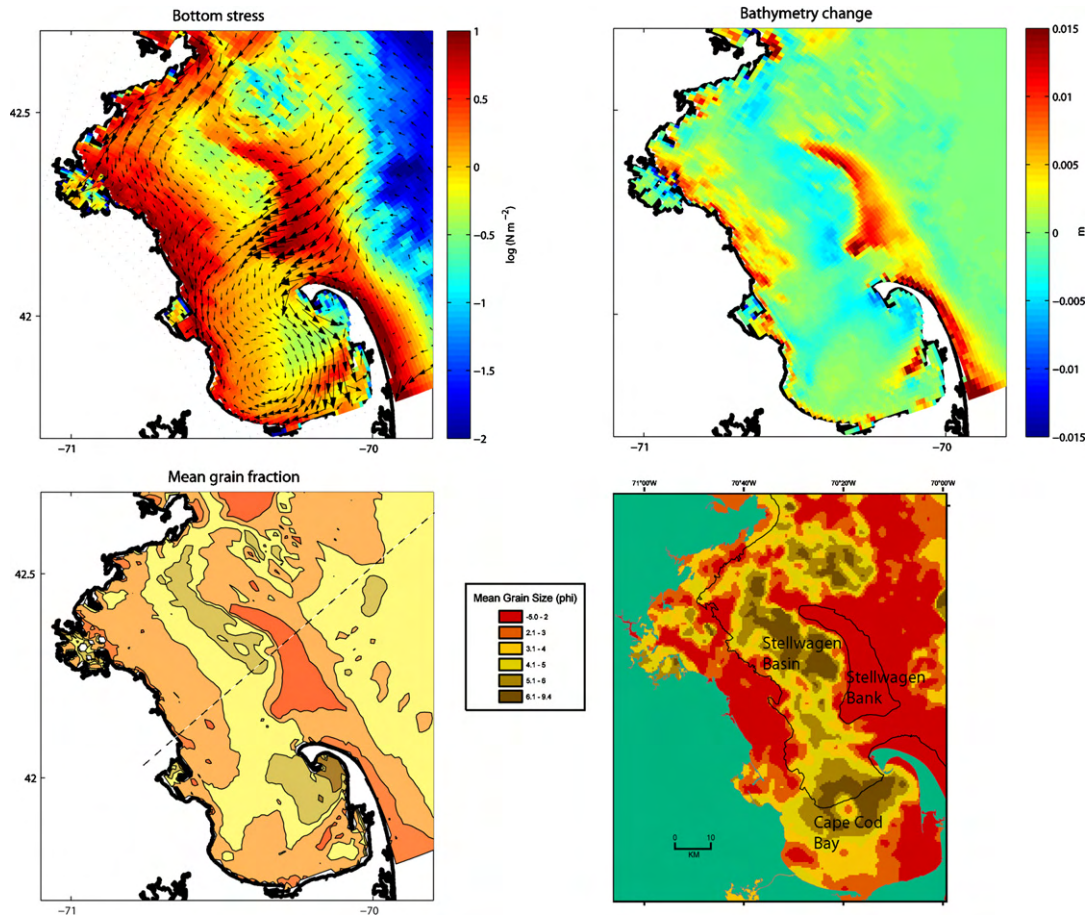


Fig. 7. Results from model simulation of Massachusetts Bay for the evolution of a mixed sediment bed in response to a sequence of 10 idealized northeast storms, modeled after the December 1992 storm with winds from 50° . Panels show instantaneous wave–current bottom stress at peak of storm (A), and change in bathymetry (B) and final mean surficial grain size (C) following the 10-storm sequence. The observed surficial grain size distribution (D) qualitatively matches the evolved sediment texture.

Massachusetts Bay (in the region opposite of Stellwagen Basin) the combined wave and current stress is high but then decreases between Plymouth and Barnstable. The instantaneous suspended-sediment concentrations during the storm (not shown) are greatest in the regions of highest stress and are lowest in Cape Cod Bay and in Stellwagen Basin. At the end of the simulation, net erosion has occurred along the crest of Stellwagen Bank, along the western shore of Massachusetts Bay (in the region of high stress), and along the outer arm of Cape Cod, reaching maximum values of 0.02 m (Fig. 7b). Deposition occurs in Stellwagen Basin immediately west of Stellwagen Bank, and in Cape Cod Bay.

The surficial grain size distribution after 10 storms (Fig. 7C) has approached a steady-state, with continued small changes that do not significantly alter the pattern described here. The sediment texture is

coarser in regions of high stress and finer in areas of low stress. The surficial sediment texture qualitatively resembles the observed distribution (Fig. 7d; Poppe et al., 2003). The crest of Stellwagen Bank, the outer Cape, and the western shore of Massachusetts Bay north of Plymouth have been winnowed to sizes of $2\text{--}3\phi$ and sediment deposition in Cape Cod Bay and Stellwagen Basin has produced a surface of $5\text{--}6\phi$ material. The material east of Stellwagen Bank is slightly finer in the model, possibly because the Gulf of Maine coastal current which could transport the 4 and 5ϕ material further to the south is not simulated.

5. Future work

Future model improvements will be implemented using an open-source, community development approach. We plan to investigate alternative approaches

to wave-induced circulation in the nearshore, including the vortex-force representation of McWilliams et al. (2004). We also are investigating other model-coupling methodologies, such as the Earth System Modeling Framework (ESMF, <http://www.esmf.ucar.edu/>). Algorithms to represent cohesive sediment behavior and biodiffusive mixing are under development. Several aspects of the BBL calculations will be improved by including effects of sediment-induced stratification, time-dependent ripple evolution, and representation of bedforms that develop under combinations of waves and currents. These processes and others are currently being investigated.

6. Conclusions

We are developing a coupled wave–current–sediment transport–morphodynamic oceanographic circulation model applicable to studies in rivers, lakes, estuaries, coastal environments, and the coastal ocean. The ocean circulation model ROMS has been coupled using the MCT to the surface wave model SWAN. We have incorporated nearshore radiation-stress terms and a surface roller model to account for surfzone (nearshore) processes. The sediment-transport algorithms have been implemented to transport an unlimited number of user-defined sediment classes. Suspended-sediment transport is computed with the advection–diffusion equation and a vertical-settling algorithm not restricted by the CFL criteria. Erosion and deposition algorithms control mass balance between suspended sediment in the water column and the evolution of a multi-level bed framework. The bed tracks the mass, fractions, thickness, and surface properties of the sediment and thus allows computations of morphological behavior and stratigraphy. Bedload transport occurs in the top layer for all the sediment classes. Additional features are being implemented to account for such conditions as mixed grain sizes, cohesive behavior, and bed biodiffusivity.

The model in its current state (ROMS 3.0) is available online and model development is being conducted as an open-source community effort. We hope for feedback that will add features and make the model more robust as the community of users and developers grows.

Acknowledgments

This work has been supported by the US Geological Survey Coastal and Marine Geology Program and by the Office of Naval Research

EuroSTRATAFORM project. We thank the reviewers for their comments and the developers of ROMS for open access to their code.

References

- Arakawa, A., 1966. Computational design for long-term numerical integration of the equations of fluid motion: Two-dimensional incompressible flow. Part I. *Journal of Computational Physics* 1, 119–143.
- Ariathurai, C.R., Arulanandan, K., 1978. Erosion rates of cohesive soils. *Journal of Hydraulics Division* 104 (2), 279–282.
- Blaas, M., Dong, C., Marchesiello, P., McWilliams, J.C., Stolzenbach, K.D., 2005. Sediment-transport modeling on Southern Californian Shelves: a ROMS case study. *Continental Shelf Research* 27, 832–853.
- Blumberg, A.F., Galperin, B., O'Connor, D.J., 1992. Modeling vertical structure of open-channel flows. *Journal of Hydraulic Engineering, ASCE* 118 (H8), 1119–1134.
- Booij, N., Ris, R.C., Holthuijsen, L.H., 1999. A third-generation wave model for coastal regions, Part I, Model description and validation. *Journal of Geophysical Research* 104 (C4), 7649–7666.
- Booij, N., Haagsma, I.J.G., Holthuijsen, L.H., Kieftenburg, A.T.M.M., Ris, R.C., van der Westhuysen, A.J., Zijlema, M., 2004. SWAN Cycle III version 40.41 User Manual. Delft University of Technology.
- Casulli, V., Cheng, R., 1992. Semi-implicit finite difference methods for three-dimensional shallow water flow. *International Journal for Numerical Methods in Fluids* 15, 629–648.
- Chassignet, E.P., Arango, H.G., Dietrich, D., Ezer, T., Ghil, M., Haidvogel, D.B., Ma, C.-C., Mehra, A., Paiva, A.M., Sirkes, Z., 2000. DAMEE-NAB: the base experiments. *Dynamics of Atmospheres and Oceans* 32, 155–183.
- Colella, P., Woodward, P., 1984. The piecewise parabolic method (PPM) for gas-dynamical simulations. *Journal of Computational Physics* 54, 174–201.
- Durski, S.M., Glenn, S.M., Haidvogel, D.B., 2004. Vertical mixing schemes in the coastal ocean: comparison of the level 2.5 Mellor-Yamada scheme with an enhanced version of the K profile parameterization. *Journal of Geophysical Research* 109, C01015.
- Fredsoe, J., Deigaard, R., 1992. Mechanics of coastal sediment transport. In: Liu, P.P.L.-F. (Ed.), *Advanced Series on Ocean Engineering*, Vol. 3. World Scientific, Singapore, p. 392.
- Grant, W.D., Madsen, O.S., 1979. Combined wave and current interaction with a rough bottom. *Journal of Geophysical Research* 84 (C4), 1797–1808.
- Grant, W.D., Madsen, O.S., 1982. Movable bed roughness in unsteady oscillatory flow. *Journal Geophysical Research* 87 (C1), 469–481.
- Haidvogel, D.B., Arango, H.G., Hedstrom, K., Beckmann, A., Malanotte-Rizzoli, P., Shchepetkin, A.F., 2000. Model evaluation experiments in the North Atlantic Basin: Simulations in nonlinear terrain-following coordinates. *Dynamics of Atmospheres and Oceans* 32, 239–281.
- Haidvogel, D.B., Arango, H.G., Budgell, W.P., Cornuelle, B.D., Curchitser, E., Di Lorenzo, E., Fennel, K., Geyer, W.R., Hermann, A.J., Lanerolle, L., Levin, J., McWilliams, J.C.,

- Miller, A.J., Moore, A.M., Powell, T.M., Shchepetkin, A.F., Sherwood, C.R., Signell, R.P., Warner, J.C., Wilkin, J., 2007. Regional Ocean forecasting in terrain-following coordinates: model formulation and skill assessment. *Journal of Computational Physics*.
- Harris, C.K., Wiberg, P.L., 1997. Approaches to quantifying long-term continental shelf sediment transport with an example from the northern California STRESS mid-shelf site. *Continental Shelf Research* 17, 1389–1418.
- Harris, C.K., Wiberg, P.L., 2001. A two-dimensional, time-dependent model of suspended sediment transport and bed reworking for continental shelves. *Computers & Geosciences* 27, 675–690.
- Jacob, R., Larson, J., Ong, E., 2005. M x N Communication and parallel interpolation in community climate system model version 3 using the model coupling toolkit. *International Journal of High Performance Computing Applications* 19 (3), 293–307.
- Jonsson, I.C., Carlsen, N.A., 1976. Experimental and theoretical investigations in an oscillatory boundary layer. *Journal of Hydraulic Research, ASCE* 14 (1), 45–60.
- Kantha, L.H., Clayson, C.A., 1994. An improved mixed layer model for geophysical applications. *Journal of Geophysical Research* 99 (C12), 25,235–25,266.
- Large, W.G., McWilliams, J.C., Doney, S.C., 1994. A review and model with a nonlocal boundary layer parameterization. *Reviews of Geophysics* 32, 363–403.
- Larson, J., Jacob, R., Ong, E., 2005. The model coupling toolkit: a new fortran90 toolkit for building multiphysics parallel coupled models. *International Journal of High Performance Computing Applications* 8 (19), 277–292.
- Lesser, G.R., Roelvink, J.A., van Kester, J.A.T.M., Stelling, G.S., 2004. Development and validation of a three-dimensional morphological model. *Coastal Engineering* 51, 883–915.
- Li, M.Z., Amos, C.L., 2001. SEDTRANS96: the upgraded and better calibrated sediment-transport model for continental shelves. *Computers & Geosciences* 27, 619–645.
- Li, M., Zhong, L., Boicourt, B., 2005. Simulation of Chesapeake Bay Estuary: sensitivity to turbulence mixing parameterizations and comparison with hydrographic observations. *Journal of Geophysical Research* 110, C12004.
- Liu, X.-D., Osher, S., Chan, T., 1994. Weighted essentially non-oscillatory schemes. *Journal of Computational Physics* 115, 200–212.
- Madsen, O.S., 1994. Spectral wave–current bottom boundary layer flows. In: *Coastal Engineering 1994. Proceedings of the 24th International Conference on Coastal Engineering Research Council, Kobe, Japan*, pp. 384–398.
- Malarkey, J., Davies, A.G., 2003. A non-iterative procedure for the Wiberg and Harris (1994) oscillatory sand ripple predictor. *Journal of Coastal Research* 19 (3), 738–739.
- McWilliams, J.C., Restrepo, J.M., Lane, E.M., 2004. An asymptotic theory for the interaction of waves and currents in coastal waters. *Journal of Fluid Mechanics* 511, 135–178.
- Mellor, G.L., 2003. The three-dimensional current and surface wave equations. *Journal of Physical Oceanography* 33, 1978–1989.
- Mellor, G.L., 2005. Some consequences of the three-dimensional currents and surface wave equations. *Journal of Physical Oceanography* 35, 2291–2298.
- Mellor, G.L., Yamada, T., 1982. Development of a turbulence closure model for geophysical fluid problems. *Reviews of Geophysics and Space Physics* 20, 851–875.
- Meyer-Peter, E., Müller, R., 1948. Formulas for bedload transport. In: *Report on the 2nd Meeting International Association Hydraulic Structure Research, Stockholm, Sweden*, pp. 39–64.
- Nielsen, P., 1986. Suspended sediment concentrations under waves. *Coastal Engineering* 10, 23–31.
- Nielsen, P., 1992. *Coastal Bottom Boundary Layers and Sediment Transport. Advanced Series on Ocean Engineering, vol. 4. World Scientific, Singapore*, 324pp.
- Phillips, O.M., 1969. *The Dynamics of the Upper Ocean. Cambridge Press, Cambridge*.
- Poppe, L.J., Paskevich, V.F., Williams, S.J., Hastings, M.E., Kelly, J.T., Belknap, D.F., Ward, L.G., FitzGerald, D.M., Larsen, P.F., 2003. Surficial sediment data from the Gulf of Maine, Georges Bank, and vicinity: A GIS Compilation. US Geological Survey Open-File Report 03-001, <<http://pubs.usgs.gov/of/2003/of03-001/index.htm>>.
- Roelvink, J.A., 2006. Coastal morphodynamic evolution techniques. *Coastal Engineering* 53, 277–287.
- Shchepetkin, A.F., McWilliams, J.C., 2005. The regional ocean modeling system (ROMS): a split-explicit, free-surface, topography-following-coordinates ocean model. *Ocean Modelling* 9, 347–404.
- Sherwood, C.R., Harris, C.K., Geyer, W.R., Butman, B., 2002. Toward a community coastal sediment-transport modeling system: Report of the Second Workshop. EOS, Transactions, American Geophysical Union 83 (51).
- Smith, J.D., 1977. Modeling of sediment transport on continental shelves. In: Goldberg, E.D., McCave, I.N., O'Brien, J.J., Steele, J.H. (Eds.), *The Sea, Vol. 6. Wiley-Interscience, New York*, pp. 539–577.
- Smith, J.D., McLean, S.R., 1977. Spatially averaged flow over a wavy surface. *Journal of Geophysical Research* 82 (12), 1735–1746.
- Soulsby, R.L., 1995. Bed shear-stresses due to combined waves and currents. In: Stive, M.J.F. (Ed.), *Advances in Coastal Morphodynamics: An Overview of the G8-Coastal Morphodynamics Project, Co-Sponsored by the Commission of The European Communities Directorate General XII* pp. 4.20–4.23.
- Soulsby, R.L., 1997. *Dynamics of Marine Sands. Thomas Telford, London*, 249pp.
- Soulsby, R.L., Damgaard, J.S., 2005. Bedload sediment transport in coastal waters. *Coastal Engineering* 52 (8), 673–689.
- Styles, R., Glenn, S.M., 2000. Modeling stratified wave and current bottom boundary layers on the continental shelf. *Journal of Geophysical Research* 105 (C10), 24,119–24,139.
- Styles, R., Glenn, S.M., 2002. Modeling bottom roughness in the presence of wave-generated ripples. *Journal of Geophysical Research* 107 (C8), 24/1–24/15.
- Svendsen, I.A., 1984. Wave heights and set-up in a surf zone. *Coastal Engineering* 8, 303–329.
- Svendsen, I.A., Haas, K., Zhao, Q., 2002. Quasi-3D nearshore circulation model SHORECIRC, User's Manual, Draft Report, Center for Applied Coastal Research, Department of Civil Engineering, University of Delaware, Newark.
- Umlauf, L., Burchard, H., 2003. A generic length-scale equation for geophysical turbulence models. *Journal of Marine Research* 61, 235–265.

- van Rijn, L.C., 1987. Mathematical modelling of morphological processes in the case of suspended sediment transport. Delft Technical University, Delft Hydraulics Communication No. 382, Delft, The Netherlands.
- van Rijn, L.C., 1993. Principles of Sediment Transport in Rivers, Estuaries, and Coastal Seas. Aqua Publications–I11, Amsterdam, The Netherlands, 614pp.
- Warner, J.C., Sherwood, C.R., Arango, H.G., Signell, R.P., 2005. Performance of four turbulence closure models implemented using a generic length scale method. *Ocean Modelling* 8, 81–113.
- Warner, J.C., Perlin, N., Skillingstad, E. (in press). Using the model coupling toolkit to couple earth system models. *Environmental Modelling and Software*.
- Wiberg, P.L., Harris, C.K., 1994. Ripple geometry in wave-dominated environments. *Journal of Geophysical Research* 99 (C1), 775–789.
- Wiberg, P.L., Nelson, J.M., 1992. Unidirectional flow over asymmetric and symmetric ripples. *Journal of Geophysical Research* 97 (C8), 12,745–12,761.
- Wiberg, P.L., Rubin, D.M., 1989. Bed roughness produced by saltating sediment. *Journal of Geophysical Research* 94 (C4), 5011–5016.
- Wiberg, P.L., Sherwood, C.R. (this issue). Calculating wave-generated bottom orbital velocity from surface wave parameters. *Computers & Geosciences*, doi:10.1016/j.cageo.2008.02.010.
- Wijesekera, H.W., Allen, J.S., Newberger, P.A., 2003. Modeling study of turbulent mixing over the continental shelf: comparison of turbulent closure schemes. *Journal of Geophysical Research* 108 (C3), 3103.



August 31 – September 05

Short course on Morphodynamics

- **Peter Mewis**

Peter MEWIS

12.10.1964 in Berlin

Current Position:

Senior Engineer, Hydraulic Laboratory, Department of Civil Engineering and Geodesy, Darmstadt University of Technology, Germany.



Education Background:

1. Oceanography, Moscow State University, Diploma(1988)
2. PhD in Hydraulic Engineering (2002)

Email: mewis@wb.tu-darmstadt.de

Professional Career :

until 1995, Research Associate at the Institute of Fluid Mechanics and Informatics, Faculty of Civil Engineering and Geodesy, University of Hanover, Germany
1995 to 2001, Research Associate at the Institute of Hydraulic Engineering and Water Resources Research, UT Darmstadt, Germany
2001, Dr.-Ing. doctoral dissertation with the thesis “Morphodynamic numerical modelling of river bends”, Institute of Hydraulic Engineering and Water Resources Research UT Darmstadt
Since 2001, head of the Hydraulic Laboratory of the Hydraulic Engineering and Water Resources Research, UT Darmstadt, Germany.

Position in Professional Association:

American Society of Civil Engineers ASCE
International Association of Hydraulic Research IAHR
German Water Association DWA
German Port Technology Association HTG

*Member of the ASCE task committee on three-dimensional model verification, organised by Prof. Sam Wang

*Speaker of the workgroup on “Sediment Transport Models” of the German Water Association.

Working fields: Morphodynamic-numerical computations, sediment transport in rivers and estuaries, bedforms, coastal morphology, tidally induced morphodynamics, physical modeling

Publications:

- P. Mewis, “Morphodynamic-Numerical Modeling of dunes in the river Elbe”, MARID-Workshop, University of Twente, 2004.
P. Mewis, “Morphodynamic Numerical Modelling of the tidal channels of the Dithmarscher Bucht”, Int. Conference on HydroScience and Engineering, Brisbane, 2004.
M. Witting, P. Mewis, U. Zanke, “Modeling of Storm Induced Island Breaching at the Baltic Sea Coast”, Coastal Dynamics 2005, 214, 59.
P. Mewis, “Nearshore morphodynamic-numerical computation of the influence of harbor jetties”, Proceedings of the 30th International Conference on Coastal Engineering, 2006, San Diego, pp. 835-8843.

Tidally induced morphodynamics



Dr.-Ing. P. Mewis

Structure

1. Morphodynamic-numerial models: SMOR3D, TIMOR, Strand
2. Three levels of severity
3. Filling of mining pits
4. Dithmarscher Bay, verification example
5. 3D modeling including density effects in the Weser estuary

ICCE 2008 | Institute of Hydraulic and Water Resources Engineering | Dr.-Ing. P. Mewis | 1



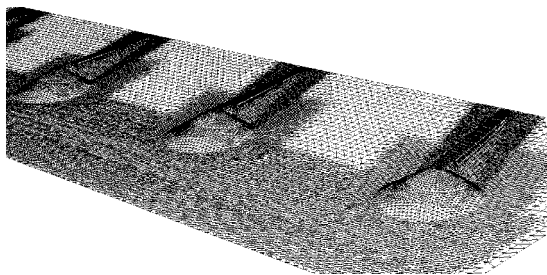
1. Morphodynamic-numerial models

SMOR3D, TIMOR, Strand

based on unstructured grids, stable and fast in computation

ICCE 2008 | Institute of Hydraulic and Water Resources Engineering | Dr.-Ing. P. Mewis | 2

Unstructured mesh



ICCE 2008 | Institute of Hydraulic and Water Resources Engineering | Dr.-Ing. P. Mewis | 3

TIMOR



TIMOR3 (Prof. Zanke and Dr. Mewis)
2D based on triangular elements (FEM)
fully coupled flow and sediment transport
applied and developed over 10 years

is capable of calculating

- bed- and suspended load
- graded sediment (24 fractions), incl. mud fractions
- dredging and dumping
- slope effect, bankline erosion
- helical flow effect
- account for wave motion (SWAN, WWM)

ICCE 2008 | Institute of Hydraulic and Water Resources Engineering | Dr.-Ing. P. Mewis | 4

SMOR3D



3D momentum equations, hydrostatic pressure
(mixing length, k-epsilon)

Continuity equation

Bed load transport (after Meier-Peter und Müller)

$$q_b(\tau') = C_{MPM} \cdot ((\tau' - \tau_c) / \rho)^{3/2}$$

Suspended load transport by Entrainment-Settlement
approach (non-cohesive material and cohesive material)

Transverse transport z.B. similar to Fredsøe, 1974

$$\tau' = \tau + C \cdot grad(a)$$

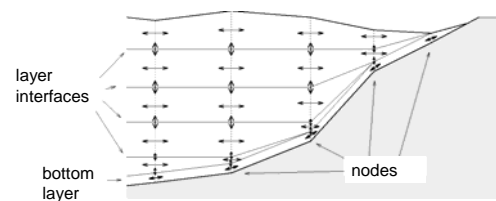
constant C from $\tau_c / tan(\phi) = 0.33 \text{ N/m}^2$

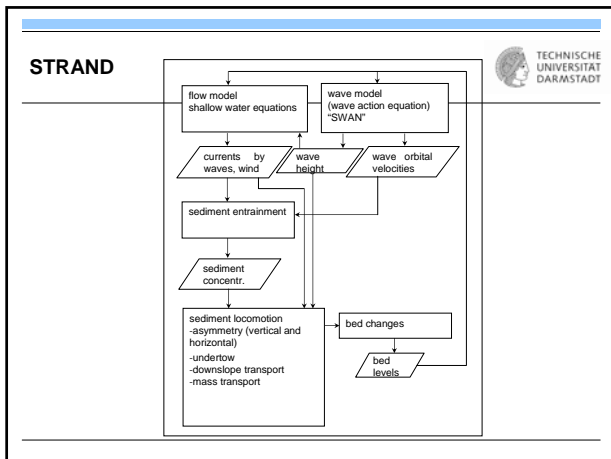
ICCE 2008 | Institute of Hydraulic and Water Resources Engineering | Dr.-Ing. P. Mewis | 5

SMOR3D



3D model SMOR3D vertical resolution





4. Three levels of severity

ICCE 2008 | Institute of Hydraulic and Water Resources Engineering | Dr.-Ing. P. Mewis | 8

Three levels of severity

Three **levels of severity** of morphodynamic model application can be distinguished:

- 1. Hard structures** like Jetties, dikes, quay walls, ...
Far from the dynamic equilibrium.
- almost caused by human activities
-> the reaction is strong, the direction is toward the equilibrium
- Development close to the **dynamic equilibrium**.
Self organization like meandering, crescentic bars a.o.
- Influences from **outside** / slow processes
Sediment fluxes across the open boundary.

ICCE 2008 | Institute of Hydraulic and Water Resources Engineering | Dr.-Ing. P. Mewis | 10

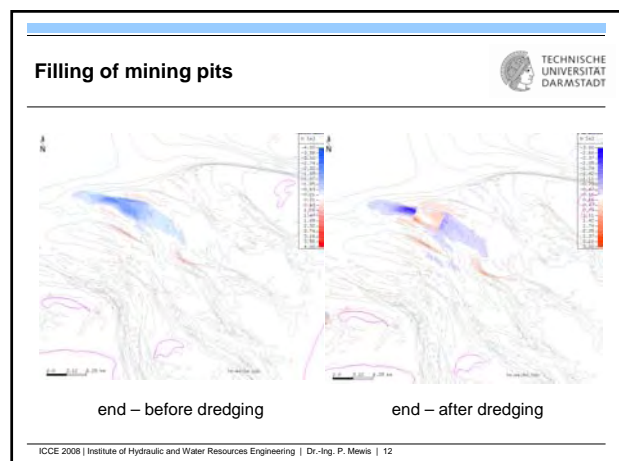
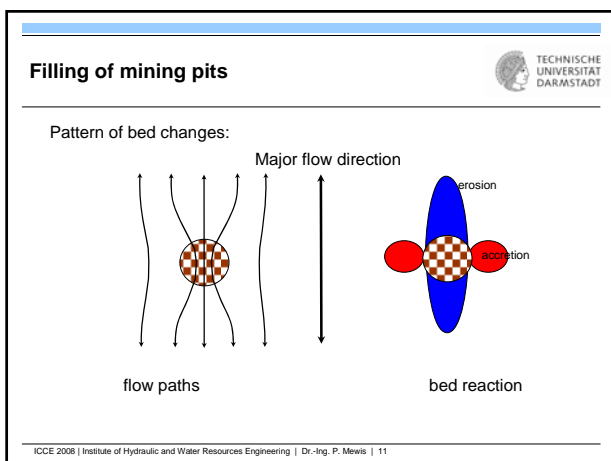
Filling of mining pits

3. Filling of mining pits

2 hypothetical examples:

1. Mining pit in the Jade tideway.
2. Mining field at a distance from the coast.

ICCE 2008 | Institute of Hydraulic and Water Resources Engineering | Dr.-Ing. P. Mewis | 10



Filling of mining pits



Migration of mining fields

1. Stretching in the flow direction.
2. More wave energy propagates across the deeper fields and may cause erosion behind it.
3. The part of the field exposed to more energy is refilling faster. This results in a „migration“ of the maximum depth location.
4. The fields influence the background depth changes at the location. If accumulation took place it is slowed down and vice versa.

ICCE 2008 | Institute of Hydraulic and Water Resources Engineering | Dr.-Ing. P. Mewis | 13



4. Verification example morphodynamics of the Dithmarscher Bucht.

ICCE 2008 | Institute of Hydraulic and Water Resources Engineering | Dr.-Ing. P. Mewis | 14

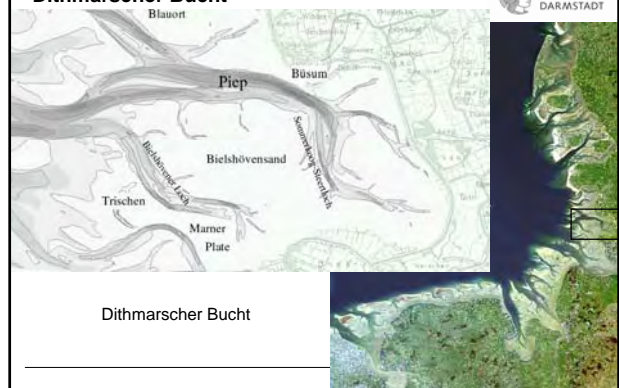
Dithmarscher Bucht



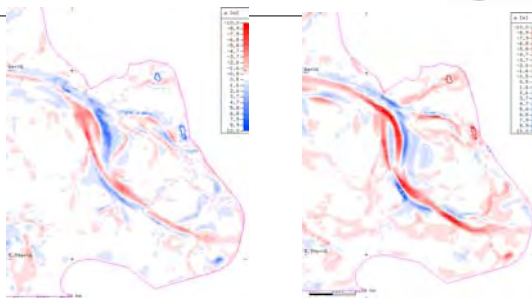
For the verification of morphodynamic-numerical models high quality data sets are needed that:

- have a high accuracy of the data,
- cover a certain minimum time span with sufficient density of the data,
- exhibit a significant morphodynamic development,
- that can well be recognized in the measurements and
- that can desirably be interpreted by experienced experts even without a model simulation.

Dithmarscher Bucht



Dithmarscher Bucht

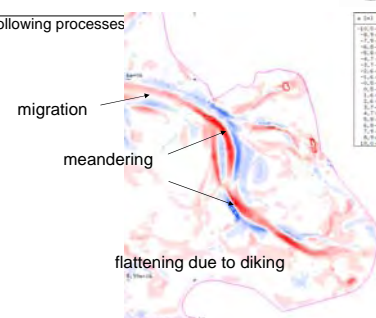


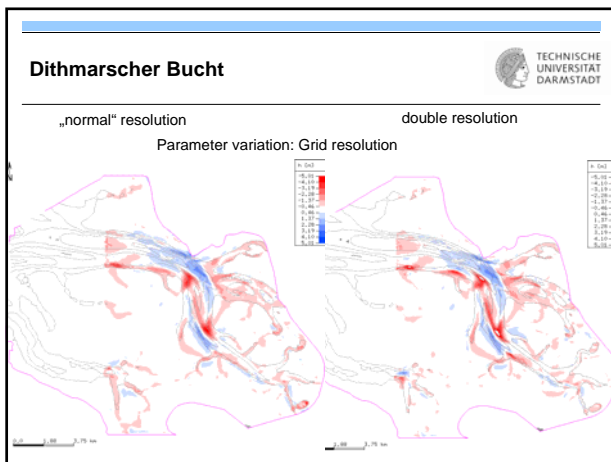
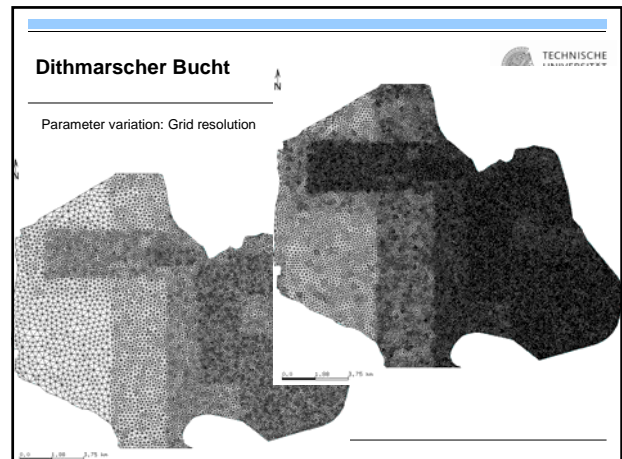
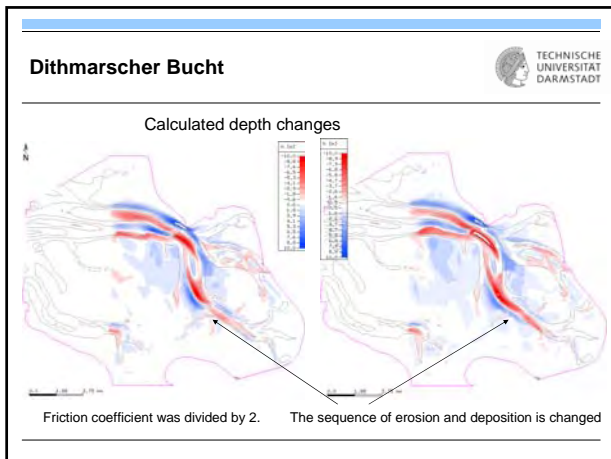
Observed depth changes: left 1969-1979, right 1979-1990
before after diking

Dithmarscher Bucht



Focus on the following processes in the channel:





Dithmarscher Bucht

Parameter variation:

Shown parameter variation

1. friction coefficient
2. numerical grid resolution/orientation

Other parameters that can be varied:

1. grain size
2. transverse transport
3. wind waves/scenarios
4. transport parameters
5. 2D/3D

Question: Is there a suitable measure of the model accuracy?

Dithmarscher Bucht

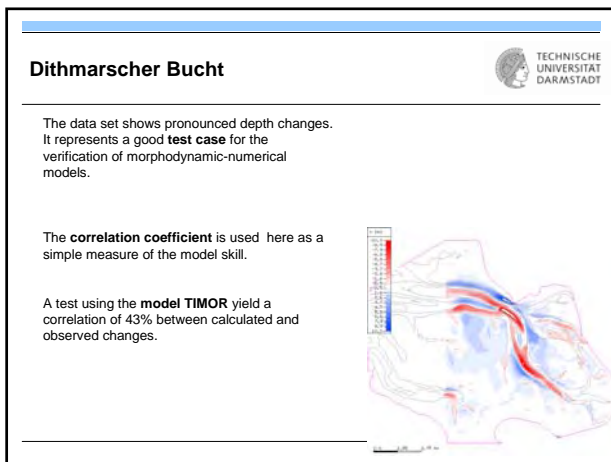
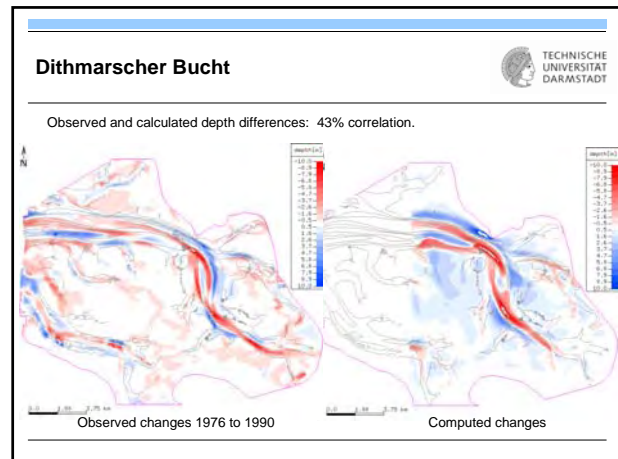
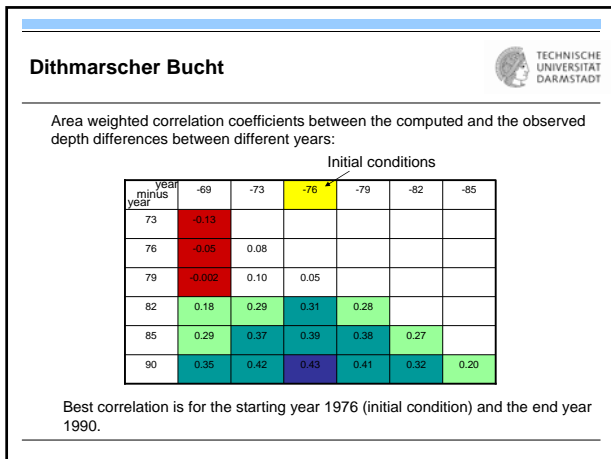
Area weighted correlation coefficients between depth distributions of different years.

year	1969	1973	1976	1979	1982	1985	1990
1969	1						
1973	0.962	1					
1976	0.951	0.975	1				
1979	0.925	0.951	0.973	1			
1982	0.898	0.926	0.952	0.965	1		
1985	0.879	0.901	0.927	0.943	0.976	1	
1990	0.852	0.875	0.899	0.913	0.943	0.968	1

Dithmarscher Bucht

Area weighted correlation coefficients between depth differences of different years (measurements):

year	73-69	76-73	79-76	82-79	85-82	90-85
73-69	1					
76-73	-0.223	1				
79-76	0.038	0.022	1			
82-79	0.119	-0.043	0.070	1		
85-82	-0.077	0.035	0.007	-0.187	1	
90-85	0.040	-0.068	-0.074	-0.157	-0.028	1



5. 3D modeling including density effects in the Weser estuary

ICCE 2008 | Institute of Hydraulic and Water Resources Engineering | Dr.-Ing. P. Mewis | 28

